uOttawa

L'Université canadienne
Canada's university

FACULTÉ DES ÉTUDES SUPÉRIEURES ET POSTOCTORALES

uOttawa

L'Université canadienne
Canada's university

FACULTY OF GRADUATE AND POSDOCTORAL STUDIES

Paul Marchand

AUTEUR DE LA THÈSE / AUTHOR OF THESIS

M.A.Sc. (Mechanical Engineering)

GRADE / DEGREE

Department of Mechanical Engineering

FACULTÉ, ÉCOLE, DÉPARTEMENT / FACULTY, SCHOOL, DEPARTMENT

Investigation of the C^2 Parameter of Force Limited Vibration Testing for Multiple Degrees-of-Freedom Systems

TITRE DE LA THÈSE / TITLE OF THESIS

Dr. D. Redekop

DIRECTEUR (DIRECTRICE) DE LA THÈSE / THESIS SUPERVISOR

Dr. R. Singhal

CO-DIRECTEUR (CO-DIRECTRICE) DE LA THÈSE / THESIS CO-SUPERVISOR

EXAMINATEURS (EXAMINATRICES) DE LA THÈSE / THESIS EXAMINERS

Dr. F. Afagh

Dr. D. Necsulescu

Gary W. Slater

Le Doyen de la Faculté des études supérieures et postdoctorales / Dean of the Faculty of Graduate and Postdoctoral Studies

Investigation of the C^2 Parameter of Force Limited Vibration Testing for Multiple Degrees-of-Freedom Systems

Paul Marchand

A thesis submitted to the Faculty of Graduate and Postdoctoral Studies
in partial fulfillment of the requirements for the degree of

Master of Applied Science

in Mechanical Engineering

Ottawa-Carleton Institute for Mechanical and Aerospace Engineering
University of Ottawa
Ottawa, Canada

June 2007

Your file Votre référence
ISBN: 978-0-494-34087-5
Our file Notre référence
ISBN: 978-0-494-34087-5

ABSTRACT

The semi-empirical method of force-limited vibration testing is used in the aerospace industry to avoid over-testing. The semi-empirical method specifies the maximum interface force based on a single parameter, often referred to as C^2, which is based on previous experience with similar structures. This thesis investigates the factors influencing the value of C^2 associated with semi-empirical force limited vibration testing. First, a base excited two degrees-of-freedom system is examined in context of the semi-empirical method. Then, the effect of different types of damping is investigated. The work is then extended to multiple degrees-of-freedom and continuous systems where a new method, based on the apparent mass, of determining the value of C^2 is presented. Finally, experimental testing is utilized to validate the conclusion and the predictions of the new method.

ACKNOWLEDGEMENTS

This thesis was made possible through the help and support of many individuals. I wish to thank and acknowledge the following persons for their aid.

I wish to thank my supervisor, Dr. Raj Singhal, for his invaluable support, encouragement, and guidance during the course of this work. This thesis would not have been possible without his help. In addition, I greatly appreciated his good humour, without which this thesis would not have been as fun.

I wish to thank my co-supervisor, Dr. David Redekop, for his useful comments and guidance. He also facilitated my transition from a work environment back to a school environment.

I wish to thank Mr. Mark O'Grady for providing me with many hours of fruitful discussions about force limited testing.

I wish to thank Mr. Tony Russiello of the David Florida Laboratory for his immense patience in conducting the many vibration tests presented in this thesis.

I wish to thank both Dr. Terry Scharton and Dr. Churn Kang for encouraging me to pursue my research in force limited testing.

I wish to thank Dr. Yvan Soucy for his useful comments and for making me appreciate some of the finer points of the force limited testing.

I wish to thank Mr. Vijayamohan Rao Dharanipathi and Mr. Swen Ritzmann for their generosity in sharing their knowledge of force limited testing.

I also wish to thank Dr. Tory Payne, Mr. Geoff Barnes, Mr. Ken Smith, Mr. Louis Piché, and Mr. Blair Gordon for their financial support and encouragement in pursuing my post-graduate studies while remaining in their employment at Routes AstroEngineering.

In addition, I wish to thank my parents for taking care of my personal affairs during my studies, allowing me to devote my full attention to both work and school.

And most of all, I wish to thank my wife Diana for encouraging me in pursuing higher education and for being so supportive throughout my studies.

TABLE OF CONTENTS

LIST OF FIGURES

LIST OF TABLES

ACRONYMS

ASD	Acceleration Spectral Density
C-of-M	Center-of-Mass
DOF	Degrees-of-freedom
FRF	Frequency Response Function
FSD	Force Spectral Density
ID	Identification
JPL	Jet Propulsion Laboratory
MAC	Mass Acceleration Curve
NASA	National Aeronautics and Space Administration
RMS	Root Mean Squared
TDFS	Two Degrees-of-Freedom System

LIST OF SYMBOLS

c	Viscous damping constant
C	Constant associated with the semi-empirical method for sine tests
e	Base of the natural logarithm, 2.718281828…
f	Frequency in Hertz
F	Un-damped natural frequency ratio of the load to the source, $F \equiv \frac{\omega_2}{\omega_1}$
H	Complex acceleration frequency response function
i	Index
i	Imaginary number equal to $\sqrt{-1}$
k	Spring constant
L	Length
m	Mass
n	Exponent associated with the semi-empirical method
Q	Quality factor
R	Ratio of input frequency to load natural frequency, $R \equiv \frac{\omega}{\omega_2}$
t	Time
x	Position
α	Bolt force correction factor
β	Overall force correction factor
γ	Structural damping factor
ζ	Damping ratio
θ	Angular position
μ	Mass ratio of the load to the source, $\mu \equiv \frac{m_2}{m_1}$
π	3.141592654…
ω	Circular frequency

$A_{test}(f)$	Test acceleration
$F_{max}(f)$	Interface force limit during testing
$F_{total}(f)$	Total vector summed force
$M_{app}(f)$	Apparent mass of the article under test
$M_{app\_load}(f)$	Load apparent mass
$M_{app\_source}(f)$	Source apparent mass
$S_{aa}(f)$	Acceleration spectral density
$S_{aa\_flight}(f)$	Acceleration spectral density when in the flight configuration
$S_{aa\_source\_free}(f)$	Acceleration spectral density of the source when the load is absent
$S_{aa\_test}(f)$	Test input acceleration spectral density
$S_{ff}(f)$	Force spectral density
$S_{ff\_flight}(f)$	Force spectral density when in the flight configuration
$S_{ff\_max}(f)$	Force spectral density limit during testing
$S_{ff\_source}(f)$	Force spectral density at interface
A_i	Zero-to-peak acceleration at position i
A_{test}	Test acceleration
C_i	Complex number
f_0	Corner frequency associated with the semi-empirical method equal to the first pronounced resonance displayed by the apparent mass of the test item
f_{max_acc}	Frequency where the maximum acceleration occurs when in the flight configuration
f_{max_force}	Frequency where the maximum force occurs when in the flight configuration
$f_{nn\_coupled}$	First natural frequency of the flight configuration
m_{eff}	Effective mass
m_{eff_max}	Largest effective mass
M_0	Mass of the article under test
M_{app}	Apparent mass of the article under test
M_{load}	Mass of the load
$M_{residual\_n}$	Residual mass of mode n

R_{11} Ratio of first coupled natural frequency to load natural frequency, $R_{11} \equiv \frac{\omega_{11}}{\omega_2}$

R_{22} Ratio of second coupled natural frequency to load natural frequency, $R_{22} \equiv \frac{\omega_{22}}{\omega_2}$

R_{ff} Either first or second coupled natural frequency to load natural frequency

S_{aa} Acceleration spectral density

S_{aa_source} Acceleration spectral density of the source

S_{aa_test} Test input acceleration spectral density

S_{ff} Force spectral density

$S_{ff\_total\_actual}$ Actual total force spectral density at interface

$S_{ff\_total\_sensor}$ Total force spectral density reported by load sensors

$\beta_{overall}$ Overall system effective force correction factor

ω_1 Un-damped fixed-base natural frequency of the source

ω_{11} First un-damped natural frequency of the coupled source-load system

ω_2 Un-damped fixed-base natural frequency of the load

ω_{22} Second un-damped natural frequency of the coupled source-load system

C^2 Constant associated with the semi-empirical method for random tests

GLOSSARY OF SELECTED TERMS

Acceleration Spectral Density (ASD)

The acceleration spectral density, or ASD, is a frequency dependent function that describes the mean square acceleration of a random vibration with a mean acceleration of zero for an infinitesimally small bandwidth. It can be obtained by taking the Fourier transform of the auto-correlation function of the time history with itself. The acceleration spectral density is sometimes referred to as the power spectral density or the auto-spectral density.

Apparent Mass

In a base-excited system, the frequency response function that describes the resultant interface force in the excitation direction divided by the base acceleration is called the apparent mass of the system. The value of the apparent mass at 0 Hertz corresponds to the actual mass of the object. At higher frequencies, the value of the apparent mass can be higher or lower than the actual mass depending on the mass, stiffness, and damping of the structure.

Complex Two Degrees-of-Freedom System Method (Complex TDFS Method)

The complex two degrees-of-freedom system method, or complex TDFS method for short, is the name given to a technique for approximating the interface force between two structures of any degrees-of-freedom when performing force-limited testing. The technique accounts for the force contribution from the residual masses.

Effective Mass

In a base-excited system, the interface force divided by the base acceleration can be expressed as the weighted sum of the force transmissibility response of N single degree-of-freedom systems, where N represents all possible modes of the structure. The weighing factor for each mode has the units of mass and is referred to as the effective mass for that mode. The effective mass expresses the contribution of each mode to the total interface force measured in the same direction as the base excitation. The effective

masses have the property that the sum of all effective masses in a common direction is equal to the actual mass of the object. The ratio of the effective mass to the total mass is called the mass participation factor for that mode.

Frequency Response Function

The frequency response function is a complex function that describes an output response to a given input at a given frequency.

Mechanical Impedance

The mechanical impedance is the frequency response function that describes the ratio of the applied force to the resulting velocity at a particular point on a structure. It is a way of describing the resistance to motion for that point. The mechanical impedance is a frequency dependent function that depends on the stiffness, mass, and damping of the structure. It is sometimes referred to as structural impedance.

Quality Factor (Q)

The quality factor Q is a value that describes the sharpness of resonance of a system. It describes the ratio of a resonant frequency to the frequency bandwidth defined by the half-power points where the response is equal to $\frac{1}{\sqrt{2}}$ of the peak response. The quality factor is often referred simply as the Q of a structure.

Residual Mass

The residual mass is a discontinuous frequency dependent term that is equal to the actual mass of the object minus the sum of all effective masses for modes up to and including the frequency of interest.

Simple Two Degrees-of-Freedom System Method (Simple TDFS Method)

The simple two degrees-of-freedom system method, or simple TDFS method for short, is the name given to a technique for approximating the interface force between two structures of any degrees-of-freedom when performing force-limited testing. The

technique is based on a simple two degrees-of-freedom system where the masses of the two degrees-of-freedom system are associated with residual masses within a given bandwidth for the actual system.

1 INTRODUCTION

Launching satellites into space is a risky venture. In particular, there is a risk that the satellite will not survive the harsh vibrations present during launch. To minimize this risk, vibration testing is performed to verify that the satellite and all of its component hardware are indeed fit for launch.

Vibration testing consists of bolting the test hardware to a shaker table and shaking the table such that the base of the hardware experiences acceleration levels that are representative of the accelerations that will be present during launch. Ideally, the exact acceleration spectrum experienced during launch would be reproduced during testing. However, for practical reasons, a simplified acceleration spectrum that envelops the peaks of the expected flight level is utilized during testing. This simplifying enveloping technique has been successfully utilized to qualify space hardware for many years. However, in 1956, Blake [1] described how the enveloping process leads to severe over-testing at the natural frequencies of the test hardware. Acceleration spectral density vibration levels as high as 10,000 times higher than required have been reported [2], but more typically the over-test levels are between 10 and 100 higher than required [3]. Such over-testing can lead to unrealistic failures that would never be present during flight. Resolving these failures by re-design and then re-testing of the hardware is both expensive and time-consuming and is therefore undesirable. Moreover, if the hardware was designed *a priori* to survive the over-test, there would be no test failures but this would be achieved at the expense of unnecessary over-design. This is also undesirable because of the required extra mass, volume, and design effort, which impact the overall cost of the spacecraft. To mitigate the over-testing problem, the acceleration test levels are reduced near the main resonant frequency of the test item. This practice is commonly referred to as notching.

Traditionally, the amount of notching is based on response limiting, which is the practice of limiting the acceleration input such that the maximum acceleration responses at critical locations never exceed a specified value. A fairly detailed and complex finite element

model is usually created in order to perform response notching. This complexity, along with required assumptions about the damping nature of the structure, creates a certain level of uncertainty as to the accuracy of the model. In addition, critical locations may not be accessible during testing, or a large number of response limiting locations might be required, limiting the usefulness of the method.

A different method of notching called force limiting has been implemented for the past 15 years at the National Aeronautics and Space Administration (NASA) Jet Propulsion Laboratory (JPL) [4]. Force limiting is now becoming the standard method of notching at NASA [5, 6] and is slowly gaining acceptance by the space agencies of other countries including the Canadian Space Agency. In this method, the acceleration input is limited such that the interface forces between the test item and the shaker do not exceed a predicted peak value experienced during launch. One of the benefits of force limiting over traditional response limiting is that the interface forces are much easier to accurately predict than the acceleration responses. Although a rudimentary finite element model can be utilized, the forces can also be predicted with reasonable accuracy without the need of any finite element model. In addition, the interface between the satellite and shaker table is always accessible and only up to six measurement channels are required to account for all the forces and moments through the interface. An example of force limiting vibration testing is given in appendix A.

In force limiting, there are many different approximate methods that can be utilized to predict the maximum interface forces without the need for a finite element analysis [5]. One of these alternate methods is the semi-empirical method. The method is gaining popularity in the international aerospace community because of its ease of use. The maximum interface forces are predicted using a semi-empirical constant called C. Since during random vibration testing, the square of the value of C is of interest, the constant is often expressed as the value C^2. The constant is based on experience with similar hardware and mounting structure as the hardware undergoing testing, as well as theoretical considerations. People have noticed that in practice this C^2 parameter is typically between 2 and 5 but can sometimes attain values of 25 or higher [6, 7, 8].

Although some investigations have been carried out on the how this C^2 parameter changes with different structures [7, 9, 10], currently no one has extensively described how the value of C^2 changes with various modal parameters, such as natural frequency and damping values, or how to predict the exact value of C^2 for a specific structure without resorting to a finite element analysis.

As such, the objective of this thesis is to provide a qualitative and quantitative understanding of the behaviour of the C^2 parameter of the semi-empirical method for any arbitrary structure.

1.1 Root of the Over-Testing Problem in Aerospace

To understand the main cause of the vibration over-testing problem, consider the acceleration time history at the spacecraft-launcher interface during launch as shown in figure 1-1.

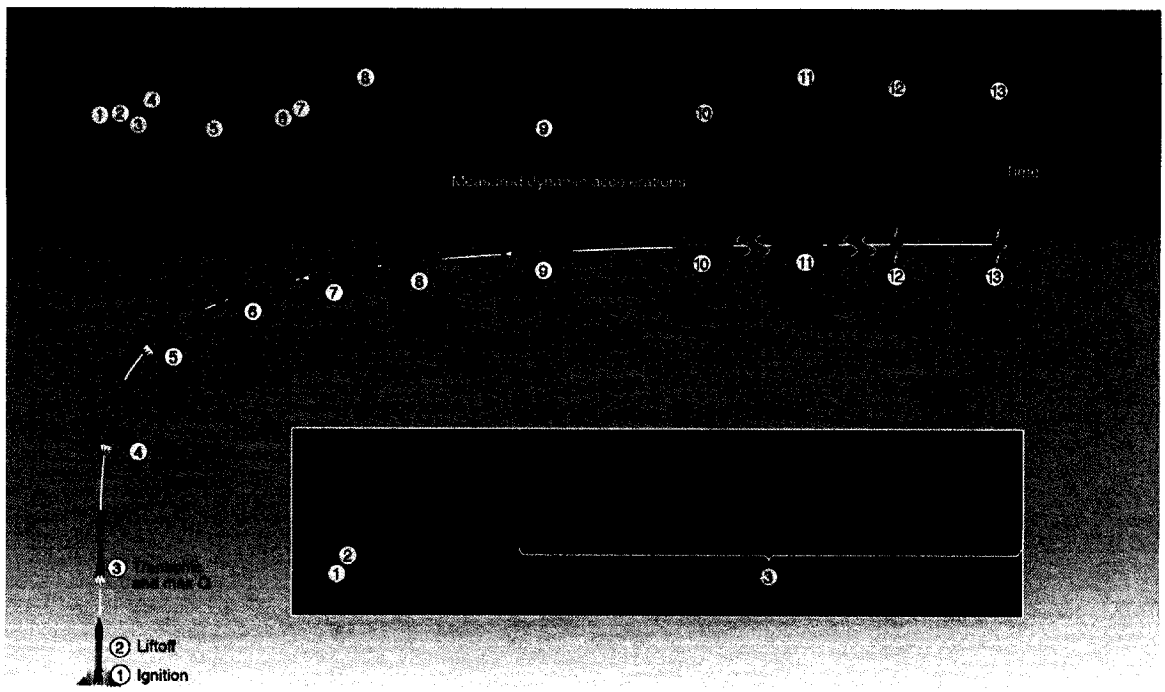

Figure 1.1: Typical Acceleration Time History for a Delta II Launch Vehicle
Reference [11] Figure used with permission.

The highest vibration levels transmitted to the spacecraft interface occur during ignition, liftoff, and at the start of the ascent. These three periods combined typically span less than the first minute of flight. In addition to the vibration transmitted through the interface, direct excitation through acoustic excitation can also be an important source of vibration input to the spacecraft. However, for many structures the acoustic contribution is negligible compared to the direct excitation transmitted through the interface. As such, only the interface forces due purely to direct excitation is investigated in this thesis.

The first step in determining an appropriate test level is to remove any steady-state contribution to the acceleration time history data and decompose the first three periods, shown in figure 1.1, into their acceleration spectral densities (ASD). The resulting acceleration spectral densities describe the value of the variance of the acceleration for a given bandwidth of a random process having a mean acceleration of zero. In aerospace, the unit of the acceleration spectral density is expressed in g^2/Hz, where a "g" is equal to the gravitational acceleration of 9.81 m/s^2. In literature, the acceleration spectral density is also referred to as the auto-spectral density, the mean square spectral density, and the power spectral density [12]. An example of the acceleration spectral densities of the first three periods of launch is shown in figure 1.2.

As demonstrated in figure 1.2, the highest levels of random vibration typically occur between 20 and 2000 Hertz. The figure also demonstrates how the simplified acceleration spectral density utilized for testing envelops the peaks of the flight acceleration spectral densities. In practice, the final test acceleration spectral density also accounts for some probabilistic variation in the flight levels and the random vibration levels required for performing a workmanship tests. The figure also shows how the simplifying enveloping process has severely over-estimated the valleys of figure 1.2, especially considering the log scale of the acceleration spectral density level.

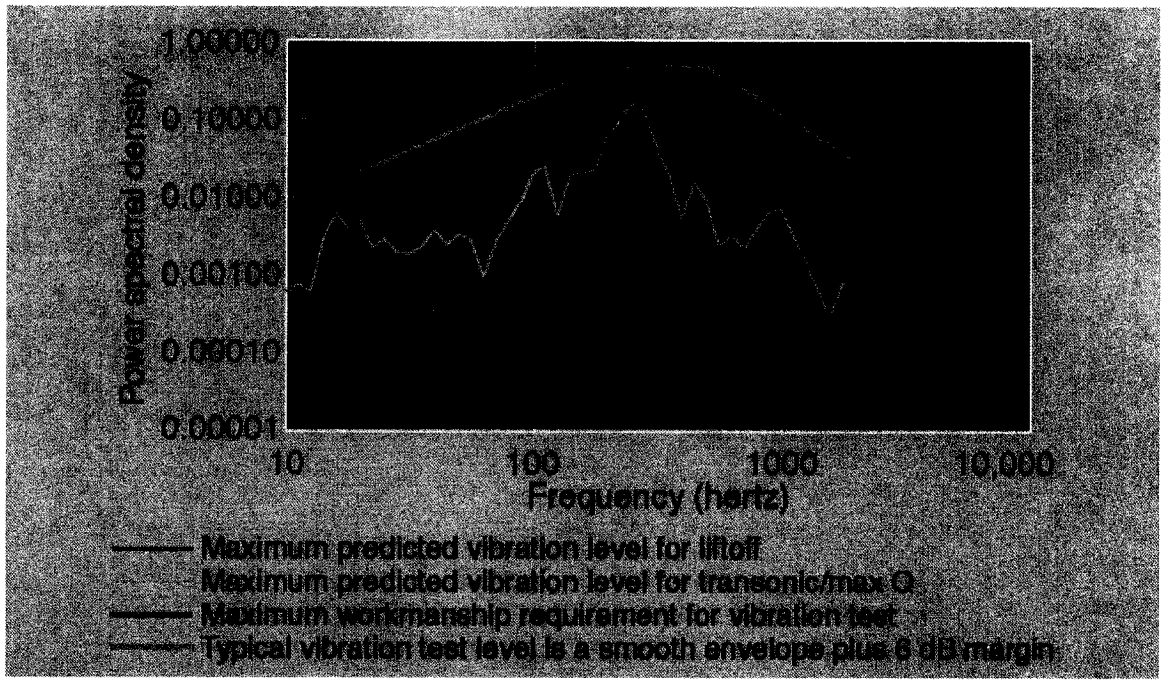

Figure 1.2: Typical Acceleration Spectral Density for a Delta II Launch Vehicle

Reference [11] Figure used with permission.

The frequency locations of the valleys shown in figure 1.2 are not arbitrary. A valley will always correspond to a natural frequency of the structure under test. This phenomenon is referred to as the vibration absorber effect and results from the differences in boundary conditions between the flight and the test configuration. For example, consider a satellite mounted on a launch vehicle. In the flight configuration, the satellite is mounted on the launch vehicle that has a natural frequency that is typically much lower than the satellite's first natural frequency. During testing however, the satellite is mounted on the shaker table that, by design, has a natural frequency that is significantly higher than the satellite's first natural frequency. This difference in boundary conditions is typically referred to as a structural impedance mismatch [5]. A more detailed example of the vibration absorber effect is given in appendix A.

Consequently, the vibration absorber effect ensures that the frequency of maximum response experienced during testing always corresponds to a valley in the acceleration levels experienced during flight. Since the input vibration levels utilized during testing

are severely over-estimated at the frequencies of maximum response, severe over-testing occurs at these frequencies unless the input is notched.

1.2 The Semi-Empirical Method

The semi-empirical method of performing force-limiting vibration testing is one way to significantly reduce the over-testing problem previously discussed. Since the purpose of this thesis is to investigate the nature of the constant associated with the semi-empirical method, the method is described in detail in this section.

The origin of the semi-empirical method can be attributed to Salter [10], who in 1964 proposed that the maximum interface force could be described as a factor times the mass of the article under testing multiplied by the peak acceleration that would be experienced during service. This peak acceleration experienced in service is related to the test acceleration spectrum since the test acceleration spectrum envelops the peak acceleration experience in service. His proposed method can be described by equation 1.1, with the constant "C" representing the factor referred to by Salter. The equivalent form for random vibration testing using spectral densities is shown in equation 1.2 [5].

For sinusoidal vibration

$$F_{\max}(f) = \mathrm{C} \cdot \mathrm{M}_0 \cdot \mathrm{A}_{\text{test}}(f) \tag{1.1}$$

Random Vibration

$$S_{ff\_\max}(f) = \mathrm{C}^2 \cdot \mathrm{M}_0^2 \cdot S_{aa\_\text{test}}(f) \tag{1.2}$$

where

$F_{\max}(f)$	Interface force limit
C	Dimensionless parameter
M_0	Mass of article under test
$A_{test}(f)$	Test acceleration
$S_{ff\_max}(f)$	Interface force spectral density limit

$S_{aa\_test}(f)$ Test input acceleration spectral density

f Test input frequency

Slater [10] claimed that the maximum value of the C parameter rarely exceeds 1.5 for structures of practical interest. As such, he suggested that a value of C = 1.5 could be utilized to predict the absolute maximum interface force.

Further research into force limit derivation by Witte and Rodeman in 1970 [13] and Hunter and Otts in 1972 [14] led to a modification of Salter's original equation based on Newton's second law. In this modified form, a simplified equation defining the maximum interface force is presented where the value of C is a constant corresponding to the value of C of equation 1.1. However, a frequency dependent term is added for frequencies above a corner frequency identified as f_0 based on considerations from Newton's second law. The equations of the modified form are shown in equation 1.3 to 1.6 [5].

For sinusoidal vibration

$$F_{\max}(f) = \mathrm{C} \cdot \mathrm{M}_0 \cdot \mathrm{A}_{s\_test}(f) \qquad f < f_0 \qquad (1.3)$$

$$F_{\max}(f) = \mathrm{C} \cdot \mathrm{M}_0 \cdot A_{s\_test}(f) \cdot \left(\frac{f_0}{f}\right)^n \qquad f \geq f_0 \qquad (1.4)$$

For random vibration

$$S_{ff\_\max}(f) = \mathrm{C}^2 \cdot \mathrm{M}_0^2 \cdot S_{aa\_test}(f) \qquad f < f_0 \qquad (1.5)$$

$$S_{ff\_\max}(f) = \mathrm{C}^2 \cdot \mathrm{M}_0^2 \cdot S_{aa\_test}(f) \cdot \left(\frac{f_0}{f}\right)^{2n} \qquad f \geq f_0 \qquad (1.6)$$

In the equations above, the corner frequency f_0 is the frequency at which the apparent mass of the test article has its first pronounced resonance. The exponent "n" of the ratio

$\left(\frac{f_0}{f}\right)$ is presented as $n = 1$ in reference [5], but in general can be any positive number. In practice, the value of n can be determined from the fall-off of the asymptotic mass of the test item for frequencies above the corner frequency f_0 [5]. By definition, the asymptotic mass is the apparent mass the test item would have if all modes had critical damping, meaning that the damping ratio ζ is equal to unity. Based on work by Skudrzyk, Scharton [5] suggests that an alternate way of estimating the asymptotic mass is "to take a geometric average of the apparent mass FRF over frequency, so that there is equal area above and below the curve on a log-log plot", where the letters FRF are short for frequency response function. The value of n is chosen such that the roll-off of the asymptotic mass function for frequencies above the corner frequency f_0, is mimicked by the ratio $M_0 \cdot \left(\frac{f_0}{f}\right)^n$.

In the semi-empirical method, the constant C is based on extrapolating interface force data from similar flight configurations. Once a value for C has been established, equation set 1.1, 1.2 or equation set 1.3 to 1.6 can be utilized to quickly estimate the maximum interface force without resorting to time consuming finite element analysis.

1.3 Literature Survey

The accuracy of the semi-empirical method rests on adequate determination of the value of C or equivalently C^2. Since the method is based on empirical data, much research has been performed in studying or validating values of C^2 for various flight structures. In addition, investigations regarding what parameters affect the value of C^2 have been performed in order to quantify what constitutes a similar structure. Both types of research are necessary to properly understand and evaluate what value of C^2 would be appropriate for testing of any new structure. The following literature survey describes previous investigations performed in regards to understanding the value of C^2 of the semi-empirical method.

As previously discussed, Salter [10] claimed in 1964 that the value of C seldom exceeded 1.5, corresponding to a C^2 of 2.25, for structures of practical interest. This estimate was based on an analogue analysis of a two degree-of-freedom system.

In 1997, Scharton [5] created a monograph for NASA describing the force limiting vibration testing technique. As part of his monograph, he describes validation tests for the semi-empirical method for three sub-systems on-board the Cassini spacecraft. The validation tests consisted of measuring interface forces for the three sub-systems during spacecraft level acoustic testing and deriving an appropriate value for C^2. A value of C^2 close to unity was found to be appropriate for all three sub-systems during force limiting vibration testing.

In 1997, the Advanced Composition Explorer spacecraft was launched using a Delta II rocket. The spacecraft was instrumented to measure the forces and acceleration during launch at the base of the Cosmic Ray Isotope Spectrometer instrument aboard the spacecraft. Scharton [15] analyzed the data and found that a C^2 value of 2 properly described the maximum interface forces during flight.

In 1998, Haile [9] examined the validity of the equations of the semi-empirical method by examining the various interface forces of a force excited eight degrees-of-freedom system. In his paper, Haile found that a C^2 of unity gave an excellent fit to the calculated interface force for all interfaces. In addition, the force results for all 7 interfaces were less than the value predicted when using a C^2 of 1.39.

In 2000, Scharton [16] described the acceleration and interface forces measured during flight for two experiments mounted to the sidewall of the space shuttle. He found that a C^2 value of 4 and 2 correctly described the maximum interface force during flight.

In 2000, Chang [6] studied whether the semi-empirical method produced response acceleration to levels that are below design loads as predicted by the Mass Acceleration Curve (MAC) data. Chang suggests that typical values of C^2 are 2 for "strut mounted

heavier equipment" and 5 for "directly mounted lightweight loads". The semi-empirical method, combined with C^2 values between 2 and 5, produced acceleration levels that are comparable with the acceleration levels predicted by the MAC data. The study also concluded that the response, and thus the C^2 parameter, is independent of damping.

Also in 2000, Kaufman and Worth [17] examined interface forces from flight data and found that an appropriate value of C^2 would have been unity.

In 2003, Rice and Buehrle [18] validated several methods of predicting the force limit during force limited vibration testing including the semi-empirical method. They did so by comparing flight data to test data of a plate like structure that flew on board a Black Brant sounding rocket. In their investigation, they found a C^2 of 2.6 described the maximum interface force.

In 2003, Dharanipathi [7] investigated how the value of C^2 changes with several different structures as part of his master's thesis. His approach entailed the analysis and testing of flight representative structures in the context of the semi-empirical method. The structures investigated had closely spaced modes, variable attachment points, variable mass, and variable flexibility characteristics. In all, 142 cases were analytically investigated of which 16 were physically tested. The finite element analytical study of the sensitivity of the different parameters showed that the damping was not an important factor in determining C^2. In the analysis, only damping ratios that produced Q values of 20 and 50 were investigated. The value of C^2 was also determined to depend on the number and position of attachment points, the effective mass ratio of the structures, the direction of excitation, and the natural frequency of the structure. Also, from the 142 test cases, 25 cases resulted in a C^2 value over 5 and the maximum value of C^2 among these 25 cases was 25. The 16 experimental results showed reasonably good correlation between the analytical results and the test results in the vertical direction. Thirteen of the 16 test cases performed had C^2 values between 0.76 and 4.37. The remaining 3 test cases had C^2 values of 5.74, 7.2, and 11.

In 2004, Nagahama et al. [8] of the Japan Aerospace Exploration Agency examined the value of C^2 by performing random vibration tests on a dummy satellite structure and a dummy instrument. Their dummy instrument, a plate mounted on four tall legs, was mounted on top of the dummy satellite and had a natural frequency close to the natural frequency of the satellite. They found that a C^2 value of 121 (C = 11) was needed to correctly predict the maximum interface force.

In 2005, Ritzmann and Jahn [19] performed an investigation on the force limited vibration method using a test article that represented an electronics box mounted on a honeycomb panel. Their test results showed that the maximal interface force was consistent with a C^2 value of 1.4.

In 2005 Marchand et al. [20] showed through analysis of a two degrees-of-freedom system that when the load's natural frequency is different from the source's natural frequency, there is a significant reduction in interface force. A natural frequency difference as low as 10% can result in over an order of magnitude reduction in the value of C^2. Since by design, an item's natural frequency is deliberately separated from its mounting structure, it is suggested to be this design requirement that produces low C^2 for aerospace structures.

The literature survey illustrates that a value of C^2 between 2 and 5 would typically be appropriate to utilize during testing. However, typical values of C^2 should not be blindly utilized for testing because some structures required values of C^2 that were an order of magnitude greater to properly estimate the interface forces. The semi-empirical method is based on data from similar hardware and mounting structure. However, the hardware and mounting structures described in the literature survey are not characterized in a way to quantitatively determine if a given new structure is similar to an existing one. This situation may reflect an incomplete understanding on what constitutes a similar structure. This fact has impeded the quick acceptance of the semi-empirical method by other space agencies because their lack of direct experience with these previous structures has lead to a fear of under-testing.

1.4 Thesis Statement

To accelerate the worldwide acceptance of the semi-empirical method of performing force limited vibration testing, the objective of this thesis is to provide a qualitative and quantitative understanding of the behaviour of the C^2 parameter of the semi-empirical method for any arbitrary structure.

The approach utilized in this thesis differs from the work performed by Dharanipathi [7]. Instead of characterizing the value of C^2 for various representative aerospace structures, this thesis focuses on the theoretical description of C^2 for the simple two degrees-of-freedom system and then extends the theory to multiple degrees-of-freedom systems and discusses the effect of multiple attachment points. In this manner, all parameters affecting the value of C^2 can be definitively identified and the conclusions obtained can be applied with confidence to any structure. In addition, this thesis presents qualitative and quantitative methods for predicting the value of C^2 for any new structure, where the equations presented are validated through experimental testing.

Force limited vibration testing has become an important way of preventing costly over-testing in the aerospace industry throughout the world. As such, this work is worthwhile in providing a better understanding of how to properly specify the force parameter, C^2, during semi-empirical force-limited vibration testing. The work also provides practical information in the form of equations and charts that can be referred to when performing force limited vibration testing.

1.5 Thesis Organization

To achieve the stated objective, chapter 2 of this thesis will first examine how the value of C^2 varies for an arbitrary viscously damped two degrees-of-freedom system. The analysis is then extended to investigate specific load-source configurations. The effect of different types of damping is investigated by comparing the value of C^2 for a two degrees-of-freedom system with structural damping to the previous viscously damped

case. This information will provide a starting point in understanding more complex structures.

Chapter 3 investigates the value of C^2 for multiple degrees-of-freedom and continuous systems. The effect of boundary conditions, including multiple attachment points, is investigated and their effect on the value of C^2 is described. The apparent mass of the item is found to be a key parameter for determining the value of C^2 and thus a new method called the apparent mass method is described. Several practical issues regarding the determination of the apparent mass are also described including their ultimate effect on the value of C^2.

Chapter 4 presents experimental testing performed to validate the equations presented in chapter 3. Actual force measurements in terms of the value C^2 are compared to the predictions of the apparent mass method.

Finally, chapter 5 summarizes the key conclusions of the work and discusses future work that could be performed to improve the semi-empirical method.

2 C^2 FOR BASE-EXCITED TWO-DOF SYSTEMS

The base-excited two degrees-of-freedom system is the simplest system exhibiting the vibration absorber effect. Consequently, a comprehensive study of how the C^2 parameter behaves for this system is a logical starting point. This will be followed by a study of how the C^2 parameter will behave for more complex systems.

2.1 Two Degrees-of-Freedom System Definition

Consider the base-excited two degrees-of-freedom system with viscous damping shown in figure 2.1.

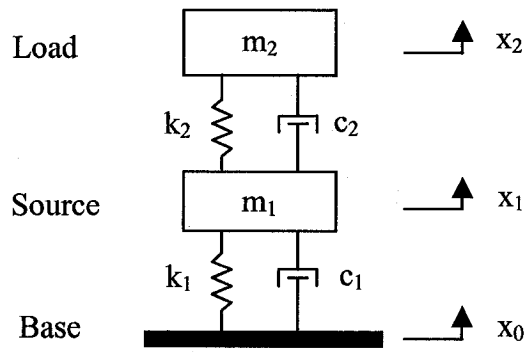

Figure 2.1: Base-Excited 2-DOF System

In force-limited vibration testing terminology, the mass closest to the input excitation is called the source and the mass mounted on the source is called the load. For example, the load could represent a scientific instrument and the source the spacecraft bus, in which case the base would be the launch vehicle structure where the spacecraft mounts. In figure 2.1, system parameters and position variables belonging to the source all have a subscript of 1 and system parameters and position variables belonging to the load all have a subscript of 2. The base position variable has a subscript of 0. The six basic system parameters are: mass, spring constant, and viscous damping constant for each the load and the source as shown in table 2.1.

Table 2.1: Basic System Parameters

Variable	Basic System Parameter
m_1	Source mass
k_1	Source spring constant
c_1	Source viscous damping constant
m_2	Load mass
k_2	Load spring constant
c_2	Load viscous damping constant

The six basic system parameters defining the two degrees-of-freedom system can be reduced to four dimensionless system parameters by considering the following definitions.

Un-damped fixed-base natural frequency of the source

$$\omega_1 \equiv \sqrt{\frac{k_1}{m_1}} \tag{2.1}$$

Un-damped fixed-base natural frequency of the load

$$\omega_2 \equiv \sqrt{\frac{k_2}{m_2}} \tag{2.2}$$

Mass ratio

$$\mu \equiv \frac{m_2}{m_1} \tag{2.3}$$

Un-damped fixed-base natural frequency ratio

$$F \equiv \frac{\omega_2}{\omega_1} \tag{2.4}$$

Critical damping ratio of the source

$$\zeta_1 \equiv \frac{c_1}{2 \cdot m_1 \cdot \omega_1} \tag{2.5}$$

Critical damping ratio of the load

$$\zeta_2 \equiv \frac{c_2}{2 \cdot m_2 \cdot \omega_2} \tag{2.6}$$

For viscous damping, the Q of the source is [21]

$$Q_1 = \frac{1}{2\zeta_1} \tag{2.7}$$

Similarly, the Q of the load is

$$Q_2 = \frac{1}{2\zeta_2} \tag{2.8}$$

The resulting dimensionless system parameters are shown in table 2.2

Table 2.2: Dimensionless System Parameters

Variable	Reduced System Parameter
F	Load to source frequency ratio
μ	Load to source mass ratio
Q_1	Q of source
Q_2	Q of load

Throughout the remainder of this work, the dimensionless system parameters F, μ, Q_1, and Q_2 of table 2.2 will be utilized in favour of the basic parameters when describing a two degrees-of-freedom system.

The positions of the base, as well as the position of the center-of-mass of the source and the load, are described by the variables x_0, x_1, and x_2 respectively as shown in table 2.3.

Table 2.3: Position Variables

Variable	Position
x_0	Base
x_1	Center-of-Mass of Source
x_2	Center-of-Mass of Load

Consider the response of the source and the load to steady harmonic acceleration at the base described as

$$\ddot{x}_0 = A_0 \cos(\omega t) \tag{2.9}$$

Where

ω	Excitation angular frequency
A_0	Zero-to-peak Acceleration
t	Time

For convenience, equation 2.9 can be written in exponential form as

$$\ddot{x}_0 = \mathrm{Re}\left[A_0 e^{i\omega}\right] \tag{2.10}$$

Similarly, the resulting acceleration response of the source and the load can be expressed in exponential form as

$$\ddot{x}_1 = \mathrm{Re}\left[A_1 e^{i\omega}\right] \tag{2.11}$$

$$\ddot{x}_2 = \mathrm{Re}\left[A_2 e^{i\omega}\right] \tag{2.12}$$

where the quantities A_1 and A_2 in equations 2.11 and 2.12 are understood to be complex quantities in general.

For a truly dimensionless analysis, the following additional dimensionless quantities relating to the base motion are identified.

Base motion frequency to load natural frequency ratio

$$R \equiv \frac{\omega}{\omega_2} \tag{2.13}$$

The complex acceleration frequency response function of the source to the base

$$H_{10} = \frac{A_1}{A_0} \tag{2.14}$$

The complex acceleration frequency response function of the load to the base

$$H_{20} = \frac{A_2}{A_0} \tag{2.15}$$

In the following sections, the above dimensionless system parameters will be utilized in determining the value of C^2 for the base-excited two degrees-of-freedom system.

2.2 Parameters Definition for Force Limited-Vibration Testing

During vibration testing, the load is attached directly to the vibration table as shown in figure 2.2.

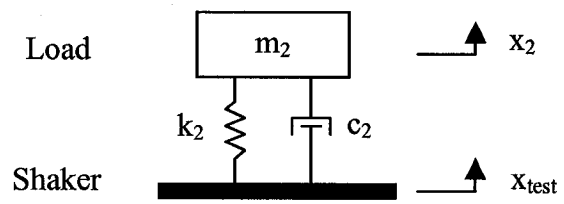

Figure 2.2: Load 1-DOF System During Testing

In order to perform a force-limited vibration test, the following two pieces of information are required:

- A description of the test input
  (A_{test} for sine test or S_{aa_test} for random test)
- The maximum source-load interface force of the coupled system
  (F_{max} for sine test or S_{ff_max} for random test)

The test input A_{test} or S_{aa_test} is a function derived by the enveloping process of the source response A_1 or S_{aa_1} of the coupled system. For the coupled system described in figure 2.1, the response of the source can be written in terms of the complex frequency response function H_{10}. For sine vibration testing, the response of the source can be described as

$$A_1 = H_{10} A_0 \tag{2.16}$$

and for random vibration testing [21], as

$$S_{aa\_1} = |H_{10}|^2 S_{aa\_0} \tag{2.17}$$

The idea behind force limiting testing is to let the force limit drive the notching. Consequently, a flat, un-notched input is chosen as the test input. To avoid both under-testing and over-testing, the test input A_{test} or S_{aa_test} is defined as being equal to the maximum response of the source A_1 or a S_{aa_1} over all frequencies. Therefore, for sine vibration testing

$$A_{test} = |H_{10}|_{max} A_0 \tag{2.18}$$

and for random vibration testing.

$$S_{aa\_test} = |H_{10}|^2_{max} S_{aa\_0} \tag{2.19}$$

From Newton's second law, the maximum interface force between the source and the load of the coupled system in figure 2.1 is simply the mass of the load times its absolute acceleration. Thus, for sine vibration testing,

$$F_{max} = m_2 \cdot |H_{20}|_{max} A_0 \tag{2.20}$$

and for random vibration testing

$$S_{ff\_test} = m_2^2 \cdot |H_{20}|^2_{max} \cdot S_{aa\_0} \tag{2.21}$$

Both required pieces of information, A_{test} or S_{aa_test} and F_{max} or S_{ff_test}, are derived from the complex frequency response functions H_{10} and H_{20} of the coupled system shown in figure 2.1. Therefore, the next logical step is to derive an expression for the source and load complex frequency responses H_{10} and H_{20}.

2.3 Complex Frequency Response Functions

To find the complex frequency response functions H_{10} and H_{20}, the equations of motion for the coupled system are required. The derivation of the equations of motion describing the absolute acceleration responses of the source and the load are detailed in appendix B. The result of the base-excited two degrees-of-freedom system equations of motion can be expressed in terms of the previously identified non-dimensional variables as

$$\left[\frac{1}{F^2}+\mu-R^2+i\cdot\left(\frac{R}{FQ_1}+\frac{\mu R}{Q_2}\right)\right]A_1-\left[\mu+i\cdot\left(\frac{\mu R}{Q_2}\right)\right]A_2=\left[\frac{1}{F^2}+i\cdot\left(\frac{R}{FQ_1}\right)\right]A_0 \tag{2.22}$$

$$\left[1-R^2+i\cdot\left(\frac{R}{Q_2}\right)\right]A_2=\left[1+i\cdot\left(\frac{R}{Q_2}\right)\right]A_1 \tag{2.23}$$

Solving for the modulus of complex frequency response functions H_{10} and H_{20} results in the following long mathematical formulas.

$$|H_{10}|=\sqrt{\frac{\left(\frac{1}{F^2}-\frac{R^2}{F^2}-\frac{R^2}{FQ_1Q_2}\right)^2+\left(\frac{R}{F^2Q_2}+\frac{R}{FQ_1}-\frac{R^3}{FQ_1}\right)^2}{\left(\frac{1}{F^2}-\frac{R^2}{F^2}-\mu R^2-R^2-\frac{R^2}{FQ_1Q_2}+R^4\right)^2+\left(\frac{R}{F^2Q_2}+\frac{R}{FQ_1}-\frac{R^3}{Q_2}-\frac{R^3}{FQ_1}-\frac{\mu R^3}{Q_2}\right)^2}} \tag{2.24}$$

$$|H_{20}|=\sqrt{\frac{\left(\frac{1}{F^2}-\frac{R^2}{FQ_1Q_2}\right)^2+\left(\frac{R}{F^2Q_2}+\frac{R}{FQ_1}\right)^2}{\left(\frac{1}{F^2}-\frac{R^2}{F^2}-\mu R^2-R^2-\frac{R^2}{FQ_1Q_2}+R^4\right)^2+\left(\frac{R}{F^2Q_2}+\frac{R}{FQ_1}-\frac{R^3}{Q_2}-\frac{R^3}{FQ_1}-\frac{\mu R^3}{Q_2}\right)^2}} \tag{2.25}$$

These long results can be expressed concisely by defining the following complex variables corresponding to the coefficients of A_1, A_2, and A_0 of equations 2.22 and 2.23.

$$C_1=\left[\frac{1}{F^2}+\mu-R^2+i\cdot\left(\frac{R}{FQ_1}+\frac{\mu R}{Q_2}\right)\right] \tag{2.26}$$

$$C_2=\left[\mu+i\cdot\left(\frac{\mu R}{Q_2}\right)\right] \tag{2.27}$$

$$C_3 = \left[\frac{1}{F^2} + i \cdot \left(\frac{R}{FQ_1}\right)\right] \tag{2.28}$$

$$C_4 = \left[1 - R^2 + i \cdot \left(\frac{R}{Q_2}\right)\right] \tag{2.29}$$

$$C_5 = \left[1 + i \cdot \left(\frac{R}{Q_2}\right)\right] \tag{2.30}$$

Using the above complex variables, the equations of motion 2.22 and 2.23 can be expressed simply as

$$C_1 A_1 - C_2 A_2 = C_3 A_0 \tag{2.31}$$

$$C_4 A_2 = C_5 A_1 \tag{2.32}$$

Solving for the complex frequency response functions H_{10} and H_{20} as defined by equation 2.14 and 2.15

$$|H_{10}| = \left|\frac{C_3 C_4}{C_1 C_4 - C_2 C_5}\right| \tag{2.33}$$

$$|H_{20}| = \left|\frac{C_3 C_5}{C_1 C_4 - C_2 C_5}\right| \tag{2.34}$$

Note that response equations 2.33 and 2.34 are relatively easy to solve numerically with a computer program that can deal with complex variables.

The complex frequency response functions H_{10} and H_{20} are dependent on the excitation frequency expressed through the value R. Of interest will be the maximum values of H_{10} and H_{20} for use with equations 2.18 to 2.21. The maximum values occur, by definition, at one of the resonant frequencies of the coupled system. The next logical step is to find the

value of R that corresponds to the natural frequencies of the base-excited two degrees-of-freedom system.

2.4 Un-Damped Natural Frequencies

The two degrees-of-freedom system of figure 2.1 will have two natural frequencies. The first and second natural frequencies of the coupled system are identified respectively as f_{11} and f_{22}, in cycles per seconds, or ω_{11} and ω_{22} in radians per second, with the double subscript emphasizing that these values pertain to the coupled system. In terms of the dimensionless variable R of equation 2.13, the natural frequencies of the coupled system of figure 2.1 are

$$R_{11} = \frac{\omega_{11}}{\omega_2} \tag{2.35}$$

$$R_{22} = \frac{\omega_{22}}{\omega_2} \tag{2.36}$$

The maximum responses of H_{10} and H_{20} occur at the damped natural frequencies of the system. However, if the damping is very light such as when $Q > 10$, then the maximum response will essentially occur at the un-damped natural frequencies of the base excited two degrees-of-freedom system. The un-damped natural frequencies of the coupled system are derived in terms of the dimensionless system parameters in appendix C. The natural frequencies in terms of the dimensionless parameter R are

First Un-Damped Natural Frequency

$$R_{11} = \sqrt{\frac{1+F^2(1+\mu)-\sqrt{\left[1+F^2(1+\mu)\right]^2-4F^2}}{2F^2}} \tag{2.37}$$

Second Un-Damped Natural Frequency

$$R_{22} = \sqrt{\frac{1+F^2(1+\mu)+\sqrt{\left[1+F^2(1+\mu)\right]^2-4F^2}}{2F^2}} \tag{2.38}$$

2.5 C^2 of the Two Degrees-of-Freedom System

From equations 1.1 and 1.2, the maximum interface force is described by the semi-empirical method as

For sinusoidal vibration

$$F_{max}(f) = C \cdot M_0 \cdot A_{test}(f) \tag{2.39}$$

For random vibration

$$S_{ff\_max}(f) = C^2 \cdot M_0^2 \cdot S_{aa\_test}(f) \tag{2.40}$$

where

$F_{max}(f)$	Interface force limit
C	Dimensionless parameter
M_0	Mass of article under test
$A_{test}(f)$	Zero-to-peak test acceleration
$S_{ff\_max}(f)$	Interface force limit spectral density
$S_{aa\_test}(f)$	Test input acceleration spectral density
f	Test input frequency

The mass M_0 is the mass of the object under test. Since the object under test is the load, as shown in figure 2.2, the following relationship holds for the two degrees-of-freedom system.

$$M_0 = m_2 \tag{2.41}$$

Equation 2.39 can be combined with equation 2.18, 2.20, and 2.41 to solve for C.

$$C = \frac{|H_{20}|_{max}}{|H_{10}|_{max}} \tag{2.42}$$

Similarly, equation 2.40 can be combined with equation 2.19, 2.21, and 2.41 to solve for C^2

$$C^2 = \frac{|H_{20}|^2_{max}}{|H_{10}|^2_{max}} \tag{2.43}$$

From equations 2.42, and 2.43, one can conclude that for the base-excited two degrees-of-freedom system, the value of C^2 is independent of whether the excitation is sinusoidal or random in nature. In addition, considering equations 2.24 and 2.25, one can further state that the value of C^2 is, in general, dependent on the system parameters F, μ, Q_1 and Q_2.

2.6 Behaviour of C^2 Based on Numerical Analysis

The behaviour of C^2 for the base-excited two degrees-of-freedom system is described by equations 2.26 to 2.30, 2.33, 2.34, 2.37, 2.38 and 2.43.

Because of the discontinuous nature of equation 2.43, determining how C^2 varies with system parameters F, μ, Q_1, and Q_2 using direct algebraic substitution is not conducive to an understanding of the behaviour of C^2 for different system parameters. Consequently, a numerical investigation of C^2 was conducted based on equations 2.26 to 2.30, 2.33, 2.34, 2.37, 2.38 and 2.43. The results are shown in figures 2.3 to 2.18.

In figures 2.3 to 2.10, the effect of changing frequency ratio F was investigated for various combinations of μ, Q_1, and Q_2. In figures 2.11 to 2.18, the effect of changing mass ratio μ was investigated for various combinations of F, Q_1, and Q_2. Although the curves from the two sets of figures look different, the curves from the first set (figures 2.3 to 2.10) are essentially the same curves depicted in the second set (figures 2.11 to 2.18).

The figures were constructed by solving the equations 2.26 to 2.30, 2.33, 2.34, 2.37, 2.38 and 2.43 with a software program capable of computing with complex numbers. MATLAB version 2.0.1.24704 (R14) was chosen for this task [22]. The MATLAB

routines utilized in the construction of the figures are shown in appendix D as program 1, for figures 2.3 to 2.10, and program 2 for figures 2.11 to 2.18.

Table 2.4 shows the system parameter values for F, μ, Q_1, and Q_2 utilized for the 112 cases investigated. Although arbitrary values were chosen for the system parameters F, μ, Q_1, and Q_2, the values are believed to encompass the majority of values that would be encountered in practice.

Table 2.4: Case Parameters

Case ID	F (see note below)	μ (see note below)	Q_1	Q_2	Figure
1	0.001 to 2.5	0.00001	10	100	2.3
2	0.001 to 2.5	0.0001	10	100	2.3
3	0.001 to 2.5	0.001	10	100	2.3
4	0.001 to 2.5	0.01	10	100	2.3
5	0.001 to 2.5	0.1	10	100	2.3
6	0.001 to 2.5	1	10	100	2.3
7	0.001 to 2.5	10	10	100	2.3
8	0.001 to 2.5	0.00001	10	50	2.4
9	0.001 to 2.5	0.0001	10	50	2.4
10	0.001 to 2.5	0.001	10	50	2.4
11	0.001 to 2.5	0.01	10	50	2.4
12	0.001 to 2.5	0.1	10	50	2.4
13	0.001 to 2.5	1	10	50	2.4
14	0.001 to 2.5	10	10	50	2.4
15	0.001 to 2.5	0.00001	10	20	2.5
16	0.001 to 2.5	0.0001	10	20	2.5
17	0.001 to 2.5	0.001	10	20	2.5
18	0.001 to 2.5	0.01	10	20	2.5
19	0.001 to 2.5	0.1	10	20	2.5
20	0.001 to 2.5	1	10	20	2.5
21	0.001 to 2.5	10	10	20	2.5
22	0.001 to 2.5	0.00001	10	10	2.6
23	0.001 to 2.5	0.0001	10	10	2.6
24	0.001 to 2.5	0.001	10	10	2.6
25	0.001 to 2.5	0.01	10	10	2.6
26	0.001 to 2.5	0.1	10	10	2.6
27	0.001 to 2.5	1	10	10	2.6
28	0.001 to 2.5	10	10	10	2.6
29	0.001 to 2.5	0.00001	100	100	2.7
30	0.001 to 2.5	0.0001	100	100	2.7
31	0.001 to 2.5	0.001	100	100	2.7
32	0.001 to 2.5	0.01	100	100	2.7
33	0.001 to 2.5	0.1	100	100	2.7
34	0.001 to 2.5	1	100	100	2.7
35	0.001 to 2.5	10	100	100	2.7
36	0.001 to 2.5	0.00001	20	10	2.8
37	0.001 to 2.5	0.0001	20	10	2.8
38	0.001 to 2.5	0.001	20	10	2.8
39	0.001 to 2.5	0.01	20	10	2.8
40	0.001 to 2.5	0.1	20	10	2.8
41	0.001 to 2.5	1	20	10	2.8
42	0.001 to 2.5	10	20	10	2.8

Table 2.4: Case Parameters (continued)

Case ID	F (see note below)	μ (see note below)	Q_1	Q_2	Figure
43	0.001 to 2.5	0.00001	50	10	2.9
44	0.001 to 2.5	0.0001	50	10	2.9
45	0.001 to 2.5	0.001	50	10	2.9
46	0.001 to 2.5	0.01	50	10	2.9
47	0.001 to 2.5	0.1	50	10	2.9
48	0.001 to 2.5	1	50	10	2.9
49	0.001 to 2.5	10	50	10	2.9
50	0.001 to 2.5	0.00001	100	10	2.10
51	0.001 to 2.5	0.0001	100	10	2.10
52	0.001 to 2.5	0.001	100	10	2.10
53	0.001 to 2.5	0.01	100	10	2.10
54	0.001 to 2.5	0.1	100	10	2.10
55	0.001 to 2.5	1	100	10	2.10
56	0.001 to 2.5	10	100	10	2.10
57	0.5	0.00001 to 10	10	100	2.11
58	0.75	0.00001 to 10	10	100	2.11
59	0.9	0.00001 to 10	10	100	2.11
60	1	0.00001 to 10	10	100	2.11
61	1.1	0.00001 to 10	10	100	2.11
62	1.5	0.00001 to 10	10	100	2.11
63	2	0.00001 to 10	10	100	2.11
64	0.5	0.00001 to 10	10	50	2.12
65	0.75	0.00001 to 10	10	50	2.12
66	0.9	0.00001 to 10	10	50	2.12
67	1	0.00001 to 10	10	50	2.12
68	1.1	0.00001 to 10	10	50	2.12
69	1.5	0.00001 to 10	10	50	2.12
70	2	0.00001 to 10	10	50	2.12
71	0.5	0.00001 to 10	10	20	2.13
72	0.75	0.00001 to 10	10	20	2.13
73	0.9	0.00001 to 10	10	20	2.13
74	1	0.00001 to 10	10	20	2.13
75	1.1	0.00001 to 10	10	20	2.13
76	1.5	0.00001 to 10	10	20	2.13
77	2	0.00001 to 10	10	20	2.13
78	0.5	0.00001 to 10	10	10	2.14
79	0.75	0.00001 to 10	10	10	2.14
80	0.9	0.00001 to 10	10	10	2.14
81	1	0.00001 to 10	10	10	2.14
82	1.1	0.00001 to 10	10	10	2.14
83	1.5	0.00001 to 10	10	10	2.14
84	2	0.00001 to 10	10	10	2.14

Table 2.4: Case Parameters (continued)

Case ID	F (see note below)	μ (see note below)	Q_1	Q_2	Figure
85	0.5	0.00001 to 10	100	100	2.15
86	0.75	0.00001 to 10	100	100	2.15
87	0.9	0.00001 to 10	100	100	2.15
88	1	0.00001 to 10	100	100	2.15
89	1.1	0.00001 to 10	100	100	2.15
90	1.5	0.00001 to 10	100	100	2.15
91	2	0.00001 to 10	100	100	2.15
92	0.5	0.00001 to 10	20	10	2.16
93	0.75	0.00001 to 10	20	10	2.16
94	0.9	0.00001 to 10	20	10	2.16
95	1	0.00001 to 10	20	10	2.16
96	1.1	0.00001 to 10	20	10	2.16
97	1.5	0.00001 to 10	20	10	2.16
98	2	0.00001 to 10	20	10	2.16
99	0.5	0.00001 to 10	50	10	2.17
100	0.75	0.00001 to 10	50	10	2.17
101	0.9	0.00001 to 10	50	10	2.17
102	1	0.00001 to 10	50	10	2.17
103	1.1	0.00001 to 10	50	10	2.17
104	1.5	0.00001 to 10	50	10	2.17
105	2	0.00001 to 10	50	10	2.17
106	0.5	0.00001 to 10	100	10	2.18
107	0.75	0.00001 to 10	100	10	2.18
108	0.9	0.00001 to 10	100	10	2.18
109	1	0.00001 to 10	100	10	2.18
110	1.1	0.00001 to 10	100	10	2.18
111	1.5	0.00001 to 10	100	10	2.18
112	2	0.00001 to 10	100	10	2.18

Note: Frequency ratio F was varied between 0.001 and 2.5 in steps of 0.001

Mass ratio μ was varied from 10^{-5} to 10 in 1000 logarithmically spaced steps using a MATLAB subroutine.

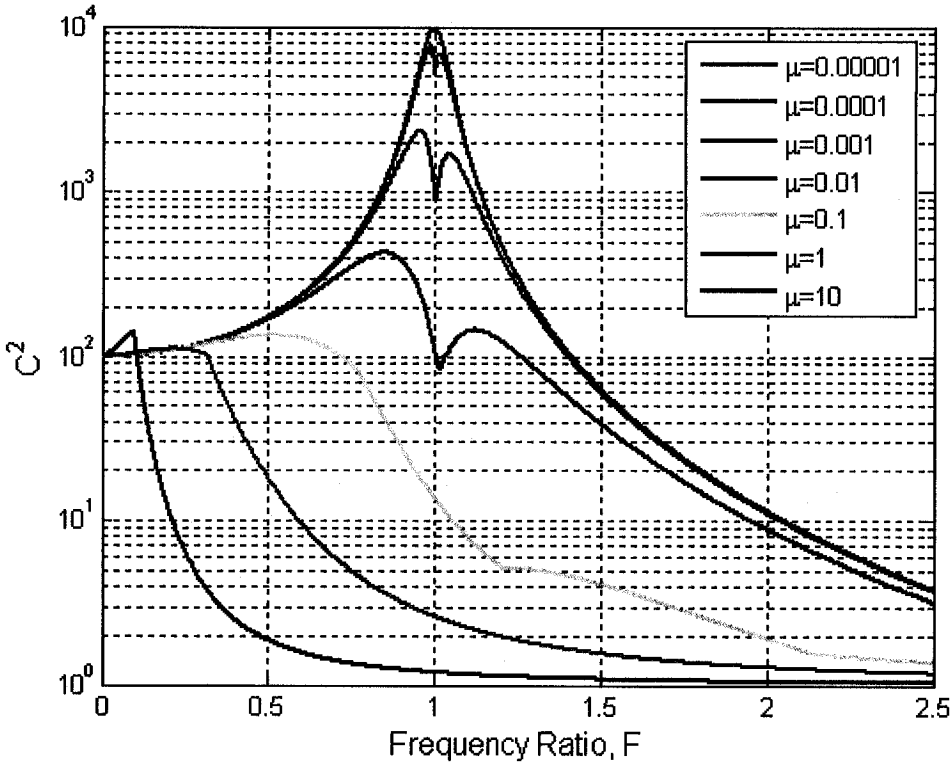

Figure 2.3: C^2 vs. Frequency Ratio for $Q_1 = 10$ and $Q_2 = 100$

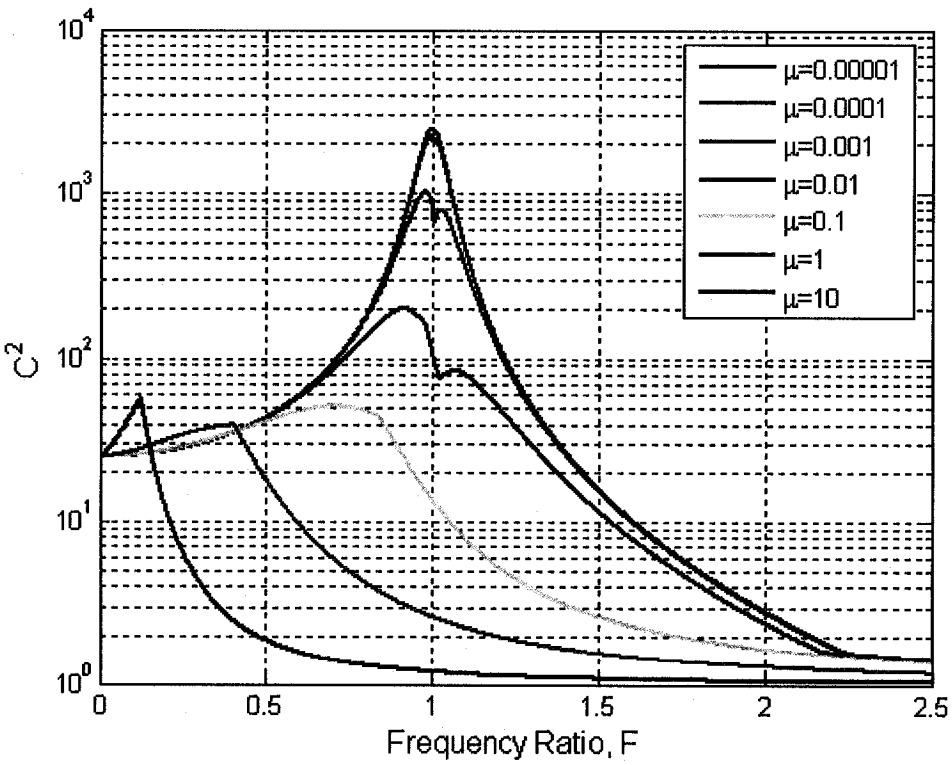

Figure 2.4: C^2 vs. Frequency Ratio for $Q_1 = 10$ and $Q_2 = 50$

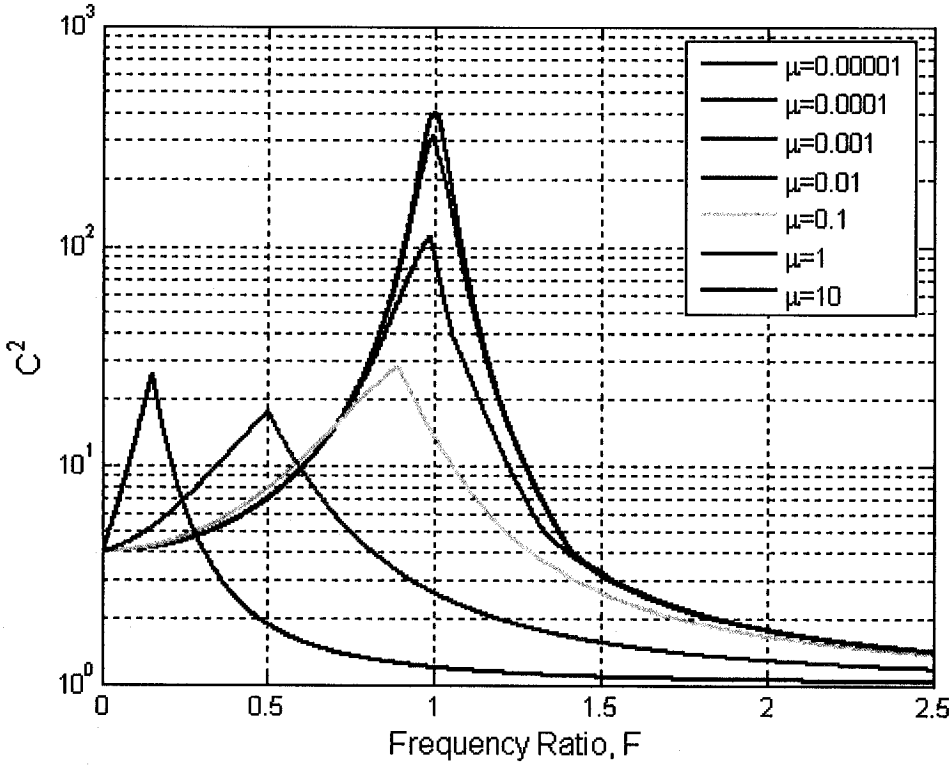

Figure 2.5: C^2 vs. Frequency Ratio for $Q_1 = 10$ and $Q_2 = 20$

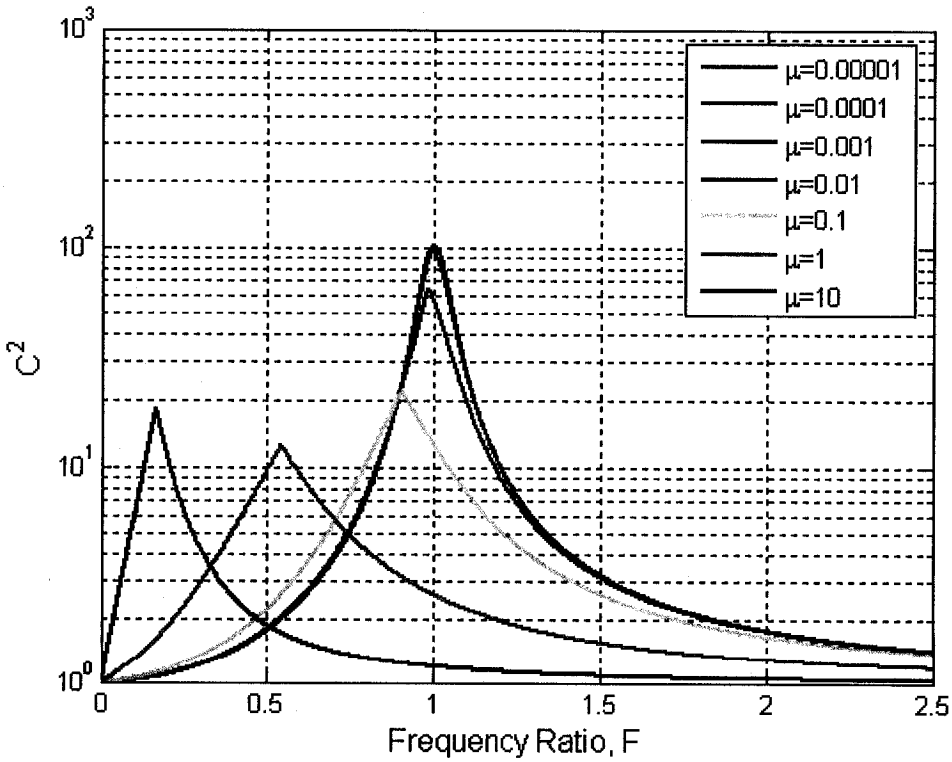

Figure 2.6: C^2 vs. Frequency Ratio for $Q_1 = 10$ and $Q_2 = 10$

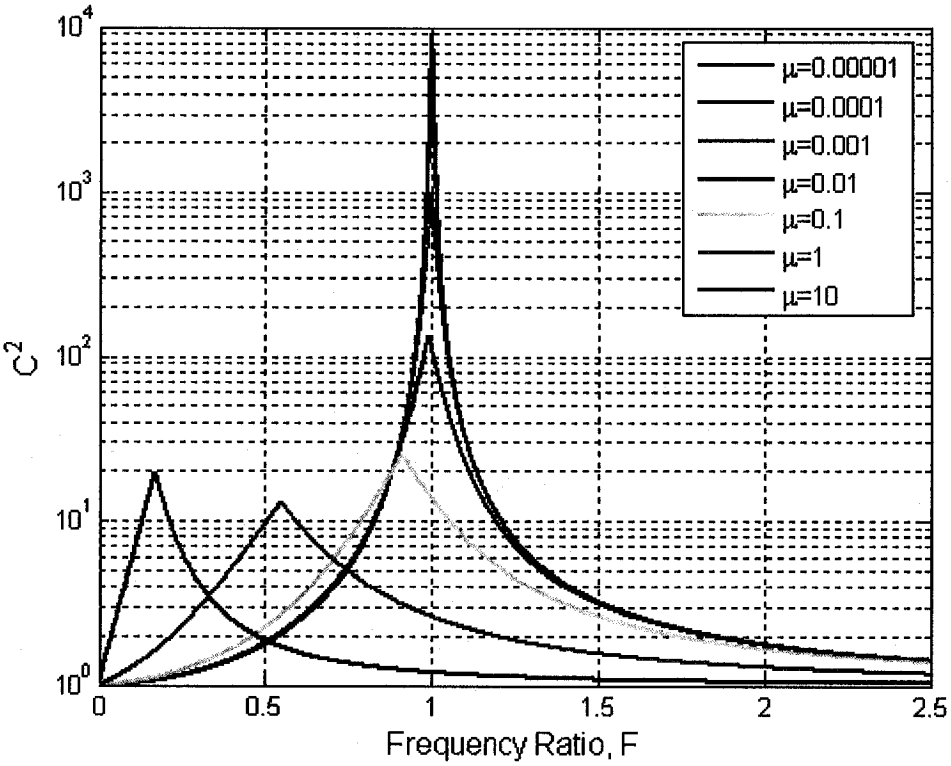

Figure 2.7: C^2 vs. Frequency Ratio for $Q_1 = 100$ and $Q_2 = 100$

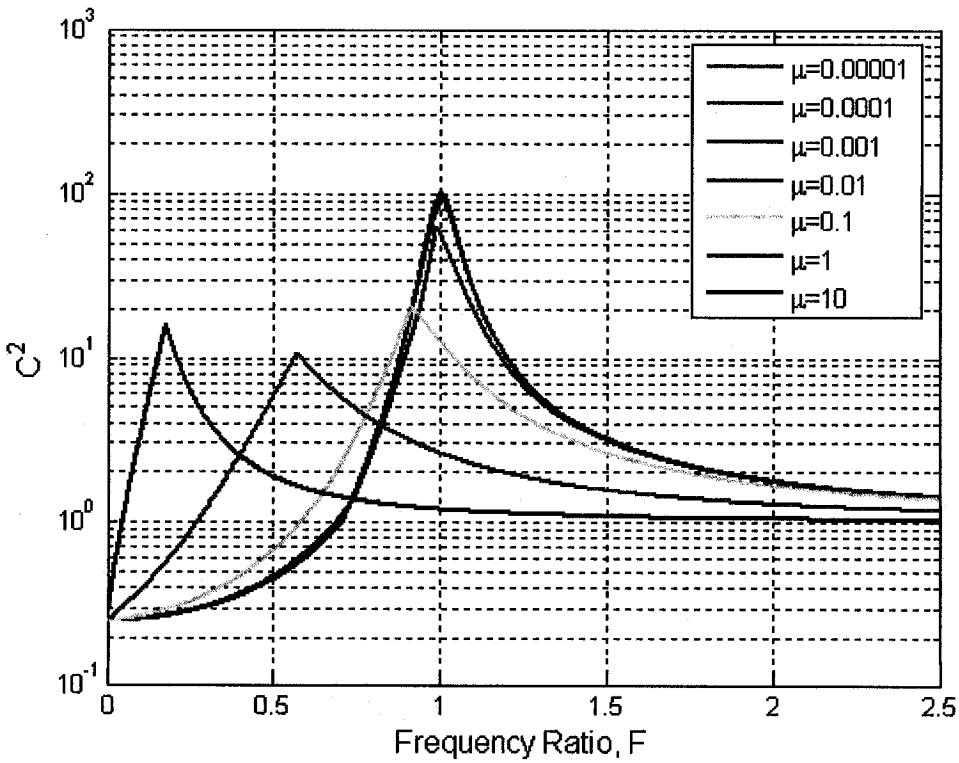

Figure 2.8: C^2 vs. Frequency Ratio for $Q_1 = 20$ and $Q_2 = 10$

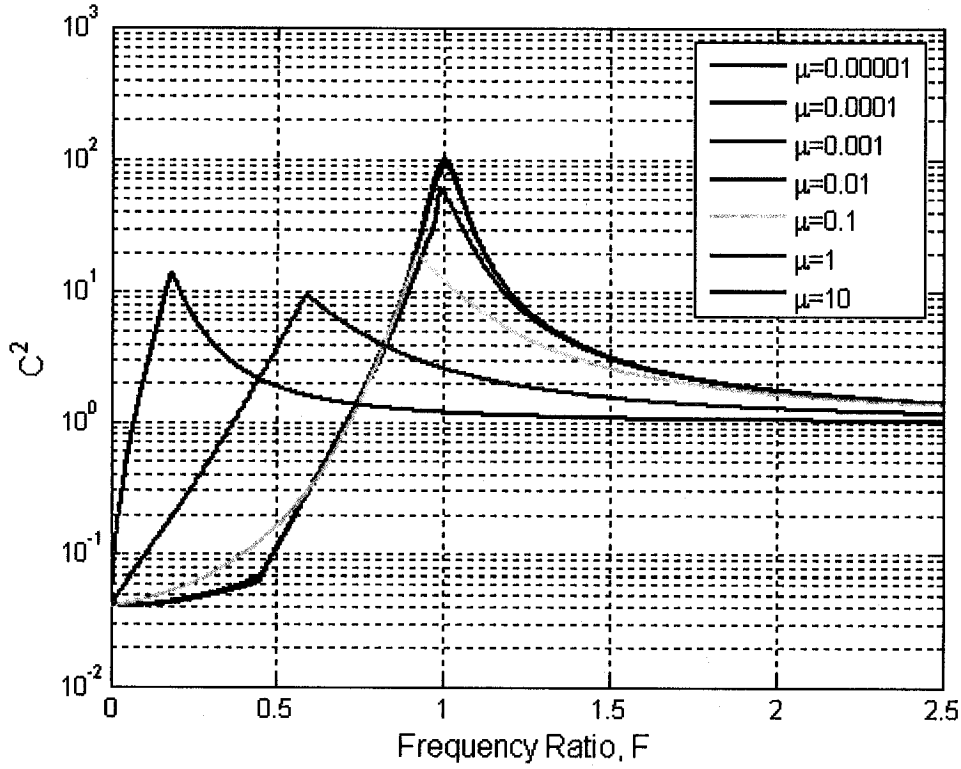

Figure 2.9: C^2 vs. Frequency Ratio for $Q_1 = 50$ and $Q_2 = 10$

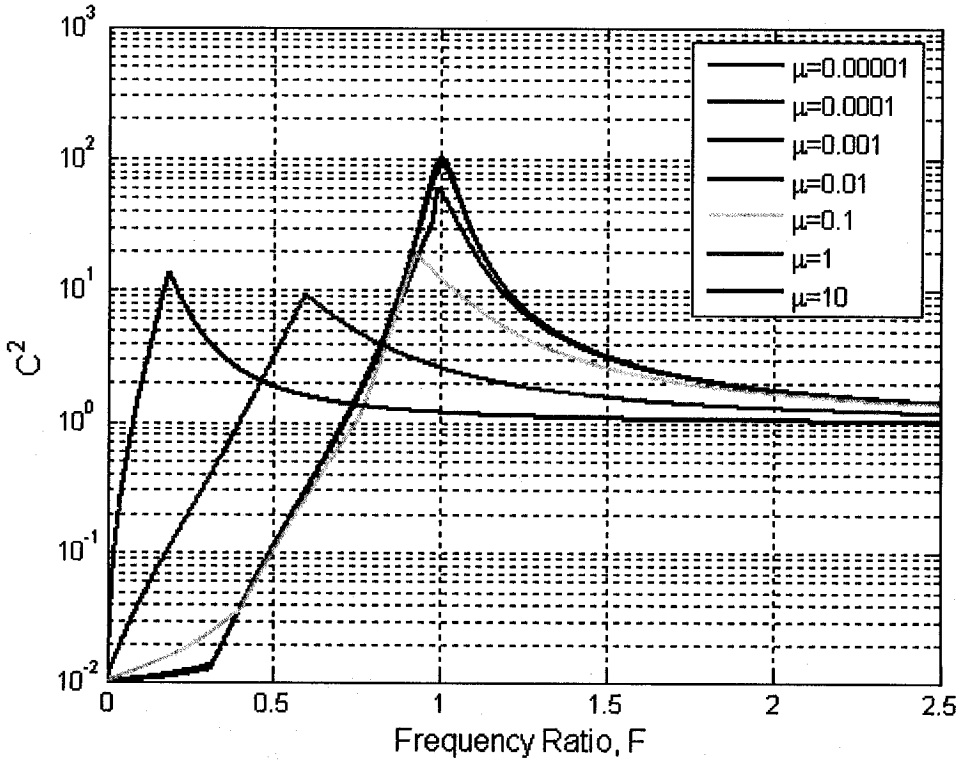

Figure 2.10: C^2 vs. Frequency Ratio for $Q_1 = 100$ and $Q_2 = 10$

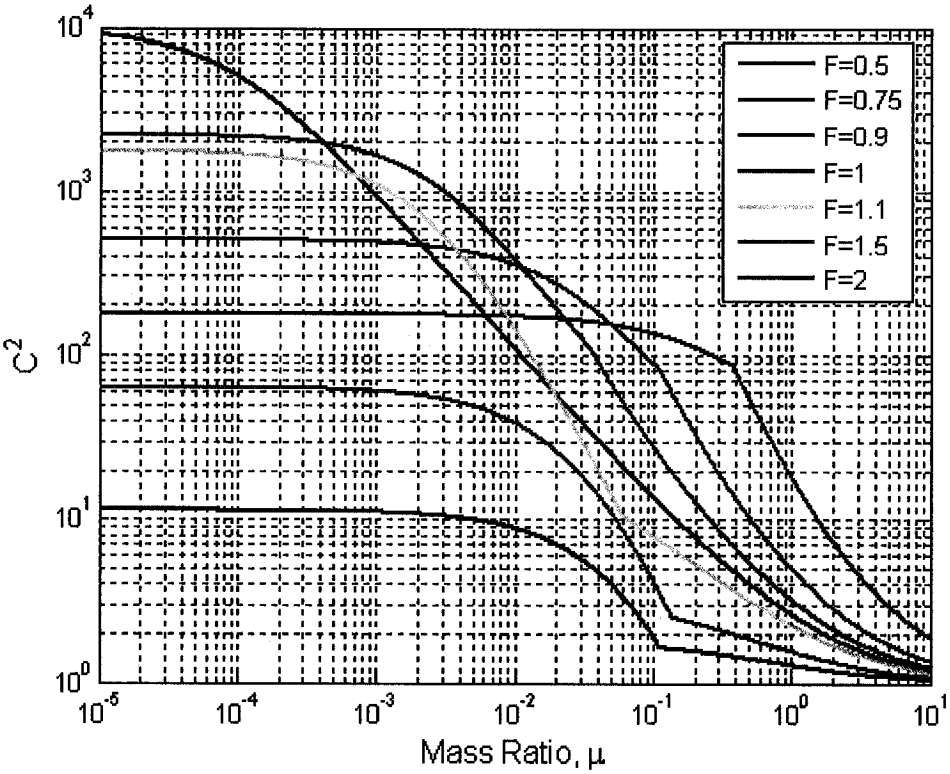

Figure 2.11: C^2 vs. Mass Ratio for $Q_1 = 10$ and $Q_2 = 100$

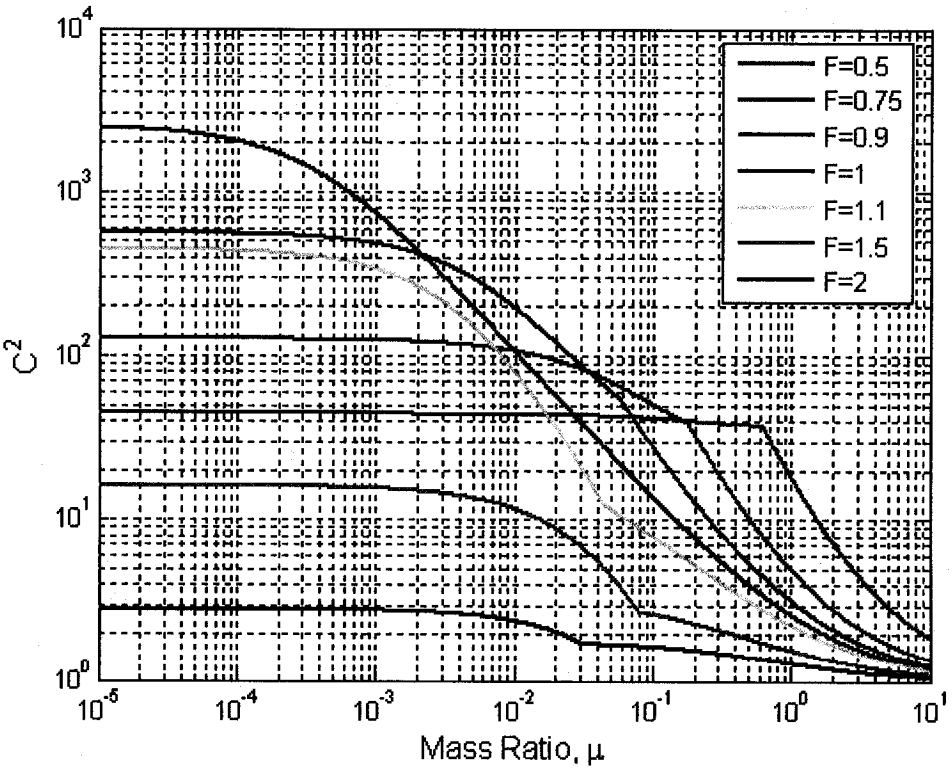

Figure 2.12: C^2 vs. Mass Ratio for $Q_1 = 10$ and $Q_2 = 50$

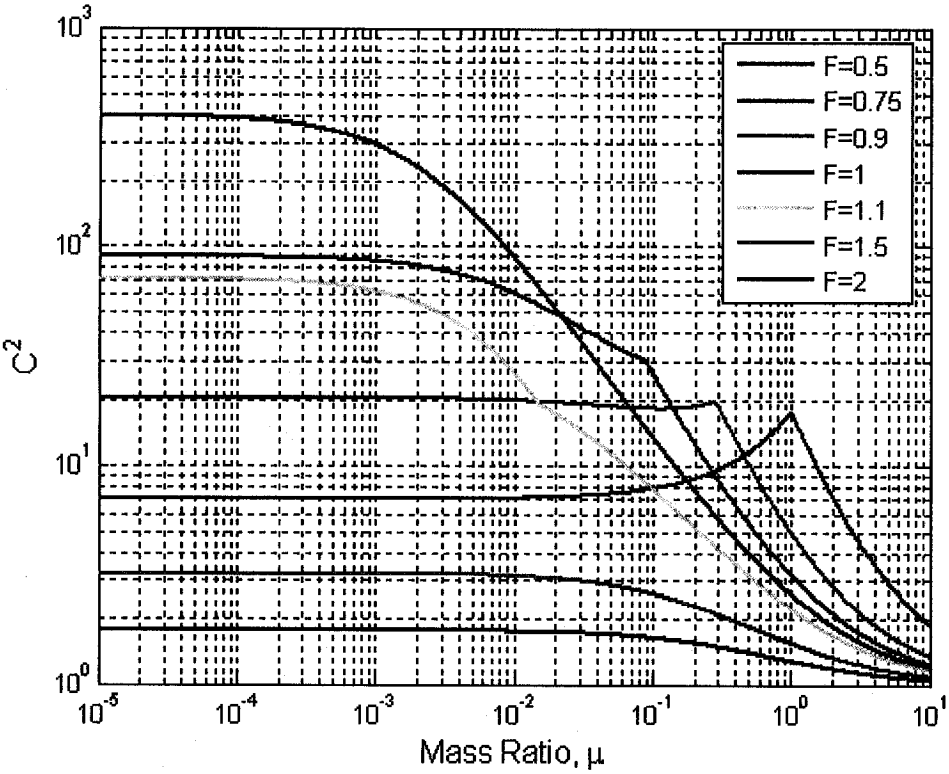

Figure 2.13: C^2 vs. Mass Ratio for $Q_1 = 10$ and $Q_2 = 20$

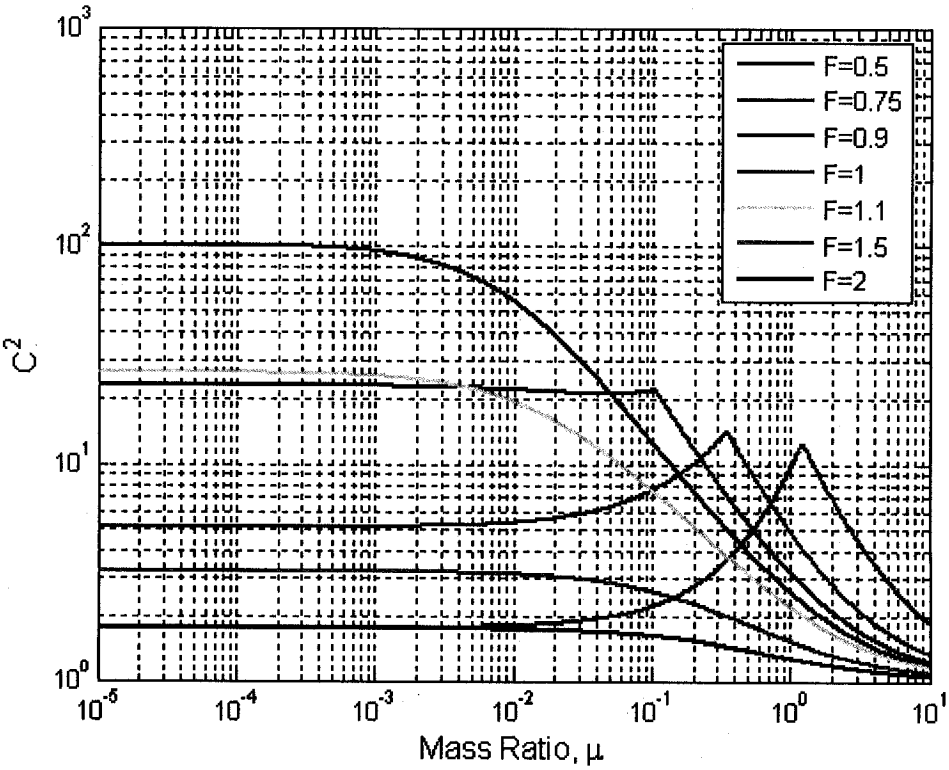

Figure 2.14: C^2 vs. Mass Ratio for $Q_1 = 10$ and $Q_2 = 10$

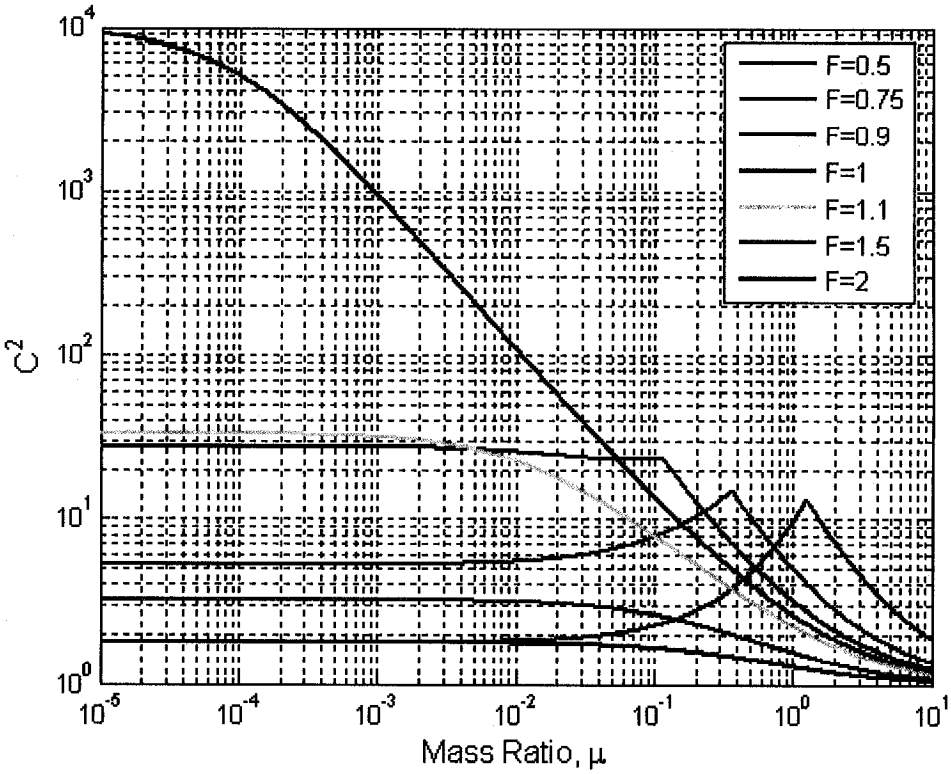

Figure 2.15: C^2 vs. Mass Ratio for $Q_1 = 100$ and $Q_2 = 100$

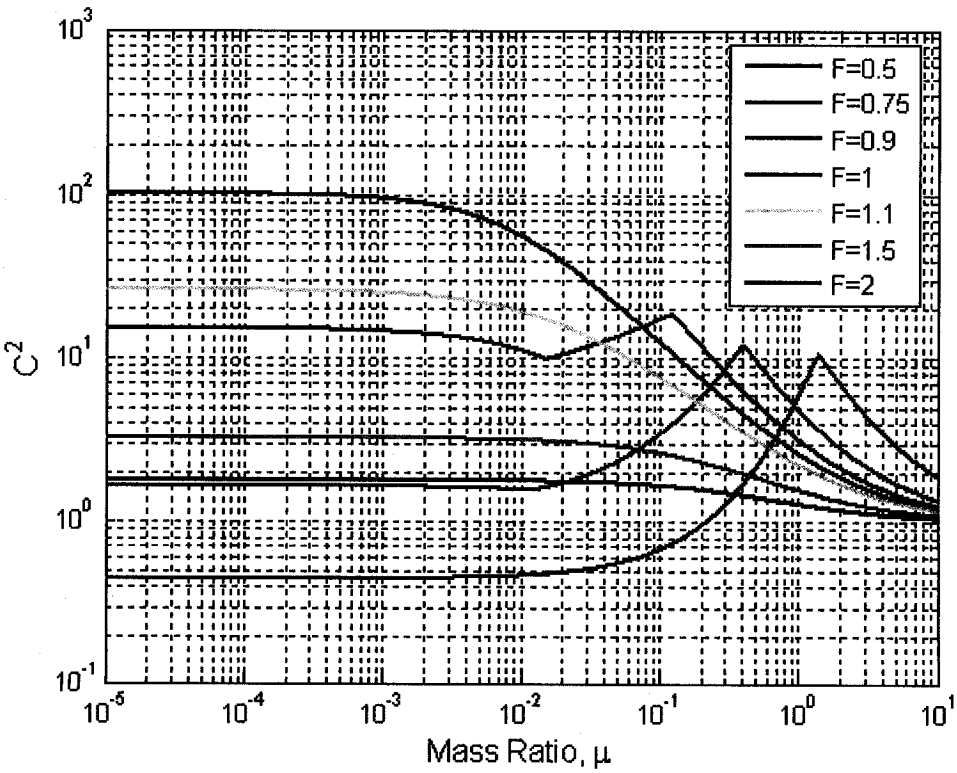

Figure 2.16: C^2 vs. Mass Ratio for $Q_1 = 20$ and $Q_2 = 10$

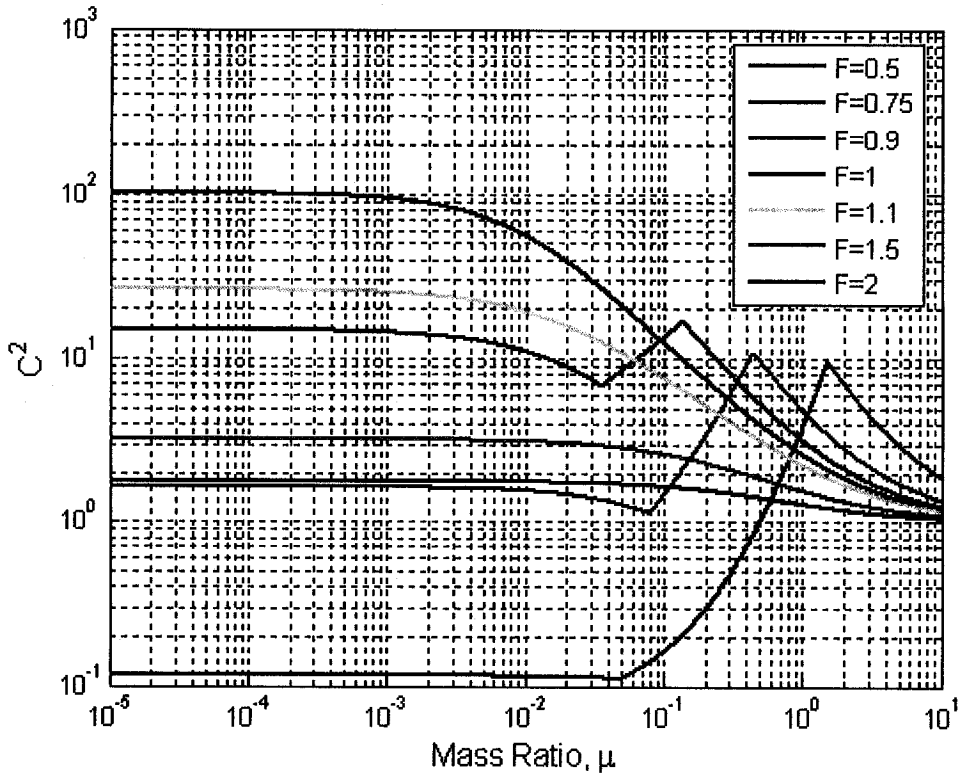

Figure 2.17: C^2 vs. Mass Ratio for $Q_1 = 50$ and $Q_2 = 10$

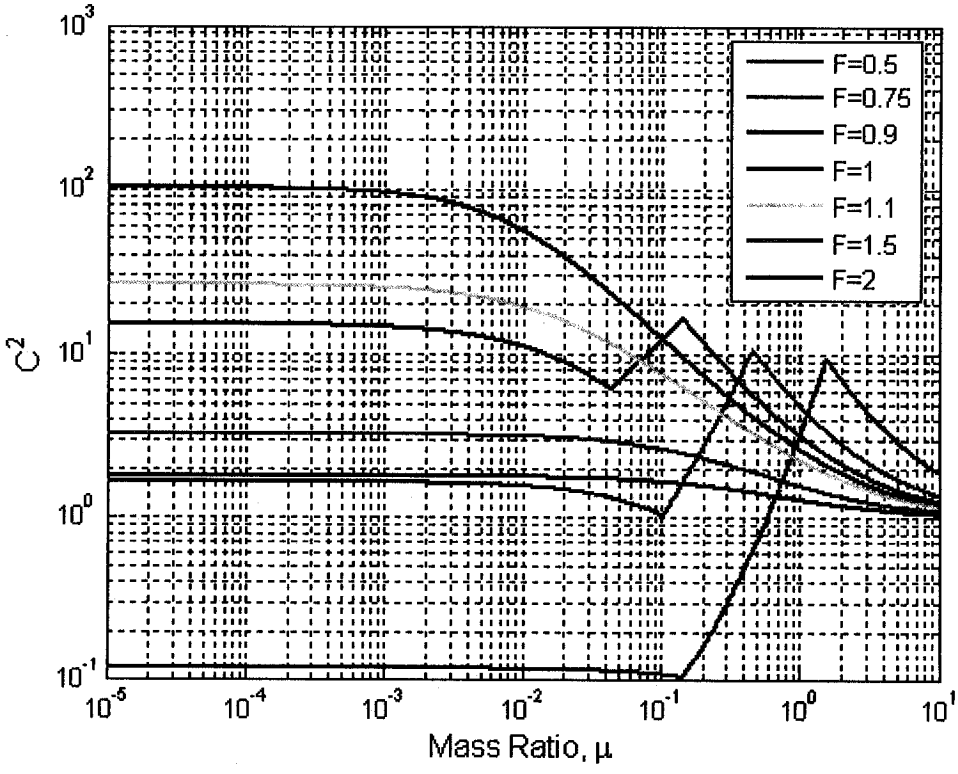

Figure 2.18: C^2 vs. Mass Ratio for $Q_1 = 100$ and $Q_2 = 10$

An examination of the curves in figures 2.3 to 2.10 reveal the general behaviour for the value of C^2. These various behaviours are demonstrated in figure 2.19 and described below.

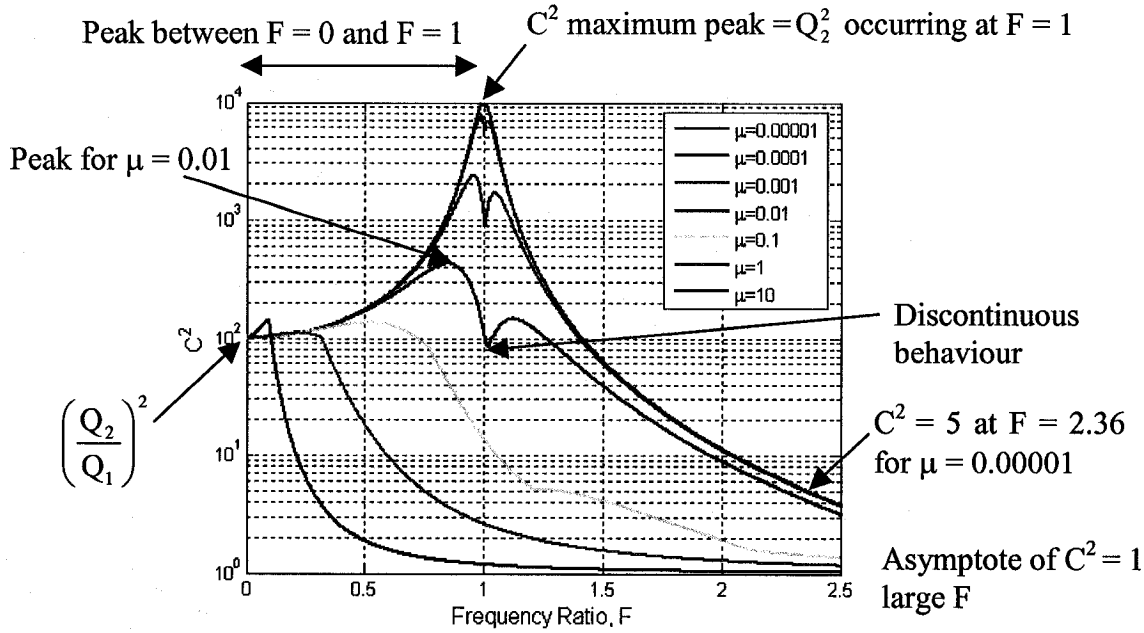

C^2 vs. Frequency Ratio for $Q_1 = 10$ and $Q_2 = 100$

Figure 2.19: General Behaviour of C^2 for the 2-DOF System, Part I

Independent of the values of the mass ratio μ, the value of C^2 approaches the value $\left(\frac{Q_2}{Q_1}\right)^2$ as the frequency ratio tends towards F = 0.

As the frequency ratio increases from F = 0, the value of C^2 starts from $C^2 = \left(\frac{Q_2}{Q_1}\right)^2$ and increases until a peak value is reached. The peak is always reached when the frequency ratio F is between F = 0 and F = 1 but tends towards F = 1 for small mass ratios μ, e.g. $\mu < 0.01$, independent of the specific values of Q_1 and Q_2.

The value of C^2 at this peak depends primarily on the mass ratio μ but also on the values Q_1 and Q_2. The largest possible peak value of C^2 occurs for systems having a frequency ratio of $F = 1$ and a mass ratio tending towards $\mu = 0$. For these conditions, the peak value occurs as $C^2 = Q_2^2$, independent of the value of Q_1. Moreover, for a given value of F, the largest possible value of C^2 occurs when $\mu \rightarrow 0$, but only if $F \geq 1$.

The value of C^2 decreases rapidly as the frequency ratio is increased passed the peak until the value of C^2 asymptotically tends towards $C^2 = 1$. Most of the systems investigated have values of $C^2 < 5$ when the frequency ratio was $F > 1.5$. Systems that were exceptions to this general observation all have very small mass ratios and very large load to source quality ratios $\frac{Q_2}{Q_1}$. All systems investigated have $C^2 < 5$ when the frequency ratio F was greater than 2.36.

Values of C^2 less than unity are observed, but only for systems where $F < 1$ and $Q_1 > Q_2$.

Discontinuous behaviour for C^2 is noted. This was expected from equation 2.43, shown again below for reference.

$$C^2 = \frac{|H_{20}|^2_{max}}{|H_{10}|^2_{max}} \tag{2.43}$$

The numerator and the denominator of equation 2.43 must be evaluated separately. Their maximum values may not occur at the same natural frequency f_{11} or f_{22} of the coupled system leading to a discontinuous behaviour for C^2.

In all, there are four possible combinations that must be evaluated using equation 2.43 to determine the value of C^2. No combination can be ruled out *a priori* because each one of these combinations can occur given the right combination of system parameters F, μ, Q_1, and Q_2.

Consider the curve in figure 2.3 for a two degrees-of-freedom system partly defined by $\mu = 0.01$, $Q_1 = 10$, and $Q_2 = 100$. The effect of this discontinuous behaviour on this C^2 curve is shown in figure 2.20. In this figure, colour has been added to the curve for C^2 to show which combinations were utilized to calculate C^2.

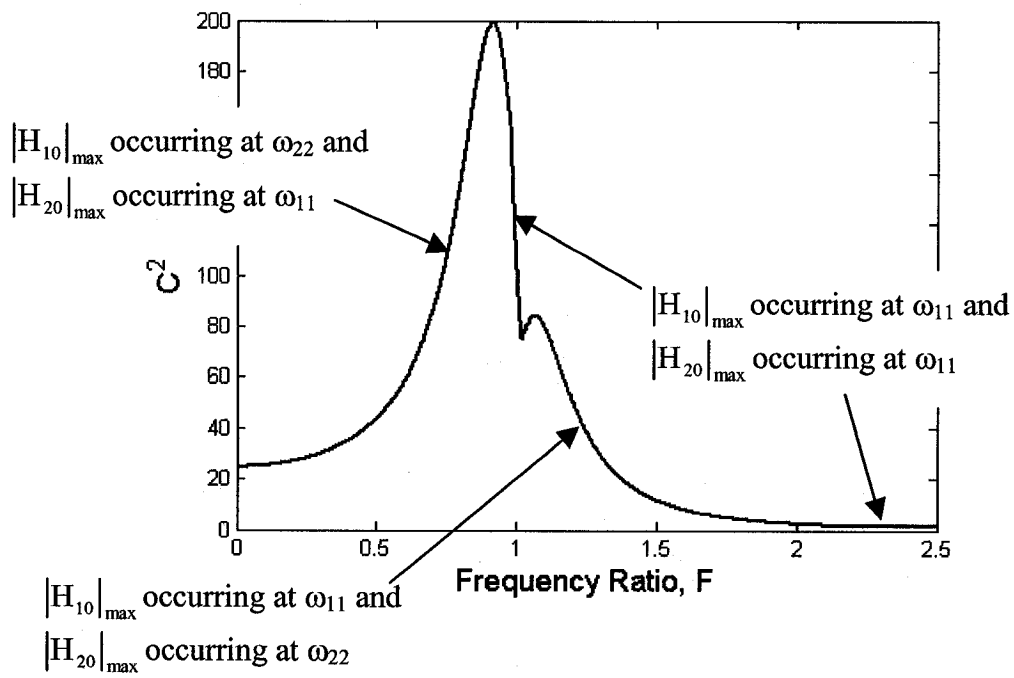

C^2 vs. Frequency Ratio F for system $\mu = 0.01$, $Q_1 = 10$, and $Q_2 = 50$

Figure 2.20: Discontinuous Behaviour of C^2 Curve

A similar examination as figure 2.19 can be performed for figures 2.11 to 2.18. Observations are shown below in figure 2.21.

Figures 2.11 to 2.18 show asymptotic behaviour for C^2 when the mass ratio μ is either very small or very large.

The asymptotic value of C^2 for small mass ratios μ is dependent on the system parameters F, Q_1 and Q_2 but never exceeds the value $C^2 = Q_2^2$. This asymptote decreases very quickly in value as the frequency ratio departs from the value F = 1.

The asymptotic value of C^2 for large mass ratios μ is equal to $C^2 = 1$, independent of the specific values of the system parameters.

For a system with a given mass ratio μ, the maximum possible value of C^2 does not necessarily occur at the tuned condition when the frequency ratio is F = 1.

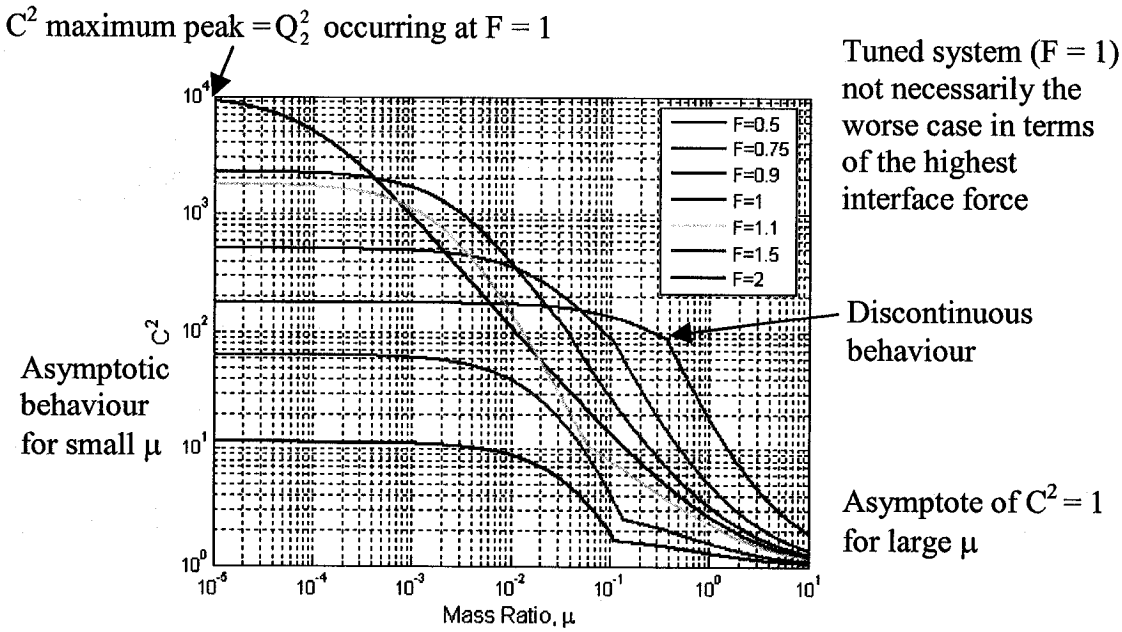

C^2 vs. Mass Ratio for $Q_1 = 10$ and $Q_2 = 100$

Figure 2.21: General Behaviour of C^2 for the 2-DOF System, Part II

2.6.1 Effect of Damping Mechanism: Structural Damping

The behaviour of C^2 presented up to date is based on analysis of a two degrees-of-freedom system with viscous damping. This particular approach of investigating the maximum interface forces by assuming viscous damping is similar to the approach

utilized by the simple and complex TDFS methods [5], which are briefly described in the glossary.

In viscous damping, the energy dissipated per oscillation increases with increasing frequency. In contrast, experimental evidence suggests that for most metallic structures, such as steel and aluminum, the energy dissipated per oscillation is independent of frequency over a large frequency range [21]. In addition, the amount of damping in these structures tends to be proportional to the square of the amplitude instead of being proportional to the velocity as in the case for viscous damping. Thus, although viscous damping is often used in the theoretical treatment of vibration of structures, experimental evidence suggests that structural damping is a more representative damping mechanism for real structures.

One particular difference between structural and viscous damping is the frequency at which the maximum frequency responses H_{10} and H_{20} occur. For systems with viscous damping, the frequency of maximum response is the damped natural frequency, which is always slightly lower than the un-damped natural frequency. However, for systems with structural damping, the frequency of maximum response is always equal to the un-damped natural frequency. In light of this, this section examines possible differences in the value of C^2 for systems with identical system parameters F and μ but with equivalent quality factors Q_1 and Q_2 for structural damping instead of viscous damping.

For viscous damping, the quality factor is equal to [21]

$$Q_{viscous} = \frac{1}{2\zeta} \tag{2.44}$$

For structural damping, the quality factor is expressed in terms of the structural damping factor γ as [21]

$$Q_{structural} = \frac{1}{\gamma} \tag{2.45}$$

The details of the derivation of the frequency response functions H_{10} and H_{20} for the base excited two degrees-of-freedom system with structural damping are contained in appendix E. The resulting solutions for the frequency response functions H_{10} and H_{20} are

$$|H_{10}| = \left| \frac{C_8 C_9}{C_6 C_9 - C_7 C_{10}} \right| \qquad \text{Structural Damping} \qquad (2.46)$$

$$|H_{20}| = \left| \frac{C_8 C_{10}}{C_6 C_9 - C_7 C_{10}} \right| \qquad \text{Structural Damping} \qquad (2.47)$$

Where

$$C_6 = \left[\frac{1}{F^2} + \mu - R^2 + i \cdot \left(\frac{1}{F^2 Q_1} + \frac{\mu}{Q_2} \right) \right] \qquad (2.48)$$

$$C_7 = \left[\mu + i \cdot \left(\frac{\mu}{Q_2} \right) \right] \qquad (2.49)$$

$$C_8 = \left[\frac{1}{F^2} + i \cdot \left(\frac{1}{F^2 Q_1} \right) \right] \qquad (2.50)$$

$$C_9 = \left[1 - R^2 + i \cdot \left(\frac{1}{Q_2} \right) \right] \qquad (2.51)$$

$$C_{10} = \left[1 + i \cdot \left(\frac{1}{Q_2} \right) \right] \qquad (2.52)$$

Note that equations 2.48 to 2.52 associated with structural damping are simpler than equation 2.26 to 2.30 associated with viscous damping.

The value of C^2 can be determined as before for viscous damping with

$$C^2 = \frac{|H_{20}|^2_{max}}{|H_{10}|^2_{max}} \qquad (2.43)$$

For purposes of determining whether or not different types of damping can affect the calculated value of C^2, only one test showing evidence of a difference is required. Consequently, only the first seven test cases presented in table 2.4, corresponding to the curves shown in figure 2.3, were evaluated for comparison.

The evaluation was performed using a MATLAB routine programmed with equations 2.26 to 2.30, 2.33, 2.34 as well as equations 2.46 to 2.52. The MATLAB routines producing the plots shown in figure 2.22 are shown as program 3 in appendix D.

The results of the comparison are shown in figure 2.22. From this data, one can conclude that the type of damping can indeed influence the value of C^2.

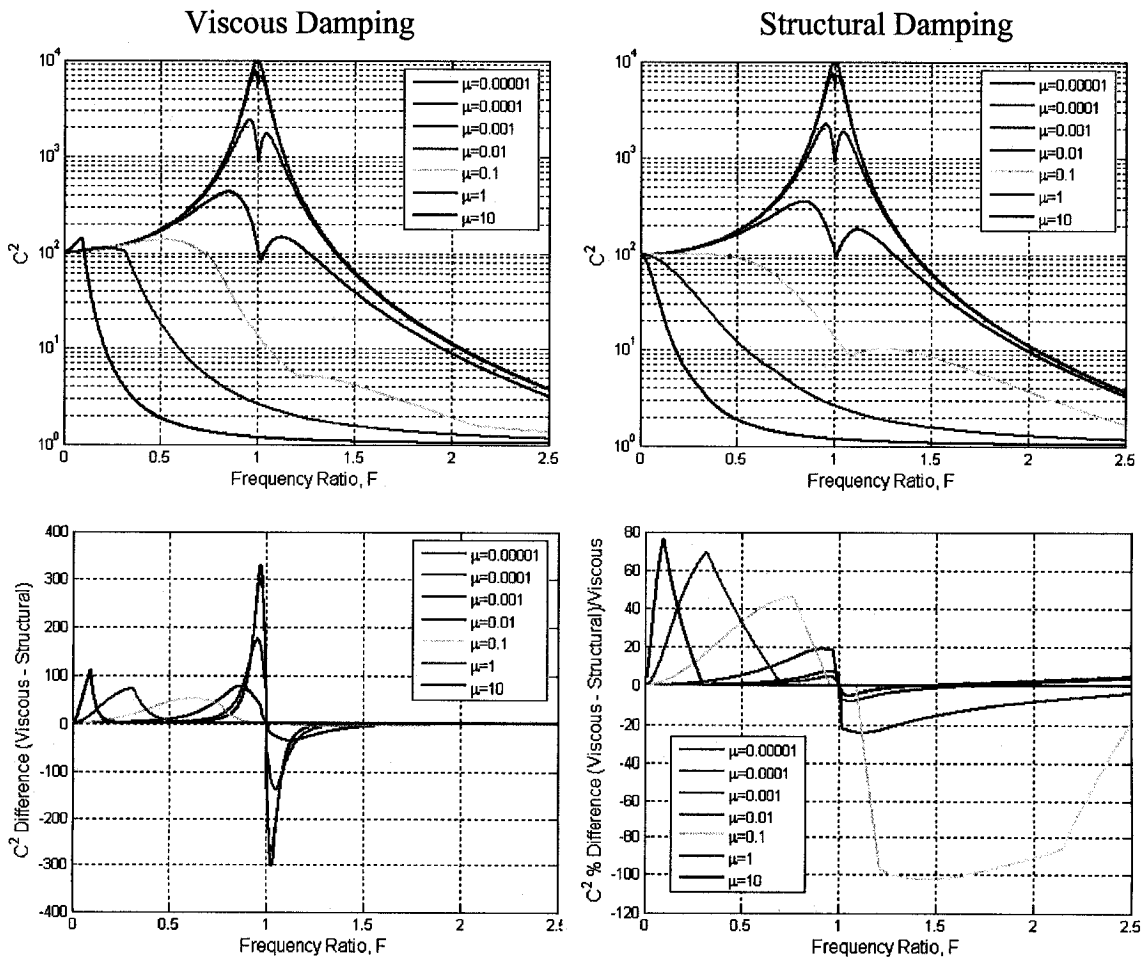

Figure 2.22: C^2 for Viscous vs. Structural Damping for $Q_1 = 10$ and $Q_2 = 100$

2.6.2 Summary of the Behaviour of C^2 Based on Numerical Analysis

For ease of reference, the previous observations based on the numerical analysis are summarized below in point form.

- $C^2 = \left(\frac{Q_2}{Q_1}\right)^2$ when $F \to 0$, independent of μ
- For any given set of F, Q_1, and Q_2, the largest possible value of C^2 occurs when $\mu \to 0$ but only if $F \geq 1$. If $F < 1$, the largest possible value of C^2 does not necessarily occur when $\mu \to 0$.
- C^2 has an asymptotic limit when $\mu \to 0$ whose exact value depends on F, Q_1, and Q_2
- C^2 peaks between $0 < F < 1$, depending mostly on μ
- For any system, $C^2_{max} = Q_2^2$, occurring when $F = 1$ and $\mu \to 0$, independent of Q_1
- For any μ, the maximum value of C^2 is $\left(\frac{Q_2}{Q_1}\right)^2 \leq C^2 \leq Q_2^2$, occurring when $F \leq 1$
- $C^2 \to 1$ for large F, independent of μ, Q_1, and Q_2
- $C^2 \to 1$ for large μ independent of F, Q_1, and Q_2
- C^2 can exhibit discontinuous behaviour
- Most of the systems investigated reached $C^2 < 5$ when $F > 1.5$
- The maximum value of C^2 does not necessary occur when $F = 1$
- Values of C^2 less than unity are possible but occur only when $F < 1$ and $Q_1 > Q_2$
- The type of damping, viscous or structural, can have an effect on C^2

2.7 Behaviour of C^2 Based on Algebraic Analysis of Special Cases

2.7.1 Special Case 1: When the Maximum Frequency Responses Occur at the Same Frequency of the Coupled System

In general, the maximum value of the frequency responses H_{10} and H_{20} can occur at either the first or second natural frequency of the coupled system shown in figure 2.1.

However, consider the special case where both of these maximum frequency responses occur at the same natural frequency of the coupled system. For this case, equations 2.43, 2.33, and 2.34 can be combined to give

$$C^2 = \left[\frac{|C_5|^2}{|C_4|^2}\right]_{R_{ff}=\text{max responses}} \tag{2.53}$$

Furthermore, equation 2.53 can be combined with equations 2.29 and 2.30 resulting in

$$C^2 = \left[\frac{1+\left(\frac{R_{ff}}{Q_2}\right)^2}{\left(1-R_{ff}^2\right)^2+\left(\frac{R_{ff}}{Q_2}\right)^2}\right]_{R_{ff}=\text{max responses}} \tag{2.54}$$

where R_{ff} has been utilized instead of R to indicate that the value R must be evaluated at the frequency of maximum response for both the source and the load corresponding to either the first un-damped natural frequency

$$R_{11} = \sqrt{\frac{1+F^2(1+\mu)-\sqrt{\left[1+F^2(1+\mu)\right]^2-4F^2}}{2F^2}} \tag{2.37}$$

or the second un-damped natural frequency

$$R_{22} = \sqrt{\frac{1+F^2(1+\mu)+\sqrt{\left[1+F^2(1+\mu)\right]^2-4F^2}}{2F^2}} \tag{2.38}$$

Examination of equations 2.54, 2.37 and 2.38 show that the value of C^2 is independent of Q_1 of the source, when the maximum frequency responses of H_{10} and H_{20} occur at the same natural frequency.

2.7.2 Special Case 2: When the Maximum Frequency Responses Occur at the Same Frequency and Q_2 is Very Large

Equation 2.54 can be further simplified by considering the special case when the maximum frequency responses H_{10} and H_{20} both occur at the same natural frequency *and* the quality factor of the load Q_2 is very large compared to the dimensionless excitation parameter R evaluated at either the first natural frequency $R = R_{11}$ or the second natural frequency $R = R_{22}$ of the coupled system. For this special case, the term $\left(\frac{R_{ff}}{Q_2}\right)^2$ approaches zero and can be ignored compared to the other terms in equation 2.54. The resulting equation is shown below as equation 2.55. Equation 2.55 approximates equation 2.54 but will always produce larger values of C^2 when $R_{ff} = R_{11}$.

$$C^2 \approx \left[\frac{1}{\left(1-R_{ff}^2\right)^2}\right]_{R_{ff}=\text{max responses}} \tag{2.55}$$

In the above equation, the dimensionless excitation parameter R_{ff} represents R evaluated at $R = R_{11}$ or $R = R_{22}$ as per equations 2.37 and 2.38.

Equation 2.37, 2.38, and 2.55 show that for systems where the load quality factor Q_2 is very large compared to the dimensionless excitation parameter R_{ff} and the maximum frequency responses of H_{10} and H_{20} both occur at the same natural frequency R_{ff}, the value of C^2 depends on the system parameter of frequency ratio F and mass ratio μ and is independent of the quality factors Q_1 and Q_2, and hence independent of the damping in either the source or the load. This finding is consistent with the findings by Chang [6] and Dharanipathi [7]. However, it is important to note that in general the value of C^2 is not independent of damping.

2.7.3 Special Case 3: When the Maximum Frequency Responses Occur at the First Natural Frequency of the Coupled System, Q_2 is Very Large, the Mass Ratio μ is Very Small, and the Frequency Ratio F is above Unity

Equation 2.55 can be further simplified by considering the additional condition when the maximum frequency responses H_{10} and H_{20} both occur at the first natural frequency of the coupled system instead of either the first or the second natural frequency. For this condition equation 2.55 can be expressed as

$$C^2 \approx \frac{1}{\left(1-R_{11}^2\right)^2} \tag{2.56}$$

Where R_{11} is shown again below for reference

$$R_{11} = \sqrt{\frac{1+F^2(1+\mu)-\sqrt{\left[1+F^2(1+\mu)\right]^2-4F^2}}{2F^2}} \tag{2.37}$$

Now consider R_{11}^2 when the mass ratio μ becomes infinitesimally small. This can be expressed by the limit function as

$$\lim_{\mu \to 0} \frac{1+F^2(1+\mu)-\sqrt{\left[1+F^2(1+\mu)\right]^2-4F^2}}{2F^2} = \frac{1+F^2-\sqrt{\left[1+F^2\right]^2-4F^2}}{2F^2} \tag{2.57}$$

Appendix F shows that equation 2.57 reduces to

$$R_{11,\mu\to 0}^2 = 1 \qquad \text{if } F \le 1 \tag{2.58}$$

$$R_{11,\mu\to 0}^2 = \frac{1}{F^2} \qquad \text{if } F \ge 1 \tag{2.59}$$

Now consider the case when the frequency ratio F is above unity. This case generally occurs in practice by design. Combining equations 2.56 and 2.59 results in

$$C^2 \approx \frac{1}{\left(1-\frac{1}{F^2}\right)^2} \qquad \text{maximum responses at } R_{11} \tag{2.60}$$

Thus, for systems with very small mass ratios μ, frequency ratios F above unity, large load quality factors Q_2, and maximum frequency response functions occurring at the first natural frequency of the coupled system, the value of C^2 is only a function of the frequency ratio F.

From equations 2.18 to 2.21, the maximum frequency response of H_{10} is associated with the maximum acceleration of the source m_1 and the maximum frequency response H_{20} is associated with the maximum force between the source m_1 and the load m_2. A plot of equation 2.60 is shown in figure 2.23.

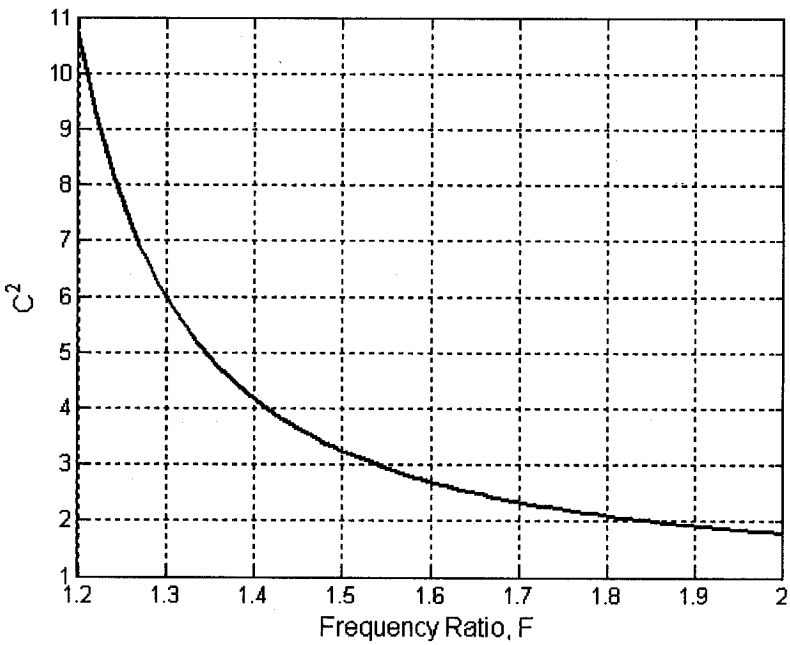

Figure 2.23: C^2 vs. Frequency for $F \geq 1$, $\mu \rightarrow 0$, and $Q_2 \rightarrow \infty$ when Both the Maximum Interface Force and the Maximum Source Acceleration Occur at the First Natural Frequency

Figures 2.3 to 2.18 show that large values of C^2 occur when the mass ratio is very small and the quality factor of the load Q_2 is very large. Consequently, provided that the maximum frequency responses of H_{10} and H_{20} occur at the first natural frequency of the coupled system, equation 2.60 can be viewed as an upper limit estimate of the value of C^2. Moreover, equation 2.60 predicts the value of the left-most asymptote for many of

the curves in figures 2.11 to 2.18. Left-most asymptote values in figures 2.11 to 2.18 not corresponding to equation 2.60 belong to two degrees-of-freedom systems where the maximum frequency responses of H_{10} and H_{20} do not occur at the first natural frequency of the coupled system. Therefore, it is logical to investigate next the necessary conditions for the maximum frequency responses of H_{10} and H_{20} to both occur at the first natural frequency of the coupled system.

2.7.3.1 Conditions When the Maximum Frequency Responses Occur at the First Natural Frequency

Of interest are the combinations of system parameters F, μ, Q_1, and Q_2, which lead to the maximum frequency responses H_{10} and H_{20} to both occur at the first natural frequency of the coupled system. This knowledge, coupled with equation 2.56, will be very useful in providing a quick and easy way of determining the value of C^2 for a base-excited two degrees-of-freedom system.

To determine if a given set of system parameters F, μ, Q_1, and Q_2 will lead to the maximum frequency responses H_{10} and H_{20} to both occur at the first natural frequency of the coupled system, the inequalities given by equations 2.61 and 2.62 need to be satisfied.

$$|H_{10}(R_{11})| > |H_{10}(R_{22})| \tag{2.61}$$

$$|H_{20}(R_{11})| > |H_{20}(R_{22})| \tag{2.62}$$

A given set of system parameters F, μ, Q_1, and Q_2 can be expressed as a four-dimensional coordinate point defined by (F,μ,Q_1,Q_2). At each coordinate point, the values $H_{10}(R_{11})$, $H_{10}(R_{22})$, $H_{20}(R_{11})$, and $H_{20}(R_{22})$ can be evaluated using equations 2.26 to 2.30, 2.33, 2.34, 2.37, and 2.38 from which the inequalities 2.61 and 2.62 can be verified.

For presentation purposes, dealing with all four system-parameters at once is cumbersome. Therefore, the four-dimensional point is reduced to a two-dimensional point by arbitrarily setting the values of Q_1 and Q_2. In this manner, only the two-dimensional points (F,μ) need to be evaluated. The result can be expressed in a contour

plot for a given Q_1 and Q_2 combination. In this plot, colour can be associated with every point depending whether or not the inequalities are satisfied.

Three sets of Q_1 and Q_2 combinations were investigated. The first set only contains combinations of the type $Q_1 < Q_2$, the second set only contains combinations of the type $Q_1 = Q_2$, and the third set only contains combinations of the type $Q_1 > Q_2$. The exact quality factor values utilized in the analysis are shown in table 2.5.

Table 2.5: Quality Factors for Inequality Investigations

Case	Source Quality Factor Q_1	Load Quality Factor Q_2
1a	10	20
1b	10	50
1c	10	100
1d	10	1000
2a	10	10
2b	20	20
2c	50	50
2d	100	100
2e	1000	1000
3a	20	10
3b	50	10
3c	100	10
3d	1000	10

The frequency ratio F was varied from 0.01 to 2.5, 0.01 to 5, or 0.01 to 15 in steps of 0.001 and was plotted on the x-axis. The mass ratio μ was varied from 0.001 to 0.5 in steps of 0.001 and was plotted on the y-axis.

A MATLAB program [22], shown as program 4 in appendix D, was written to perform all the necessary calculations. The results are shown in figure 2.24, 2.25, and 2.26.

To determine if a given combination of system parameters F, μ, Q_1, and Q_2 will lead to the maximum frequency responses of H_{10} and H_{20} to both occur at the first natural frequency of the coupled system, simply find the plot corresponding to the Q_1 and Q_2 of the system, then on that plot read the colour at the point defined by (F,μ). If the colour is

blue, then the maximum frequency responses of H_{10} and H_{20} both occur at the first natural frequency of the coupled system and equation 2.60 can be utilized to calculate the value of C^2. If the colour is red, then the maximum frequency responses of H_{10} and H_{20} do not both occur at the first natural frequency of the coupled system and equation 2.60 cannot be utilized. In this case equation 2.43 should be utilized. When F = 1, both the maximum interface force and the maximum source acceleration will always occur at the first natural frequency of the coupled system [23]. This fact is reflected in figures 2.24 to 2.26.

Examination of figures 2.24 to 2.26 reveals that for frequency ratios F greater than unity, the maximum frequency responses of H_{10} and H_{20} both occur at the first natural frequency of the coupled system for most of the selected combinations of system parameters, F, μ, Q_1, and Q_2. Figures 2.24 to 2.26 suggest that if the quality factors Q_1 and Q_2 satisfy the conditions $Q_1 \geq Q_2$ and $F \geq 1$, then the maximum frequency responses of H_{10} and H_{20} will always occur at the first natural frequency of the coupled system. However, if the quality factors Q_1 and Q_2 satisfy the conditions $Q_1 < Q_2$ and $F \geq 1$ then the maximum frequency responses of H_{10} and H_{20} will occur at the first natural frequency of the coupled system only if F is large enough or if the mass ratio μ is above a critical value. This critical mass ratio increases with increasing Q_2 to Q_1 ratio such that for systems with Q_2 to Q_1 ratios below 100, the critical mass ratio is about $\mu > 0.236$ as shown in table 2.6.

Table 2.6: Conditions for Maximum Frequency Responses of H_{10} and H_{20} to both Occur at the First Natural Frequency

Frequency Ratio Condition	Quality Ratio Condition	Mass Ratio Condition
$F > 1$	$(Q_2/Q_1) \leq 1$	$\mu \geq 0$
$F > 1$	$(Q_2/Q_1) = 2$	$\mu \geq 0.018$
$F > 1$	$(Q_2/Q_1) = 5$	$\mu \geq 0.082$
$F > 1$	$(Q_2/Q_1) = 10$	$\mu \geq 0.135$
$F > 1$	$(Q_2/Q_1) = 100$	$\mu \geq 0.236$

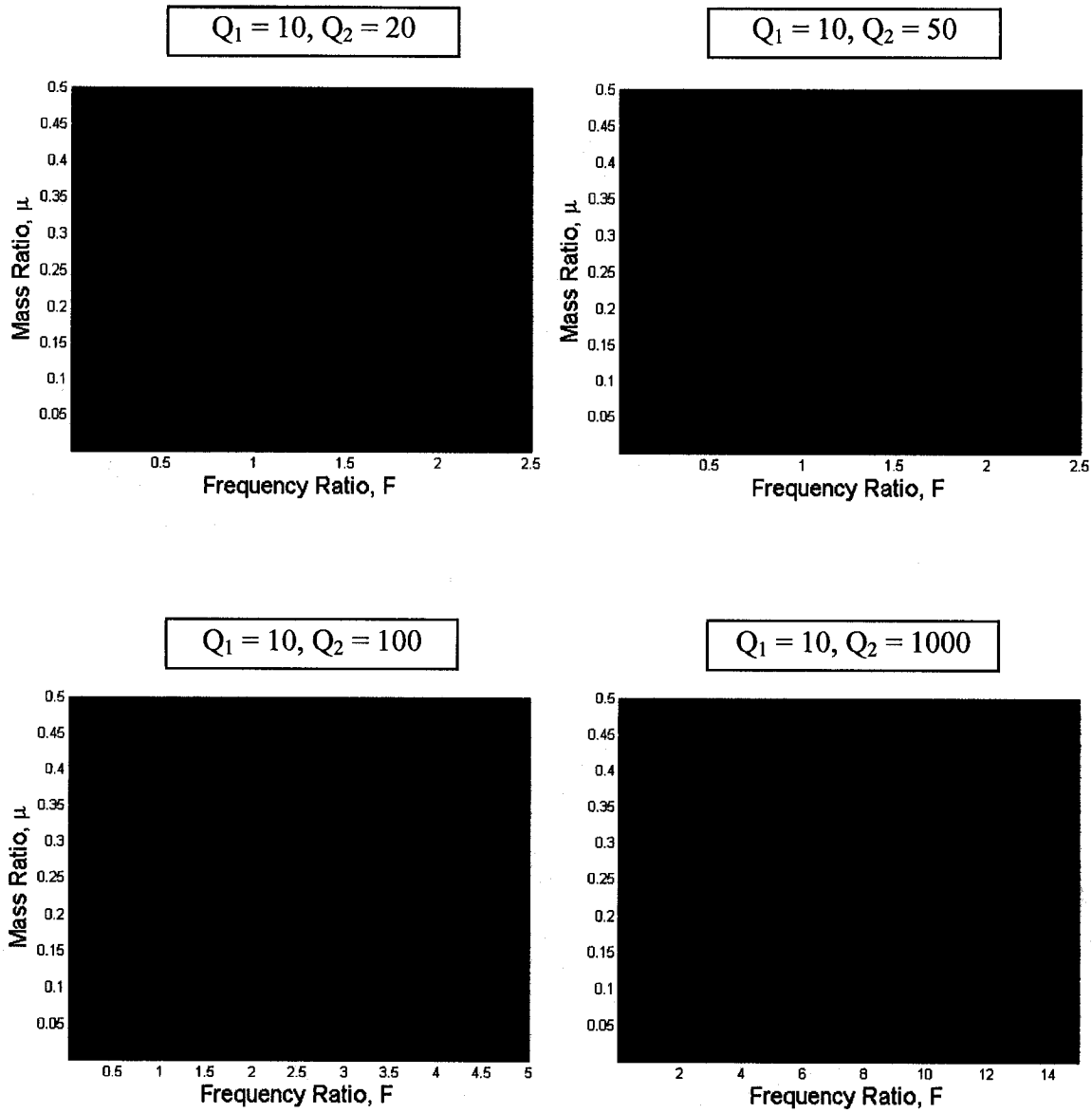

Legend

Blue = H_{10} and H_{20} both occur at the first natural frequency ω_{11}
Red = H_{10} and/or H_{20} do(es) not occur at the first natural frequency ω_{11}

Figure 2.24: System Parameters for the Maximum Responses H_{10} and H_{20} to Both Occur at ω_{11} for a Viscously Damped 2-DOF System where $Q_1 < Q_2$

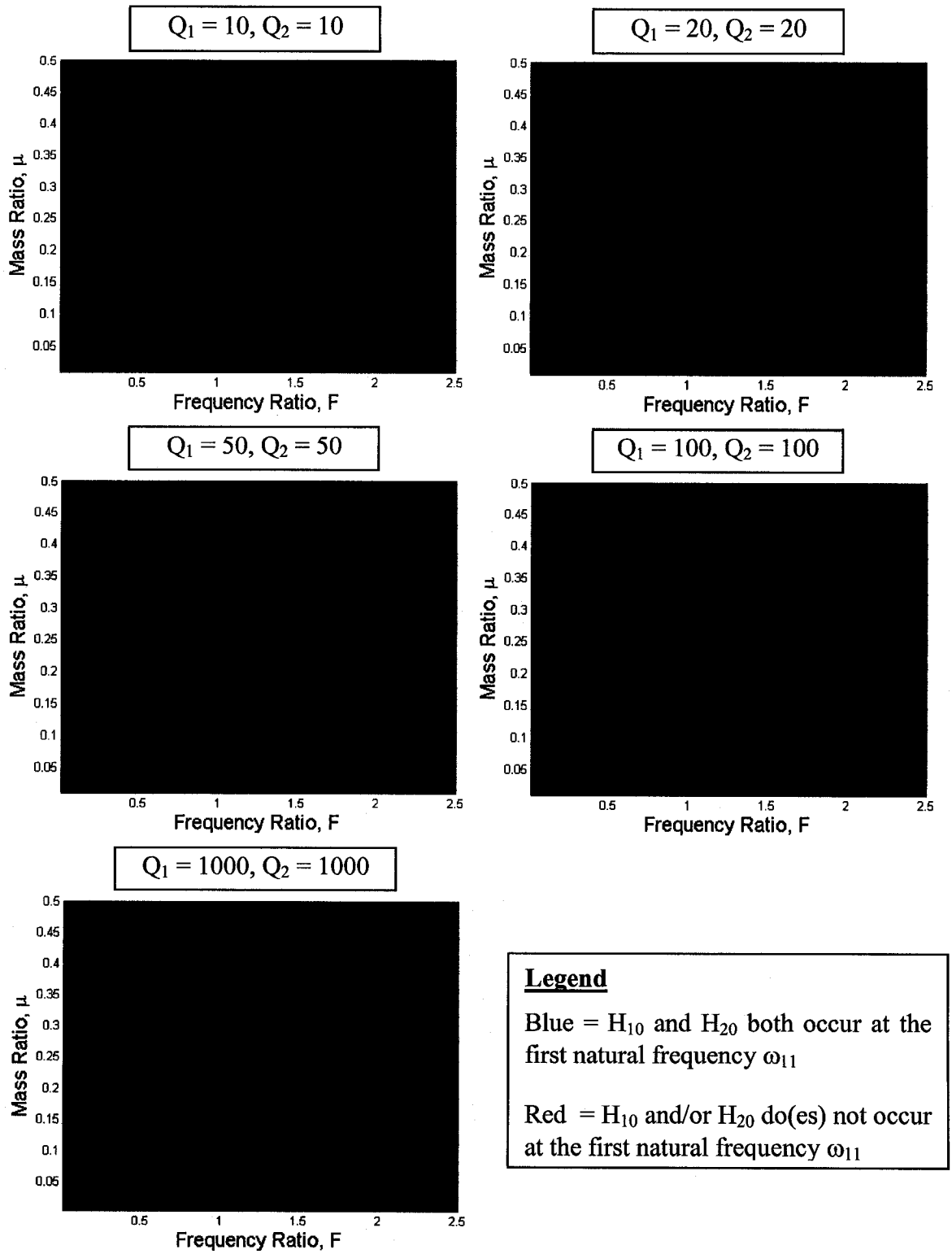

Figure 2.25: System Parameters for the Maximum Responses H_{10} and H_{20} to Both Occur at ω_{11} for a Viscously Damped 2-DOF System where $Q_1 = Q_2$

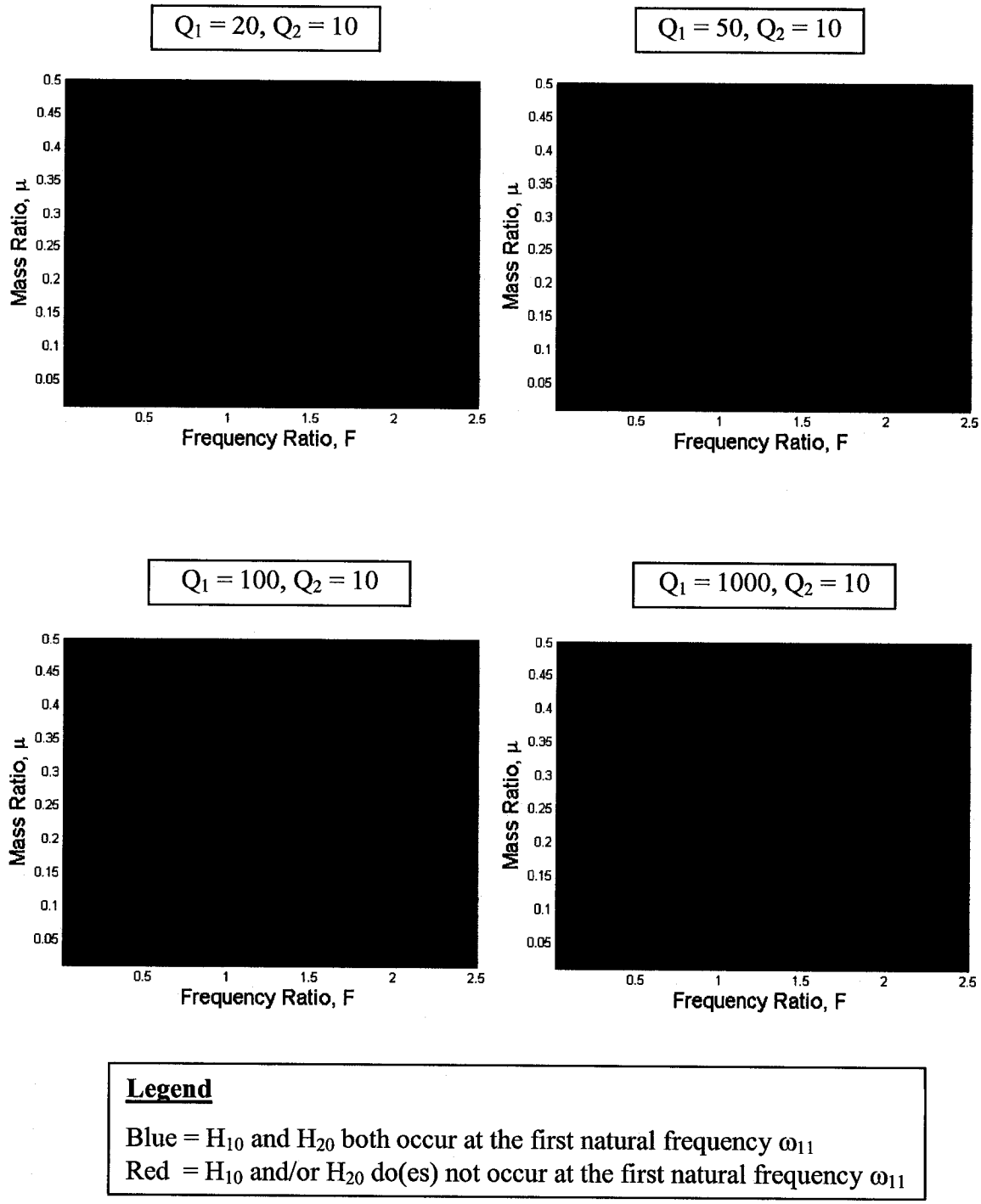

Figure 2.26: System Parameters for the Maximum Responses H_{10} and H_{20} to Both Occur at ω_{11} for a Viscously Damped 2-DOF System where $Q_1 > Q_2$

2.7.4 Summary of the Behaviour of C^2 Based on Analytical Analysis of the Special Cases

For ease of reference, the previous observations for the analytical analysis of the special cases are shown below in point form.

- In general, the value of C^2 depends on all four system-parameters F, μ, Q_1, and Q_2.
- When the maximum frequency responses of H_{10} and H_{20} occur at the same natural frequency R_{11} or R_{22}, the equation for calculating C^2 reduces to equation 2.54 and becomes independent of the source quality factor Q_1.
- When the maximum frequency responses of H_{10} and H_{20} are at the same natural frequency R_{11} or R_{22} and the quality factor of the load is very large compared to R_{11} or R_{22}, the equation for calculating C^2 reduces to equation 2.56 and becomes independent of the quality factors Q_1 and Q_2.
- When the maximum frequency responses of H_{10} and H_{20} are at the first natural frequency R_{11}, the quality factor of the load is very large compared to R_{11}, and the frequency ratio F is above unity, the equation for calculating C^2 reduces to equation 2.60 and becomes dependent only on the frequency ratio F.
    - Systems with $F > 1$ and quality factors satisfying the condition $Q_1 \geq Q_2$ will always have the maximum frequency responses H_{10} and H_{20} at the first natural frequency.
    - Systems with $F > 1$ and quality factors satisfying the condition $Q_1 < Q_2$ will have their maximum frequency responses H_{10} and H_{20} occurring at the first natural frequency if the frequency ratio F or the mass ratio μ is large enough.

3 C^2 FOR BASE-EXCITED MULTIPLE DEGREES-OF-FREEDOM AND CONTINUOUS SYSTEMS

The previous chapter dealt with understanding of the value C^2 for a two degrees-of-freedom system. This chapter presents a method for calculating the value of C^2 for any arbitrary multiple degrees-of-freedom or continuous system. Since the method is based on the concept of the apparent mass, the method is referred to as the apparent mass method. The chapter is divided into six main sections.

The first section derives the equations necessary to calculate the value of C^2 for any base-excited multiple degrees-of-freedom or continuous system with a single attachment point between itself and its supporting structure. The derived equations form the basis of the apparent mass method.

The second section discusses multiple degrees-of-freedom or continuous systems with multiple-point attachments and explains how the apparent mass method can deal with these systems.

The third section discusses parameters affecting the apparent mass of a system. Since the apparent mass is a key parameter in determining the value of C^2, knowledge of how the apparent mass can change with various parameters will lead to a better understanding regarding the behaviour of the value of C^2.

The fourth section examines practical issues regarding the measurement of the apparent mass of a system. In theory, measuring the apparent mass is simple. However, there are many practical complications that must be appreciated in order to properly evaluate the value of C^2 using the apparent mass method.

The fifth section summarizes the apparent mass method and gives two examples demonstrating its use and accuracy.

The sixth section presents a summary of the apparent mass method.

3.1 Multiple Degrees-of-Freedom or Continuous Systems with Single Attachment Point

3.1.1 Apparent Mass

Consider the apparent mass for a multiple degrees-of-freedom or continuous load-structure mounted through a single attachment point on a multiple degrees-of-freedom or continuous source-structure. Since there is only a single attachment point between the source and the load, the interface force spectral density S_{ff} between the source and the load can be expressed in terms of the apparent mass of the load M_{app} and the source acceleration spectral density at the base of the attachment point S_{aa} as follows [5].

$$S_{ff}(f) = \left|M_{app}(f)\right|^2 \cdot S_{aa}(f) \tag{3.1}$$

The apparent mass of the load is by definition a frequency response function describing the ratio of the interface force to the single attachment point base acceleration. Being a frequency response function, the apparent mass of the load is purely a structural characteristic of the load in terms of its stiffness, mass, and damping, and is independent of the structural characteristics of the structure it is mounted on. As such, if a specific acceleration spectral density is applied at the base of the load, the same interface force will develop regardless of whether the load is mounted on the source or on the vibration shaker, as long as all external forces on the load are either absent or negligible [12]. Consequently, the apparent mass function measured on a shaker table is the same apparent mass function of the test article when mounted on the source in the flight configuration. This apparent mass can be measured prior to testing by exciting the structure with a known acceleration spectral density S_{aa} and measuring the resulting force spectral density S_{ff} at the interface. Thus, according to equation 3.1 the apparent mass squared of the load can be measured using

$$\left|M_{app}(f)\right|^2 = \frac{S_{ff}(f)}{S_{aa}(f)} \tag{3.2}$$

Note that measuring the apparent mass directly as per equation 3.2 curtails the problem of determining what type or types of damping mechanisms are present, be it viscous damping, structural damping or any other type or combination of damping that may be present.

3.1.2 Relationship Between Apparent Mass and C^2

First, consider the interface acceleration spectral density $S_{aa\_flight}(f)$ and the interface force spectral density $S_{ff\_flight}(f)$ occurring between a load and a source during launch. The maximum value of $S_{aa\_flight}(f)$ occurs at a specific frequency labeled f_{max_acc} such that the maximum interface acceleration can be expressed as $S_{aa\_flight}(f_{max\_acc})$. Similarly, the maximum value of $S_{ff\_flight}(f)$ occurs at a specific frequency labeled f_{max_force} such that the maximum interface force can be expressed as $S_{ff\_flight}(f_{max\_force})$. Note that, in general, the frequencies f_{max_acc} and f_{max_force} are not necessarily the same frequency.

The value of C^2 describes the maximum interface force spectral density occurring during flight, $S_{ff\_flight}(f_{max\_force})$, normalized by the mass of the load squared M_0^2 and the maximum flight interface acceleration spectral density (ASD) $S_{aa\_flight}(f_{max\_acc})$ [5]. This can be written as

$$C^2 = \frac{S_{ff\_flight}(f_{max\_force})}{M_0^2 \cdot S_{aa\_flight}(f_{max\_acc})} \tag{3.3}$$

But according to equation 3.1, the maximum interface force spectral density $S_{ff\_flight}(f_{max\_force})$ can be expressed as

$$S_{ff\_flight}(f_{max\_force}) = \left|M_{app}(f_{max\_force})\right|^2 \cdot S_{aa\_flight}(f_{max\_force}) \tag{3.4}$$

Consequently, the value of C^2 is

$$C^2 = \frac{\left|M_{app}(f_{max\_force})\right|^2}{M_0^2} \cdot \frac{S_{aa\_flight}(f_{max\_force})}{S_{aa\_flight}(f_{max\_acc})} \tag{3.5}$$

Consider the ratio $\frac{S_{aa\_flight}(f_{max\_force})}{S_{aa\_flight}(f_{max\_acc})}$ of equation 3.5. By definition, the value of the maximum interface acceleration spectral density $S_{aa\_flight}(f_{max\_acc})$ must be equal to or greater than the value of the acceleration spectral density evaluated at any other frequency. Therefore, the following relationship is always applicable.

$$\frac{S_{aa\_flight}(f_{max\_force})}{S_{aa\_flight}(f_{max\_acc})} \leq 1 \tag{3.6}$$

Consequently, the maximum value of C^2 is

$$C^2 \leq \frac{\left|M_{app}(f_{max\_force})\right|^2}{M_0^2} \tag{3.7}$$

Equations 3.5, 3.6, and 3.7 form the basis of a new proposed method of determining the value of C^2. The new method is called the apparent mass method.

3.1.3 Usefulness of the Apparent Mass Method

Equation 3.5 gives the theoretically exact relationship for evaluating the value of C^2 for any multiple degrees-of-freedom or continuous system with a single attachment point. Similarly, equation 3.7 describes the maximum possible value of C^2 for any multiple degrees-of-freedom or continuous system with a single attachment point. At first glance, one might think that these equations are not very useful since the value f_{max_force} can only be known if the value of $S_{ff\_flight\_max}$ is known and the point of the semi-empirical method

is to find an estimate for $S_{ff\_flight\_max}$. However, as will be demonstrated, these equations help understand the factors affecting the interface force and the presented equations can be most useful in many practical situations.

Consider equation 3.5. This equation shows that the maximum interface force depends on the dynamics of the coupled source-load system through the three values f_{max_force}, $S_{aa\_flight}(f_{max\_force})$, and $S_{aa\_flight}(f_{max\_acc})$. The remaining required pieces of information, M_{app} and M_0, are purely characteristics of the load, which can be measured directly during testing. In addition, equation 3.5 shows that the only two frequencies of interest are f_{max_force} and f_{max_acc}, which by definition of resonance occur at one of the natural frequencies of the coupled system. The response of the source, the load, or the source-load system at any other frequency is irrelevant in calculating the value of C^2. Thus, equation 3.5 shows that even if a structure has several pronounced modes in its apparent mass function, even if some of which are very closely spaced natural modes, only the responses at f_{max_force} and f_{max_acc} are relevant in calculating the value of C^2.

Equation 3.5 also shows that if $f_{max\_force} \neq f_{max\_acc}$ then C^2 depends on the damping of both the source and the load because S_{aa_flight} will be a function of these parameters. If the situation $f_{max\_force} = f_{max\_acc}$ occurs, then C^2 depends only on the damping of the load since C^2 will be independent of S_{aa_flight}; and M_{app} is a function of the damping in the load but not the damping in the source. However, if f_{max_force} is not near any resonance or anti-resonance of M_{app}, then the value of C^2 will essentially be independent of damping. This fact is demonstrated later on in figure 3.5.

Next, consider the case when the function S_{ff_flight} is unknown but the function S_{aa_flight}, the acceleration spectral density of the source in the coupled flight configuration, is known. Note that it is with the function S_{aa_flight} that the simplified test spectrum is based on. With this single piece of information one can determine S_{ff_flight} by measuring the normalized apparent mass of the load and applying equation 3.1 resulting in

$$S_{ff\_flight}(f) = \left|M_{app}(f)\right|^2 \cdot S_{aa\_flight}(f) \tag{3.8}$$

Once S_{ff_flight} is known, the maximum value $S_{ff\_flight}(f_{max\_force})$, and the associated frequency f_{max_force}, can be identified. Similarly, the values of $S_{aa\_flight}(f_{max\_acc})$ and $S_{aa\_flight}(f_{max\_force})$ can be identified from the given function S_{aa_flight}. Thus, with knowledge of the function of S_{aa_flight} the correct value of C^2 can be predicted because M_{app} and M_0 can be measured directly during testing.

The correct value of C^2 can be obtained with even less information. Consider that the frequencies f_{max_force} and f_{max_acc} must coincide with one of the natural frequencies of the coupled system. Consequently, the full function S_{aa_flight} need not be known, only the values of S_{aa_flight} at the natural frequency of the coupled source-load system are required.

Now consider the case when S_{aa_flight} is not known at the time of testing. For example, an arbitrary test spectrum, assumed to envelop the peaks of the actual unknown spectrum S_{aa_flight}, may have been specified for testing without actual knowledge of S_{aa_flight}. In this case, no information regarding the value of the ratio $\frac{S_{aa\_flight}(f_{max\_force})}{S_{aa\_flight}(f_{max\_acc})}$ can be obtained. However, this value is known not to exceed unity. Previous work in section 2.7.3.1 has identified the necessary conditions for f_{max_force} and f_{max_acc} to both occur at the first natural frequency for the two degrees-of-freedom system. When this occurs, the ratio $\frac{S_{aa\_flight}(f_{max\_force})}{S_{aa\_flight}(f_{max\_acc})}$ will be unity. The criteria for the two degrees-of-freedom system may be used as a basis to judge when the value of the ratio $\frac{S_{aa\_flight}(f_{max\_force})}{S_{aa\_flight}(f_{max\_acc})}$ will be unity for higher order systems. By assuming that the ratio $\frac{S_{aa\_flight}(f_{max\_force})}{S_{aa\_flight}(f_{max\_acc})}$ is equal to unity, the maximum value of C^2 can be found using equation 3.7, repeated below

$$C^2 \leq \frac{\left|M_{app}(f_{max\_force})\right|^2}{M_0^2} \tag{3.7}$$

The only piece of information required to utilize equation 3.7 is the value of f_{max_force}. The value of f_{max_force} is known to correspond to one of the natural frequencies of the coupled source-load system. Consequently, if the natural frequencies of the coupled source-load system are known, then a maximum value for C^2 can be determined by applying equation 3.7 to all known resonant frequencies and taking the largest resulting value for C^2. Alternatively, consider the fact that the value of the apparent mass reduces considerably for frequencies greater than the corner frequency f_0, identified as the most pronounced resonance on the apparent mass function. This fact is captured in the semi-empirical method in equations 1.4 and 1.6. Using the same assumption as in the semi-empirical method that the maximum force occurs at a frequency that is equal to or less than the corner frequency f_0 [5], then only the few natural frequencies of the coupled source-load system that are equal to or less than the corner frequency f_0 need to be evaluated.

If the natural frequencies of the uncoupled source $S_{aa\_source\_free}$ are known instead of the natural frequencies of the coupled source-load system S_{aa_flight}, then one must estimate the shifts in natural frequency that will occur in the coupled system. For a source-load system with a single attachment point, the value of S_{aa_flight} can be calculated exactly by knowing the apparent mass function of both the source and the load using [12, 24]

$$S_{aa\_flight}(f) = \left| \frac{\mathrm{M}_{app\_source}(f)}{\mathrm{M}_{app\_source}(f) + \mathrm{M}_{app\_load}(f)} \right|^2 \cdot S_{aa\_source\_free}(f) \tag{3.9}$$

In the literature, it is sometimes unclear what constitutes M_{app_source}. In equation 3.9, the value of M_{app_source} is defined as the ratio of a force applied on the uncoupled source, at the location where the load would be attached, to the resulting acceleration of the source at the location of the source-load attachment point. Thus, the apparent mass must be evaluated with an uncoupled source having the same boundary condition as the coupled source-load system. For example, in the case where the load is an instrument on a spacecraft and the source is a spacecraft that can be modeled as a two degrees-of-freedom system, then the required model to determine the apparent mass of the source is as shown

in figure 3-1 a. However, in the case where the load is the spacecraft and the source is the launch vehicle that can be modeled as a two degrees-of-freedom system, then the required model to determine the apparent mass of the source is shown in figure 3-1 b. In both instances, the apparent mass of the uncoupled source is $M_{app\_source} = F/\ddot{x}_2$.

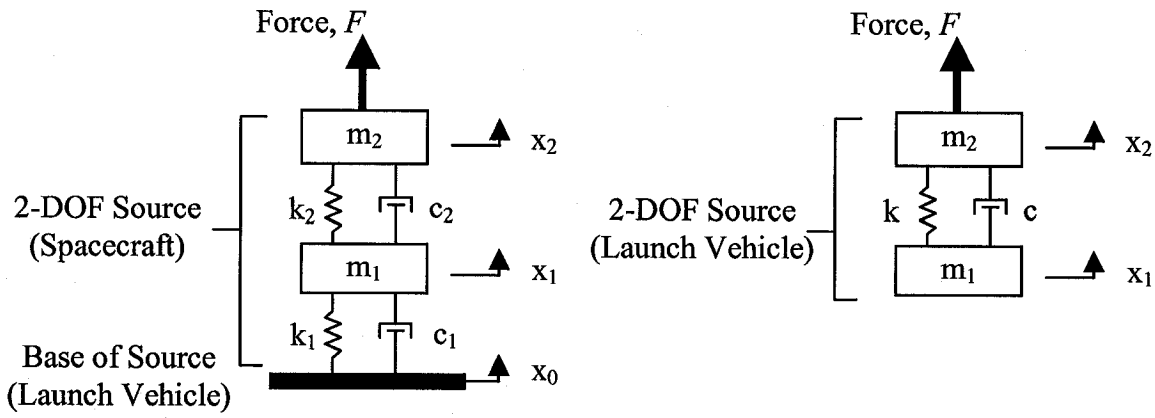

Figure a Figure b

Figure 3.1: Source Apparent Mass Definition

Previous work on the two degrees-of-freedom system has shown through equations 2.37 and 2.38 that, for the two degrees-of-freedom system, the frequency shifts will be a function of the uncoupled load-to-source natural frequencies ratio, F, as well as the load to source mass ratio μ. This information can be utilized as a basis to estimate the frequency shift for multiple degrees-of-freedom or continuous systems. The force limited method works best with load structures that exhibit a single pronounced mode [25]. Thus, the corner frequency f_0 associated with the frequency of maximum response of the apparent mass function of the load can arguably be considered as a single degree-of-freedom system. In addition, since the natural frequencies of interest are below the corner frequency f_0, only the lowest natural frequency predicted by the two degrees-of-freedom system is considered. Consequently, the natural frequencies of the coupled system can be approximated using equations 2.37, shown below in a more useful form.

$$f_{nn\_coupled} = \sqrt{\frac{1+F^2(1+\mu) - \sqrt{\left[1+F^2(1+\mu)\right]^2 - 4F^2}}{2F^2}} \cdot f_0 \qquad (3.10)$$

Equations 3.10 would be utilized once for every uncoupled source natural frequency below the load corner frequency f_0. In equation 3.10, the mass ratio μ would be taken as the ratio of the physical masses of the system. In the absence of mass information for the source, the value of the mass ratio μ could be taken as infinitesimally small resulting in the least possible amount of frequency shift. In this case, the coupled natural frequencies of the source-load system will essentially be equal to the uncoupled natural frequencies of the free source if the uncoupled natural frequency is below the corner frequency f_0. The frequency ratio F in equation 3.10 would be defined as the ratio of the load corner frequency f_0 to the uncoupled natural frequency of the source of interest: $F = \frac{f_0}{f_{n\_uncoupled\_source}}$.

Finally, consider the case where neither the natural frequencies of the source-load system nor the natural frequencies of the uncoupled source are known. One could still estimate the value of C^2 based on the minimum natural frequency design requirement. In the aerospace industry, a minimum natural frequency requirement is imposed on the designers of the load to ensure that natural frequencies of the load will be well separated from the main natural frequencies of the source. The requirement is imposed specifically to ensure that the load dynamics will not significantly affect the source dynamics. Steinberg [26] has suggested that the uncoupled natural frequency of the load should be at least a factor of 2 higher or lower than the uncoupled natural frequency of the source. Since the design requirement is a minimum natural frequency, the uncoupled natural frequency of the load will be higher than the uncoupled natural frequency of the source. Thus, if a 100 Hz minimum natural frequency requirement is imposed on a load, the main natural frequency of the uncoupled source will be around 50 Hz or lower. Since the factor of 2 is somewhat arbitrary, one could assume a less conservative factor on the natural frequency spacing, such as 1.3. For example, if the load structure had a minimum natural frequency requirement of 100 Hz, the source would be assumed to have its

uncoupled natural frequency of 100 Hz / 1.3 = 77 Hz. Assuming that the mass of the load is small compared to the mass of the source, the assumed natural frequency of 77 Hz for the uncoupled source would essentially be the same as the coupled source-load system. As such, one would assume a value of 77 Hz for f_{max_force} and equation 3.7 could be utilized to estimate an upper value for C^2.

The above suggestions regarding how the equations 3.5 and 3.7 of the apparent mass method may be utilized are meant to give a defensible reasoning why a particular value of C^2 was chosen. For instance, it may be easier to justify that the coupled natural frequency source-load system will be within a certain range, resulting in a specific maximum value for C^2, than to justify a particular value for C^2 based on personal experience. Therein lies the usefulness of the apparent mass method.

The equations developed for the apparent mass method assume that a single attachment point is present between the load and the source. The next section considers the implications of load structures with multiple attachment points.

3.2 Multiple Degrees-of-Freedom or Continuous Systems with Multiple Attachment Points

For structures with a single attachment point, the force at the interface is determined by the knowledge of the apparent mass function and the input acceleration. Since there is a single point, no phase information is required.

Structures with multiple attachment-points may have different amplitudes and phase relationships between the accelerations at the different attachment points when in the flight configuration. These effects are typically not captured during vibration testing since the single axis shaker commonly utilized to perform vibration testing produces only one excitation. As such, these differences in excitation between the flight configuration and the test configuration affect vibration testing in general, regardless of whether or not a force limiting method is utilized to perform notching. However, since almost all practical structures have multiple attachment points, it is useful to understand how

multiple attachment points affect the interface forces. The following text describes the differences in acceleration between the flight and test configuration in terms of the excitation of the attachment points with the aid of an example.

3.2.1 Differences Between Flight and Test Excitation

Consider any structure with linear response. The response of this structure to any excitation can be described as a weighted linear combination of its normal modes [21]. The weighing factor for each mode depends on how the structure is excited. To better understand this statement, consider the two degrees-of-freedom system (2-DOF) with two attachment-points shown in figure 3.2.

Being a two degrees-of-freedom system, this system will have two natural frequencies and two corresponding mode-shapes. For this symmetrical system, the first mode shape is a pure up down motion in x and the second mode shape is a pure rotation in θ about the center-of-mass (C-of-M) of the system [21].

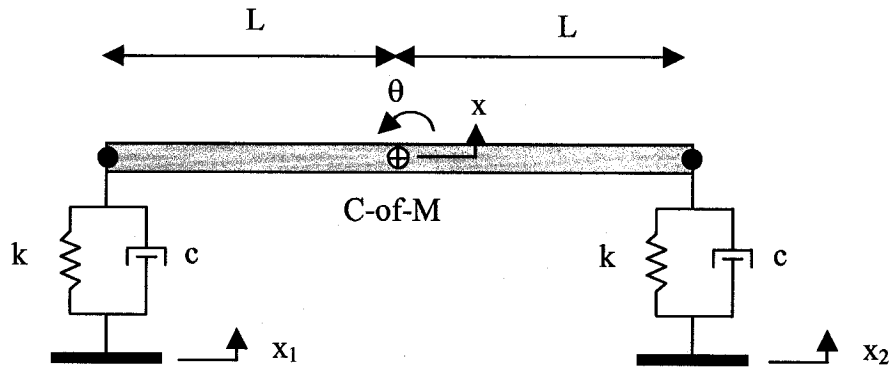

Figure 3.2: 2-DOF System with 2 Attachment-Points

First, consider what happens when the two attachment-points x_1 and x_2 experience the same excitation magnitude and the excitations are in phase with one another. The result will be a response described purely by the first mode shape because there are no moments about the center-of-mass of the bar to cause rotation. Consequently, the second mode shape is not excited. As a result, the total interface force will be at its maximum and the total moment about the center-of-mass will be zero.

Next, consider what happens when the two attachment-points x_1 and x_2 experience the same excitation magnitude as in the previous example but the excitations are now 180° out of phase with one another. The result will be a response described purely by the second mode shape because a pure moment is applied at the center-of-mass of the bar. Consequently, the first mode shape is not excited. As a result, the total interface force is zero and the total moment about the center-of-mass is at its maximum.

Note that in both previous examples, the acceleration spectral density function that would be utilized to describe the base motion from random excitation would be identical, since the acceleration spectral density contains no phase information; yet two very different responses can be observed depending on the phase relationship between the attachment points. In the general case where the magnitude of the accelerations at the attachment points are not identical and the phase between the excitation points is arbitrary, the resulting motion will be a linear combination of up-down movement from the first mode and rotation from the second mode leading to both a force and moment at the interface.

3.2.2 Effect on the Interface Forces

The previous example shows that both forces and moments are present at the interface and that both are required to properly describe the excitation of a structure with multiple attachment points. Changes in amplitude or phase in the excitation of the attachment points will necessarily modify both the forces and the moments at the interface. Thus, the forces at the source-load interface is a function of the apparent mass of the load and the manner in which the load is excited, including any amplitude and phase difference of the attachment points. The excitation of the load depends in turn on the attachment point responses for the source-load structure experience during the flight.

3.2.3 Effect on Testing in General

Consider the source and load in their flight configuration as a single structure. Every point on the source will have a different acceleration amplitude and phase relationship depending on the frequency of the excitation and the mode-shapes of the source-load

system. At low excitation frequencies well below any resonance, the source will behave essentially as a rigid body and all points on it will have nearly equal acceleration time histories. As such, the amplitude and phase will be similar at every point on the source at the low frequencies. In addition, all points on the source will have similar acceleration spectral densities and cross-spectral densities since the time histories are similar. As the excitation frequency at the base of the source is increased, the differences in responses in terms of magnitude and phase at different load attachment points on the source become more pronounced until responses can no longer be considered similar based on arbitrary chosen comparison criteria for both magnitude and phase. As the excitation frequency is further increased, the responses at different attachment points may become similar again. The first frequency at which the responses at the different attachment points are no longer considered similar is identified as the critical test frequency. This critical test frequency depends on the mode-shapes of the source-load flight configuration and the location of the attachment points on the source. In practice, the critical test frequency could be computed from a frequency response analysis of the coupled system. For frequencies greater than this critical test frequency, the responses between attachment points may or may not be considered similar, depending on the mode shapes being excited.

Now consider the acceleration experienced at the attachment points during testing. Although multiple degrees-of freedom shakers are available, typically, vibration tests are performed on a single degree-of-freedom shaker where the shaker excites all attachment points with essentially the same acceleration time history throughout all test frequencies. Thus, all attachment points are excited with equal amplitude and are in phase with each other. Also, because the attachment points have the same time history, all points will have the same acceleration spectral density and the cross-spectral densities will all be identical to the acceleration spectral densities. Assuming that the first natural frequency of the vibration table and test fixture structure is significantly higher than the greatest test frequency, the manner in which the load is excited during testing in terms of amplitude and phase at the attachment points essentially does not change with frequency.

Thus, the response of the load during testing is guaranteed to be representative of the flight response only up to the critical test frequency chosen by an arbitrary definition of similar phase and magnitude acceleration response between attachment points. This critical test frequency depends on the source-load flight response and the location of the attachment points. However, the critical test frequency will likely be higher for loads having smaller distances between their attachment points since the response between these closer attachment points are more likely to be similar to each other for a greater range of frequencies.

At frequencies higher than the critical test frequency, the load may be excited differently during testing compared to during flight. Since the measured apparent mass determined from vibration testing only accounts for in-phase and same-magnitude excitations, the interface forces experienced in-flight will be different than the ones experienced during testing if the attachment points do not receive the same excitation. In other words, for frequencies greater than the critical test frequency, the flight interface force may be significantly different than the measured interface force during testing, even if the input acceleration spectral densities in both cases are identical.

Note that during traditional vibration testing, only the value of the acceleration spectral density from a specific location or from the average of several locations can be controlled. The phase between the attachment points cannot be controlled using a single shaker.

3.2.4 Effect on the Apparent Mass Method

For multiple-attachment point systems, the apparent mass method can be utilized to correctly predict and limit the interface forces for frequencies up to the critical test frequency with certainty and possibly beyond the critical test frequency depending on the details of the modes of the coupled system and the location of the attachment points. As such, the frequency corresponding to the maximum force in the flight configuration should ideally be below the critical test frequency.

If this critical test frequency is lower than the frequency where the maximum force occurs in the flight configuration, there is a risk of either over-testing or under-testing the load, when using a single axis shaker. This occurs regardless of what method is utilized to perform notching since the test input may no longer excite the same modes as the flight configuration.

In practice, the maximum flight interface force and the maximum flight acceleration often occur below the frequency corresponding to the load's most pronounced apparent mass resonance, which is usually the load's first natural frequency and is identified as the corner frequency f_0. This statement is part of the assumptions utilized in the semi-empirical method [5]. If the load has its largest apparent mass response at its first mode, notching the input near the first mode of the load will account for a significant reduction in the root-mean-square (RMS) level of the interface force. Thus, the apparent mass method can be used successfully in reducing over-testing without causing under-testing in many practical instances.

In summary, the following guidelines for structures with multiple attachment points will ensure that the force-limited method, including the apparent mass method, will successfully and significantly notch the acceleration input such that under-testing or over-testing due to differences between the test and flight excitation levels are minimized.

- In the flight configuration, the relative magnitude of the acceleration of the attachment points can be considered identical and in phase with each other to an arbitrary degree up to a critical test frequency.
    - Smaller distances between the attachment points will increase the value of the critical test frequency.
- Ideally, notching should only be performed up to the critical test frequency. The modes excited during testing for excitation frequencies larger than the critical test frequency may not be representative of the modes excited in the flight environment.

- The critical test frequency should be higher than the maximum force frequency of the flight configuration to correctly estimate the interface force during flight using the apparent mass method.
- The critical test frequency should be higher than all load natural frequencies that are of interest for possible notching. This condition ensures that the test excitations at these frequencies are similar to the flight excitations.

3.3 Parameters Affecting Apparent Mass

Since per equation 3.5, the apparent mass was found to be a necessary parameter that must be evaluated in order to determine the value of C^2, an understanding of the parameters that can affect the value of the apparent mass is required to understand the parameters that will affect the value of C^2.

The apparent mass can be expressed in terms of all the effective masses of the system. For a system with N modes, the apparent mass is equal to [27]

$$M_{app}(f) = \sum_{j=1}^{N} m_{eff\,j} \cdot H_{1\text{-}DOF\,j}(f) \tag{3.11}$$

Where $H_{1\text{-}DOF}$ is the force transmissibility function for a fixed base single degree-of-freedom system. This force transmissibility is dependent on the type of damping present. For example, for a viscously damped system, the transmissibility function can be expressed as [27]

$$H_{1\text{-}DOF} = \frac{1 + i \cdot \frac{f}{f_n} \cdot \frac{1}{Q}}{1 - \left(\frac{f}{f_n}\right)^2 + i \cdot \frac{f}{f_n} \cdot \frac{1}{Q}} \tag{3.12}$$

While for a structurally damped system, the force transmissibility function can be expressed as (see appendix G)

$$H_{1\text{-DOF}} = \frac{1+\frac{i}{Q}}{1-\left(\frac{f}{f_n}\right)^2+\frac{i}{Q}} \tag{3.13}$$

In situations where only a subset of all possible natural frequencies is known, the apparent mass can be approximated with [27]

$$M_{app}(f) \approx M_{residual\_n} + \sum_{j=1}^{n} m_{eff\,j} \cdot H_{1\text{-DOF}\,j}(f) \tag{3.14}$$

Where $n < N$ and the residual mass, $M_{residual\_n}$, is defined as

$$M_{residual\_n} = M_0 - \sum_{j=1}^{n} m_{eff\_j} \tag{3.15}$$

The apparent mass, and therefore the value of C^2, is consequently a function of the effective masses, the natural frequencies, and the type and amount of damping present in the load. Since the natural frequencies and the effective masses depend on the boundary conditions as well as the structural parameters of the load, the boundary conditions such as the number of attachment points will also have an effect on the value of C^2.

From equation 3.11, one can conclude that the maximum peak value of the apparent mass of a system with many small effective masses will not be as high as for a system with a single dominant effective mass, assuming the same Q factor between both systems. Thus, by equation 3.7, structures that have many small, distributed effective masses with low Q will tend to have lower maximum values for C^2. Conversely, high maximum values of C^2 are only possible for systems that have a pronounced effective mass and high Q.

Consider what happens to the apparent mass of the load when the number of attachment points is increased. By changing the boundary conditions in this manner, the mode shapes of the system will change, resulting in a different effective mass distribution for

each new mode. This change in effective masses will affect the apparent mass as per equation 3.11, and in turn will affect the value of C^2 as per equation 3.5.

To better appreciate how the apparent mass can change with different boundary conditions, the apparent mass of two arbitrary objects is calculated and compared to each other in the next subsection.

3.3.1 Effective Mass and Boundary Conditions

As a demonstration of the effects entailed by a boundary condition change and differences in the magnitude of the effective masses, consider the apparent mass of a square aluminum plate with two different boundary conditions. The plate has dimensions of 20 cm x 20 cm x 0.2 cm thick. A density of 2700 kg/m^3 and a modulus of elasticity of 69 GPa were assumed for the properties of the aluminum. In the first instance, the plate is simply supported along its entire perimeter. In the second instance, the plate is also simply supported along its perimeter but has four additional fixed points located at 5 cm inside the edges of the plate. The two different boundary conditions are shown below in figure 3.3.

To find apparent mass of each object in the direction normal to the view presented in figure 3.3, the COSMOS/Works [28] finite element program was utilized to calculate the mass participation factors for the first 50 modes. The mass participation factor of each mode was then multiplied by the total mass of 2.16 kg to get the effective mass for that mode. The sum of the 50 effective masses totaled more than 90% of the entire mass of the simply supported plate and totaled over 87% of the entire mass for the simply supported plate with 4 fixed-points.

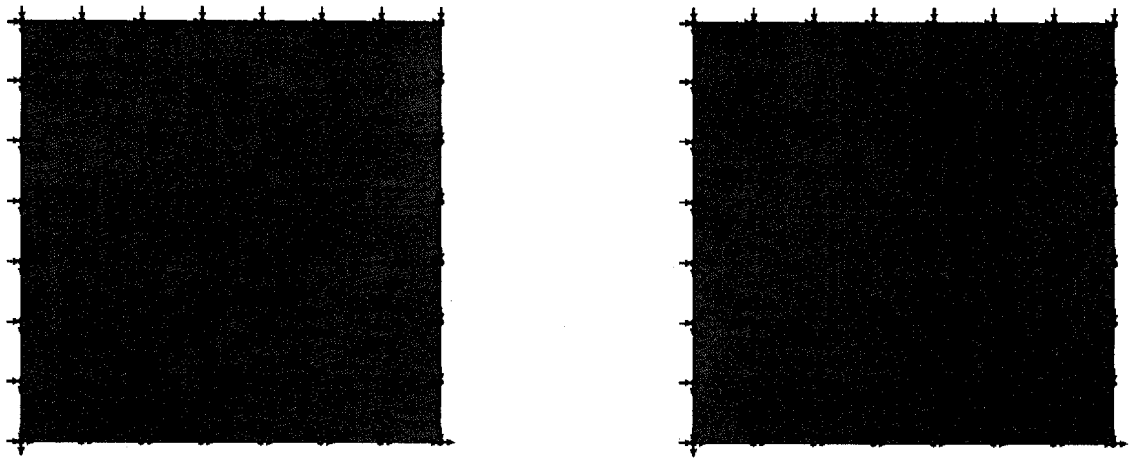

Simply Supported along Perimeter

Simply Supported along Perimeter and Fixed at 4 Points

Figure 3.3: Plate Configurations

The normalized apparent mass of each configuration was then calculated with the aid of equations 3.14 and 3.15 using a MATLAB program [22] as shown as program 6 in appendix D, where each mode was assumed to have viscous damping with a Q of 20. The results are shown in figure 3.4 and table 3.1.

The data in table 3.1 shows that the boundary conditions have an influence on the effective masses, which according to equation 3.11 will have an influence on the apparent mass, which in turn influences the value of C^2 as per equation 3.5. The value of C^2 is therefore observed to be a function of the number of attachment points. This observation is consistent with the observations reported by Dharanipathi [7].

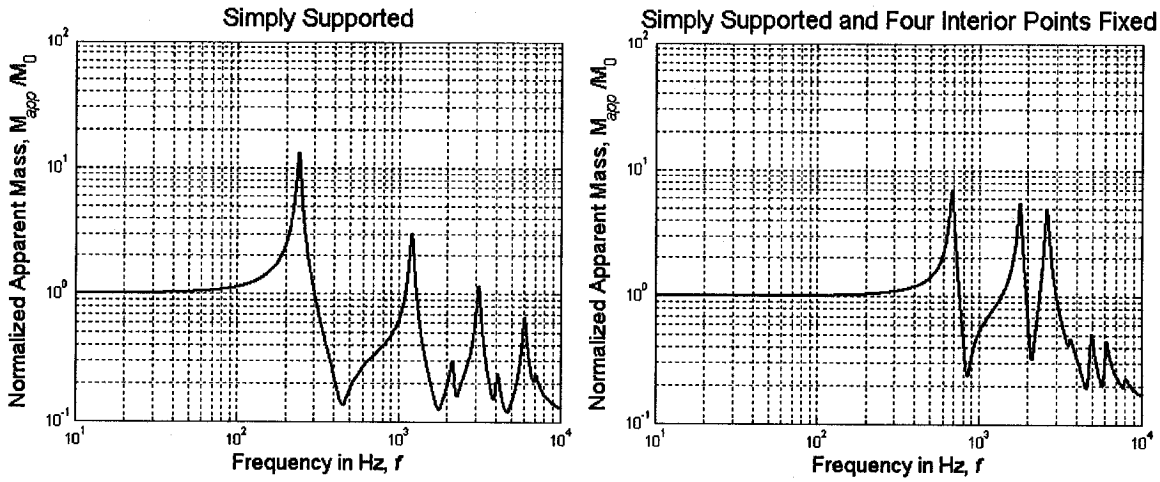

Figure 3.4: Apparent Mass Comparison

Table 3.1: Comparison of Selected Values

Peak Normalized Apparent Mass and C^2 Comparison	**Simply Supported**	**Fixed**
Peak Normalized Apparent Mass	13.26	7.00
Maximum Value of C^2	176 (= 13.26^2)	49 (= 7.00^2)
Mode Number Associated with peak	1	1
Mode 1 Details		
Frequency	242 Hz	684 Hz
Effective Mass	66% of total mass	34% of total mass
Q	20	20

3.3.2 Damping

The maximum value of C^2 in table 3.1 can be explained by examining equation 3.11. In this equation, the apparent mass, which determines the value of C^2, is expressed as a finite sum of the product of the effective mass and the force transmissibility for every mode.

The effective masses are constants and their sum is equal to the actual mass of the object.

The single degree-of-freedom force transmissibility $H_{1\text{-}DOF}$ is a frequency dependent function equal to Q at the natural frequency of the single degree-of-freedom system. The function is approximately equal to unity for frequencies well below the natural frequency and approaches zero for frequencies well above the natural frequency. The above approximations are valid for both viscous and structural damping.

Consequently, for systems with well-separated modes, such as when the half-power points of the modes do not overlap, and similar Q, the maximum value of equation 3.11 can be approximated as

$$M_{app\_max} \approx m_{eff\_max} Q + M_{residual\_max} \tag{3.16}$$

Where, as per equation 3.15, $M_{residual\_max}$ is the residual mass associated with m_{eff_max} and not necessarily the maximum residual mass. Assuming that the product $m_{eff\_max} \cdot Q$ is large compared to $M_{residual\_max}$, then equation 3.16 can be further simplified to

$$M_{app\_max} \approx m_{eff\_max} Q \tag{3.17}$$

Thus, the largest effective mass and the amount of damping can significantly affect the maximum possible value of the apparent mass and therefore the maximum possible value of C^2. From equation 3.7 and 3.17, the maximum possible value for C^2 can be approximated as

$$C^2_{max} \approx \left(\frac{m_{eff\_max}}{M_0} Q \right)^2 \tag{3.18}$$

For example, using data from table 3.1, equation 3.18 gives a maximum value of C^2 as $(0.66 \times 20)^2 = 174$ for the simply supported case and $(0.34 \times 20)^2 = 46$ for the fixed case. These results are very close to the actual values of 176 and 49 reported in table 3.1.

Equation 3.18 is useful for understanding why the force limited method is not well suited for structures that do not have well defined resonance peaks, such as an electronic box

with several printed circuit boards [25]. Structures that do not have well defined resonance peaks have many small effective masses as compared to their total mass and low Q for each resonant mode. Thus, according to equation 3.18, the largest possible value of C^2 will naturally be a low value for these structures. For example, a structure that has a maximum effective mass of 10% of its total mass and a Q of 20 would have a maximum C^2 value of 4.0 according to equation 3.17. If a value of C^2 greater than this maximum value were utilized during testing, there would not be any notching in the input acceleration.

3.4 Practical Issues in Calculating C^2

The previous sections have identified a method for calculating the value of C^2 based on theoretical considerations. The following section presents real life issues that must be appreciated in order to properly estimate the value of C^2 using the apparent mass method.

3.4.1 Force Sensor Correction Factor

For practical reasons, force sensors must be mounted using bolts. The force sensor measures the force through itself and does not report the fraction of the force passing through the bolt. A correction factor is usually applied to the force sensor calibration such that the force sensor reports the actual total force at the interface. The correction factor applied to an individual force sensor's calibration factor must be above unity to account for the part of the force that is transferred through the bolt. However, in special situations, tests utilizing multiple force sensors can require a correction factor that is either much greater than unity or even less than unity if the force sensor signals are added together before a single average calibration factor is applied to the summed signal. Such a special situation did arise during the experimental testing and is discussed in chapter 4. Moreover, the mechanism leading to the correction factor being below unity, or significantly above unity, is discussed in that chapter.

The correction factor should be included when measuring the interface force to determine the measuring apparent mass of the system because it will affect the value of C^2. If it is not included, then the resulting value for C^2 will be off by the square of the correction factor, which could lead to either unnecessary over-testing or undesirable under-testing.

3.4.2 Accuracy of f_{max_force}

The apparent mass method requires the evaluation of the normalized apparent mass squared at the frequency where the maximum force occurs when in the flight configuration. This frequency will correspond to one of the natural frequencies of the flight configuration. The accuracy of this frequency is usually determined to within about 5% of the actual frequency [29], which will entail a corresponding error in the evaluation of C^2. The slope of the normalized apparent mass function squared at the maximum force frequency gives an indication to the sensitivity of C^2 to the predicted value.

3.4.3 Variations in Damping

The apparent mass depends on the damping of the test article, expressed as the Q in equation 3.12 or 3.13. Although the previous statement is true, consider the apparent mass function of two arbitrary viscously damped four degrees-of-freedom systems having identical effective masses but with different Q shown in figure 3.5.

Figure 3.5 shows that the value of the apparent mass is significantly affected by the amount of damping only near resonant and anti-resonant frequencies of the article under test. If the frequency f_{max_force} were to occur away from any resonant or anti-resonant frequencies of the apparent mass, then the value of C^2 could be considered independent of the amount of damping. This observation is consistent with the findings of Chang [6] and Dharanipathi [7].

Now consider that the frequency f_{max_force} must occur at one of the resonant frequencies of the coupled system. Assuming behaviour akin to a two degrees-of-freedom system, equations 2.37 and 2.38 describe the natural frequencies of the coupled two degrees-of-freedom system. From these equations one can see that the only way f_{max_force} will be near a resonant frequency of the load is if the un-coupled source has a natural frequency near the resonant frequency of the load ($F \approx 1$) *and* that the load to source mass ratio is very small ($\mu \rightarrow 0$). In the aerospace industry, a minimum frequency design requirement is imposed to ensure that any load will have a first natural frequency that is significantly higher than the source structure upon which it is mounted on. As such, the apparent mass and the value of C^2 will be essentially independent of the damping for aerospace structures meeting the minimum natural frequency design requirements, regardless of its mass.

For structures where the frequency f_{max_force} is close to a resonant or anti-resonant frequency of the load, the apparent mass has the advantage that the amount of damping does not need to be estimated since it is included in the measurement of the apparent mass. However, one must be aware that in practice the damping characteristic of a structure, described by the Q, can change dramatically with input level, frequency, and boundary condition [26]. A simple tightening of the bolts at the interface can significantly change the Q in some structures resulting in a large difference in the apparent mass value near its resonant or anti-resonant frequencies. Thus, for structures where f_{max_force} is close to a resonant or anti-resonant frequency, the value of C^2 will be highly dependent on the damping and the value of C^2 may change significantly from one test to another, especially if the hardware was removed from the shaker table between tests.

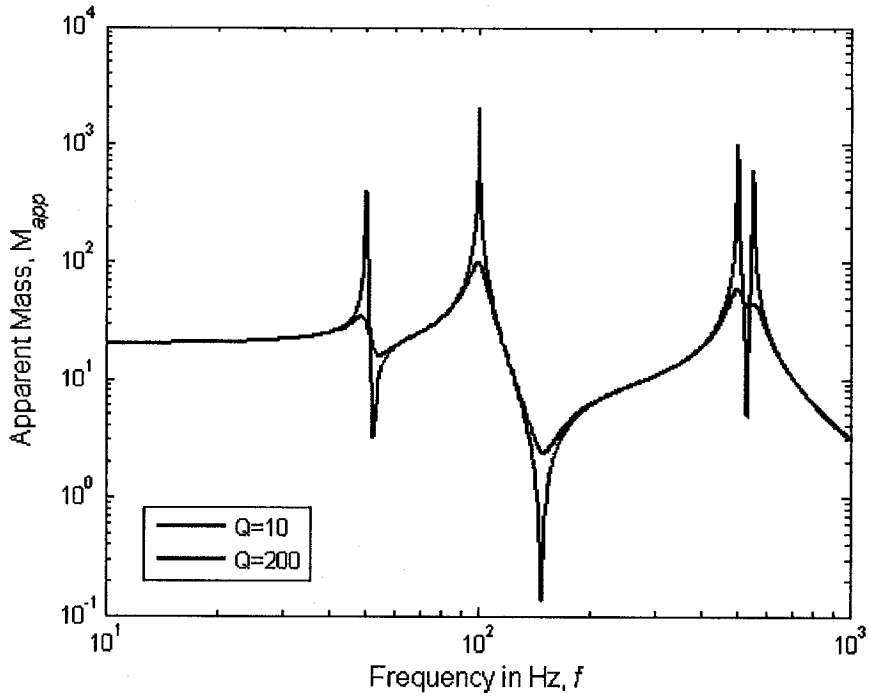

Figure 3.5: Effect of Q on Apparent Mass

3.4.3.1 Excitation Type and Level To Determine Apparent Mass

Since the previous subsection showed that the Q reduces with increasing excitation levels, the apparent mass function determined by a low level excitation may be significantly higher than the apparent mass function determined by a higher excitation level.

The effect of changes in damping with excitation level that results in changes in the measured apparent mass extends to different types of excitation. For example, consider the differences in the measured apparent mass for a random test with constant acceleration spectral density and a slow sine sweep test with constant peak amplitude such that the peak amplitude of the sine test is equal to the RMS level of the random test. Which test will result in a higher apparent mass? Since any response has to build to its full level over a certain number of cycles, it has been suggested [30] that a slow sine sweep test would produce higher responses because the response at each frequency can build up to near its full level. However, consider that the random vibration levels vary

continuously with a normal distribution with a mean of zero. As such, over 68% of the time, the random vibration levels will be under the RMS value [31]. Since Q reduces with increasing excitation levels for many practical structures, these lower vibration levels will contribute to a higher Q and consequently, a higher apparent mass function. The result is that the flat spectrum acceleration spectral density random vibration can produce a higher apparent mass function than the slow sine sweep with peak amplitude equal to the RMS of the random vibration for structures exhibiting a non-linear response to excitation level. This effect was verified experimentally in the next section.

During launch, a structure is excited by both the vibration through its interface and directly by acoustical excitation. Traditionally, these two different types of excitations are tested separately. The acoustical contribution to the interface force can vary from negligible to dominant, depending if the area-to-mass ratio of the structure is small or large. All shaker based vibration tests assume that the base driven excitations are the dominant method of excitation. If this is not the case during flight, then the force measured at the interface during a base-driven test may not be representative of the actual force encountered during flight, since the acoustical excitations may excite different modes of the structure.

3.4.4 Accuracy of Statistical Measurement of $|M_{app}|^2$

When measuring any spectral density, one is actually performing a statistical estimate of the actual value of the spectral density of the process. Thus, there may be differences between the measured estimate of the spectral density and the actual value of the spectral density that can lead to errors in calculating the value of C^2. The statistical distribution of the spectral density has a chi-squared distribution [32].

The accuracy of the measured spectral density to the actual spectral density can be described in terms of the statistical degrees-of-freedom, labeled "r", associated with the chi-squared distribution. The degree of accuracy is controlled by the desired frequency

effective bandwidth resolution B_e, in Hz, of the spectral density measurement and the time duration T_e, in seconds, of the test as [12]

$$r = 2T_eB_e \tag{3.19}$$

The higher the statistical degree-of-freedom is, the better chance that the measured spectral density will be representative of the actual spectral density.

The square modulus of the apparent mass is calculated by taking the ratio of two quantities both having a chi-squared distribution as shown in equation 3.2. Identifying the statistical degree-of-freedom of the force measurement as r_{ff} and the statistical degree-of-freedom of the input acceleration measurement as r_{aa}, the square modulus of the apparent mass will have an F-type distribution with (r_{ff}, r_{aa}) degrees-of-freedom [31].

Consequently, if one wanted to be ϕ = 90% confident, that the actual square modulus of the apparent mass was below a certain value, the measured value would be multiplied by the factor given by the $F_{1-\phi}(r_{ff},r_{aa})$ distribution as

$$\left|M_{app}\right|^2_{\text{actual}} \leq F_{1-\phi}(r_{ff}, r_{aa}) \cdot \left|M_{app}\right|^2_{\text{measured}} \tag{3.20}$$

For example, if the force and acceleration spectral densities both had a statistical degrees-of-freedom of 80, and one wanted to be 90% confident that the actual value of $\left|M_{app}\right|^2_{\text{actual}}$ was equal to or below a certain value, that certain value would be equal to $F_{0.1}(80,80)$ = 1.34 times the measured value $\left|M_{app}\right|^2_{\text{measured}}$.

The value $F_{1-\phi}(r_{ff},r_{aa})$ can easily be obtained using the Microsoft Excel software with the optional analysis toolpack add-in installed and using the command "=FINV(1-ϕ,r_{ff},r_{aa})".

For comparison, table 3.2 shows some values for $F_{1-\phi}(r_{ff},r_{aa})$ for various statistical degrees-of-freedoms (r_{ff},r_{aa}) and confidence intervals ϕ.

The factor $F_{1-\phi}(r_{ff},r_{aa})$ can be used as a basis for a safety factor on the measured value of $|M_{app}|^2$. Note that a safety factor based solely on $F_{1-\phi}(r_{ff},r_{aa})$ would only account for statistical distribution of the measured value of $|M_{app}|^2$. Other unknowns, such as the variation in apparent mass due to changes in damping characteristics at different vibration levels, are not accounted for by this factor.

Table 3.2: $F_{1-\phi}(r_{ff},r_{aa})$ Statistical Factor for $|M_{app}|^2_{actual}$

Confidence Interval ϕ	$F_{1-\phi}(r_{ff},r_{aa})$ for $(r_{ff},r_{aa})=(80,80)$	$F_{1-\phi}(r_{ff},r_{aa})$ for $(r_{ff},r_{aa})=(120,120)$	$F_{1-\phi}(r_{ff},r_{aa})$ for $(r_{ff},r_{aa})=(150,150)$
80%	1.208	1.167	1.148
90%	1.334	1.265	1.233
95%	1.448	1.352	1.309
99%	1.690	1.533	1.465
99.9%	2.014	1.767	1.662

3.4.5 Maximum Force and Acceleration Occurring at Different Frequencies

Equation 3.5 shows that the ratio $\frac{S_{aa\_flight}(f_{max\_force})}{S_{aa\_flight}(f_{max\_acc})}$ can have a very pronounced effect on the value of C^2. Both $S_{aa\_flight}(f_{max\_force})$ and $S_{aa\_flight}(f_{max\_acc})$ depend on the system parameters of the source and the load, including the type and level of damping. If the ratio $\frac{S_{aa\_flight}(f_{max\_force})}{S_{aa\_flight}(f_{max\_acc})}$ is required to estimate C^2 because f_{max_force} is not equal to f_{max_acc}, then the ratio must be derived from analysis since the opportunity to measure $S_{aa\_flight}(f_{max\_force})$ and $S_{aa\_flight}(f_{max\_acc})$ during fully assembled spacecraft testing typically occurs at a later time than vibration testing for sub-systems. In order to perform these

analyses, a damping type such as viscous or structural, as well as a damping level, in terms of a Q, must be assumed. Consequently, the resulting ratio $\frac{S_{aa\_flight}(f_{max\_force})}{S_{aa\_flight}(f_{max\_acc})}$ will be dependent on the nature of the damping assumption and may not be representative of the actual flight condition. In addition, the ratio may be very sensitive to the value of the assumed Q utilized for the analysis. This uncertainty in damping will in turn produce uncertainty in the predicted value for C^2. To alleviate this uncertainty, a sensitivity analysis of the ratio $\frac{S_{aa\_flight}(f_{max\_force})}{S_{aa\_flight}(f_{max\_acc})}$ to different values of Q is recommended. That said, solace can be found in the fact that the ratio can never exceed unity, as shown by equation 3.7.

3.5 Numerical Examples of the Apparent Mass Method

The following two examples have been selected to demonstrate the accuracy of the apparent mass method in two different circumstances. The examples have been chosen such that similar magnitudes of interface force occur at two different natural frequencies.

In the first example, the maximum acceleration occurs at the first natural frequency of the flight configuration but the maximum force occurs at the second natural frequency. In the second example, both the maximum acceleration and the maximum force occur at the first natural frequency of the flight configuration.

3.5.1 Example 1

Consider the example of a scientific instrument mounted on a spacecraft bus where each of the scientific instrument and the spacecraft bus can be modeled as a two degrees-of-freedom system as shown in figure 3.6. During launch, the vibration from the launch vehicle excites the entire spacecraft structure through the base of the spacecraft at the launch vehicle-spacecraft interface and produces a yet undetermined interface force. The

same vibration imparts a yet undetermined acceleration at the base of the scientific instrument.

During vibration testing, the scientific instrument dynamic can be modeled as shown in figure 3.7. It is in this test configuration that the apparent mass of the scientific instrument is measured. The spacecraft bus in its free state is shown in figure 3.8.

The vibration system parameters of the scientific instrument and the spacecraft bus are shown in table 3.3 and the resulting natural frequencies are shown in table 3.4.

Table 3.3: System Parameters Utilized in Example 1

Variable	Value	Variable	Value	Variable	Value
m_1	150 kg	k_1	1E7 N/m	c_1	4000 N·s/m
m_2	50 kg	k_2	1E7 N/m	c_2	20 N·s/m
m_3	10 kg	k_3	4.2E6 N/m	c_3	20 N·s/m
m_4	2 kg	k_4	1E6 N/m	c_4	10 N·s/m

Table 3.4: Un-Damped Natural Frequencies for System of Example 1

Structure	Mode	Natural Frequency
Load, test configuration	1	85.1 Hz
	2	136.3 Hz
Source, free configuration	1	34.3 Hz
	2	85.2 Hz
Coupled System	1	32.7 Hz
	2	72.7 Hz
	3	102.0 Hz
	4	140.2 Hz

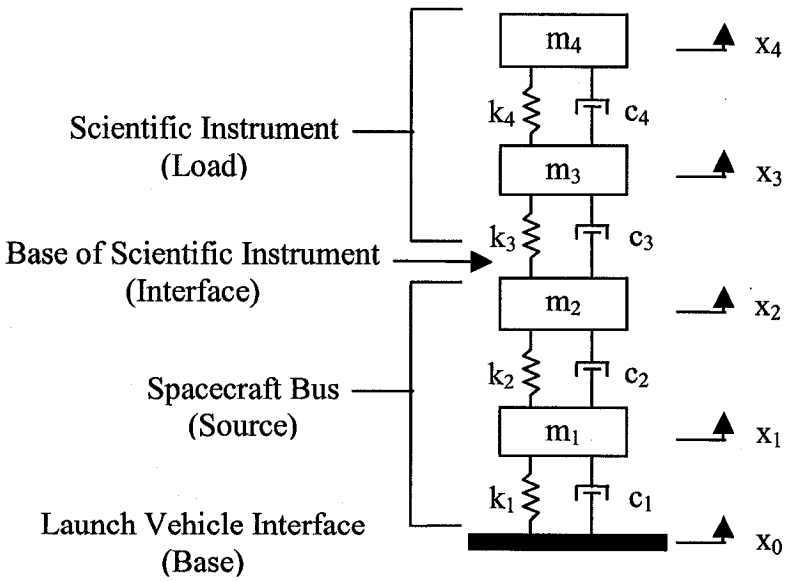

Figure 3.6: Coupled Flight Configuration

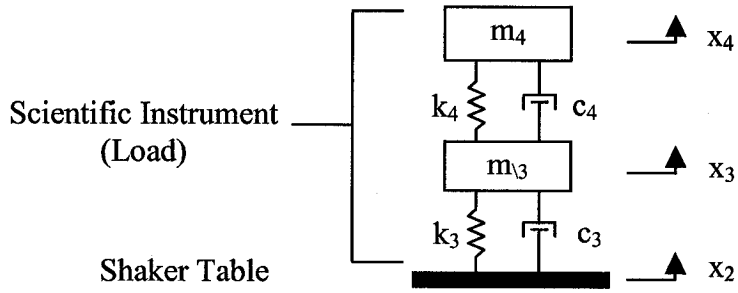

Figure 3.7: Load, Test Configuration

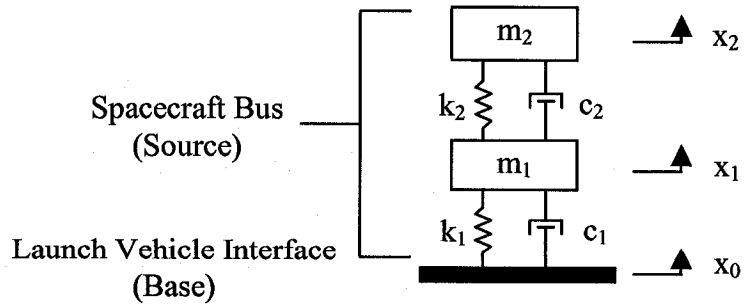

Figure 3.8: Source, Free Configuration

The arbitrary system parameters of table 3.3 were chosen such that:

- The total mass of the load is small compared to the total mass of the source.
- The first natural frequency of the load is over twice the first natural frequency of the source.
- The first natural frequency of the load effectively coincides with the second natural frequency of the source when the source is in the free interface state.
- The maximum acceleration occurs at the first natural frequency of the coupled system.
- The maximum force occurs at the second natural frequency of the coupled system.

The launch vehicle excitation, at the base x_0 in figure 3.5, is assumed to have a flat random acceleration spectral density of 0.001 g^2/Hz between 10 Hz and 1000 Hz.

In order to be able to compare the apparent mass method prediction for the interface force to the actual interface force, the in-flight acceleration spectral density $S_{aa\_flight}(f)$ and the interface force spectral density $S_{ff\_flight}(f)$ will first be determined. The values of $S_{aa\_flight}(f_{max\_force})$ and $S_{aa\_flight}(f_{max\_acc})$ will be noted for future use with equation 3.5.

Then, the apparent mass function of the scientific instrument in the test configuration will be determined. With the apparent mass and the information of $S_{aa\_flight}(f_{max\_force})$ and $S_{aa\_flight}(f_{max\_acc})$, the value of C^2 will be calculated using equation 3.5. The maximum interface force predicted by the calculated value of C^2 will be compared to the actual maximum interface force in the flight configuration using [5]

$$S_{ff\_max\_test} = C^2 \cdot M_0^2 \cdot S_{aa\_test} \tag{3.21}$$

To begin, the interface force spectral density $S_{ff\_flight}(f)$, the interface acceleration spectral density $S_{aa\_flight}(f)$, and the apparent mass of the scientific instrument $M_{app\_load}(f)$ were determined by numerically solving for the four degrees-of-freedom system and the two degrees-of-freedom system to within a 0.1 Hz accuracy using MATLAB [22]. The relevant equations are derived in appendix E and the MATLAB code is described in program 7 of appendix D.

The force spectral density $S_{ff\_flight}(f)$ at the interface between the spacecraft bus and the scientific instrument is labeled as S_{ff_flight} and is shown in figure 3.9.

From figure 3.9, the maximum spectral density interface force has a maximum value of 5477 N^2/Hz and occurs at the second natural frequency of 72.6 Hz. As shown in figure 3.9, the value of the interface force at the second natural frequency is slightly higher than the interface force at the first natural frequency.

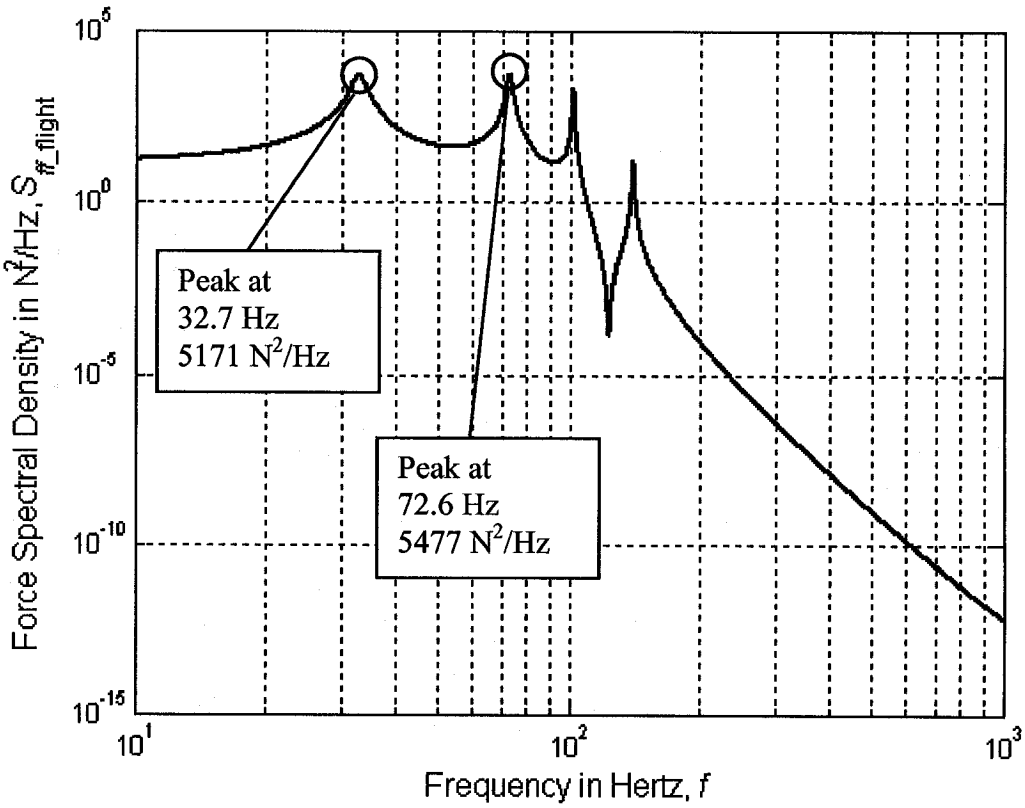

Figure 3.9: Flight Interface Force Spectral Density vs. Frequency

The acceleration spectral density of mass m_2 in the flight configuration, $S_{aa\_flight}(f)$, is shown in figure 3.10.

The base of the scientific instrument is identified as position x_2, which is the position of mass m_2 of the spacecraft bus. As seen in figure 3.10, the maximum value of the interface acceleration spectral density $S_{aa\_flight}(f)$ clearly occurs at the first natural frequency of 32.7 Hz and has a value of $S_{aa\_flight}(f_{max\_acc}) = 0.2787\ g^2/Hz$.

Recall that the maximum value of the force spectral density previously identified in figure 3.9 occurred at the frequency of $f_{max\_force} = 72.6$ Hz. The acceleration spectral density at this frequency is noted to be $S_{aa\_flight}(f_{max\_force}) = 0.03541\ g^2/Hz$ for future use with equation 3.5.

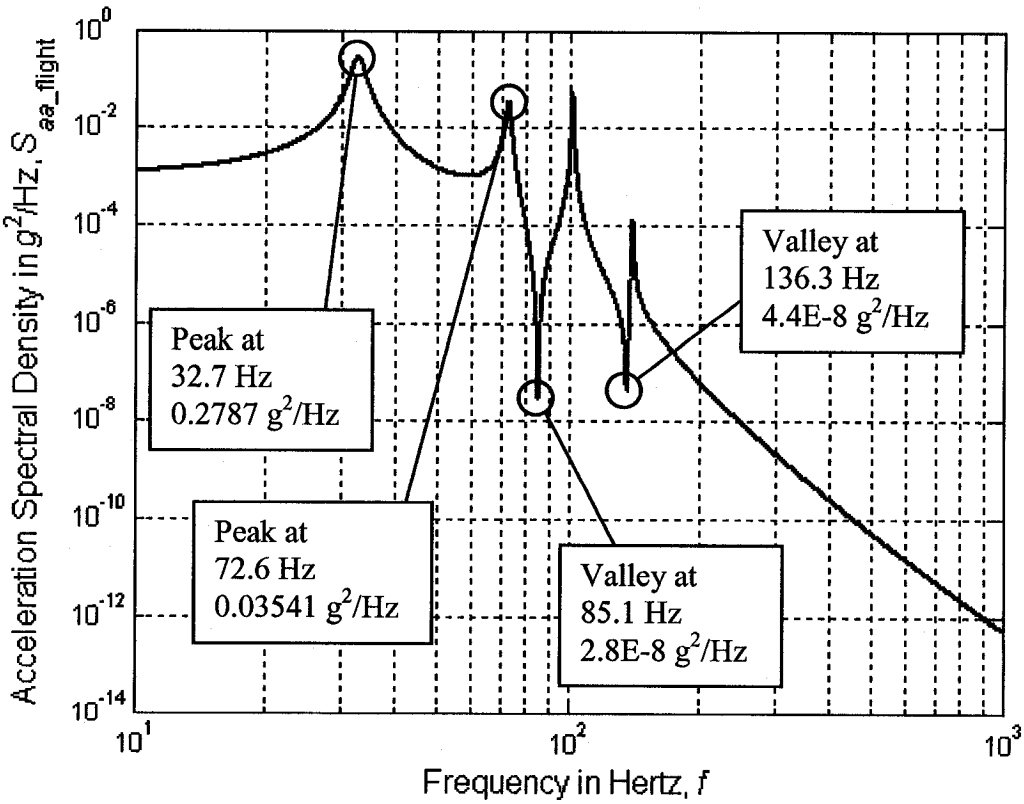

Figure 3.10: Flight Acceleration Spectral Density for Source Mass m_2

The force limits are based on the assumption that the value of S_{aa_test} exactly envelops the maximum peak value of S_{aa_flight}. This assumption ensures that any conservatism, or lack of conservatism, in the test acceleration spectral density, S_{aa_test}, will also be applied to the force limit. As such, S_{aa_test} has the constant value of 0.2787 g^2/Hz, which is the highest peak of figure 3.10.

Now that a test acceleration spectral density S_{aa_test} has been defined, consider the normalized apparent mass of the load $M_{app\_load}(f)$. The function $M_{app\_load}(f)$ can be measured during testing using an arbitrary input. The apparent mass function of the scientific instrument is shown in figure 3.11.

From figure 3.11, the two resonant frequencies of the load are 85.1 Hz and 136.4 Hz. Note that these resonant frequencies are almost identical to the un-damped natural frequencies identified in table 3.4, but shifted a small amount because of the damping.

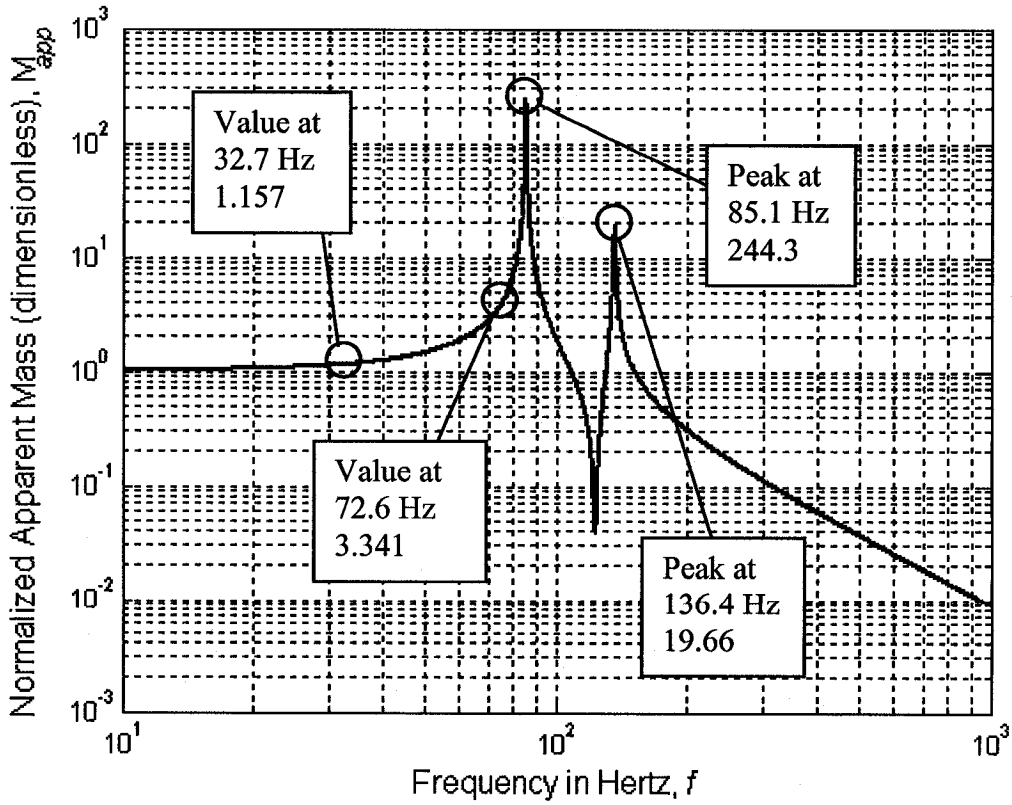

Figure 3.11: Normalized Apparent Mass of Load

Note that the two un-damped natural frequencies of 85.1 Hz and 136.3 Hz correspond to the valleys of the flight acceleration spectral density $S_{aa\_flight}(f)$ at the base of the scientific instrument as shown in figure 3.10 as described by the vibration absorber effect.

Recall from figure 3.9 that the maximum flight interface force of 5 477 N^2/Hz occurs at 72.6 Hz. The value of the normalized apparent mass at 72.6 Hz is 3.341 as shown in figure 3.11. Also recall that the flight interface acceleration spectral density evaluated at the frequency of 72.6 Hz is $S_{aa\_flight}(f_{max\_force}) = 0.03541\ g^2/Hz$. In addition, recall that the maximum acceleration spectral density is $S_{aa\_flight}(f_{max\_acc}) = 0.2787\ g^2/Hz$.

The value of C^2 can be computed with equation 3.5 as

$$C^2 = \frac{\left|M_{app}(f_{max\_force})\right|^2}{M_0^2} \cdot \frac{S_{aa\_flight}(f_{max\_force})}{S_{aa\_flight}(f_{max\_acc})} \tag{3.5}$$

$$C^2 = 3.341^2 \cdot \frac{0.03541\ g^2/Hz}{0.2787\ g^2/Hz} = 1.418$$

Recall that the test acceleration spectral density S_{aa_test} was defined to be 0.2787 g^2/Hz at all frequencies. Recall also, the total mass of the scientific instrument is 12 kg as shown in table 3.4. Thus, according to equation 3.21 the maximum interface force for a C^2 value of 1.418 and a test acceleration spectral density of $S_{aa\_test} = 0.2787\ g^2/Hz$ is

$$S_{ff\_max\_test} = C^2 \cdot M_0^2 \cdot S_{aa\_test} \tag{3.21}$$

$$S_{ff\_max\_test}(f) = 1.418 \cdot (12\ kg)^2 \cdot 0.2787\ g^2/Hz \cdot \left(\frac{9.81\ m/s^2}{1g}\right)^2 = 5477\ N^2/Hz$$

The result of 5477 N^2/Hz is identical to the predicted maximum flight interface force of 5477 N^2/Hz shown if figure 3.9.

It is interesting to note that a low value of C^2 resulted even if the system had two identical natural frequencies at 85.2 Hz and a low mass ratio of 0.06.

3.5.2 Example 2

As further demonstration of the method, consider a second example with almost identical system parameters but with an increase in damping for c_2 as shown in bold in table 3.5.

Table 3.5: Constants Utilized in Second Example

Variable	Value	Variable	Value	Variable	Value
m_1	150 kg	k_1	1E7 N/m	c_1	4000 N·s/m
m_2	50 kg	k_2	1E7 N/m	c_2	**50 N·s/m**
m_3	10 kg	k_3	4.2E6 N/m	c_3	20 N·s/m
m_4	2 kg	k_4	1E6 N/m	c_4	10 N·s/m

For this system, the maximum force of 5160 N^2/Hz is nearly identical to the previous example but now occurs at the first natural frequency of 32.7 Hz instead of 72.6 Hz as shown in figure 3.12.

As before, the maximum acceleration spectral density of the mass m_2 occurs at the first frequency of 32.7 Hz but this time has the lightly different value of 0.2781 g^2/Hz, as shown in figure 3.13, instead of the previous value of 0.2787. From this, the test acceleration spectral density, S_{aa_test}, is set at 0.2781 g^2/Hz.

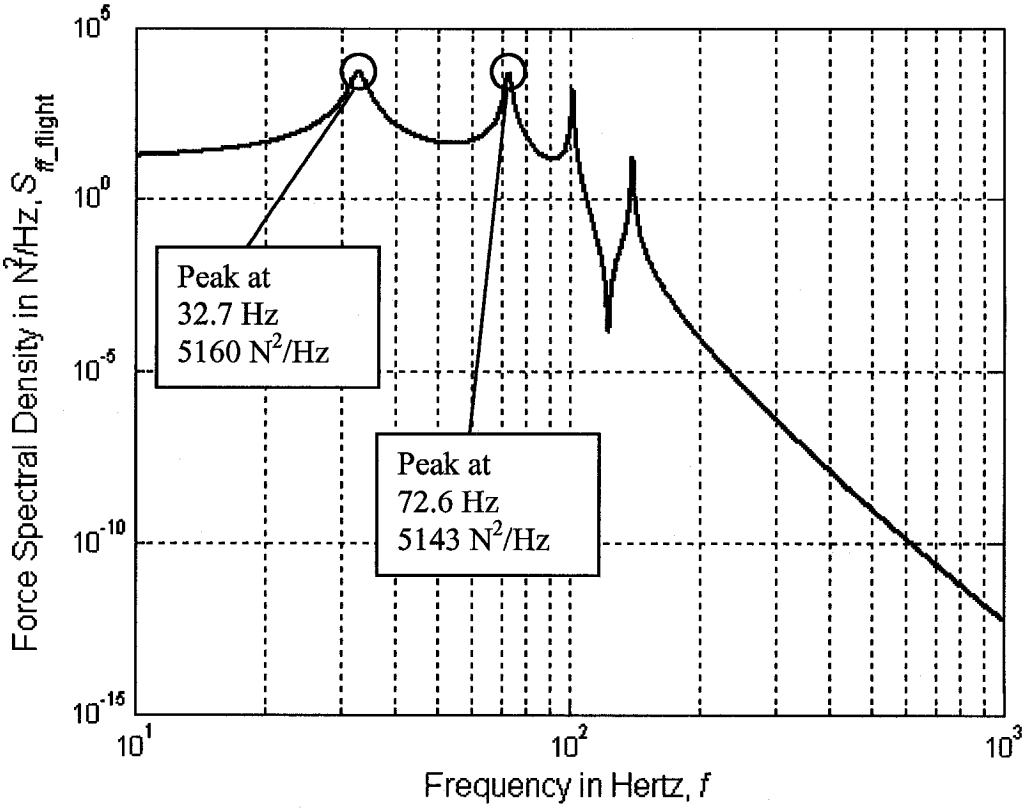

Figure 3.12: Flight Force Spectral Density vs. Frequency of Second Example

The normalized apparent mass of the load remains the same as in figure 3.9. However, this time the normalized apparent mass is evaluated at 32.7 Hz instead of 72.6 Hz. At 32.7 Hz, the value of the normalized mass is 1.157. This time, the ratio $S_{aa\_flight}(f_{max\_force})/S_{aa\_flight}(f_{max\_acc})$ is equal to unity because both the numerator and the denominator occur at the same frequency. The exact value of C^2 can be computed using equation 3.5 as

$$C^2 = \frac{\left|M_{app}(f_{max\_force})\right|^2}{M_0^2} \cdot \frac{S_{aa\_flight}(f_{max\_force})}{S_{aa\_flight}(f_{max\_acc})} \tag{3.5}$$

$$C^2 = 1.157^2 = 1.339$$

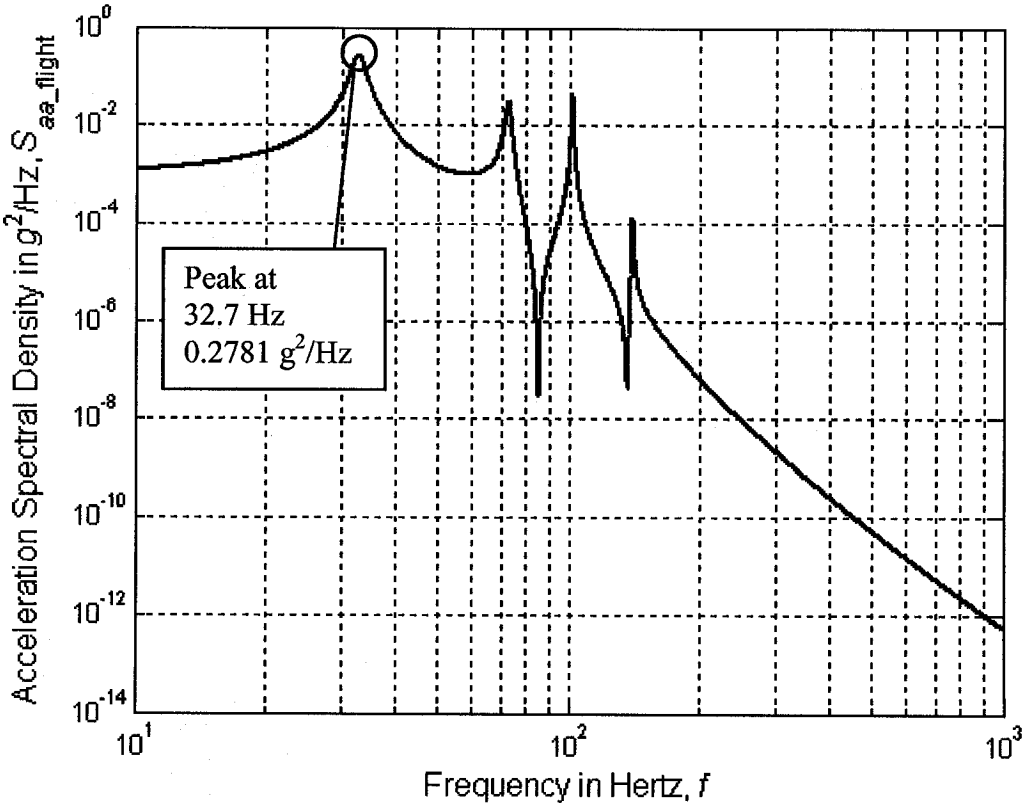

Figure 3.13: Flight Acceleration Spectral Density for Source Mass m_2 of Example 2

The force limit with $C^2 = 1.339$ and $S_{aa\_test} = 0.2781$ g^2/Hz is

$$S_{ff\_max\_test} = C^2 \cdot M_0^2 \cdot S_{aa\_test} \tag{3.21}$$

$$S_{ff\_max\_test}(f) = 1.339 \cdot (12\text{ kg})^2 \cdot 0.2781 \, {}^{g^2}\!/_{\text{Hz}} \cdot \left(\frac{9.81\text{ m/s}^2}{1\text{g}} \right)^2 = 5160 \, {}^{\text{N}^2}\!/_{\text{Hz}}$$

Again, the result of 5160 N^2/Hz is identical to the predicted maximum flight interface force of 5160 N^2/Hz shown if figure 3.12.

3.6 Apparent Mass Method Summary

In summary, the apparent mass method is based on the multiple degrees-of-freedom or continuous system with single attachment point model but is also applicable to multiple-

attachment point structures up to a critical test frequency that must be determined according to a desired arbitrary definition of similar phase and magnitude at the attachment points. This applicability of the method up to the critical test frequency is not a limitation of the apparent mass method as much as a limitation on how representative the test environment is compared to the actual flight environment. For similar reasons, the method is only applicable to structures where base excitation is the dominant type of excitation.

The apparent mass method predicts the value of C^2 to be utilized in conjunction with the semi-empirical method. However, since the value of C^2 is based entirely on vibration theory, the apparent mass method is not a semi-empirical method but a true theoretical method.

The apparent mass method calculates the value of C^2 based on equation 3.5, shown below for reference.

$$C^2 = \frac{\left|M_{app}(f_{max\_force})\right|^2}{M_0^2} \cdot \frac{S_{aa\_flight}(f_{max\_force})}{S_{aa\_flight}(f_{max\_acc})} \tag{3.5}$$

Where by definition of $S_{aa\_flight}(f_{max\_acc})$, it is noted that

$$\frac{S_{aa\_flight}(f_{max\_force})}{S_{aa\_flight}(f_{max\_acc})} \leq 1 \tag{3.6}$$

To utilize the apparent mass method, one would start by measuring the actual mass of the test item and then determining the apparent mass of the test item using a low level run, such as –15 dB of the desired test acceleration spectral density. The low level run is necessary to reduce incidents of accidental over-testing, since no notching is performed during this initial run and the amount of damping is unknown.

The values of f_{max_force}, $S_{aa\_flight}(f_{max\_force})$, and $S_{aa\_flight}(f_{max\_acc})$ are either noted from available data or estimated using one of the techniques outlined in section 3.1.3. The

apparent mass modulus squared is evaluated at the frequency f_{max_force}, from which the value of C^2 can be determined through equation 3.5. The slope of the apparent mass function at the frequency f_{max_force} is noted and retained for consideration regarding the sensitivity of the prediction. If desired, a factor of safety based on equation 3.20, repeated below, can be applied to the calculated value from equation 3.5.

$$\left|M_{app}\right|^2_{actual} \leq F_{1-\varphi}(r_{ff}, r_{aa}) \cdot \left|M_{app}\right|^2_{measured} \tag{3.20}$$

Since the apparent mass function is dependent on damping, and damping is dependent on excitation level for many practical structures, the next step is to perform a force-limited test with an input of –9 dB of the test level and force-limits set to $S_{ff\_max} = C^2 \cdot M_0 \cdot S_{aa\_-9\_dB\_of\_test}$ using the previously determined value for C^2.

The apparent mass is then re-calculated and the value of C^2 is re-evaluated based on the data from the –9 dB run. Since damping increases with excitation level for some structures, the re-calculated value of C^2 may have decreased from its previous value, depending at which frequency the apparent mass was evaluated.

The above process is repeated for input levels of –6 dB, and –3 dB. From the data points of C^2 versus input level, an appropriate value of C^2 at 0 dB can be extrapolated and utilized for the final 0 dB test. After the test, calculating the value of C^2 based on the 0 dB test data and comparing the result to the actual value utilized for testing will verify that an appropriate value of C^2 was utilized during the final 0 dB test.

In the next chapter, the apparent mass method will be validated using a structure that simulates a two degrees-of-freedom system. The predicted values for C^2 using the apparent mass method will be compared to the experimental values.

4 EXPERIMENTAL TESTING

This chapter describes the experimental testing and results done to validate the previously developed equations and trends regarding the value of C^2. In addition, some tests were performed to investigate the dependence of damping on input excitation amplitude. To this end, a two degrees-of-freedom system with adjustable system parameters was constructed and tested. In all, 28 system parameter combinations were investigated. The combinations included variations in frequency ratio F, mass ratio μ, and source quality factor Q_1. Both the source and load accelerations, as well as the interface forces between the source and the load, were monitored experimentally. The value of C^2 was then determined by measurement and the results compared to the theoretical predictions based on the apparent mass of the load.

4.1 Description of the Test Article

A test article was designed to simulate the two degrees-of-freedom system shown schematically in figure 4.1.

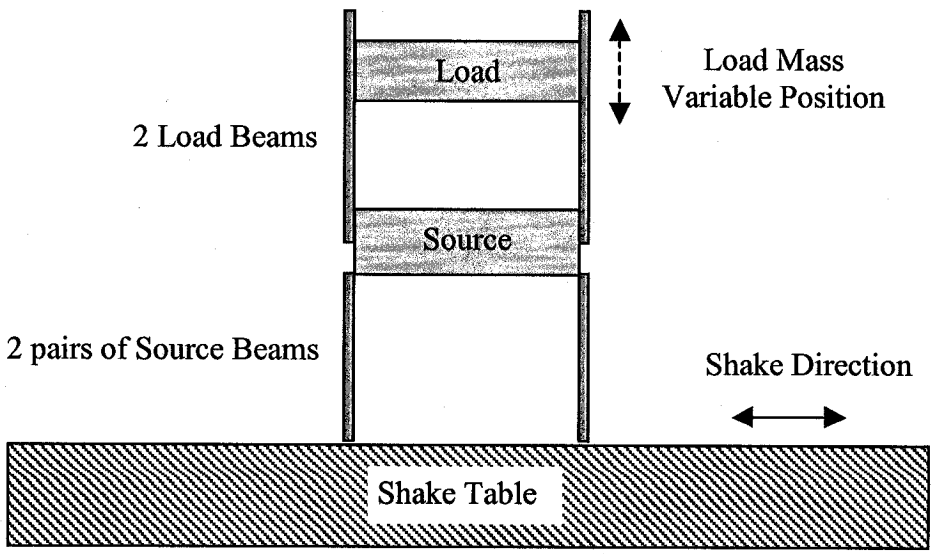

Figure 4.1: Schematic of Test 2-DOF System

With the cantilevered design, the natural frequency of the load could be changed significantly without the need for an excessively large structure.

4.1.1 Description of the Source Structure

The source is essentially a single degree-of-freedom system consisting of a 20 kg nominal mass mounted on four beams in an inverted pendulum fashion as shown in figure 4.2. As part of the source structure, two pairs of force sensors were attached to two opposite sides of the 20 kg nominal mass. These force sensors served as mounting points for the load.

The 20 kg nominal mass does not include the mass for extra equipment required for assembly and testing such as the support beams, the fasteners, force sensors, and the accelerometers. When these are taken into account, the actual mass of the source structure is 23.692 kg.

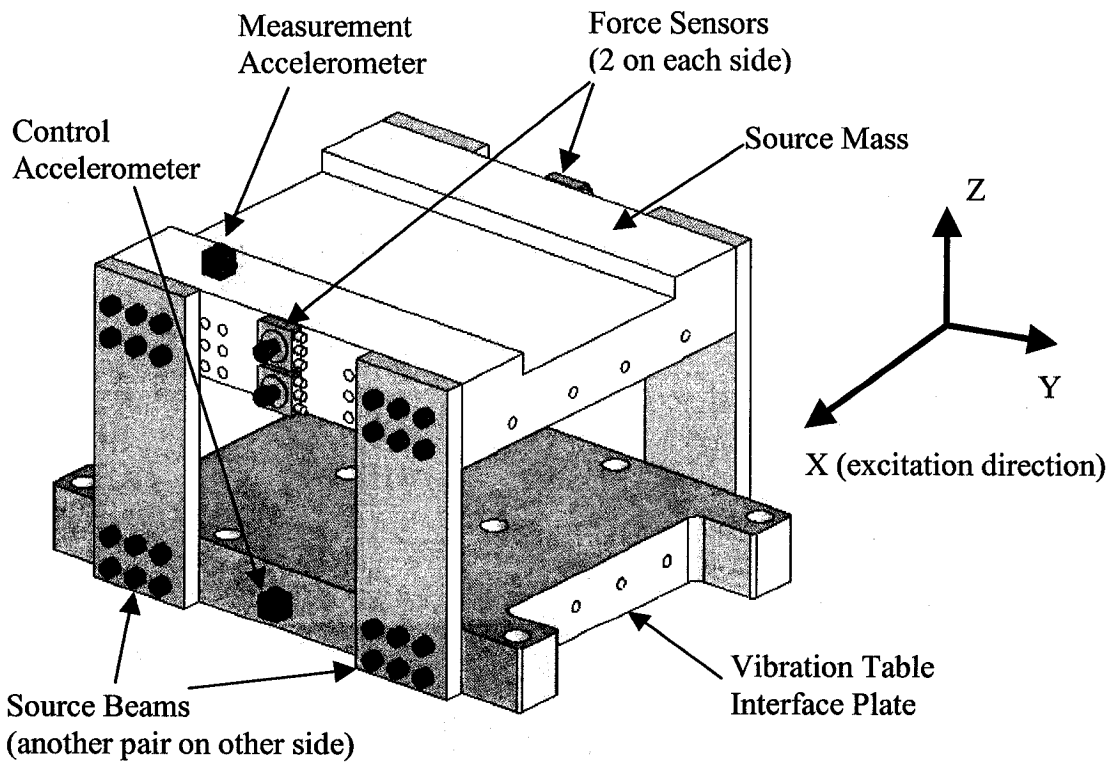

Figure 4.2: Source, Un-damped (Configuration 20U)

The mass is mounted at a fixed length on the four beams giving a fixed un-coupled natural frequency of about 250 Hz.

Optional sidewalls could be bolted to the source in order to lockdown the source in such a way as to increase the un-coupled natural frequency to over 700 Hz. The optional sidewall configuration is shown in figure 4.3. This 700 Hz configuration was not utilized directly as a test configuration but rather acted as an extension of the vibration table to test the load in an un-coupled state without changing the setup.

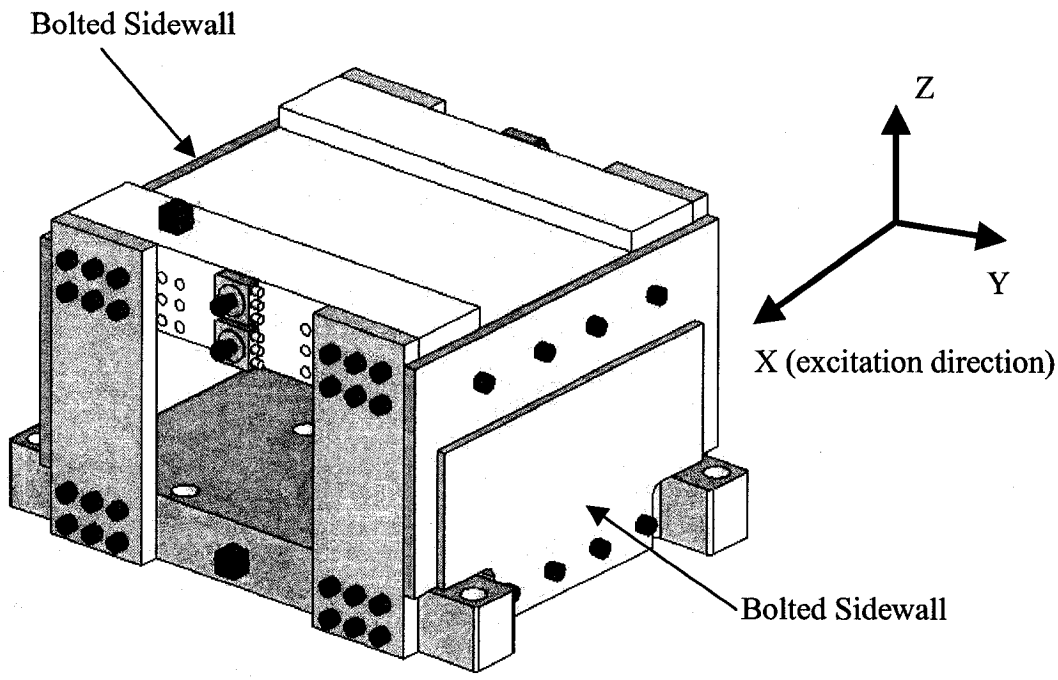

Figure 4.3: Source with Sidewalls (Configuration 20F)

In order to investigate the effect of damping, a secondary structure was installed around the source for some tests. This secondary structure surrounded but did not touch the source mass. The 0.20 inch gap between this secondary structure and the source mass was filled with Sorbothane, a soft material with very high damping characteristics [33]. In this manner, the damping of the source could be increased without significantly

affecting its un-coupled natural frequency. An example of this particular setup is shown in figure 4.4.

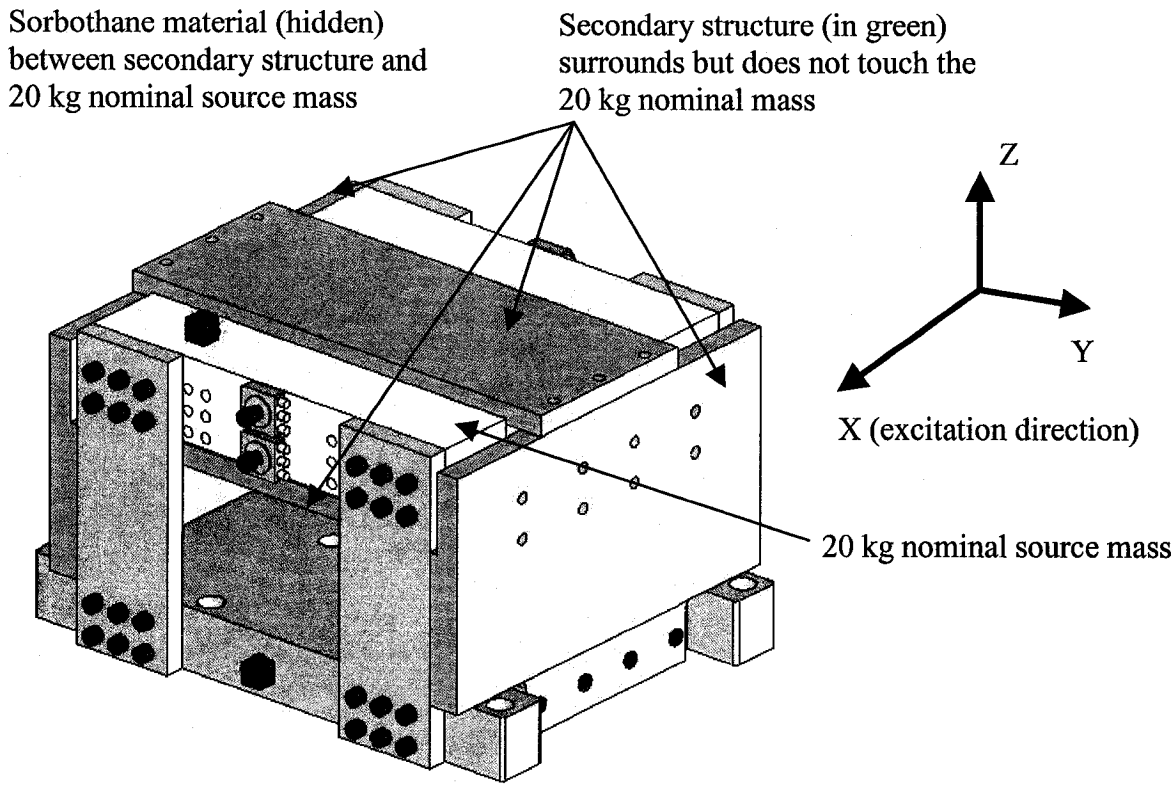

Figure 4.4: Source, Damped (Configuration 20D)

A summary of the source configurations is shown in table 4.1.

Table 4.1: Source Configurations

Source Number	Nominal Source Mass	Actual Source Mass	Optional Attachments	Source Configuration	Approximate Natural Frequency
1	20 kg	23.692 kg	None	20U	250 Hz
2	20 kg	23.692 kg	Sorbothane	20D	250 Hz
3	20 kg	23.692 kg	Sidewalls	20F	700 Hz

4.1.2 Description of the Load Structure

Fourteen different load structures were utilized in the experimental testing. All these load structures were also designed to approximate a single degree-of-freedom system in an inverted pendulum fashion.

The first group of seven loads consisted of a 2 kg nominal mass clamped on two beams as shown in figure 4.5. Similarly, the second group of seven loads consisted of a 10 kg nominal mass clamped on two beams as shown in figure 4.6.

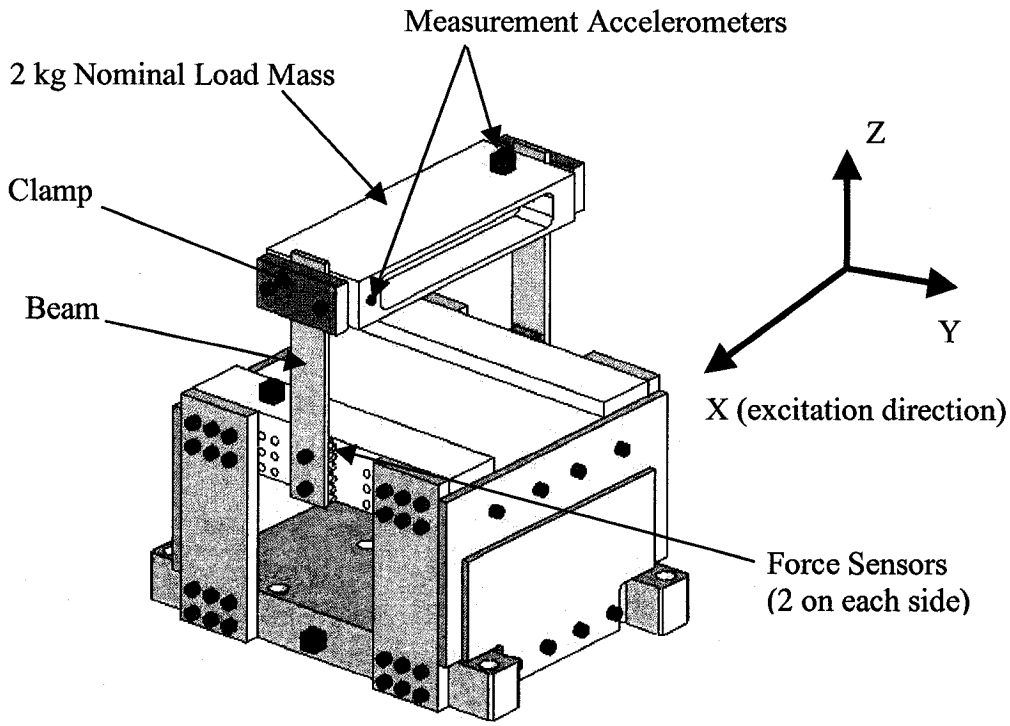

Source configuration 20F shown with 2kg load structure

Figure 4.5: 2 kg Nominal Load

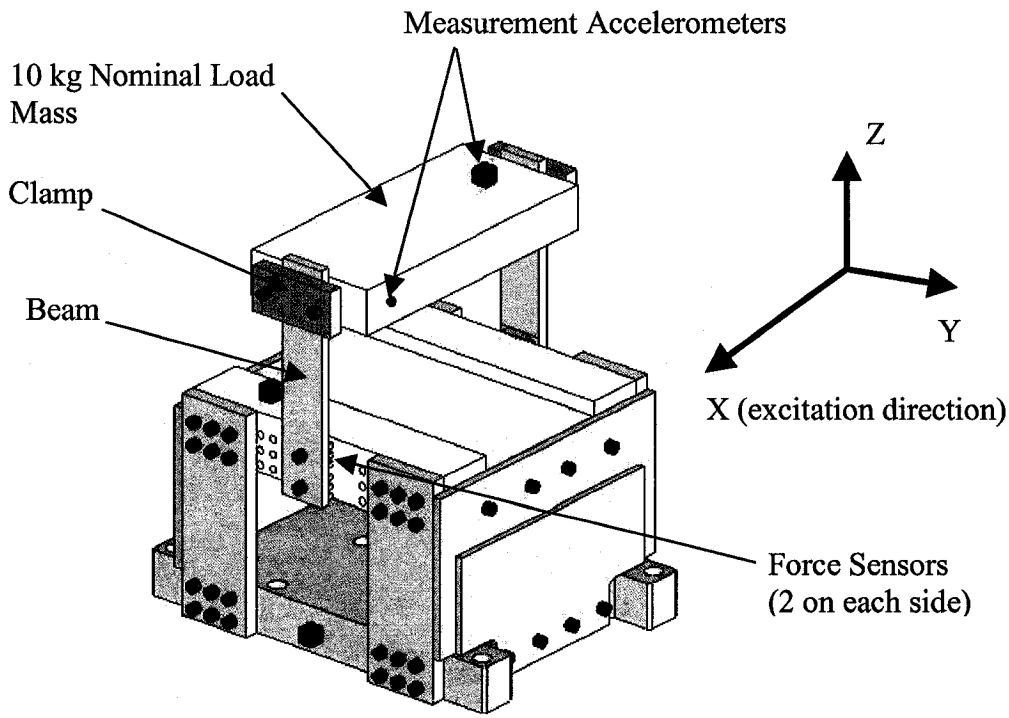

Source configuration 20F shown with 10kg load structure

Figure 4.6: 10 kg Nominal Load

The beams for the 2 kg nominal load were different in width and thickness than the beams of the 10 kg nominal load such that comparable natural frequencies of the single degree-of-freedom systems resulted when either mass was positioned at identical height.

The purpose of having comparable uncoupled natural frequencies for the 2 kg and 10 kg loads was to investigate the effect of varying mass ratio when the uncoupled natural frequency is unchanged.

For repeatability, the height of a mass along the beam was controlled using a pair of spacers that were removed before every test. An example of the use of the spacers is shown in figure 4.7. The exact length of the spacers is arbitrary but was chosen such that the resulting natural frequencies of the single degree-of-freedom systems were somewhat separated from each other. In all, 7 different spacers were combined with the 2 different

load masses to create 14 different load configurations as shown in table 4.2. The damping of the load structures was not controlled to any specific value.

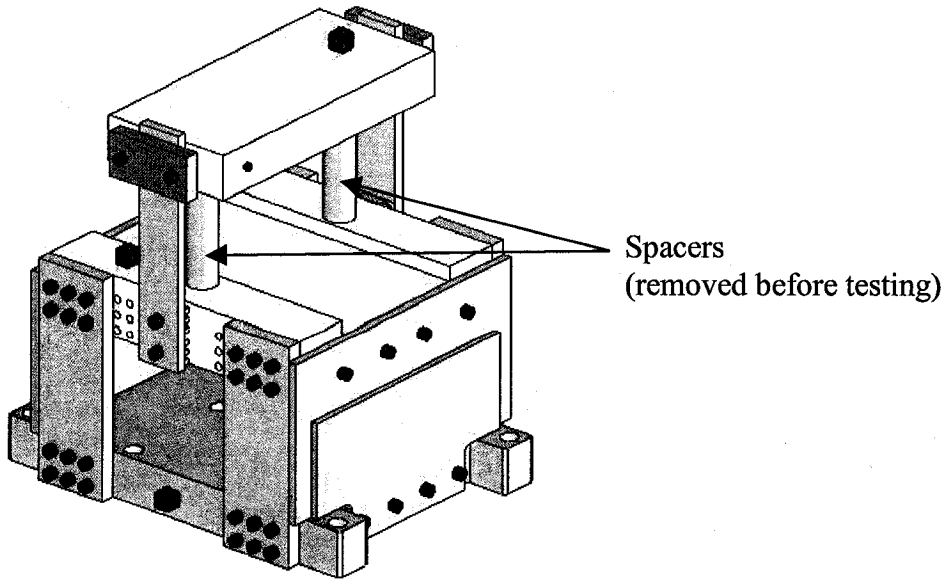

Figure 4.7: Spacer Use Example

Table 4.2: Load Configurations

Load Configuration	Nominal Load Mass	Actual Load Mass	Spacer ID	Approximate Design Natural Frequency
1	2 kg	2.080 kg	1	125 Hz
2	2 kg	2.080 kg	2	190 Hz
3	2 kg	2.080 kg	3	270 Hz
4	2 kg	2.080 kg	4	320 Hz
5	2 kg	2.080 kg	5	360 Hz
6	2 kg	2.080 kg	6	410 Hz
7	2 kg	2.080 kg	7	455 Hz
8	10 kg	9.224 kg	1	125 Hz
9	10 kg	9.224 kg	2	190 Hz
10	10 kg	9.224 kg	3	270 Hz
11	10 kg	9.224 kg	4	320 Hz
12	10 kg	9.224 kg	5	360 Hz
13	10 kg	9.224 kg	6	410 Hz
14	10 kg	9.224 kg	7	455 Hz

The 2 kg and 10 kg nominal load masses do not account for extra equipment required for assembly and testing such as the support beams, the fasteners, and the accelerometers. The actual load masses, identified as the mass M_0 in equations dealing with the semi-empirical method, are 2.080 kg and 9.224 kg for the 2 kg and 10 kg nominal masses respectively. The actual mass of the 10 kg nominal mass is slightly less than the anticipated 10 kg due to manufacturing error.

4.1.3 Test Configurations

To keep track of the data, a naming convention was created to represent different test configurations. The name for each test configuration was made up from a group of four elements, each element representing a piece of information of the setup. The first two elements provided information on the source and the last two elements provided information on the load.

The first element represents the nominal mass of the source in kilograms. Since only one 20 kg nominal source was ever utilized, this number is always 20.

The second element indicated whether the source was free to move normally, had increased damping from the Sorbothane material, or had the optional sidewalls installed to increase its natural frequency. The letter U represents a source that is essentially un-damped in that no additional damping was provided as shown in figure 4.2. The letter D represented a source with increased damping using the Sorbothane material as shown in figure 4.4. The letter F indicated that the optional sidewalls were installed to increase the natural frequency of the source as shown in figure 4.3.

The third element represented the nominal mass of the load in kilograms. As such the third element can take the value of either 2 or 10.

An underscore delimiter symbol was included between the third and fourth element to clearly show the separation between the third and fourth elements.

The fourth element is an identification spacer number that varies between 1 and 7.

A summary of the naming convention for the various test configurations is shown in table 4.3.

Table 4.3: Nomenclature Convention for Test Configurations

Element	First	Second	Third	Delimiter	Fourth
Represents	Nominal Mass of Source in kg	Source Attachments	Nominal Mass of Load in kg		Spacer Identification
Possible Values	20	U (Un-damped)	10	_	1
		D (Damped)	2		2
		F (Fixed)			3
					4
					5
					6
					7

As an example of the naming convention, configuration 20U10_4 would indicate the two degrees-of-freedom system with the 20 kg nominal source in un-damped condition and the 10 kg nominal load whose height along the beam is fixed using spacer number 4.

For the single degree-of-freedom source configurations, the third and fourth element and the delimiter were omitted. Thus, the three tests labeled 20U, 20D, and 20F respectively represent the source by itself as a single degree-of-freedom system in its un-damped, damped, and fixed configuration without any load.

For the single degree-of-freedom load configurations, the source was fixed using the optional sidewalls. As such, all single degree-of-freedom configurations for the load start with the 20F descriptor and have two more elements describing the load configuration. For example, the configuration 20F2_1 represents the single degree-of-freedom load system with the 2 kg nominal load using space number 1.

4.2 Description of the Test Setup

Testing was performed at the vibration facilities of the Canadian Space Agency, located at the David Florida Laboratory in Ottawa Ontario, Canada. As previously discussed, two different series of tests were performed. For scheduling reasons, all of the tests pertaining to the investigation of the value of C^2 were performed on their 17k shaker, while all of the tests pertaining to the investigation of the dependence of damping with acceleration input amplitude were performed on their larger 40k shaker.

Accelerometers were utilized to monitor the acceleration of the coupled system. The accelerometers were glued either directly to the test item or, in the case of tri-axial measurements, to a 1 cm aluminum block, which was in turn glued to the test item with ethyl hybrid cyanoacrylate glue. This particular mounting technique provides a reasonable flat response for frequencies up to 4 000 Hertz [34].

In addition, force sensors were used to measure the interface forces between the source and the load.

The LMS vibration control system utilized by the David Florida Laboratory is capable of providing acceleration response plots, frequency response functions plots, and force measurements plots. The LMS system can also export the measured data in universal file format. The data in universal file format was imported into Microsoft Excel for further analysis and re-plots.

In the following, the accelerometers and force sensors details are provided.

4.2.1 Accelerometers

A tri-axial accelerometer block with three accelerometers labeled as CX1, CY1, and CZ1 was installed at the base of the vibration table interface plate next to the shaker table as a control as shown in figure 4.2. The CX1 accelerometer was utilized as the control during

testing. Two more tri-axial accelerometer blocks were installed, one on the source mass and one on the load mass. The accelerometers of the source mass were labeled as MS1X, MS1Y, and MS1Z and the accelerometers of the load mass were labeled as ML1X, ML1Y, and ML1Z. An additional accelerometer, labeled as ML2Y, was installed on the load mass to monitor any rotation. The naming convention for the accelerometers was chosen as follows: the first letter is either C for control or M for measurement. The second letter is either S for source or L for load. The following digit identifies the location of the accelerometer on the source or the load. The X, Y, or Z following the digit indicates the direction of measurement. For example, ML2Y indicates that the measurement location is on the load located at position 2, and the direction of measurement is Y. Figures 4.8 and 4.9 show the locations of the accelerometers and force sensors during testing for coupled two degrees-of-freedom source-load tests. The same accelerometer locations and naming conventions were utilized for the single degree-of-freedom source or load tests.

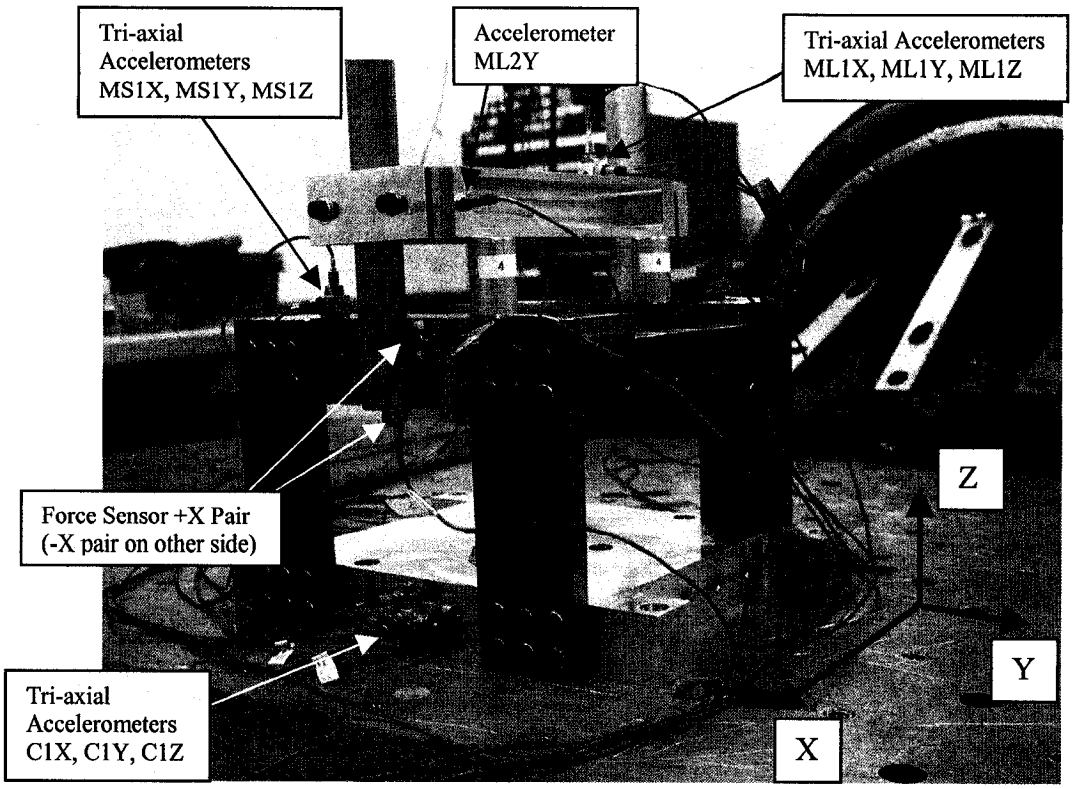

Figure 4.8: Accelerometer and Force Sensor Position with 2 kg Load

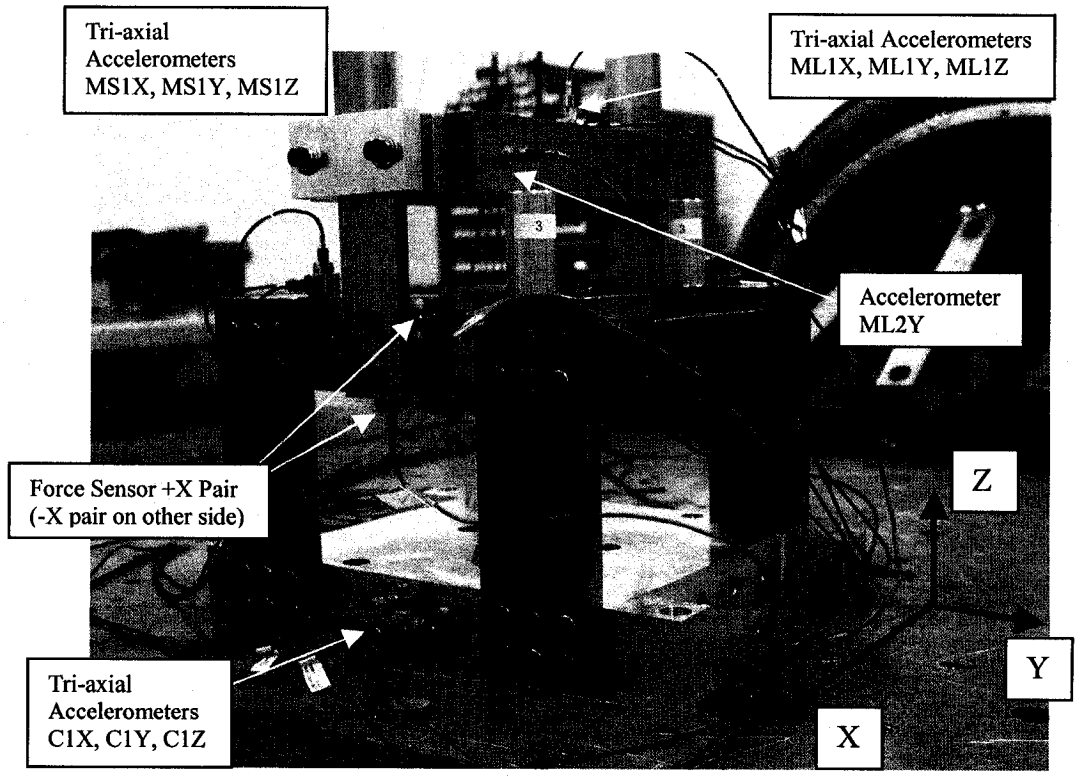

Figure 4.9: Accelerometer and Force Sensor Position with 10 kg Load

4.2.2 Force Sensors

Four Kistler force sensors, model 9251A, were utilized to measure the force during the coupled two degrees-of-freedom tests. The four sensors were divided into two pairs labeled +X and –X as shown in figures 4.8 and 4.9. Each pair of sensors had matched calibration values as shown in table 4.4.

Table 4.4: Force Sensor Details

Force Sensor Pair	Force Sensor Location	Sensor Serial Number	Manufacturer Sensitivity
+X	+X Top	1034000	4.15 pC/N
	+X Bottom	1040410	4.16 pC/N
-X	-X Top	1040408	4.14 pC/N
	-X Bottom	1040407	4.15 pC/N

The charge output from a given pair of force sensors was summed with an analogue device and then converted into a voltage using a charge amplifier and converter as shown schematically in figure 4.10.

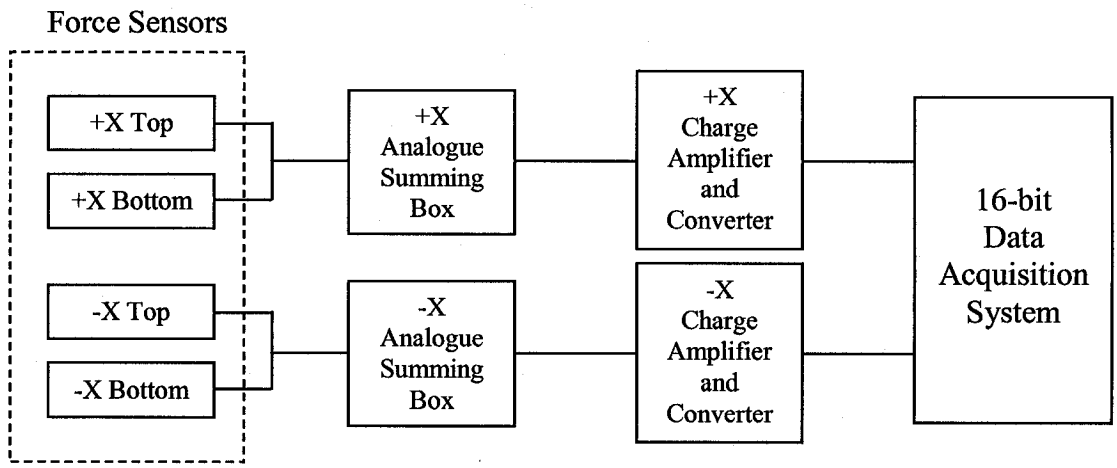

Figure 4.10: Force Sensors Schematic Setup

The data from each force sensor pair was then summed manually taking into account the fact that the summed forces at each pair are 180° out of phase with each other because

when one end is in tension, the other end must be in compression. After applying the phase correction, the value of the summed forces was labeled F_{total} for sine tests and S_{ff_total} for random tests.

Force sensors are attached to the test equipment using bolts. There are two major issues regarding these bolts when performing force limiting vibration testing. The first issue concerns the required bolt pre-load and the second issue concerns the effect of the bolt on the *in situ* calibration factor of the force sensor. Since these issues relate to the accurate measurement of the total force at the interface and to any potential damage to the equipment, these issues must both be understood in order to perform a successful test. As such, the next sub-sections present an overview of these issues in regards to the previously described test setup.

4.2.2.1 Force Sensor Issue: Bolt Pre-Load

The bolt pre-load must be high enough to prevent both separation and slippage of the interface during testing. Separation and slippage are undesirable effects because they involve changes in boundary conditions, which have been shown in section 3.3.1 to affect the apparent mass and thus the interface forces. In addition, separation and slippage could lead to unwanted structural damage to the test article.

To avoid separation and slippage, a high pre-load tension in the bolt is desirable. However, if the pre-load is too high, the force sensor reading may become saturated during testing or worse, the bolt or the sensor may be permanently damaged. Calculation of the required bolt pre-load must take into account the maximum tensile force in the bolt and the maximum compressive force in the force sensor during testing.

The maximum allowable tensile force on the bolt can be calculated knowing the tensile area of the bolt, $A_{\text{bolt tensile area}}$, and the yield stress of the bolt material $\sigma_{\text{yield bolt}}$ as follows [35]

$$F_{\text{max bolt}} = \sigma_{\text{yield bolt}} \cdot A_{\text{bolt tensile area}} \tag{4.1}$$

The bolts utilized for testing are ¼-20 unified course thread steel bolts. The tensile area for such a bolt is given as 2.05E-5 m^2 [36] and the yield point of the high strength steel bolts was given by the David Florida Laboratory as 1.02E9 Pa giving a maximum allowable tension load of about 20 000 N when rounded down to the nearest 1 000 N.

The maximum allowable compressive load on the sensor is given in the manufacturer's data sheet. For the Kistler 9251A force sensor, the maximum range of the compressive load is 30 000 N [37].

Assuming that separation of the joint interface at the force sensor never occurs, the forces in the bolt and the forces in the force sensor can be calculated using the following formulas [35]

$$F_{bolt} = F_{pre-laod} + \frac{k_{bolt}}{k_{bolt} + k_{clamped}} F_{applied} \tag{4.2}$$

$$F_{sensor} = F_{pre-laod} - \frac{k_{clamped}}{k_{bolt} + k_{clamped}} F_{applied} \tag{4.3}$$

Where k_{bolt} and $k_{clamped}$ indicate the spring stiffness of the bolt and the clamped surfaces respectively and a positive applied force $F_{applied}$ indicates an increase in tension in the bolt. For the test setup, the value of k_{bolt} and $k_{clamped}$ were calculated in appendix I and are shown below in table 4.5.

Table 4.5: Bolt and Clamped Member Stiffness

Load Mass	Bolt Stiffness k_{bolt}	Clamped Member Stiffness $k_{clamped}$
2 kg	2.714 E8 N/m	1.476 E9 N/m
10 kg	2.172 E8 N/m	1.296 E9 N/m

If separation of the joint interface at the force sensor does occur, the forces in the bolt and the forces in the force sensor are simply [35]

$$F_{bolt} = F_{applied} \tag{4.4}$$

$$F_{sensor} = 0 \tag{4.5}$$

The force constraints set by equations 4.2 to 4.5 can best be understood by plotting the applied force as the x-axis and the forces in the bolt and the force sensor as the y-axis of an X-Y plot. The plot for an initial tension of 17 500 N for the 2 kg load setup is shown in figure 4.11.

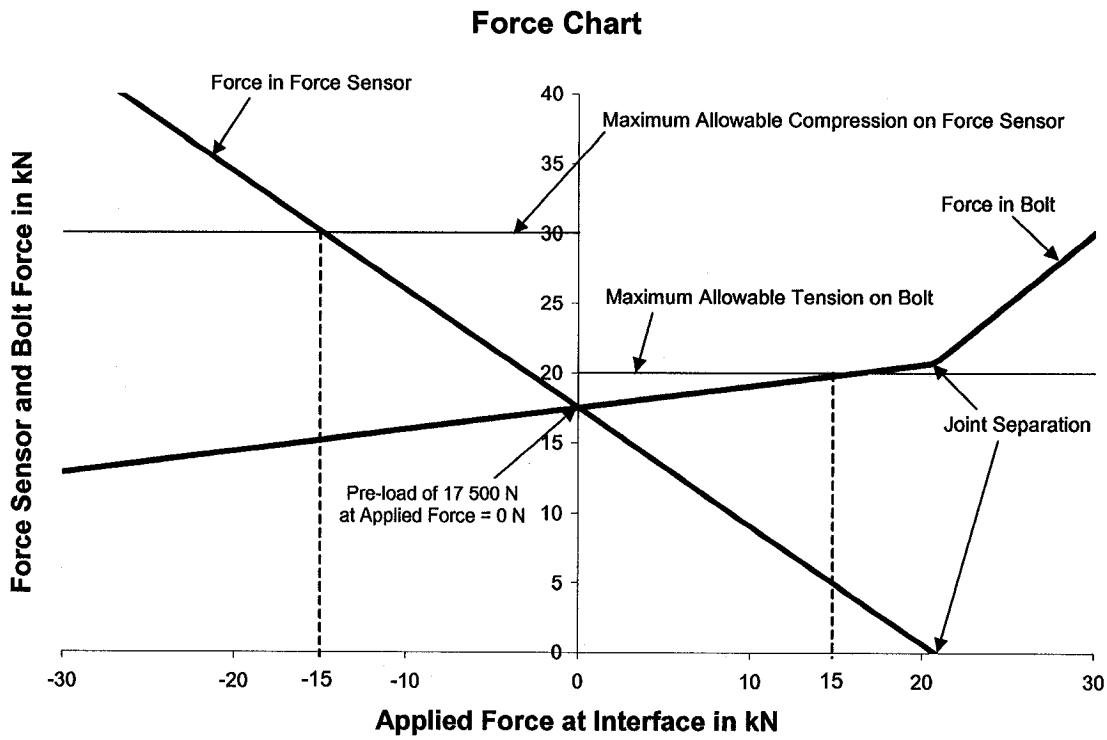

Figure 4.11: Forces in Force Sensor and Bolt for 2 kg Load Setup

Figure 4.11 shows that a pre-load value of 17 500 N will allow a force of about ±15 000 N to be applied and measured by the force sensor before either damaging the bolt or exceeding the measurement range of the force sensor. In addition, joint separation is found to occur at over 20 000 N of applied force, which is well above the 15 000 N limit in tension. A similar pre-load of 17 500 N has been found suitable for the 10 kg load setup and thus a 17 500 N pre-load was also utilized for the configurations with the 10 kg load mass.

The bolt pre-load is based on an idealized linear theory. Although a bolt pre-load of 17 500 N was utilized successfully for initial tests, the high pre-load combined with the vibration levels were causing some undesirable local yielding. To protect the equipment, the vibration levels and the pre-load were reduced. The details of the changes in vibration levels are discussed in a later section. The pre-load was reduced from 17 500 N to 9 000 N resulting in a measurement range of about ±10 500 N, corresponding to about ± 2 400 lb, before joint separation due to tension occurs.

The exact pre-load in the bolt was measured directly by the load cell during installation by setting its charge amplifier to a long time constant.

The 16-bit data acquisition system utilized by the vibration laboratory is set to read voltages ranging from –1 V to +1 V. During testing, the charge amplifiers were set to a scale factor of 2 000 N/V giving a resolution of 0.1 N.

4.2.2.2 Force Sensor Issue: Overall Calibration Value

When performing force limited vibration testing, one is interested in measuring the total force at the mounting interface. However, the total interface force is not equal to the load measured by the load cell because the bolt carries part of the load. Thus, the force sensor will only measure a fraction of the actual total load.

Assuming that separation never occurs, the force in the force sensor is predicted by equations 4.3, shown again for reference.

$$F_{sensor} = F_{pre-laod} - \frac{k_{clamped}}{k_{bolt} + k_{clamped}} F_{applied} \tag{4.3}$$

In equation 4.3, tension is a positive quantity and compression is a negative quantity. However, the particular force sensor utilized defines compression as a positive quantity. With this convention, the force sensor behaves as

$$F_{sensor} = -F_{pre-laod} + \frac{k_{clamped}}{k_{bolt} + k_{clamped}} F_{applied} \tag{4.6}$$

During testing, the force sensor is operated using a small time constant on the charge amplifier. The effect of this practice allows measurement of dynamic loads while ignoring constant loads. Thus, the sensor will not register the constant pre-load and the force sensor will behave as

$$F_{sensor} = \frac{k_{clamped}}{k_{bolt} + k_{clamped}} \cdot F_{applied} \tag{4.7}$$

Note that for any given flange, the factor $\frac{k_{clamped}}{k_{bolt} + k_{clamped}}$ is a constant that depends only on the geometry and material properties of the clamped elements and the bolt.

The quantity of interest is the actual force at the interface $F_{applied}$. However, what is measured is the force through the sensor F_{sensor}. A correction factor α needs to be applied to the force sensor in order to get the actual applied force. This correction factor is

$$\alpha = \frac{k_{bolt} + k_{clamped}}{k_{clamped}} \tag{4.8}$$

Such that

$$F_{applied} = \alpha F_{sensor} \tag{4.9}$$

Since the scaling factor only depends on initial geometry and material properties, it is a constant, unless some plastic deformation occurs.

For the test setup utilized in this thesis, both the 10 kg and the 2 kg setup are estimated to have a scaling factor of about 1.2 as shown in appendix I. The charge sensitivity of the charge amplifier/converter shown in figure 4.10 for each pair of force sensors can now be adjusted such that the force sensor directly reports the applied force during testing.

Ordinarily, only the scaling factor α that accounts for the load passing through the bolt is utilized for force limited vibration testing. However, in the particular setup utilized in this thesis, another effect contributing to the *in situ* calibration was found to be significant. The effect is explained as follows.

Consider the free body diagram of one of the load beams with the two force sensors as shown in figure 4.12. The whole point of the force measurement is to measure the force P from the force reading of the top and bottom force sensors.

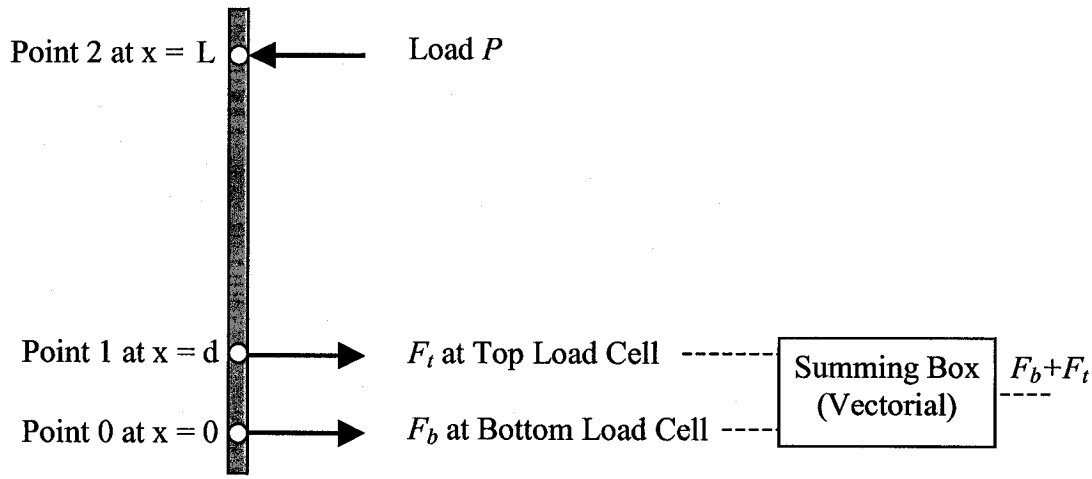

Figure 4.12: Free Body Diagram of the Load Beam

From Newton's second law and the sum of moments about point 0, the forces at the top force sensor F_t, the force at the bottom force sensor F_b, and the unknown force P obey the following two relationships.

$$F_b + F_t = P \tag{4.10}$$

$$F_t \mathrm{d} = P\mathrm{L} \tag{4.11}$$

Solving the above two equations in terms of the forces F_b and F_t

$$F_b = \left(1 - \frac{\mathrm{L}}{\mathrm{d}}\right) P \tag{4.12}$$

$$F_t = \frac{\mathrm{L}}{\mathrm{d}} P \tag{4.13}$$

From equation 4.10, one can see that the output of the summing box will be the desired force P.

Now consider the fact that the load reported by the load cell is not the actual load F_b or F_t. This is because part of the load has to pass through the bolt as previously discussed. In addition, differences in the effective sensitivity of the top and bottom force sensor arising from such effects as small differences in scaling factor, small differences in manufacturer sensitivity, and small differences from hysteresis effects will result in two sensors having slightly different overall calibration constant at any given time. Consequently, each force sensor will have a different overall correction factor β that represents the amount the measured force value must be multiplied to get the true value of the force P. This can be expressed as

$$F_b = \beta_b F_{bm} \tag{4.14}$$

$$F_t = \beta_t F_{tm} \tag{4.15}$$

Where F_{bm} represents the reported or measured force in the bottom sensor and β_b represents the overall correction factor for the bottom sensor. Similarly, F_{tm} is the measured force in the top sensor and β_t represents the overall correction factor for the top sensor.

Combining equations 4.12 with 4.14 and 4.13 with 4.15

$$\beta_b F_{bm} = \left(1 - \frac{L}{d}\right) P \tag{4.16}$$

$$\beta_t F_{tm} = \frac{L}{d} P \tag{4.17}$$

Re-arranged to

$$F_{bm} = \frac{1}{\beta_b}\left(1 - \frac{L}{d}\right) P \tag{4.18}$$

$$F_{tm} = \frac{1}{\beta_t} \cdot \frac{L}{d} P \tag{4.19}$$

In the test setup, it is the signals from the top and bottom force sensors that are vector-summed through the analogue-summing device. Thus, instead of simulating equation 4.10 to get the value of P, what is actually performed by the analogue summation device is

$$F_{bm} + F_{tm} = \frac{1}{\beta_b}\left(1 - \frac{L}{d}\right) P + \frac{1}{\beta_t} \cdot \frac{L}{d} P \tag{4.20}$$

Re-written as

$$P_m = \left[1 + \left(\frac{\beta_b}{\beta_t} - 1\right) \cdot \frac{L}{d}\right] \frac{1}{\beta_b} P \tag{4.21}$$

Where P_m represents the measured value of the load P.

Similarly to equations 4.14 and 4.15, an effective calibration factor for the measured load P using the summed forces from the top and bottom force sensors can be defined as

$$P = \beta_{eff} P_m \tag{4.22}$$

Where

$$\beta_{eff} = \frac{\beta_b}{\left[1+\left(\frac{\beta_b}{\beta_t}-1\right)\cdot\frac{L}{d}\right]} \tag{4.23}$$

Equation 4.23 shows that if the top force sensor overall correction factors β_t was equal to bottom force sensor overall correction factor β_b, then the effective calibration factor β_{eff} would simply be equal to β_b and β_t as would be expected. However, if a small difference between β_t and β_b exist and the ratio L/d is greater than unity, then the effective calibration factor can be much different than β_b. In fact, the calibration factor can be made to be less than unity or much greater than unity depending on whether β_t or β_b is larger than the other.

For the particular set of tests presented in this thesis, the value of L/d varies from 3 to 6. Table 4.6 demonstrates how easily the effective calibration factor β_{eff} can be different from either calibration constants β_b or β_t for small differences in percentages between β_b and β_t.

Table 4.6: Normalized Effective Calibration Factor β_{eff}/β_b Due to Equipment Setup

β_b/β_t	β_{eff}/β_b	
	L/d = 3	**L/d = 6**
0.95	1.18	1.43
0.98	1.06	1.14
1.00	1.00	1.00
1.02	0.94	0.89
1.05	0.87	0.77

The force sensors utilized for the testing have a full-scale linearity of 1%, a full-scale hysteresis of 0.5%, and a cross talk specification of less than 3% of full scale. In addition, the top and bottom force sensors can have slightly different bolt scaling factors due to one sensor being at the edge of the beam while the other sensor is not. As such, a 5% overall calibration difference between the top and bottom sensor is plausible and would explain why the measured overall calibrations factor varied between 0.8 and 1.5 between setups.

4.2.2.3 Force Sensor Issue: Overall Calibration Utilized in Testing

Taking into consideration the issues presented in sections 4.2.2.1 and 4.2.2.2, the total force measured by the sensors $F_{\text{total\_sensors}}$ must therefore be adjusted by an overall calibration factor β_{overall} in order to get the true total force F_{total} at the interface. This can be expressed as

$$F_{\text{total\_actual}} = \beta_{\text{overall}} F_{\text{total\_sensors}} \qquad \text{for sine vibration} \qquad (4.24)$$

$$S_{ff\_\text{total\_actual}} = \beta^2_{\text{overall}} S_{ff\_\text{total\_sensors}} \qquad \text{for random vibration} \qquad (4.25)$$

The overall calibration factor β_{overall} described in equations 4.24 and 4.25 accounts for both the forces going through the bolt as discussed by section 4.2.2.1 and the effects of geometry discussed in section 4.2.2.2.

The actual value of overall calibration factor β_{overall} can be measured directly by performing any arbitrary vibration test and extrapolating the force and acceleration measured to a frequency of 0 Hz. The value β_{overall} will be a scaling factor such that the force and acceleration at 0 Hz agree with the value predicted by Newton's second law. Consequently, depending on the type of excitation, the overall calibration factor β_{overall} is calculated as

$$\beta_{\text{overall}} = \frac{M_0 \cdot A_{0\text{-to-peak}}(0\text{Hz})}{F_{\text{total\_sensors}}(0\text{Hz})} \qquad \text{for sine excitation} \qquad (4.26)$$

$$\beta^2_{\text{overall}} = \frac{M_0^2 \cdot S_{aa}(0\text{Hz})}{S_{ff\_total\_sensors}(0\text{Hz})} \qquad \text{for random excitation} \qquad (4.27)$$

Where M_0 is the mass of the article, $A_{0\text{-to-peak}}$ is the zero-to-peak acceleration at any location on the load, and S_{aa} is the acceleration spectral density at any point on the load, $F_{\text{total\_sensors}}$ is the total vector summed force reported by the force sensors, and $S_{ff\_\text{total\_sensors}}$ is the total vector summed force spectral density of the force sensors.

In order to properly account for phase differences between force sensor pairs, the total force from each force sensor pair, in universal file format, was exported from the LMS vibration control system into Microsoft Excel. There, they could be properly added together to compute the total interface force F_{total_sensor} or $S_{ff\_total\_sensors}$ and the overall correction factor $\beta_{overall}$. This corrected total interface force was utilized to calculate the normalized apparent mass.

4.3 Description of the Tests and the Results

Two different and separate series of tests were performed. The first series of tests investigated how the damping, indicated by the value Q, changes with input acceleration amplitude and how changes in damping affect the measurement of the apparent mass. The second series of tests validated the apparent mass method by comparing the value of C^2 predicted by the apparent mass method, $C^2_{predicted}$, to the experimentally determined value, $C^2_{experimental}$, of a coupled two degree-of-freedom system. Both series of tests are described in sequence in this section.

4.3.1 Investigation of Q Dependence on Input Amplitude

The amount of damping, described by the quality factor Q of a structure, will influence the apparent mass function as described by equations 3.10 to 3.12. Since the value of C^2 is determined by the apparent mass, information regarding how Q varies is essential in evaluating an appropriate value for C^2.

To investigate the dependence of Q with input level, the load single degree-of-freedom system configuration labeled 20F10_1, as shown in figure 4.7, was exposed to various sine acceleration inputs. For each test, accelerometer C1X was utilized as the single control accelerometer. Since the load structure behaves as a single degree-of-freedom system, the value of Q was taken to be the peak value of the frequency response function defined by $\frac{A_{ML1X}}{A_{MS1X}}$, where A represents zero-to-peak acceleration. The natural frequency

was measured as the frequency at which the peak value of $\frac{A_{ML1X}}{A_{MS1X}}$ occurs. The details of the sine tests, along with the resulting Q values, are shown in table 4.7 and plotted in figure 4.13. All tests were performed sequentially in a single session.

Table 4.7: Effect of Varying Inputs Levels

0-to-Peak Amplitude in *g*	Frequency Range in Hz	Frequency Resolution in Hz	Sweep Rate in octave/minute	Natural Frequency in Hz	Q
0.1	110 to 140	0.25	1 upward	123.75	218
0.5	110 to 140	0.25	1 upward	123.25	119
1.0	110 to 140	0.25	1 upward	122.25	78
1.5	110 to 140	0.25	1 upward	121.75	65
2.0	110 to 140	0.25	1 upward	121.00	60
2.5	110 to 140	0.25	1 upward	120.50	55
3.0	110 to 140	0.25	1 upward	119.50	54
3.5	110 to 140	0.25	1 upward	119.25	47
4.0	110 to 140	0.25	1 upward	118.75	43
4.5	110 to 140	0.25	1 upward	118.25	39
5.0	110 to 140	0.25	1 upward	117.75	35
5.5	110 to 140	0.25	1 upward	117.25	32
6.0	110 to 140	0.25	1 upward	116.75	30

The data in table 4.7 presents clear and systematic changes in the natural frequency and Q value. This behaviour is evidence that the system under investigation is non-linear.

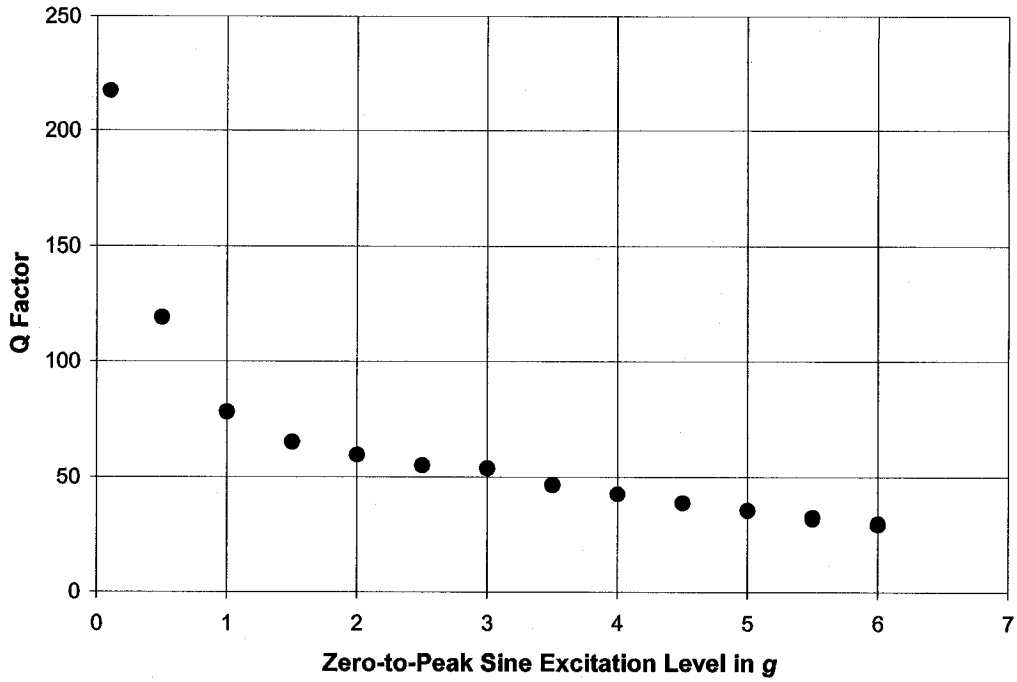

Figure 4.13: Dependence of Q factor with Sinusoidal Input Levels

Table 4.7 and figure 4.13 clearly show that input level has a significant effect on the Q value of a structure. Similar damping dependency on amplitude has been documented for other structures [26]. The phenomenon can be understood by noting that damping comes from different damping mechanisms. For example, possible damping mechanisms include

- Internal damping in the material
- Viscous damping from movement through the air
- Structural damping from microscopic slippage at the bolted interfaces

From the three damping mechanisms identified, the structural damping mechanism is the most significant source of damping in many structures [21]. At very low input levels, static friction prevents any significant movement between bolted interfaces and thus, the interface is very stiff and the low damping is characteristic of a structure with predominantly internal material damping. As the level is increased, slippage at the bolted interfaces also increases. The damping arising from structural damping is dependent on

the amplitude of the slippage. Consequently, as the input vibration levels are increased, the amplitude of the slippage also increases resulting in more energy being dissipated in the form of heat. In addition, the slippage reduces the joint stiffness leading to a reduction in the natural frequency of the structure as shown in table 4.7.

4.3.1.1 Differences in Random and Sine Excitation

Consider the response of a structure exposed to a 1 *g* sine sweep though its natural frequency and the response of the same structure exposed to a constant random acceleration spectral density spanning its natural frequency where the root-mean-square of the acceleration is 1 *g*. Tustin [30] has proposed that the peak response of a structure exposed to random vibration will tend to be less than if a slow sweeping sinusoidal vibration excites the same structure. His argument is based on the observation that several full-amplitude cycles, at or near the structure's natural frequency, are required in order to fully develop the response. The excitation from random vibration is by definition not constant in both amplitude and in phase resulting in an underdeveloped response.

The above reasoning would be true if the damping of the structure was independent of the amplitudes of excitations. In reality, the damping dependence on excitation amplitude can have a very pronounced effect on the damping experienced during random vibration. Consider the input levels experienced during random vibration testing. The acceleration amplitudes from the random vibration have a Normal distribution with a mean acceleration of zero and a standard deviation that depends on the ASD spectrum definition. The probability density $f(x)$ of the Normal distribution in terms of the mean $\bar{x}$ and the standard deviation σ is shown by equation 4.28 [31] and plotted in figure 4.14.

$$f(x) = \frac{1}{\sigma\sqrt{2\pi}} e^{-\left[\frac{(x-\bar{x})^2}{2\sigma^2}\right]} \tag{4.28}$$

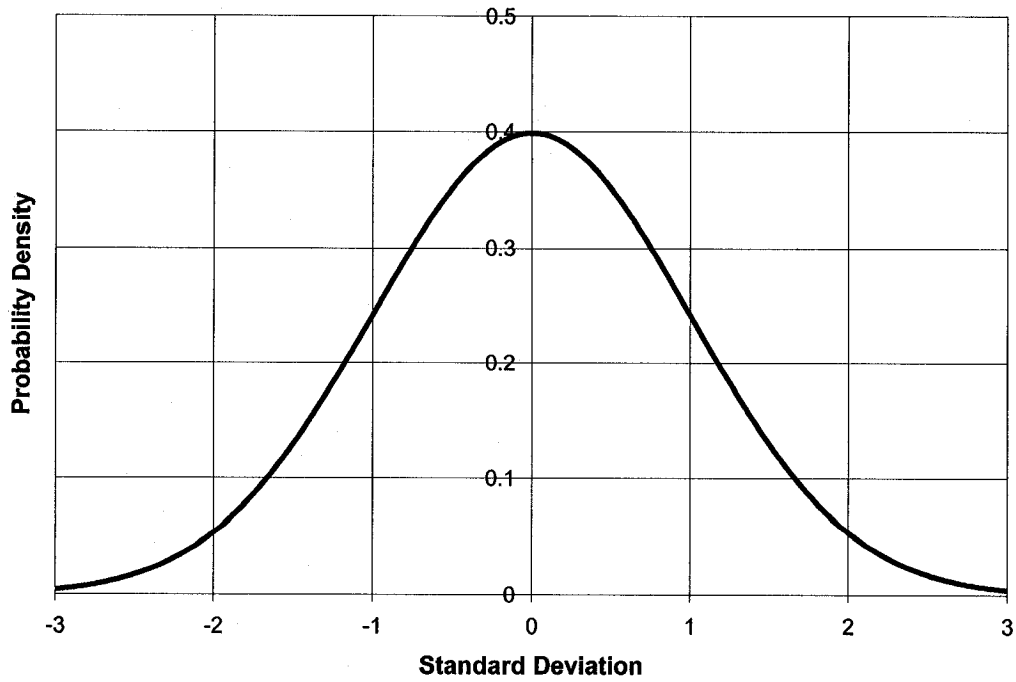

Figure 4.14: Normal Probability Density Distribution

Figure 4.14 shows clearly that the random vibration amplitudes at any given moment are more likely to occur close to the mean of zero. These small amplitudes are associated with very large Q as shown in figure 4.13. Consequently, even though the full response of the structure is never attained, the structure can exhibit very large responses due to the much lighter damping associated with the smaller input amplitudes.

The above effect must be appreciated when measuring the apparent mass of a structure in that a sine test will likely give a lower peak apparent mass than a random vibration test. This statement was verified experimentally with 5 tests, described in table 4.8, using the single degree-of-freedom load system defined by the 20F2_1 configuration shown in figure 4.5. For each test, accelerometer C1X was utilized as the single control accelerometer. The peak normalized apparent mass was calculated as $\frac{|F_{total}(f_n)|}{M_0 \cdot |A_{MS1X}(f_n)|}$ for sine tests and as $\sqrt{\frac{|S_{ff\_total}(f_n)|}{M_0^2 \cdot |S_{aa\_MS1X}(f_n)|}}$ for random tests, where f_n represents the

natural frequency of the single degree-of-freedom load system where the peak response occurs. The total force F_{total} or the total force spectral density S_{ff_total} was corrected utilizing calibration factors as per equations 4.26 and 4.27. The test results, shown in table 4.8, support the notion that significantly larger values of the peak apparent mass can be obtained when measuring the apparent mass using random vibration as opposed to sine vibration.

Table 4.8: Apparent Mass from Sine and Random Excitation

	Test 1	**Test 2**	**Test 3**	**Test 4**	**Test 5**
Vibration Type	Sine	Sine	Sine	Random	Random
Frequency Range in Hz	10-600	10-600	10-600	10-600	10-600
Frequency Resolution in Hz	0.25	0.25	0.25	0.25	0.25
Input Amplitude	0.5 *g* 0-to-peak	1.0 *g* 0-to-peak	3.0 *g* 0-to-peak	0.0017 g^2/Hz	0.0153 g^2/Hz
Test Duration in minutes	3	3	3	4	4
Sweep Rate in octaves/minute	2 upward	2 upward	2 upward	not applicable	not applicable
Input Vibration Root-Mean-Square	not applicable	not applicable	not applicable	1.0 *g*	3.0 *g*
Input and Output Statistical Degree-of-Freedom	not applicable	not applicable	not applicable	120	120
Normalized Peak Apparent Mass	**80**	**51**	**21**	**223**	**123**

4.3.2 Investigation of Apparent Mass Method to Determine C^2

This section describes the second series of tests that investigated the apparent mass method by comparing the value of C^2 predicted by the apparent mass method to the actual value from a two degrees-of-freedom coupled system.

To perform the comparison, the uncoupled source, as a single degree-of-freedom system, and all uncoupled loads, as single degree-of-freedom systems, were vibrated using an arbitrary sine sweep. The natural frequency of the uncoupled source was determined

from its measured acceleration frequency response function. The normalized apparent mass of the uncoupled load was determined from the total force and input acceleration measurements at the base of the load using the mass of the load and the following equation.

$$\left[\frac{\left|\mathrm{M}_{app}(f)\right|}{\mathrm{M}_{\mathrm{load}}}\right]_{\mathrm{uncoupled\_load}} = \frac{F_{\mathrm{total}}(f)}{\mathrm{M}_{\mathrm{load}} \cdot \mathrm{A}_{\mathrm{input}}(f)} \tag{4.29}$$

From the normalized apparent mass function, the natural frequency of the load was determined and the various uncoupled load-to-source natural frequency ratios F were computed.

Then, the two systems were coupled, as a two degree-of-freedom system, and exposed to random vibration. The interface forces and source acceleration of the coupled system were measured such that the experimental value, $\mathrm{C}^2_{\mathrm{experimental}}$, could be computed using equation 3.3 as

$$\mathrm{C}^2_{\mathrm{experimental}} = \left[\frac{\left[S_{ff\_\mathrm{interface}}\right]_{\max}}{\mathrm{M}^2_{\mathrm{load}} \cdot \left[S_{aa\_\mathrm{source}}\right]_{\max}}\right]_{\mathrm{coupled\_system}} \tag{4.30}$$

Where $[S_{ff\_\mathrm{interface}}]_{\max}$ is the maximum force spectral density between the load and the source, $\mathrm{M}_{\mathrm{load}}$ is the mass of the load, and $[S_{aa\_\mathrm{source}}]_{\max}$ is the maximum measured acceleration of the source.

Also noted during the coupled system tests was the frequency $f_{\max\_\mathrm{force}}$ where the maximum force spectral density occurs. In addition, the following ratio was noted.

$$\left[\frac{S_{aa\_\mathrm{source}}\left(f_{\max\_\mathrm{force}}\right)}{S_{aa\_\mathrm{source}}\left(f_{\max\_\mathrm{acc}}\right)}\right]_{\mathrm{coupled\_system}} \tag{4.31}$$

The value of the ratio given by equation 4.31 will be a number less than or equal to unity.

The value of C^2 as predicted by the apparent mass method was then computed using equation 3.5 of the apparent mass method re-written as

$$C^2_{predicted} = \left[\frac{\left|M_{app}\left(f_{max\_force\ (coupled\_system)}\right)\right|}{M_{load}}\right]^2_{uncoupled\_load} \cdot \left[\frac{S_{aa\_source}\left(f_{max\_force}\right)}{S_{aa\_source}\left(f_{max\_acc}\right)}\right]_{coupled\_system} \quad (4.32)$$

Finally, the value of $C^2_{predicted}$ was compared to the value of $C^2_{experimental}$ for the different values of uncoupled load-to-source natural frequency ratios F. The comparison demonstrates that the value of $C^2_{experimental}$, given by equation 4.30, can be determined if the normalized apparent mass of the load is measured, as per equation 4.29, and if the values f_{max_force}, $S_{aa\_source}(f_{max\_force})$, and $S_{aa\_source}(f_{max\_acc})$ of the coupled system are known.

In the following, the results for both the uncoupled source and the uncoupled loads are presented.

4.3.2.1 Uncoupled Source Test Results

The source only tests were performed using the configurations 20U, 20F, and 20D, which are shown in figures 4.2, 4.3, and 4.4 respectively.

The source was vibrated with a slow sine sweep as described in table 4.9. Some typical plots produced by the LMS vibration control system are shown in appendix J for reference. The natural frequency and the Q of the structure were determined from the frequency response function $\frac{A_{MS1X}}{A_{C1X}}$. The natural frequency was determined as the frequency where the peak value of the frequency response function occurs. Since the structure behaves as a single degree-of-freedom system, the Q corresponds to the peak response of the frequency response function. The Q was calculated to determine the amount of increase in damping provided by the 20D configuration.

The measured natural frequencies of the uncoupled source and the corresponding Q are shown in table 4.10. The plots of the frequency response functions are shown in figures 4.15 to 4.17, which have been re-plotted from the universal file data using Microsoft Excel.

Indeed, table 4.10 shows that the deliberately damped configuration 20D has significantly more damping than the essentially un-damped configuration 20U.

Table 4.9: Uncoupled Source Vibration Test Details

Test Details	Value
Vibration Type	Sine
Frequency Range in Hz	10-1000
Frequency Resolution in Hz	1.0
Input Amplitude	0.5 *g* 0-to-peak
Test Duration in minutes	2.82
Sweep Rate in octaves/minute	2 – upward
Control Accelerometer	C1X

Table 4.10: Measured Uncoupled Source Natural Frequencies and Q

Test Configuration	Natural Frequency in Hz	Q
20F	707	14
20U	246	44
20D	260	18

Although the Sorbothane has added a significant amount of damping to the source structure, it has also added some amount of stiffness resulting in a small increase in natural frequency as shown in table 4.10.

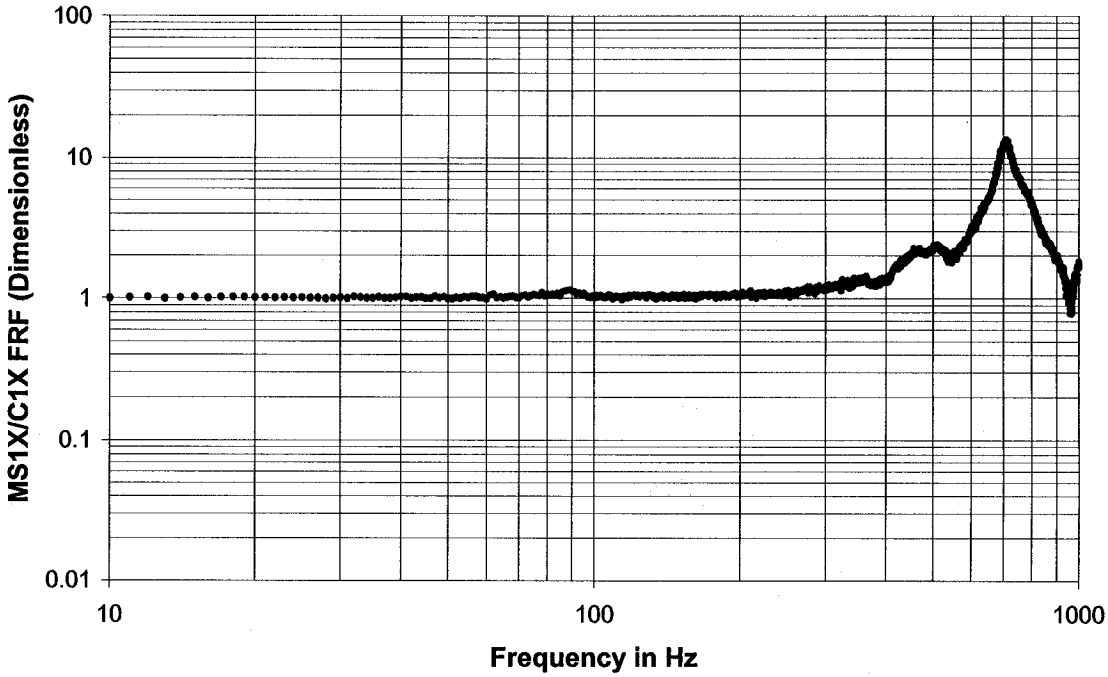

Figure 4.15: 20F Frequency Response Function Test Results

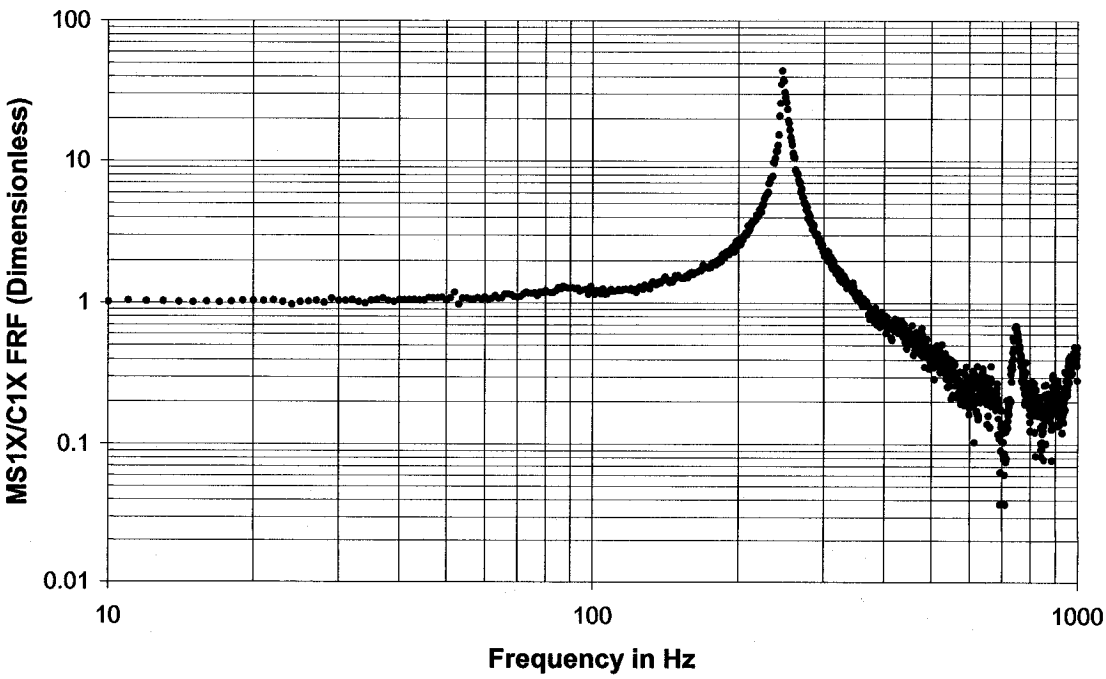

Figure 4.16: 20U Frequency Response Function Test Results

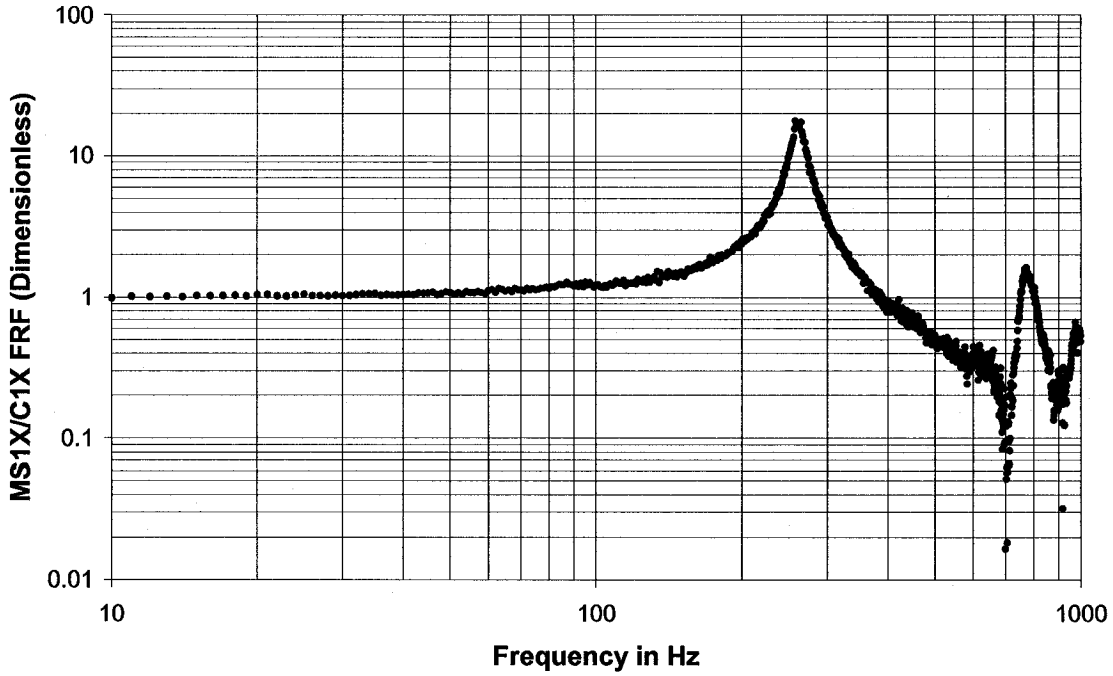

Figure 4.17: 20D Frequency Response Function Test Results

4.3.2.2 Uncoupled Load Test Results

For the uncoupled load tests, the source was fixed with the optional sidewalls, as shown in figures 4.5 and 4.6, such that the source structure acted as an extension of the vibration table up to about 400 Hz as shown in figure 4.15. The slow sine sweep utilized for testing is described in table 4.11. The configurations utilized for these tests are described in table 4.12. In addition, to completely remove the dynamic effects of the source, the apparent mass function was computed relative to the acceleration of the source MS1X instead of the control accelerometer C1X.

The apparent mass can be computed from either a sine or random vibration test. At the time of these tests, the previous experiment of section 4.3.1 investigating the difference between the sine and random vibrations had not yet been completed. Based on the reasoning given by Tustin [30], that a slow sine sweep is better than random vibration at fully exciting the resonance of a structure, a slow sine sweep test was utilized to find the apparent mass for all uncoupled load tests.

The normalized apparent mass was computed using $\frac{|F_{total}(f)|}{M_0 \cdot |A_{MS1X}(f)|}$ with the LMS data provided in universal file format, where the total force F_{total} is the total force calibrated as per equations 4.24 and 4.26 and M_0 is 2.080 kg for the 2 kg nominal mass and 9.224 kg for the 10 kg nominal mass. The resulting apparent mass functions for each load configuration are shown in figures 4.18 to 4.31. These apparent mass functions will be utilized later on to predict the value of C^2 for the coupled source-load system.

As shown in figures 4.18 to 4.31, most of the load configurations can be described as a single degree-of-freedom system with four configurations 20F2_5, 20F2_6, 20F2_7 and 20F10_7 being more akin to a two degrees-of-freedom system. The extra degree-of-freedom for these four configurations are due to the presence of higher order modes in the structure. The measured first natural frequencies of the uncoupled load are shown in table 4.12.

In view of equation 4.32, the next logical step is to investigate the coupled systems.

Table 4.11: Uncoupled Load Vibration Test Details

Test Details	Value
Vibration Type	Sine
Frequency Range in Hz	20-1000
Frequency Resolution in Hz	1.0
Input Amplitude	0.5 *g* 0-to-peak
Test Duration in minutes	2.82
Sweep Rate in octaves/minute	2 – upward
Control Accelerometer	C1X

Table 4.12: Measured Uncoupled Load First Natural Frequencies

Test Configuration	First Natural Frequency in Hz
20F2_1	124
20F2_2	193
20F2_3	273
20F2_4	333
20F2_5	383
20F2_6	432
20F2_7	453
20F10_1	127
20F10_2	193
20F10_3	264
20F10_4	309
20F10_5	352
20F10_6	393
20F10_7	459

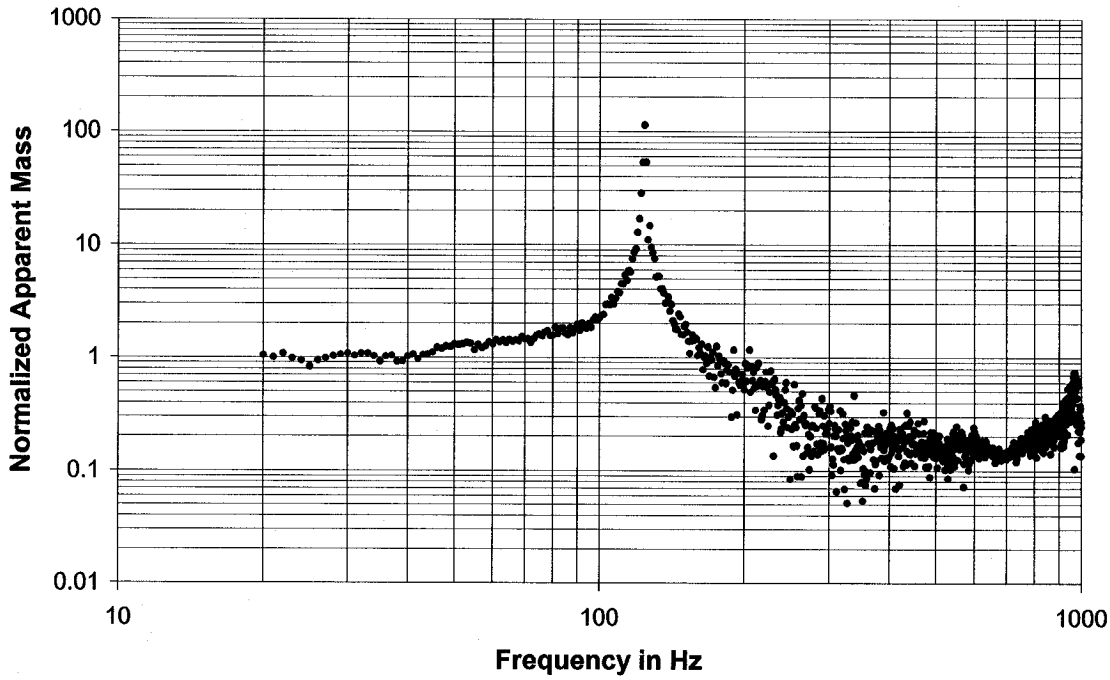

Figure 4.18: Normalized Apparent Mass Results for Test Configuration 20F2_1

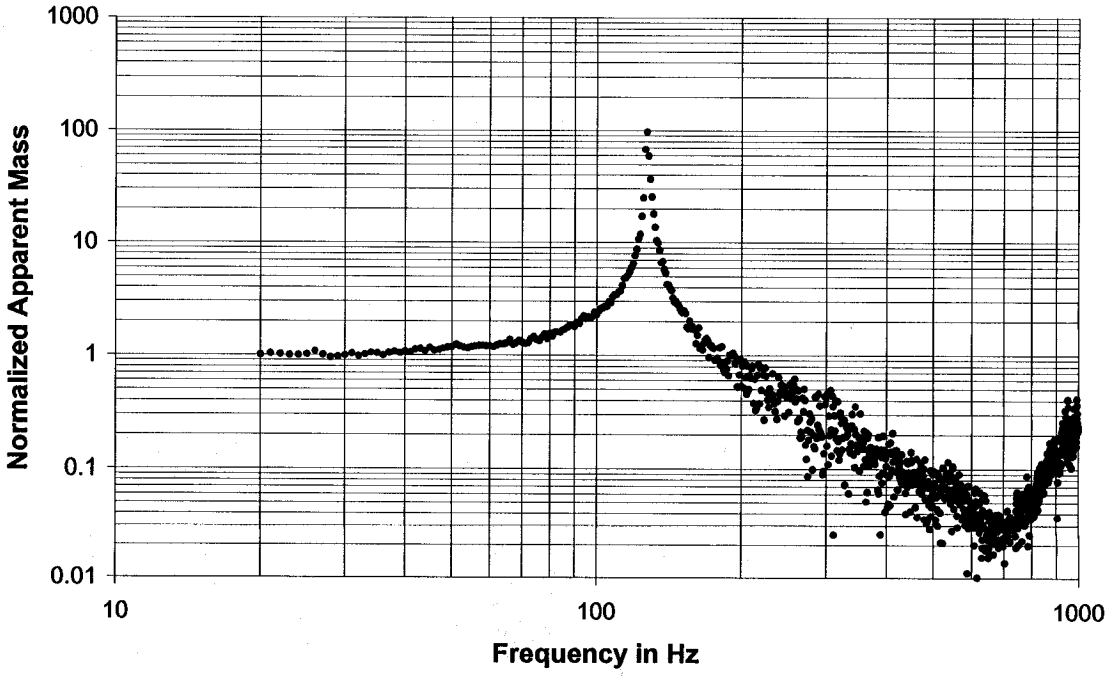

Figure 4.19: Normalized Apparent Mass Results for Test Configuration 20F10_1

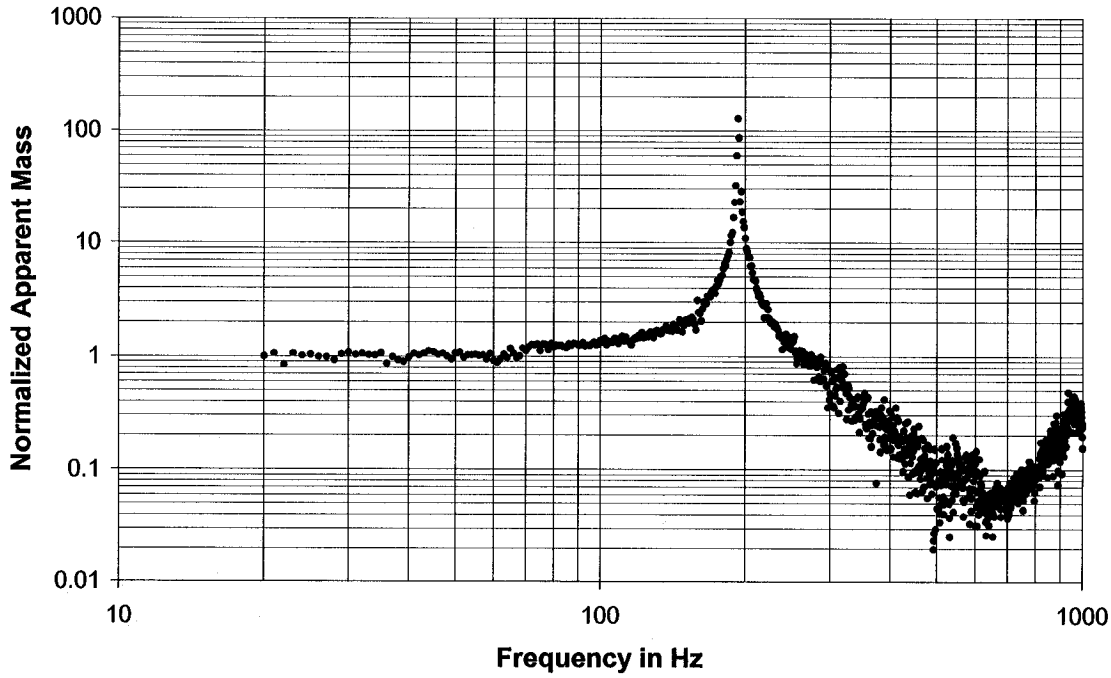

Figure 4.20: Normalized Apparent Mass Results for Test Configuration 20F2_2

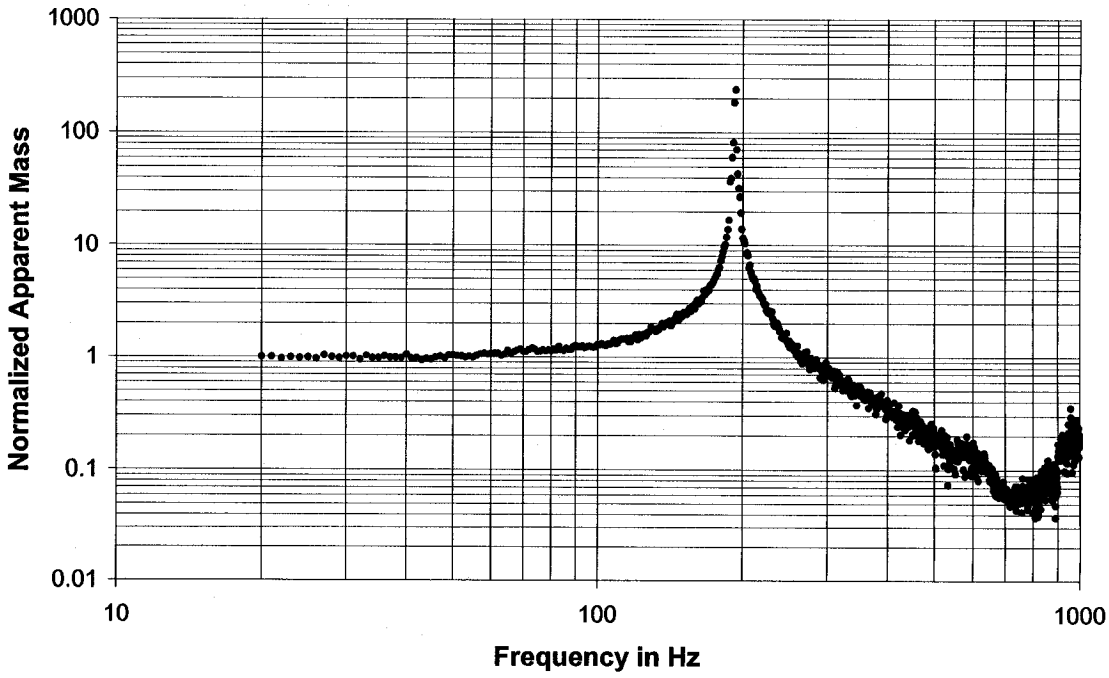

Figure 4.21: Normalized Apparent Mass Results for Test Configuration 20F10_2

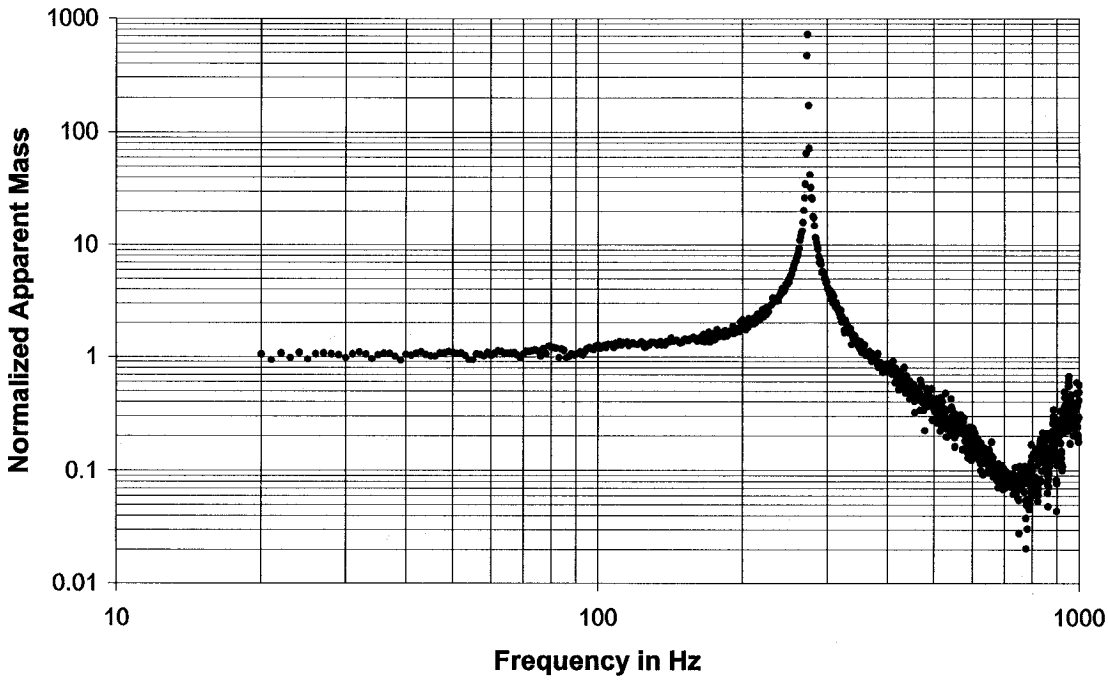

Figure 4.22: Normalized Apparent Mass Result for Test Configuration 20F2_3

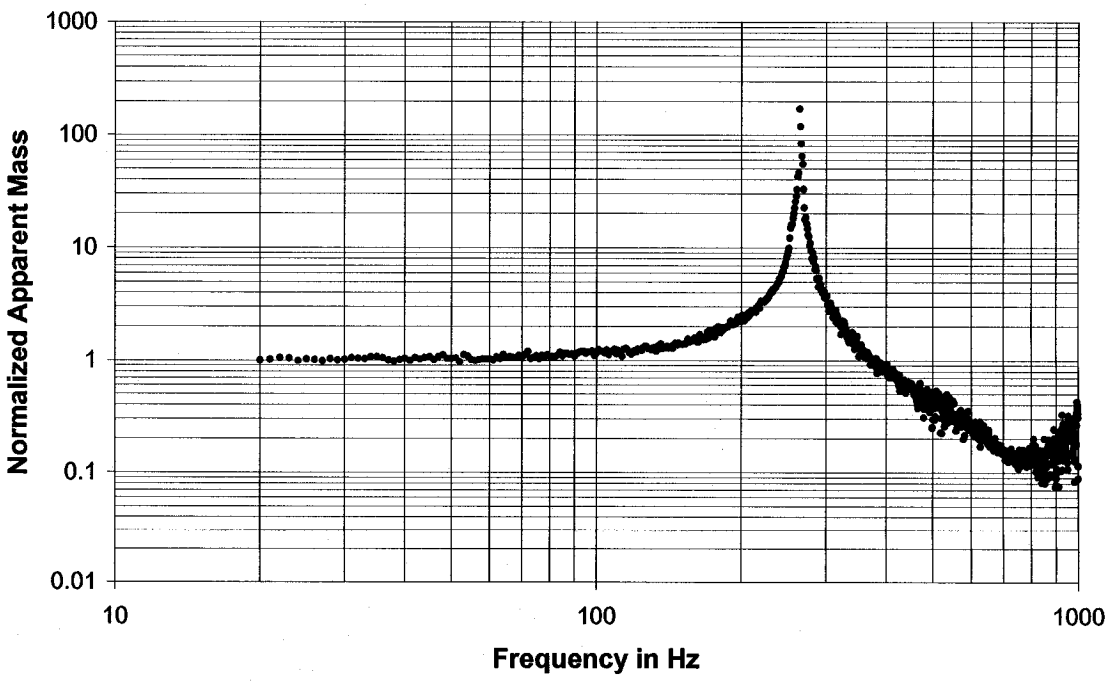

Figure 4.23: Normalized Apparent Mass Results for Test Configuration 20F10_3

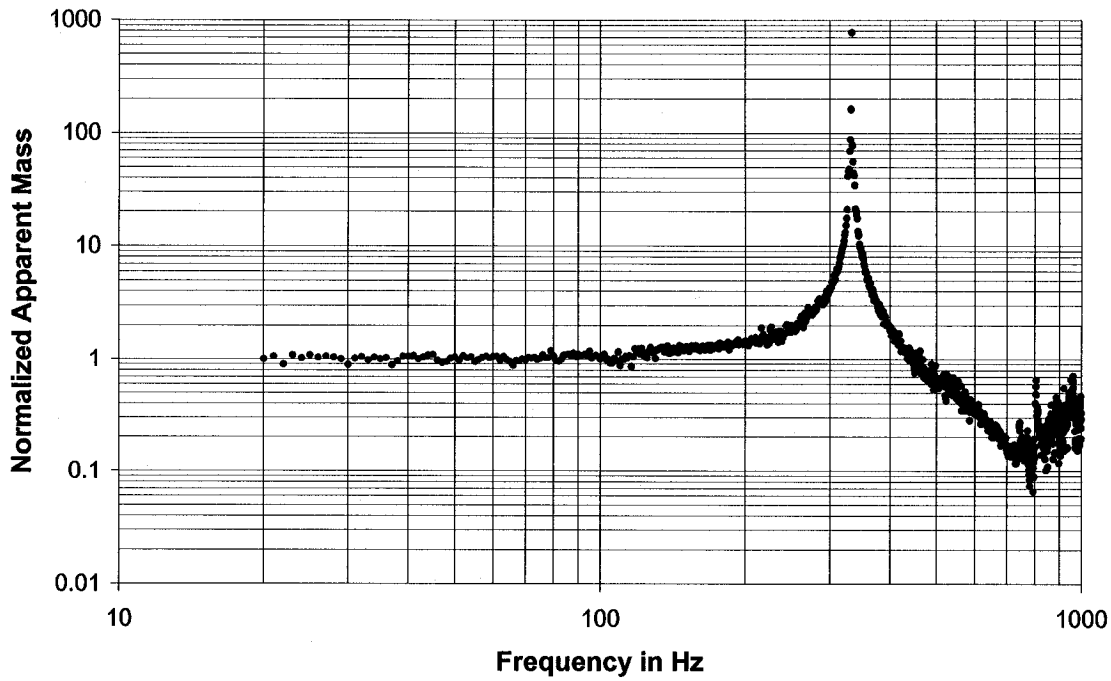

Figure 4.24: Normalized Apparent Mass Results for Test Configuration 20F2_4

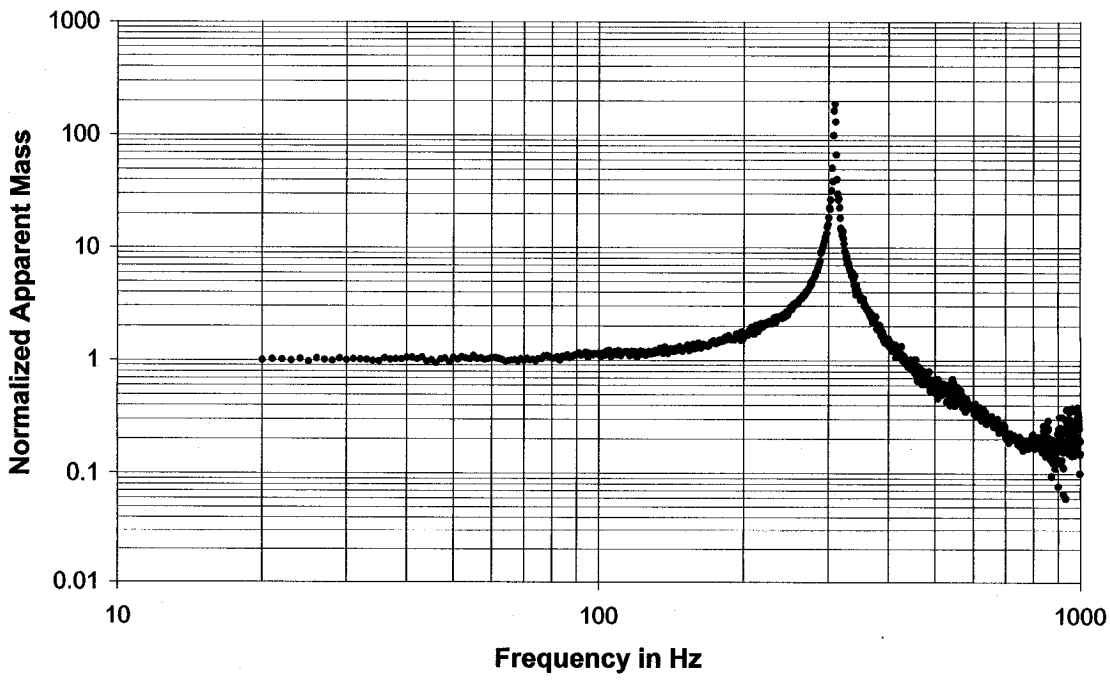

Figure 4.25: Normalized Apparent Mass Results for Tests Configuration 20F10_4

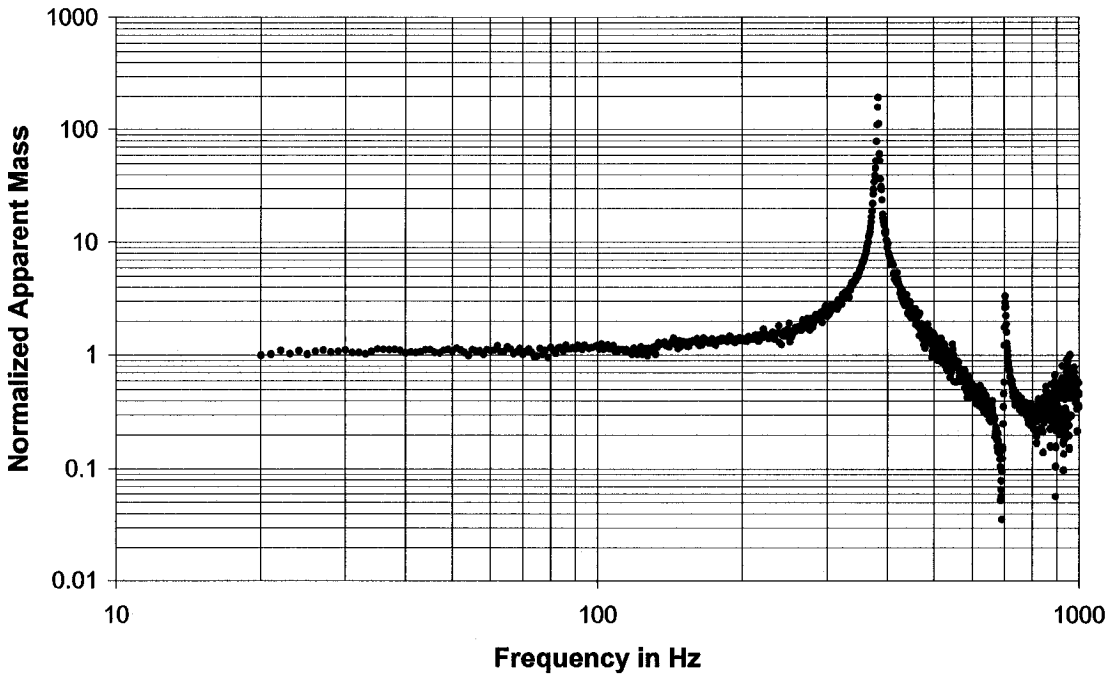

Figure 4.26: Normalized Apparent Mass Results for Test Configuration 20F2_5

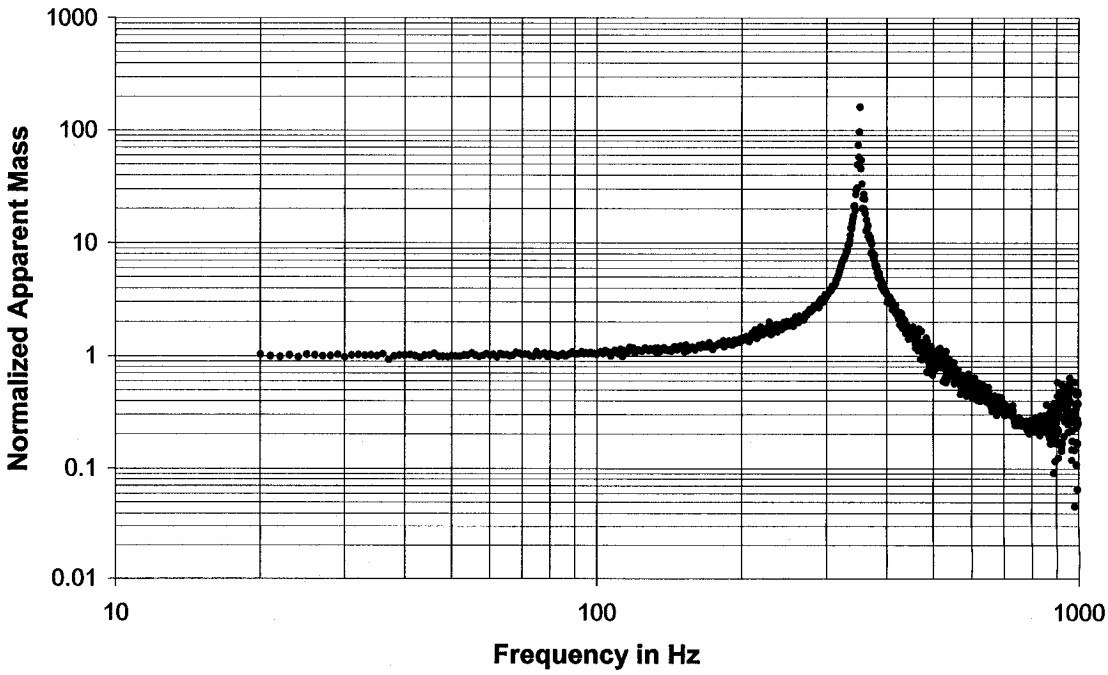

Figure 4.27: Normalized Apparent Mass Results for Test Configuration 20F10_5

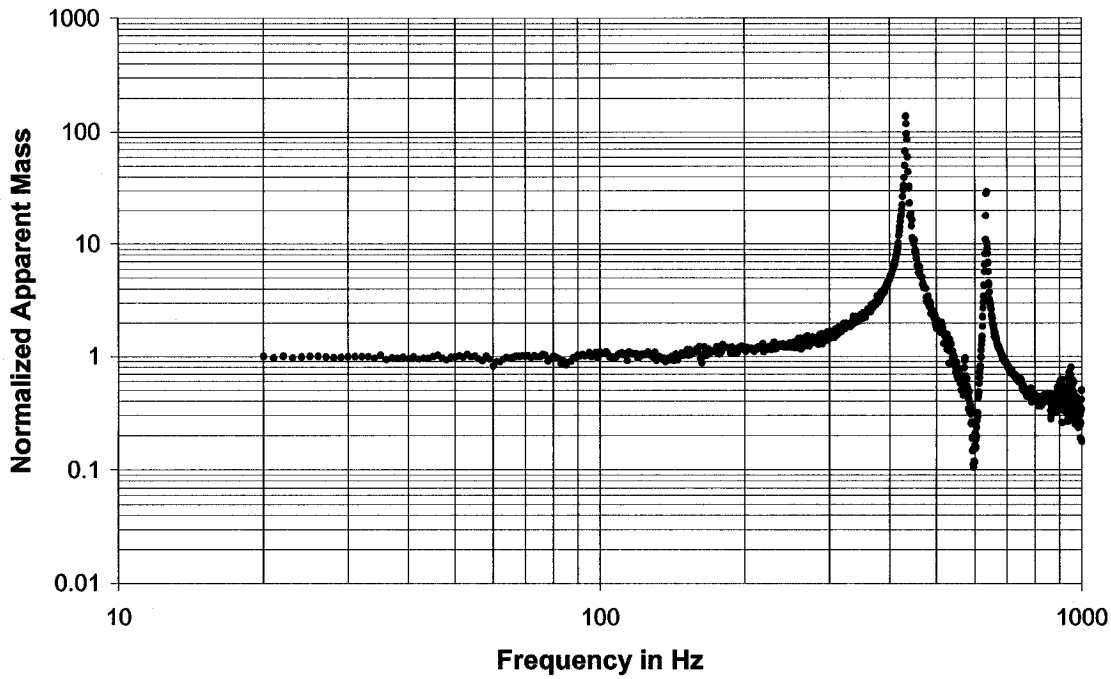

Figure 4.28: Normalized Apparent Mass Results for Test Configuration 20F2_6

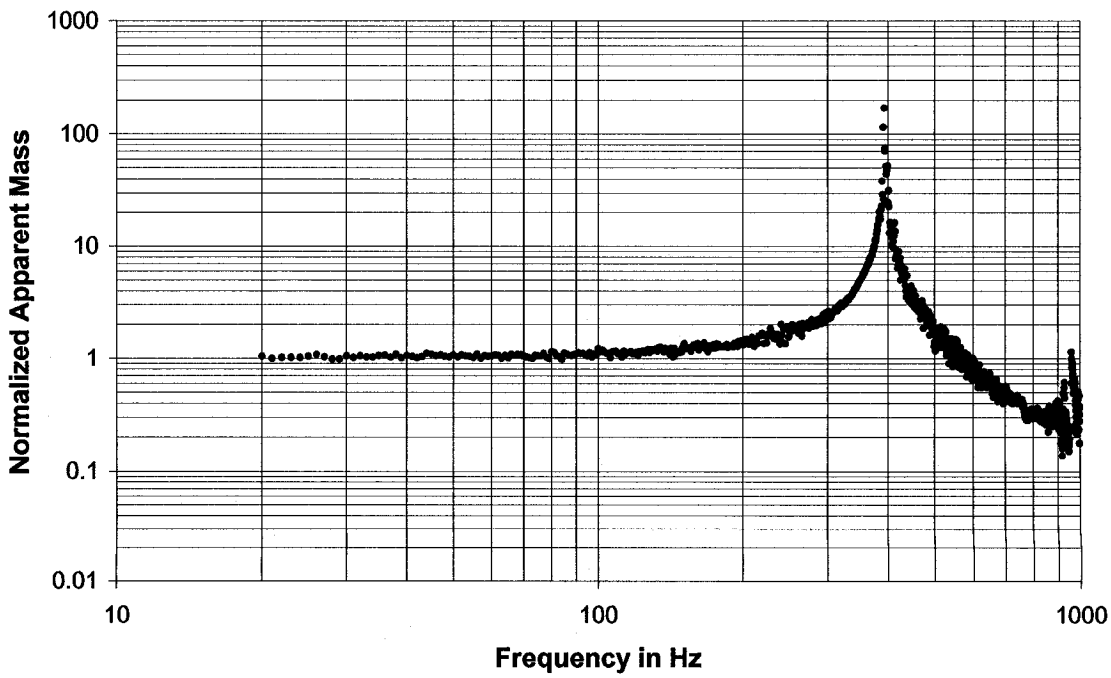

Figure 4.29: Normalized Apparent Mass Results for Test Configuration 20F10_6

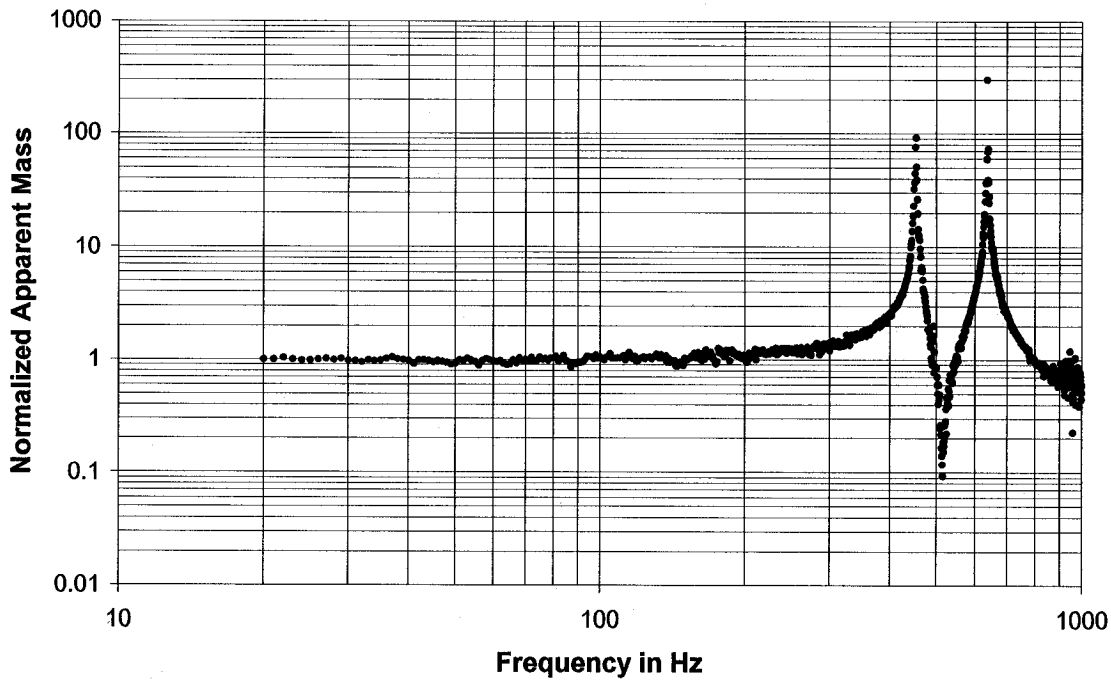

Figure 4.30: Normalized Apparent Mass Results for Test Configuration 20F2_7

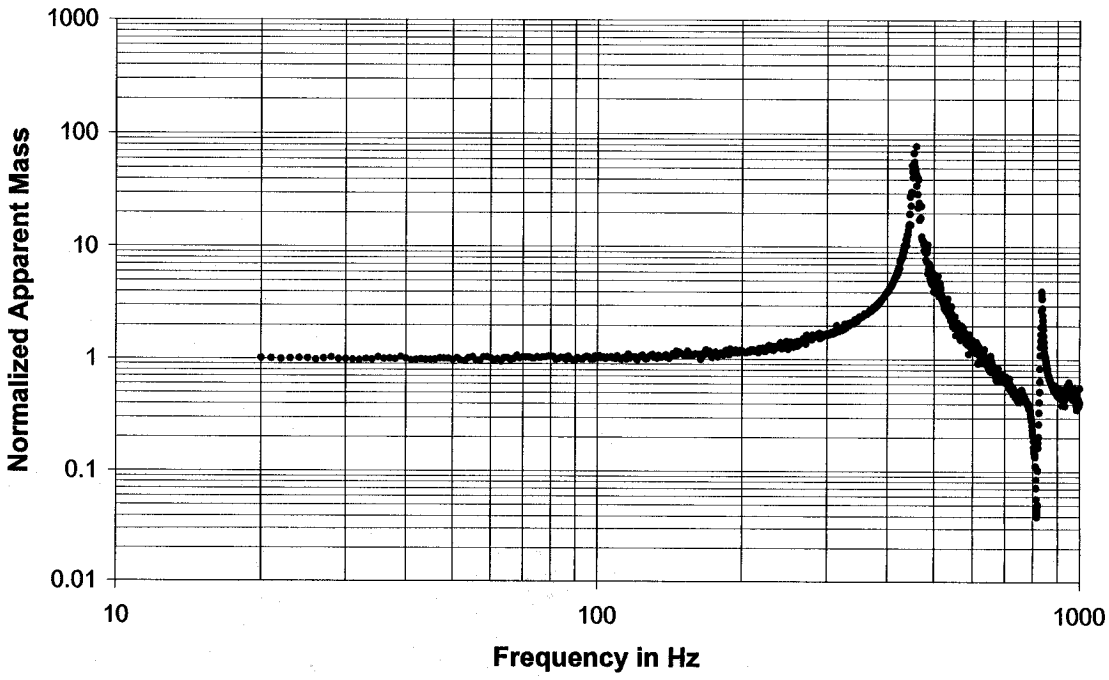

Figure 4.31: Normalized Apparent Mass Results for Test Configuration 20F10_7

4.3.2.3 Coupled Systems Test Results

The coupled systems were vibrated using random vibration as described in table 4.13. As previously discussed in section 4.2.2.1, part way during the testing the vibration levels were reduced from 0.1 g^2/Hz to 0.01 g^2/Hz to protect the equipment. Also part way during the testing, the resolution was increased from 1 Hz to 0.5 Hz because it was realized that the resolution could be increased without affecting the desired 150 statistical degrees-of-freedom for the measurements.

The tests were performed using the coupled configurations identified in table 4.14. Examples of a coupled configuration for the 2 kg nominal load mass and the 10 kg nominal load mass are shown in figures 4.8 and 4.9 respectively.

All coupled tests were performed on the 17k shaker at the Canadian Space Agency's David Florida Laboratory. Unfortunately, this particular shaker is an older model that has poor signal-to-noise ratio. As such, the best control that could be achieved was ±3 dB of the desired control amplitudes as identified in table 4.13. The noisy input is reflected as noisy data as demonstrated in the acceleration and force data shown in figures 4.32 and 4.33 for the 20D2_4 configuration. The corresponding plots from the LMS vibration control system are shown in appendix J. However, since the value of C^2 is dependent on the ratio of the interface force spectral density to the source spectral acceleration, the fact that the input was noisy had little impact on the experimentally measured value for C^2.

The coupled system force data shown in figure 4.33 show periodic super-harmonic responses indicative of a non-linear system [39]. The super-harmonics are only present in all of the random vibration tests that include a load configuration as demonstrated in appendix J. This indicates that when the load is integrated with the source, it makes the coupled system non-linear. The non-linear behaviour can be attributed to the Coulomb friction in the bolted interfaces that attach to the load. The reason that the sine sweep tests do not show any super-harmonics is because the reported data from the sine sweep

tests is filtered to only include the response at the excitation frequency. Consequently, any super-harmonics are filtered out in the reported frequency response function of a sine sweep. In contrast, the filtering process is not present during random vibration tests.

A random vibration test is preferred over a sine sweep test to determine the apparent mass because the random vibration produces larger responses than sine sweep, for reasons discussed in section 4.3.1. This is desirable to avoid under-estimating the value of the apparent mass and consequently under-estimating the value of C^2, which would lead to under-testing of the test article.

The apparent mass method is based on the notion that the apparent mass of the load is independent of the structure it is mounted on. The presence of super-harmonics in the coupled system random test data but not in the uncoupled system sine test data does not significantly affect the apparent mass method for the tests presented in this thesis. This is because the apparent mass is always evaluated at frequencies that are well below any super-harmonics.

The experimental value, $C^2_{experimental}$, for the coupled system was computed using equation 4.30, repeated below.

$$C^2_{experimental} = \left[\frac{\left[S_{ff\_interface} \right]_{max}}{M^2_{load} \cdot \left[S_{aa\_source} \right]_{max}} \right]_{coupled\_system} \tag{4.30}$$

For example, figure 4.33 shows that the value of $[S_{ff\_interface}]_{max}$ for the 20D2_4 configuration is 2 579 lb^2/Hz occurring at 365 Hz. Similarly, figure 4.32 shows that the value of $[S_{aa\_source}]_{max}$ is 33.4 g^2/Hz. The value of S_{aa_source} evaluated at 365 Hz, the frequency where the maximum force occurs, is identified as 6.26 g^2/Hz.

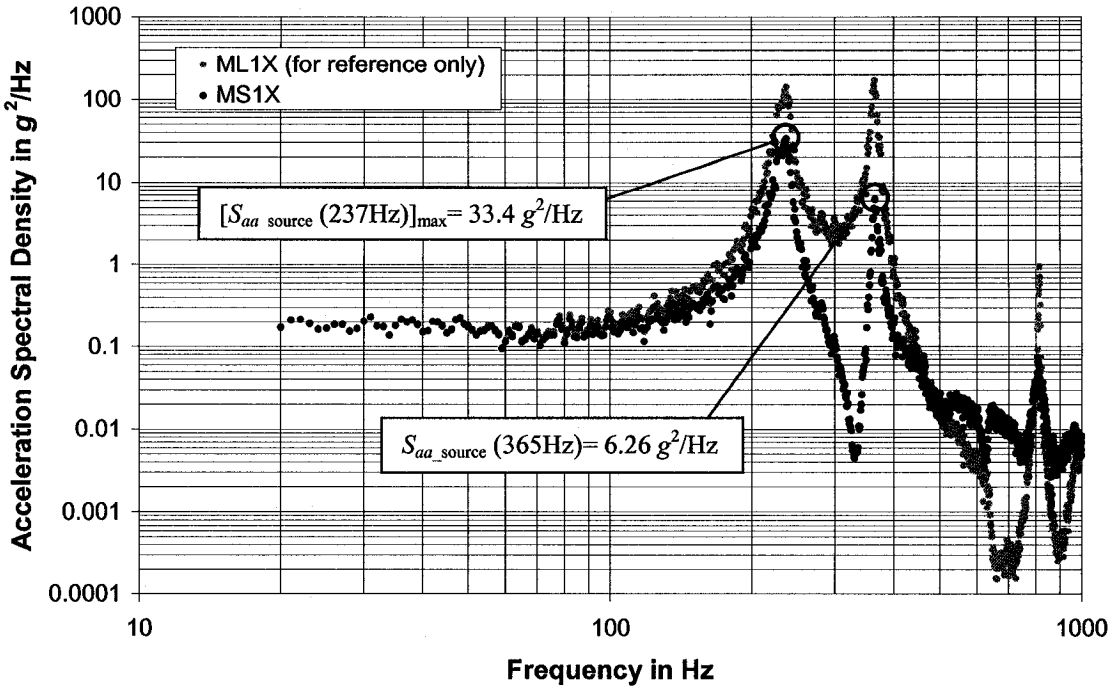

Figure 4.32: Acceleration Data for Test Configuration 20D2_4

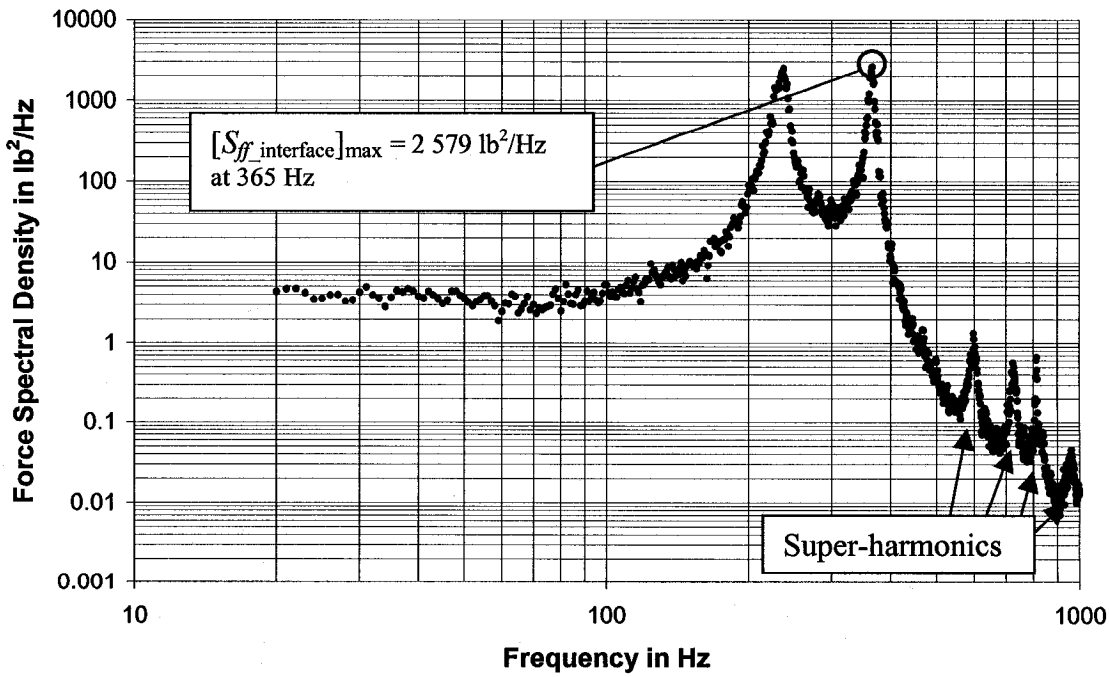

Figure 4.33: Summed and Corrected Interface Force Spectral Density Data for Test Configuration 20D2_4

Since the actual mass of the load is 2.080 kg or 4.586 lb/g, the value of $C^2_{experimental}$ for the 20D2_4 configuration is

$$C^2_{experimental\_20D2\_4} = \frac{2\,579\,lb^2/Hz}{\left(4.586\ lb/g\right)^2 \cdot 33.4\,g^2/Hz} = 3.67$$

Note that the value of C^2 is dimensionless. The experimental values, $C^2_{experimental}$, for the remaining coupled system test configurations are listed in table 4.14.

In addition, figure 4.31 shows that the ratio given by equation 4.31 is

$$\left[\frac{S_{aa\_source}\left(f_{max\_force}\right)}{S_{aa\_source}\left(f_{max\_acc}\right)}\right]_{coupled\_system} \tag{4.31}$$

$$\left[\frac{S_{aa\_source}(365\ Hz)}{S_{aa\_source}(237\ Hz)}\right]_{20D2\_4} = \frac{6.26\,g^2/Hz}{33.4\,g^2/Hz} = 0.1874$$

The ratios for the remaining coupled system tests configurations are listed in table 4.14.

Table 4.13: Vibration Test Details

Test Details	Rand1	Rand2	Rand3
Vibration Type	Random	Random	Random
Frequency Range in Hz	20-1000	20-1000	20-1000
Frequency Resolution in Hz	1.0	1.0	0.5
Test Duration	150 seconds	150 seconds	150 seconds
Control Accelerometer	C1X	C1X	C1X
Control Amplitude	0.1 g^2/Hz	0.01 g^2/Hz	0.01 g^2/Hz
Control Vibration Root-Mean-Square	9.9 g	3.1 g	3.1 g
Control Statistical Degrees-of-Freedom	150	150	150
Acceleration Measurement Statistical Degrees-of-Freedom	150	150	150
Force Measurement Statistical Degrees-of-Freedom	150	150	150

Table 4.14: Coupled System Test Results and Experimental C^2

Test Config.	Load to Source Uncoupled Natural Frequency Ratio, F	Test Type see table 4.12	Coupled System f_{max_force} in Hz	Coupled System f_{max_acc} in Hz	Source $S_{aa}(f_{max\_force})/S_{aa}(f_{max\_acc})$	C^2 Experimental (Eq. 4.30)
20U2_1	0.50	Rand3	121.5	245	0.005237	**4.75**
20U2_2	0.78	Rand3	182.0	259	0.09180	**8.25**
20U2_3	1.11	Rand3	306.5	217	0.6296	**6.89**
20U2_4	1.35	Rand3	359.0	224	0.1639	**3.95**
20U2_5	1.56	Rand3	413.0	225	0.08137	**3.03**
20U2_6	1.76	Rand3	456.5	227	0.05702	**2.62**
20U2_7	1.84	Rand3	230.0	230	1	**1.55**
20D2_1	0.48	Rand1	120	260	0.02254	**17.91**
20D2_2	0.74	Rand1	181	267	0.2128	**16.03**
20D2_3	1.05	Rand1	227	222	0.9077	**7.50**
20D2_4	1.28	Rand1	365	237	0.1874	**3.67**
20D2_5	1.47	Rand1	239	239	1	**2.27**
20D2_6	1.66	Rand1	470	241	0.04449	**1.93**
20D2_7	1.74	Rand1	243	243	1	**1.61**
20U10_1	0.52	Rand3	117.5	261	0.01114	**0.61**
20U10_2	0.78	Rand3	158.5	296	0.3262	**3.43**
20U10_3	1.07	Rand3	179.0	179	1	**3.78**
20U10_4	1.26	Rand3	186.5	187	1	**2.59**
20U10_5	1.43	Rand3	189.5	190	1	**2.11**
20U10_6	1.60	Rand3	190.5	191	1	**1.76**
20U10_7	1.87	Rand3	196.0	196	1	**1.55**
20D10_1	0.49	Rand2	110	269	0.01426	**1.15**
20D10_2	0.74	Rand2	155	295	0.2558	**3.42**
20D10_3	1.02	Rand2	182	182	1	**4.30**
20D10_4	1.19	Rand2	194	194	1	**2.81**
20D10_5	1.35	Rand1	199	199	1	**2.15**
20D10_6	1.51	Rand1	202	202	1	**1.79**
20D10_7	1.77	Rand1	206	206	1	**1.47**

4.3.2.4 Predicted Value of C^2 Based on Measured Apparent Mass of Uncoupled Load

The value of $C^2_{predicted}$ was computed using the apparent mass method described by equation 3.5. The apparent mass data and acceleration spectral density data required to utilize equation 3.5 were taken from the data collected in sections 4.3.2.2 and 4.3.2.3 respectively. Equation 3.5, rewritten as equation 4.32, is shown below for reference.

$$C^2_{predicted} = \left[\frac{\left|M_{app}\left(f_{max\_force\ (coupled\_system)}\right)\right|}{M_{load}}\right]^2_{uncoupled\_load} \cdot \left[\frac{S_{aa\_source}\left(f_{max\_force}\right)}{S_{aa\_source}\left(f_{max\_acc}\right)}\right]_{coupled\_system} \quad (4.32)$$

Equation 4.32 shows that if the frequencies f_{max_force} and f_{max_acc} of the coupled system are known, as well as the acceleration spectral density data at those frequencies, then the value of $C^2_{predicted}$ can be computed by measuring the normalized apparent mass of the uncoupled load. In addition, since the maximum value that the ratio $\frac{S_{aa\_source}\left(f_{max\_force}\right)}{S_{aa\_source}\left(f_{max\_acc}\right)}$ can attain is unity, the maximum value of C^2 can be predicted if the frequency of the coupled system f_{max_force} is known. Note that the frequency f_{max_force} will correspond to one of the natural frequencies of the coupled system.

After having determined $C^2_{experimental}$, it is now desirable to compute the value of $C^2_{predicted}$ for configuration 20D2_4. Table 4.14 identifies the maximum force as occurring at the frequency of 365 Hz. Table 4.14 also identifies the value of the ratio $\frac{S_{aa\_source}(365\ \text{Hz})}{S_{aa\_source}(237\ \text{Hz})}$ as 0.1874.

Next, in order to evaluate the first term of equation 4.32, consider configuration 20F2_4. Figure 4.34 shows the normalized apparent mass of the uncoupled load in configuration 20F2_4. The value of the normalized apparent mass of the uncoupled load evaluated at f_{max_force} = 365 Hz, is 4.18.

Thus, based on equation 4.32, the value of $C^2_{predicted}$ for the 20D2_4 configuration with a normalized apparent mass of 4.18 at f_{max_force} is

$$C^2_{predicted\_20D2\_4} = 4.18^2 \cdot 0.1874 = 3.27$$

A similar calculation was performed for all test configurations listed in table 4.14. The results are reported and compared to the experimental value of C^2 in table 4.15 and figures 4.35 to 4.38.

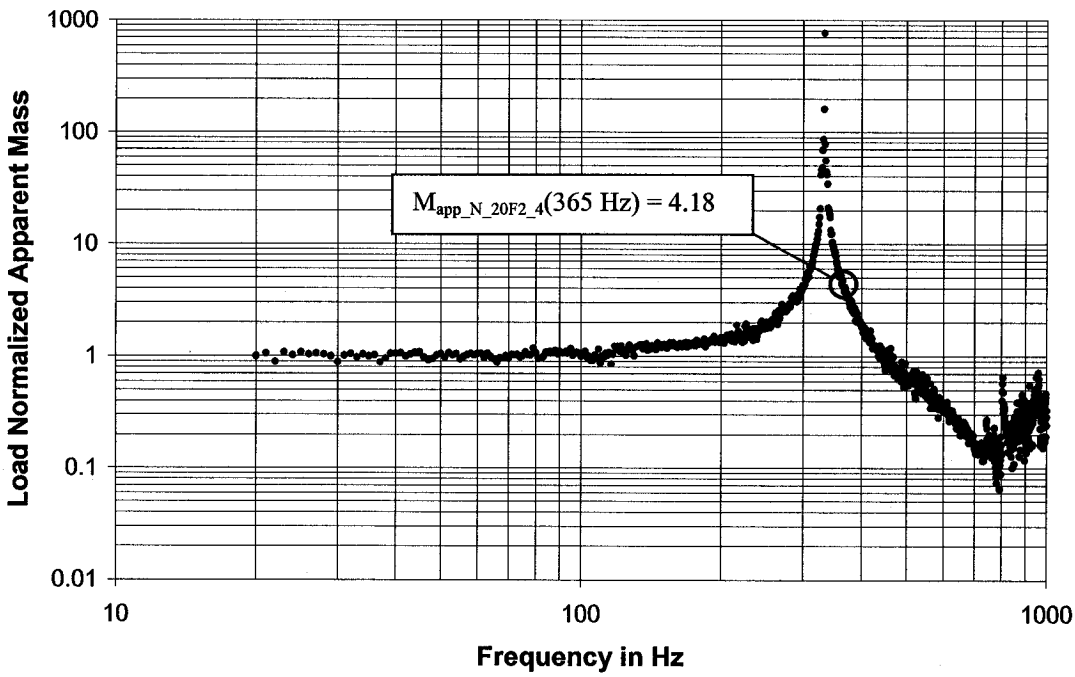

Figure 4.34: Load Normalized Apparent Mass for 20F2_4

Table 4.15: Predicted vs. Experimental Values for C^2

Test Config.	Uncoupled Load to Source Natural Frequency Ratio, F	C^2 Predicted (Eq. 4.32)	C^2 Experimental (Eq. 4.30)	Difference Experimental -Predicted	% Difference Difference / Experimental
20U2_1	0.50	**2.71**	**4.75**	2.04	43%
20U2_2	0.78	**3.61**	**8.25**	4.64	56%
20U2_3	1.11	**8.00**	**6.89**	-1.11	-16%
20U2_4	1.35	**4.69**	**3.95**	-0.74	-19%
20U2_5	1.56	**2.36**	**3.03**	0.67	22%
20U2_6	1.76	**2.40**	**2.62**	0.22	8%
20U2_7	1.84	**1.31**	**1.55**	0.24	16%
20D2_1	0.48	**3.76**	**17.92**	14.16	82%
20D2_2	0.74	**9.00**	**16.03**	7.03	44%
20D2_3	1.05	**7.25**	**7.50**	0.25	3%
20D2_4	1.28	**3.27**	**3.67**	0.40	11%
20D2_5	1.47	**1.64**	**2.27**	0.63	28%
20D2_6	1.66	**0.81**	**1.93**	1.12	58%
20D2_7	1.74	**1.59**	**1.61**	0.02	1%
20U10_1	0.52	**0.37**	**0.61**	0.24	40%
20U10_2	0.78	**2.56**	**3.43**	0.86	25%
20U10_3	1.07	**3.98**	**3.78**	-0.20	-5%
20U10_4	1.26	**2.55**	**2.59**	0.03	1%
20U10_5	1.43	**1.59**	**2.11**	0.52	25%
20U10_6	1.60	**1.62**	**1.76**	0.15	8%
20U10_7	1.87	**1.30**	**1.55**	0.26	17%
20D10_1	0.49	**0.17**	**1.15**	0.98	85%
20D10_2	0.74	**3.00**	**5.90**	2.90	49%
20D10_3	1.02	**3.87**	**5.20**	1.33	26%
20D10_4	1.19	**2.56**	**2.81**	0.25	9%
20D10_5	1.35	**2.02**	**2.15**	0.13	6%
20D10_6	1.51	**2.16**	**1.79**	-0.37	-21%
20D10_7	1.77	**1.41**	**1.47**	0.06	4%

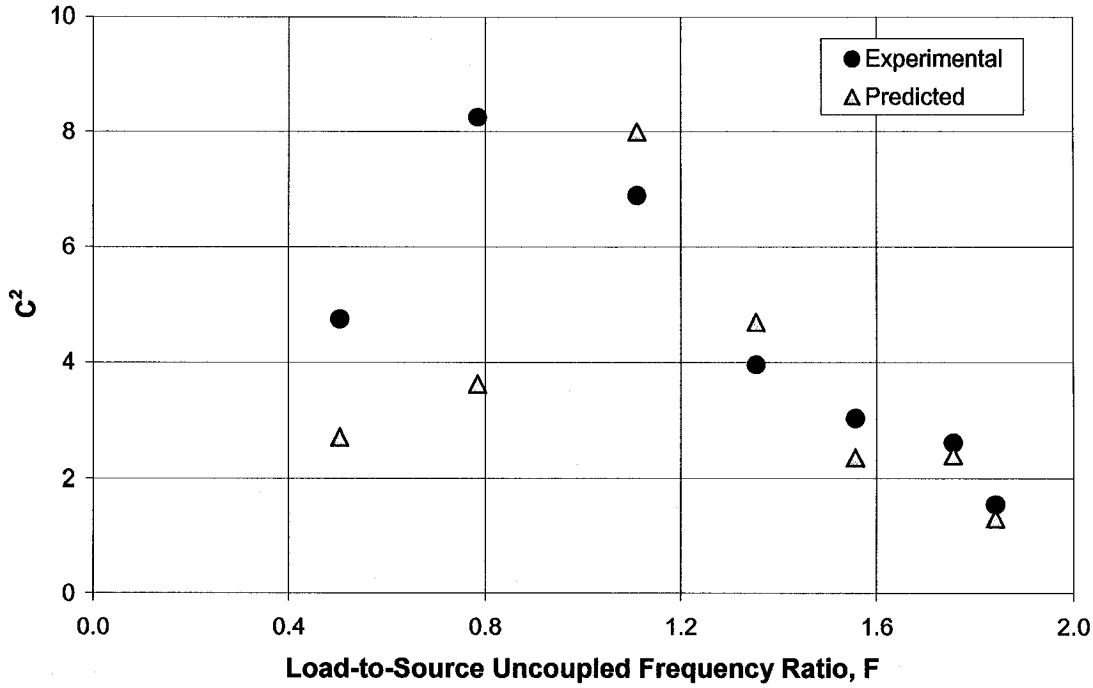

Figure 4.35: C^2 Comparison for Setup 20U2

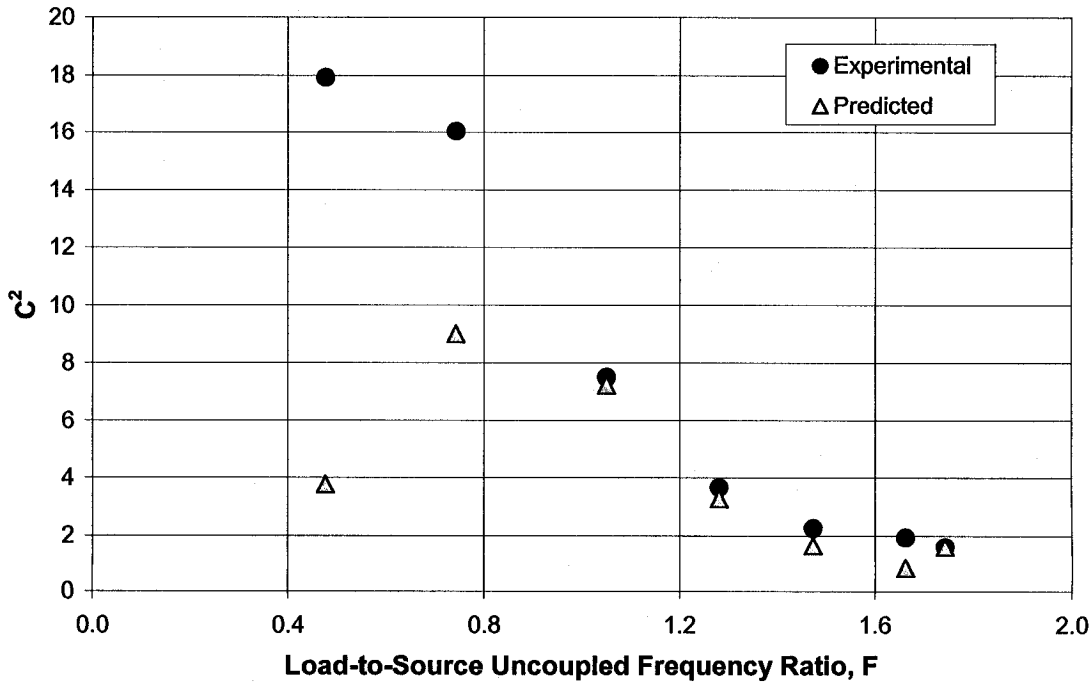

Figure 4.36: C^2 Comparison for Setup 20D2

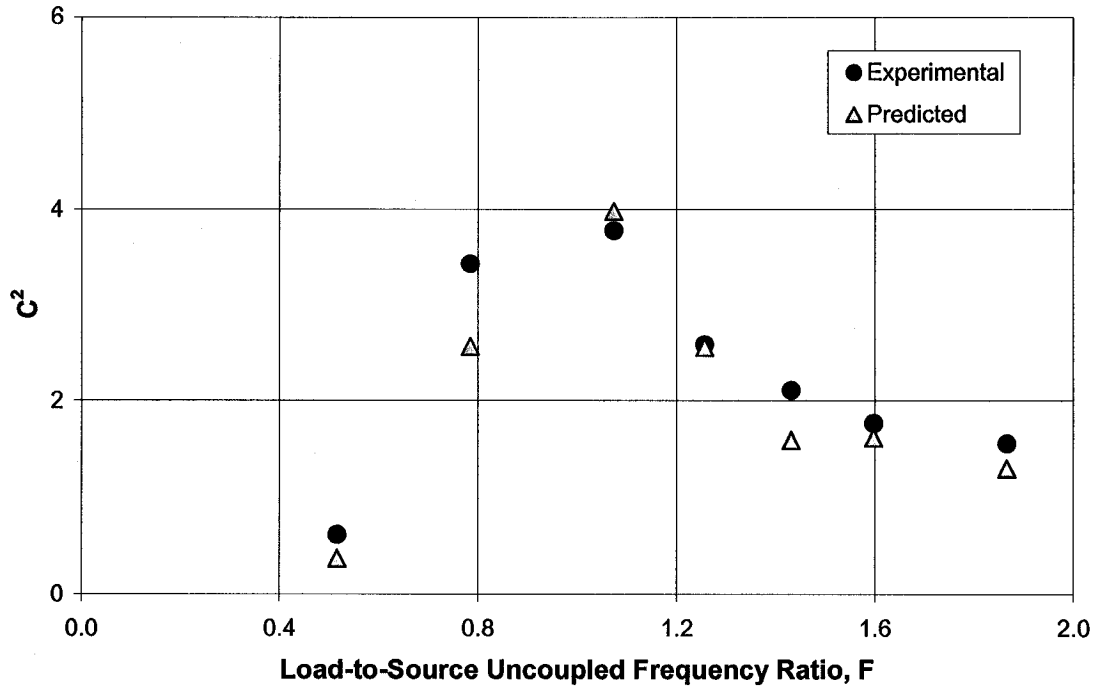

Figure 4.37: C^2 Comparison for Setup 20U10

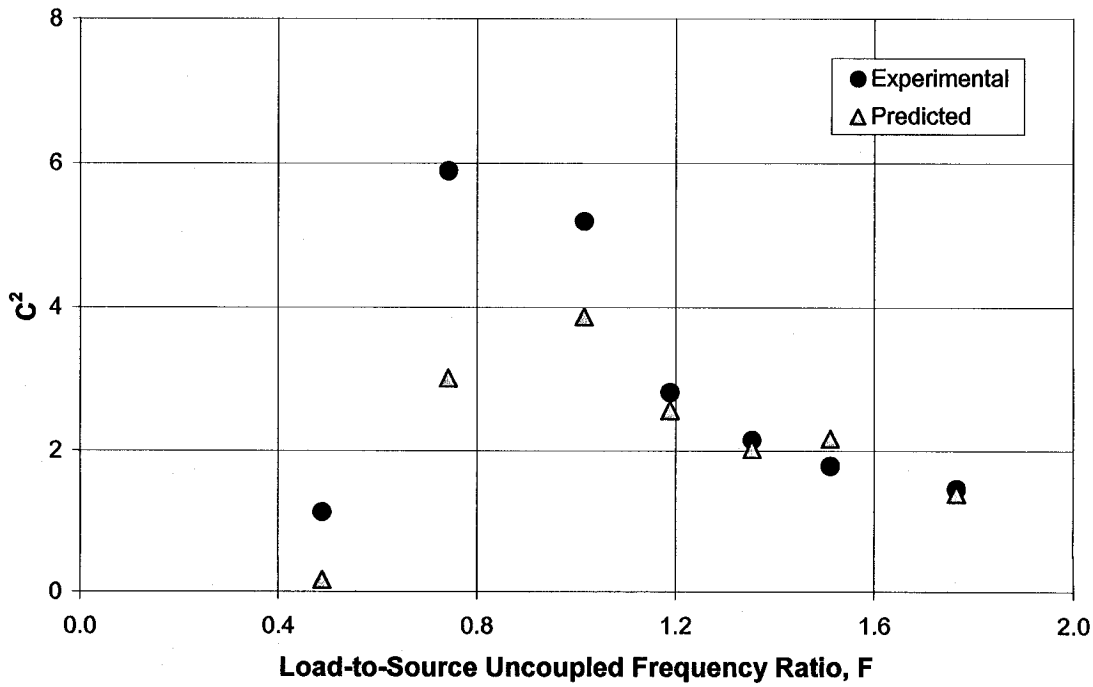

Figure 4.38: C^2 Comparison for Setup 20D10

4.3.2.5 Comment on the Predicted Value of C^2 Based on Measured Apparent Mass of Uncoupled Load

Except for test configurations 20U2_2, 20D2_1, 20D2_2, and 20D10_2, the data shown in figures 4.35 to 4.38 show excellent correlation between the predicted values and the experimental values of C^2. The less than ideal correlation for the configurations 20U2_2, 20D2_1, 20D2_2, and 20D10_2 is attributed to the combined effect of

- Small shift in the frequency of the peak apparent mass of the load between the coupled and uncoupled configuration as described in table 4.16.
- The frequency f_{max_force} being very close to a first natural frequency of the load as described in table 4.17.
- Differences in response arising from the non-linearity of the structure. The presence of non-linearity was demonstrated in table 4.7.

One of the assumptions of the semi-empirical method, described by equations 1.3 to 1.6, is that the frequency f_{max_force} corresponds to the first natural frequency of the coupled instrument-spacecraft system. Note that in practice, typically there is a minimum natural frequency design requirement to ensure that the first natural frequency of an instrument is significantly above the first natural frequency of the spacecraft. Therefore, f_{max_force} is typically well separated from the first natural frequency of the load, which will avoid the situation of the frequency f_{max_force} being very close to a first natural frequency of the load. Because of this, the value of C^2 predicted for typical aerospace structures can be expected to be relatively insensitive to small shifts in the fundamental frequency of the load and differences in response, due to changes in boundary conditions and non-linear effects when using the apparent mass method.

Table 4.16: Peak Apparent Mass Frequency Shift between Coupled and Uncoupled Test Configurations

Peak M_{app} (Coupled System) in Hz	Peak M_{app} (Uncoupled System) in Hz	Frequency Shift in Hz	Frequency Shift in %
123.5 (20U2_1)	124 (20F2_1)	0.5	0.4 %
191.5 (20U2_2)	193 (20F2_2)	1.5	0.8 %
272.0 (20U2_3)	273 (20F2_3)	1.0	0.4 %
329.0 (20U2_4)	333 (20F2_4)	4.0	1.2 %
387.0 (20U2_5)	383 (20F2_5)	-4.0	-1.0 %
433.0 (20U2_6)	432 (20F2_6)	-1.0	-0.2 %
455.5 (20U2_7)	453 (20F2_7)	-2.5	-0.5 %
122 (20D2_1)	124 (20F2_1)	2.0	1.6 %
190 (20D2_2)	193 (20F2_2)	3.0	1.6 %
270 (20D2_3)	273 (20F2_3)	3.0	1.1 %
335 (20D2_4)	333 (20F2_4)	-2.0	-0.6 %
392 (20D2_5)	383 (20F2_5)	-9.0	-2.3 %
447 (20D2_6)	432 (20F2_6)	-15.0	-3.4 %
466 (20D2_7)	453 (20F2_7)	-13.0	-2.8 %
125.5 (20U10_1)	127 (20F10_1)	1.5	1.2 %
187.5 (20U10_2)	193 (20F10_2)	5.5	2.9 %
259.0 (20U10_3)	264 (20F10_3)	5.0	1.9 %
304.0 (20U10_4)	309 (20F10_4)	5.0	1.6 %
341.0 (20U10_5)	352 (20F10_5)	11.0	3.2 %
375.0 (20U10_6)	393 (20F10_6)	18.0	4.8 %
457.5 (20U10_7)	459 (20F10_7)	1.5	0.3 %
115 (20D10_1)	127 (20F10_1)	12.0	10.4 %
172 (20D10_2)	193 (20F10_2)	21.0	12.2 %
241 (20D10_3)	264 (20F10_3)	23.0	9.5 %
291 (20D10_4)	309 (20F10_4)	18.0	6.2 %
351 (20D10_5)	352 (20F10_5)	1.0	0.3 %
378 (20D10_6)	393 (20F10_6)	-3.0	-0.8 %
467 (20D10_7)	459 (20F10_7)	-8.0	-1.7 %

Table 4.17: Frequency of f_{max_force} and First Natural Frequency of Uncoupled Load

Test Config.	f_{max_force} Coupled System in Hz	Load First Natural Frequency Uncoupled System in Hz	Ratio f_{max_force} to First Natural Frequency of Uncoupled System
20U2_1	121.5	124	0.98
20U2_2	182	193	0.94
20U2_3	306.5	273	1.12
20U2_4	359	333	1.08
20U2_5	413	383	1.08
20U2_6	456.5	432	1.06
20U2_7	230	453	0.51
20D2_1	120	124	0.97
20D2_2	181	193	0.94
20D2_3	227	273	0.83
20D2_4	365	333	1.10
20D2_5	239	383	0.62
20D2_6	470	432	1.09
20D2_7	243	453	0.54
20U10_1	117.5	127	0.93
20U10_2	158.5	193	0.82
20U10_3	179	264	0.68
20U10_4	186.5	309	0.60
20U10_5	189.5	352	0.54
20U10_6	190.5	393	0.48
20U10_7	196	459	0.43
20D10_1	110	127	0.87
20D10_2	155	193	0.80
20D10_3	182	264	0.69
20D10_4	194	309	0.63
20D10_5	199	352	0.57
20D10_6	202	393	0.51
20D10_7	206	459	0.98

The less than ideal correlation for the few tests with the 20U2 and 20D2 configurations can, by and large, be attributed to the combination of a small shift in the natural frequency of the apparent mass of the 2 kg load and the value of frequency f_{max_force} being very close to a first natural frequency of the load. This effect is explained as follows.

The apparent mass is defined as the frequency response function of the interface force to the input acceleration. Therefore, the apparent mass of the 2 kg load can be measured either during the 20F2 tests, as described in section 4.3.2.2, or during the 20U2 and 20D2 coupled system tests. Theoretically, for a linear structure, the same apparent mass function would result regardless of whether the load structure is mounted on a fixed base, as in configuration 20F2, or as a coupled system, as in configurations 20U2 and 20D2. Furthermore, the apparent mass is also independent of the type of excitation such as sine or random. However, because of non-linearity in the load structure, subtle changes in boundary conditions, and the filtering of non-linear effects during the sine excitation, the apparent mass as determined by the 20F2 configuration with sine excitation and the 20U2 and 20D2 configurations with random excitation are not identical. This is demonstrated in figure 4.39 for the 20F2_1 and the 20D2_1 configurations. In particular, the frequency corresponding to the peak normalized apparent mass has shifted from 122 Hz, for the 20D2_1 configuration, to 124 Hz for the 20F2_1 configuration, giving a frequency shift of 2 Hz as shown in table 4.16.

Appendix K shows the details of how C^2 experimental and predicted are calculated for the 20D2_1 configuration. In that appendix, the value of f_{max_force} is found to be 120 Hz for the 20D2_1 configuration.

As shown in figure 4.39, the value of the normalized apparent mass of the load evaluated at f_{max_force} = 120 Hz was found to be 12.92 when using the data from the uncoupled 20F2_1 configuration and 28.19 when using the data from the coupled 20D2_1 configuration. The large difference in the value of the normalized load apparent mass evaluated at f_{max_force} = 120 Hz arises, in part, by the coincidence that the frequency f_{max_force} is very close to the peak value of the normalized apparent mass, which has shifted by 2 Hz.

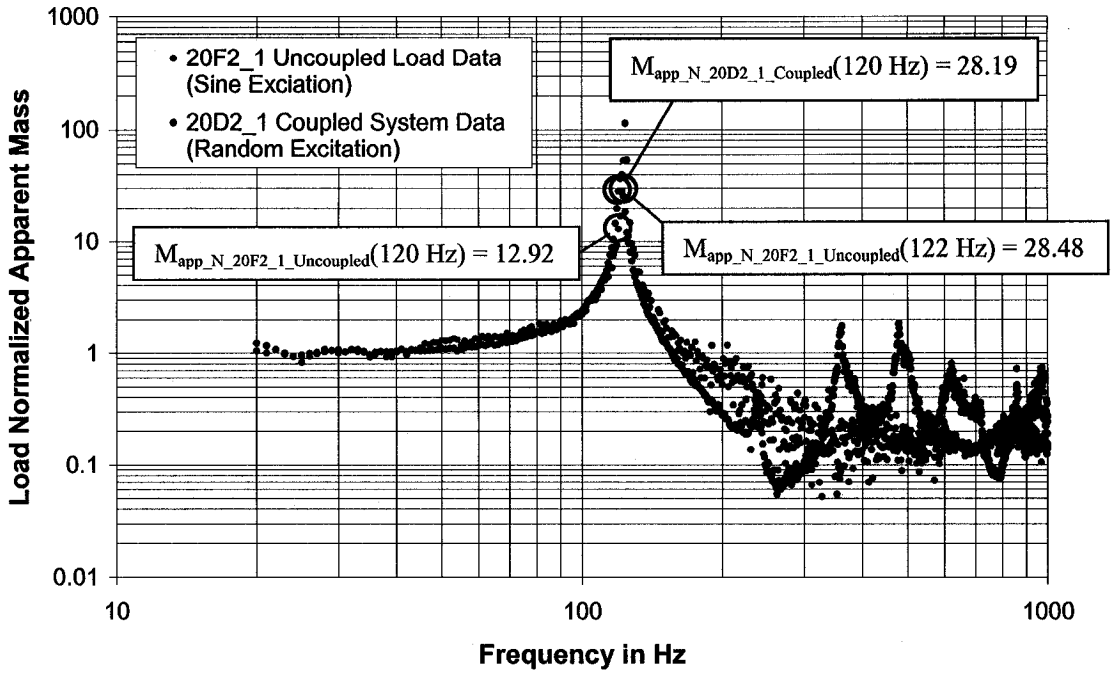

Figure 4.39: Load Normalized Apparent Mass, Coupled and Uncoupled Data Comparison for 20F2_1 and 20D2_1 Configurations

To further understand the effect of the frequency shift, consider the normalized apparent mass for the 20F2_1 configuration evaluated at $f_{max\_force\_shifted}$ instead of at f_{max_force} to take into account the shift in frequency. Note that normally, any shift that might occur in the natural frequencies of the load's apparent mass between the uncoupled and the coupled configurations will be unknown at the time of testing because coupled configuration vibration testing typically has not yet occurred. The value of $f_{max\_force\_shifted}$ is

$$f_{max\_force\_shifted} = f_{max\_force} + (\text{frequency shift}) \tag{4.33}$$

$$f_{max\_force\_shifted} = 120\ Hz + (124\ Hz - 122\ Hz)$$

$$f_{max\_force\_shifted} = 120\ Hz + 2\ Hz$$

$$f_{max\_force\_shifted} = 122\ Hz$$

By pure coincidence, the value $f_{max\_force\_shifted}$ of 122 Hz is equal to the value of the peak apparent mass of the coupled 20D2_1 configuration. The value of the normalized apparent mass of the load evaluated at $f_{max\_force\_shifted}$ is 28.48 instead of 12.92 when using

the un-shifted value f_{max_force} of 120 Hz, as shown in figure 4.39. Note that the value of 28.48 calculated at the frequency $f_{max\_force\_shifted}$ is almost identical to the value of 28.19 found using the un-shifted value f_{max_force}. This will result in similar values for C^2 supporting the notion that the poor correlation for the 20D2_1 configuration was due to f_{max_force} being close to the frequency corresponding to the peak normalized apparent mass combined with a small frequency shift.

For comparison, consider configuration 20U10_3 as an example of when the value of f_{max_force} is not near the frequency of the peak normalized apparent mass. The calculations for C^2 for the 20U10_3 configuration are shown in appendix K. From appendix K, the value of f_{max_force} is found to be 179 Hz, while the value of the frequency corresponding to the peak normalized apparent mass is 259 Hz, for the coupled 20U10_3 configuration; and is 264 Hz, for the uncoupled 20F10_3 configuration, as shown in table 4.16. Note the presence of a 5 Hz frequency shift between the uncoupled and coupled configurations. Figure 4.40 shows that the value of the normalized apparent mass evaluated at f_{max_force} is nearly the same for the two configurations even though there is a 5 Hz frequency shift between the coupled 20U10_3 and uncoupled 20F10_3 configurations.

Consequently, since the frequency f_{max_force} is away from the frequency of the peak normalized apparent mass, the 5 Hz shift did not produce any significant differences in value between $C^2_{predicted}$ and $C^2_{experimental}$.

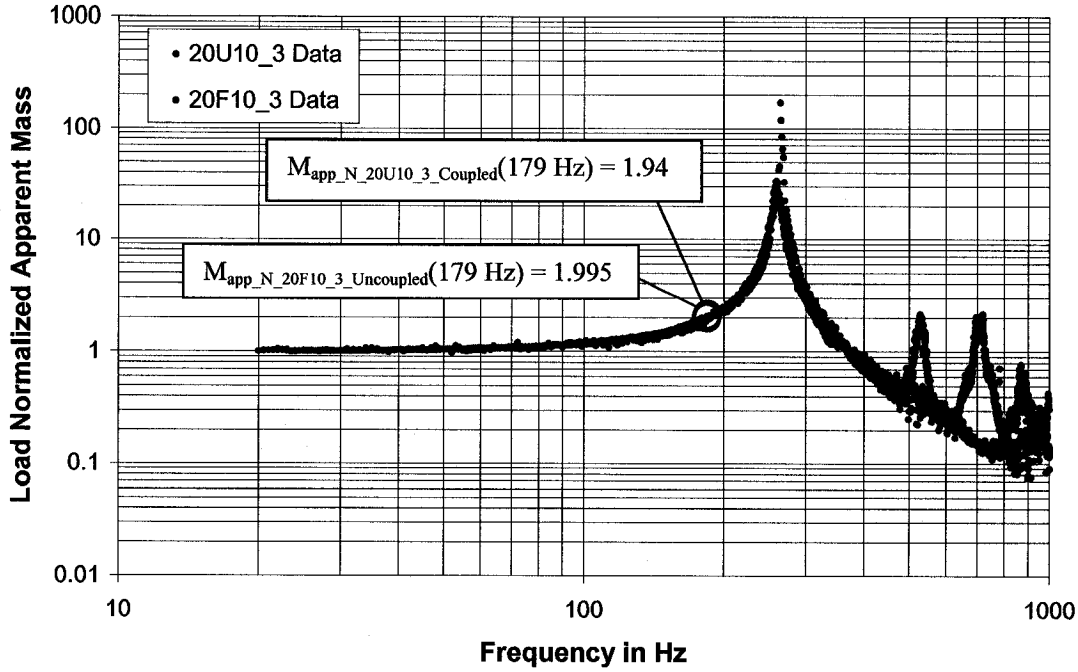

Figure 4.40: Load Normalized Apparent Mass, Coupled and Uncoupled Data Comparison for 20U10_3 and 20F10_3 Configurations

From the examination of the above two examples, it is now logical to apply the frequency shift correction to the previous data in figures 4.35 to 4.38 and table 4.15.

The value of f_{max_force} utilized in equation 4.32 to calculate the value of the uncoupled normalized apparent mass was substituted with the value $f_{max\_force\_shifted}$ to take into account the small frequency shift listed in table 4.16. The value of $C^2_{predicted}$ was then re-computed based on the shifted value $f_{max\_force\_shifted}$. The results are shown in figures 4.41 to 4.44 and table 4.18.

Table 4.18: Predicted using $f_{max\_force\_shifted}$ vs. Experimental Values for C^2

Test Config.	Uncoupled Load to Source Natural Frequency Ratio, F	C^2 Predicted using $f_{max\_force\_shifted}$ (Eq. 4.32)	C^2 Experimental (Eq. 4.30)	Difference Experimental -Predicted	% Difference Difference / Experimental
20U2_1	0.50	**4.25**	**4.75**	0.50	10%
20U2_2	0.78	**5.02**	**8.25**	3.23	39%
20U2_3	1.11	**7.02**	**6.89**	-0.14	-2%
20U2_4	1.35	**3.07**	**3.95**	0.88	22%
20U2_5	1.56	**3.47**	**3.03**	-0.45	-15%
20U2_6	1.76	**2.74**	**2.62**	-0.12	-5%
20U2_7	1.84	**1.47**	**1.55**	0.08	5%
20D2_1	0.48	**18.29**	**17.92**	-0.37	-2%
20D2_2	0.74	**12.45**	**16.03**	3.58	22%
20D2_3	1.05	**7.89**	**7.50**	-0.39	-5%
20D2_4	1.28	**3.51**	**3.67**	0.16	4%
20D2_5	1.47	**2.35**	**2.27**	-0.08	-3%
20D2_6	1.66	**2.44**	**1.93**	-0.51	-26%
20D2_7	1.74	**1.31**	**1.61**	0.31	19%
20U10_1	0.52	**0.47**	**0.61**	0.14	23%
20U10_2	0.78	**3.22**	**3.43**	0.21	6%
20U10_3	1.07	**3.64**	**3.78**	0.14	4%
20U10_4	1.26	**2.36**	**2.59**	0.22	9%
20U10_5	1.43	**1.98**	**2.11**	0.12	6%
20U10_6	1.60	**2.07**	**1.76**	-0.31	-17%
20U10_7	1.87	**1.37**	**1.55**	0.18	12%
20D10_1	0.49	**1.65**	**1.15**	0.98	85%
20D10_2	0.74	**7.48**	**5.90**	2.90	49%
20D10_3	1.02	**6.23**	**5.20**	1.33	26%
20D10_4	1.19	**4.18**	**2.81**	0.25	9%
20D10_5	1.35	**1.85**	**2.15**	0.13	6%
20D10_6	1.51	**2.07**	**1.79**	-0.37	-21%
20D10_7	1.77	**1.45**	**1.47**	0.06	4%

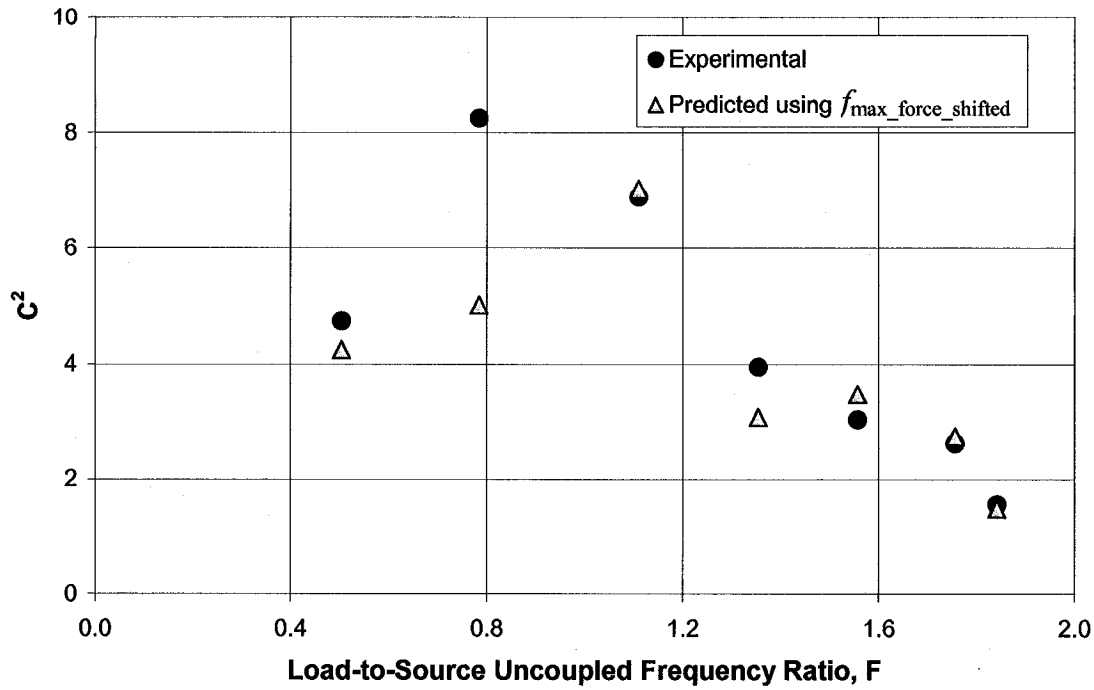

Figure 4.41: C^2 Comparison for Setup 20U2, using $f_{max\_force\_shifted}$

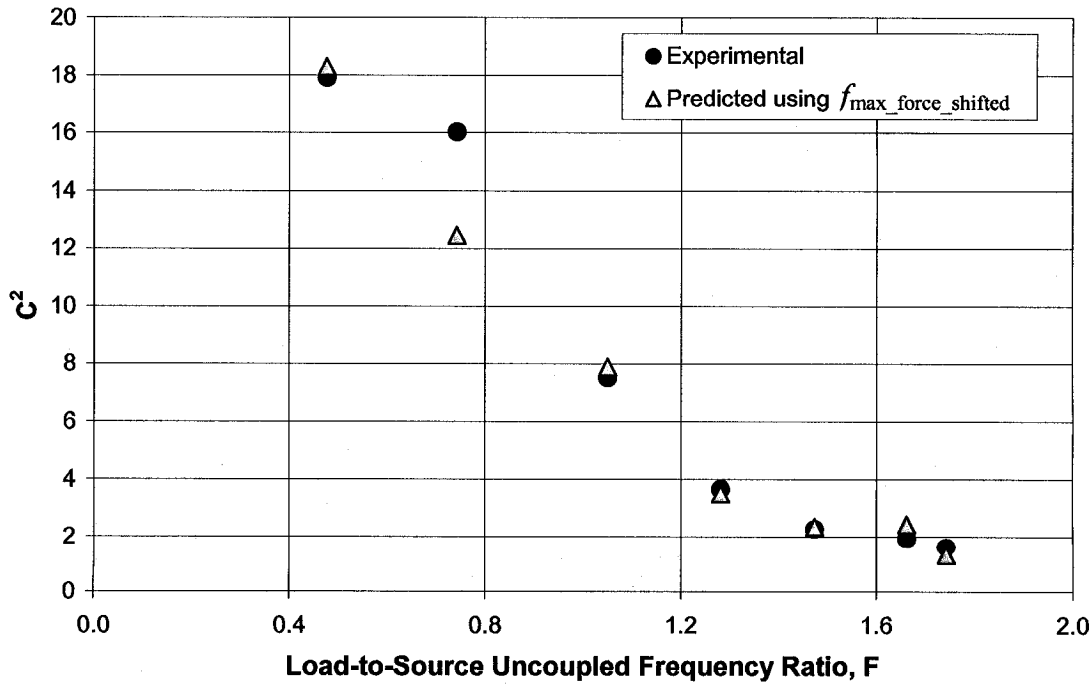

Figure 4.42: C^2 Comparison for Setup 20D2, using $f_{max\_force\_shifted}$

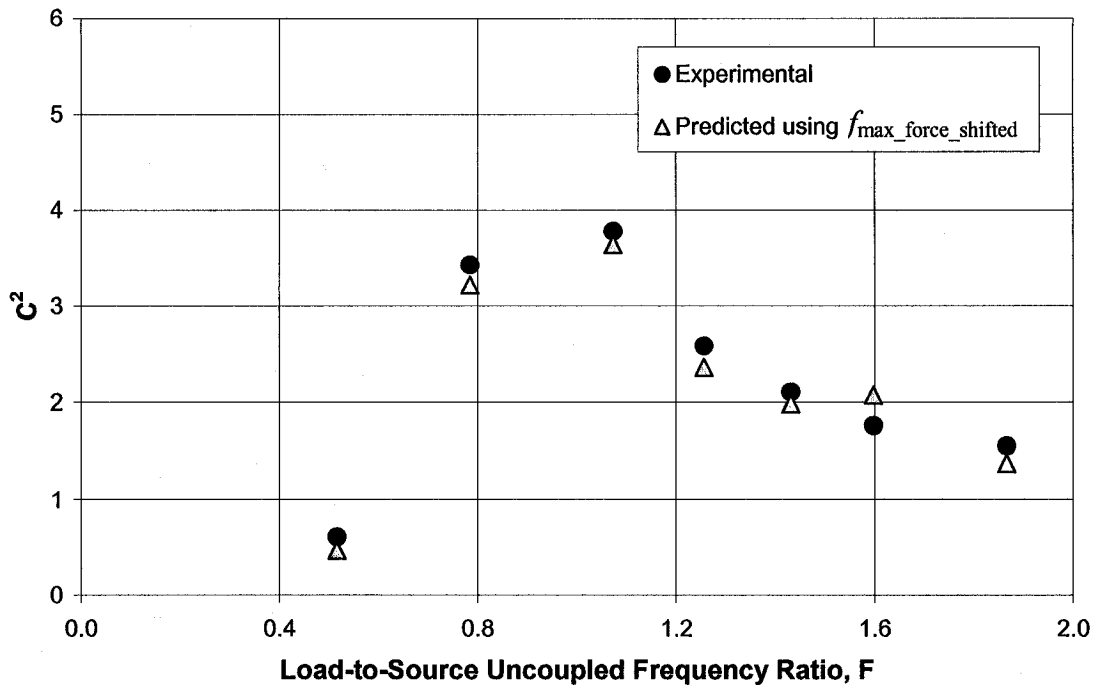

Figure 4.43: C^2 Comparison for Setup 20U10, using $f_{max\_force\_shifted}$

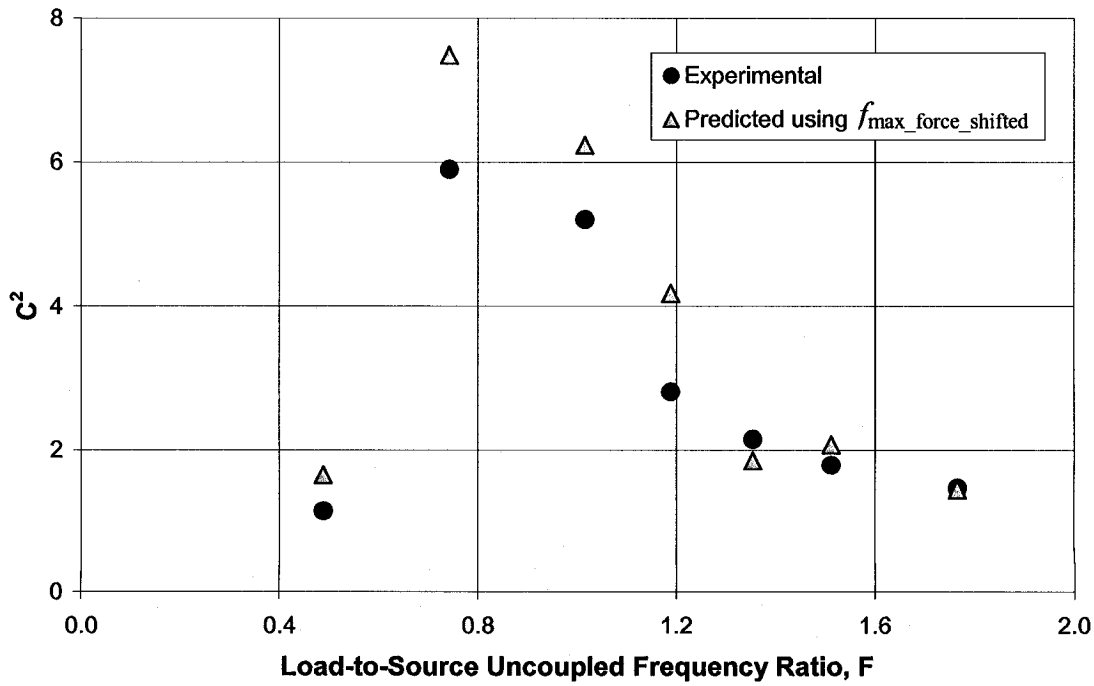

Figure 4.44: C^2 Comparison for Setup 20D10, using $f_{max\_force\_shifted}$

Overall, the apparent mass method predicted the value of C^2 reasonably well, considering the pronounced non-linear effects and small shifts in natural frequencies of the various test configurations. In addition, the remaining errors, after correcting for the frequency shift, can be attributed to non-linear effects, the noisy data, and other experimental errors associated with the measuring equipment.

In both sets of figures, 4.35 to 4.38 and 4.41 to 4.44, the apparent mass method captured the dependency of C^2 on system parameters of uncoupled natural frequency ratio F and mass ratio μ.

A significant trend that is noted from the data in table 4.14 is that the ratio $\frac{S_{aa\_source}(f_{max\_force})}{S_{aa\_source}(f_{max\_acc})}$ is more likely to be unity as the uncoupled natural frequency ratio F increases. The frequency of maximum force f_{max_force} occurs at one of the natural frequencies of the coupled system, as is demonstrated in the typical plots given in appendix J.

Testing revealed that non-linearity in the response can have a pronounced effect on the apparent mass of the load. Consequently, care must be taken to when applying the apparent mass method to a non-linear system.

Figures 4.35 and 4.36 describing the un-damped 20U2 configuration and the damped 20D2 configuration, show that damping can indeed significantly affect the value of C^2 if the uncoupled frequency ratio F is below unity, as was predicted by the two degrees-of-freedom model discussed in chapter 2.0. In addition, the test configuration 20U10_1 demonstrated that a value of C^2 below unity is possible, as was discussed in chapter 2.

5 CONCLUSIONS

The system parameters affecting the value of C^2 for both a two degrees-of-freedom system and for any arbitrary multiple degrees-of-freedom or continuous system have been described in this thesis. From these investigations, a new method, called the apparent mass method, was developed to predict the value of C^2 for any arbitrary structure using a minimal amount of information.

The investigations of the two degrees-of-freedom system were summarized in chapter 2. From these investigations, the following conclusions regarding the behaviour of C^2 can be made.

- In general, the value of C^2 depends on all four system parameters F, μ, Q_1, and Q_2 as well as the type of damping present. However, investigation of a two degrees-of-freedom system with viscous damping revealed that
  - If $F > 1$ and $Q_1 \geq Q_2$ then C^2 is always independent of Q_1
  - If $F > 1$ and $Q_1 < Q_2$ then C^2 is independent of Q_1 if either F or μ is large enough (see figure 2.24 for what qualifies as large enough)
- For any given mass ratio μ, the maximum value of C^2 is between $\left(\frac{Q_2}{Q_1}\right)^2 \leq C^2 \leq Q_2^2$, occurring when $F \leq 1$
- For any given set of F, Q_1, and Q_2, the largest possible value of C^2 occurs when $\mu \rightarrow 0$ but only if $F \geq 1$. If $F < 1$, the largest possible value of C^2 does not necessarily occur when $\mu \rightarrow 0$.
- For any system, $C^2_{max} = Q_2^2$, when $F = 1$ and $\mu \rightarrow 0$, whatever the value of Q_1
- $C^2 \rightarrow 1$ for large F, independent of μ, Q_1, and Q_2
- $C^2 \rightarrow 1$ for large μ independent of F, Q_1, and Q_2
- Most of the systems investigated had $C^2 < 5$ when $F > 1.5$. This behaviour is consistent with the experimental results discussed in chapter 4.

- Values of C^2 less than unity are possible. However, this can only occur when $F < 1$ and $Q_1 > Q_2$.

Figures 2.3 to 2.18 show how the system parameters affect the value of C^2 for selected systems with viscous damping. These figures are useful as a quick reference in estimating the value of C^2 of a two degrees-of-freedom system.

For multiple degrees-of-freedom or continuous systems, the value of C^2 can be predicted by equation 3.5

$$C^2 = \left| \frac{M_{app}(f_{max\_force})}{M_0} \right|^2 \cdot \frac{S_{aa\_flight}(f_{max\_force})}{S_{aa\_flight}(f_{max\_acc})} \tag{3.5}$$

where

- f_{max_force} is the forcing frequency that produces the maximum interface force between the load and the source
- $S_{aa\_flight}(f_{max\_force})$ is the coupled system acceleration spectral density located at the load-to-source interface and evaluated at f_{max_force}
- $S_{aa\_flight}(f_{max\_acc})$ is the maximum acceleration spectral density of the load-to-source interface for the coupled system
- f_{max_acc} is the frequency where the maximum acceleration occurs
- $M_{app}(f_{max\_force})$ is the apparent mass of the load evaluated at f_{max_force} of the coupled system
- M_0 is the mass of the load

Consequently, the only frequencies of interest are the two natural frequencies f_{max_force} and f_{max_acc} of the coupled system. All other frequencies are irrelevant in determining the value of C^2.

By definition of $S_{aa\_flight}(f_{max\_acc})$, the ratio $\frac{S_{aa\_flight}(f_{max\_force})}{S_{aa\_flight}(f_{max\_acc})}$ must be a number less than or equal to unity as described below in equation 3.6.

$$\frac{S_{aa\_flight}(f_{max\_force})}{S_{aa\_flight}(f_{max\_acc})} \leq 1 \tag{3.6}$$

Consequently, the maximum possible value of C^2 for any multiple degrees-of-freedom or continuous system is given below.

$$C^2 \leq \left| \frac{M_{app}(f_{max\_force})}{M_0} \right|^2 \tag{3.7}$$

In addition, in section 3.3.2 the maximum value for the normalized apparent mass for system with well separated modes and similar Q for each mode was found to be approximately equal to the product of the largest effective mass and the Q of the mode, normalized by the actual mass of the load as shown in equation 3.18 below.

$$C^2_{max} \approx \left(\frac{m_{eff\_max}}{M_0} Q \right)^2 \tag{3.18}$$

Equations 3.7 and 3.18 explains why structures without a dominant effective mass, relative to their actual mass, do not benefit as much from force limiting vibration, since for such structures the maximum possible value of C^2 is intrinsically very low. Note that for a load structure behaving as an idealized single degree-of-freedom system, equation 3.18 reduces to $C^2_{max} = Q^2_{load}$, which is the same relationship previously described for a single degree-of-freedom load mounted on a single degree-of-freedom source.

A new method called the apparent mass method was presented in this thesis showing how the value of C^2 can be predicted, or how the value of C^2 can be approximated using a minimum amount of information or assumptions.

The apparent mass method has several advantages, such as

- The ability to estimate the maximum possible value for C^2.

- The predicted value of C^2 is easier to defend because the value is produced through theoretical considerations.
- The ability to estimate the accuracy of the predicted value C^2 through
    - The statistical degrees-of-freedom of the measured apparent mass.
    - Consideration of the slope of the apparent mass at the frequency f_{max_force}.
    - Consideration of the sensitivity of the ratio $\frac{S_{aa\_flight}(f_{max\_force})}{S_{aa\_flight}(f_{max\_acc})}$ to assumed damping values and non-linear effects.
    - The location of f_{max_force} relative to peaks or valleys of M_{app}.

The results of the tests described in section 4.3.1 showed that the Q of a practical structure increased with an increase in excitation level. This can greatly affect the apparent mass measurement if f_{max_force} is evaluated near its resonant frequency but, as seen in section 4.3.2.4, it can have negligible effect at frequencies only a few Hertz away from a resonant frequency.

By design, the first natural frequency of an aerospace structure is typically well above the first natural frequency of the structure it is designed to be mounted on, i.e. $F > 1$. This explains why aerospace structures typically have low values of C^2. This behaviour is evident in both the theoretical results of chapter 2 and the experimental results of chapter 4.

Although this thesis has outlined the major parameters affecting the value of C^2, more research regarding how the value of C^2 changes with the type of damping, changes in boundary conditions, and the effects of non-linearity is suggested.

To summarize, the above information gives a test director a better understanding of how the value of C^2 can change for a particular structure. Additionally, a simple and practical method to determine the appropriate value of C^2 called the "apparent mass method" has been presented. This work will help reduce over-testing and under-testing of aerospace structures during vibration testing.

REFERENCES

1 Blake, R. E., "The Need to Control the Output Impedance of Vibration and Shock Machines", *Shock and Vibration Bulletin*, U.S. Naval Research Laboratory, Washington, D. C., No. 23, June 1956, pp. 59-64.

2 Scharton, T. D., Boatman, D. J., and Kern, D. L., "Dual Control Vibration Testing", *Proceedings of 60th Shock and Vibration Symposium*, David Taylor Research Centre, Bethesda, Vol. IV, 1989, pp. 199-217.

3 Judkins, N. J., and Ranaudo, S. M., "Component Internal Vibration Response Accelerations—System Level Versus Component Level", *Proceedings of the 10th Aerospace Testing Seminar*, The Aerospace Corporation, El Segundo, March 1987, pp. 97–104.

4 "Force Limited Vibration Testing", NASA-STD-7004B, January 2003.

5 Scharton, T. D., "Force Limited Vibration Testing Monograph", NASA RP-1403, May 1997.

6 Chang, K. Y., "Force Limit Specifications vs. Design Limit Loads in Vibration Testing", *Proceedings of the European Conference on Spacecraft Structures, Materials and Mechanical Testing*, ESA SP-468, Paris, March 2001, pp.295-300.

7 Dharanipathi, V. R., "Investigation of the Semi-Empirical Method for Force Limited Vibration Testing", Master's Thesis, Concordia University, Montréal, Québec, September 2003.

8 Nagahama, K., Shi Q., Ando S., and Saegusa H., "Validation of Force Limited Vibration Testing Using Dummy Satellite Structure", *Proceedings of the 5th*

International Symposium on Environmental Testing for Space Programmes, ESA SP-558, Paris, June 2004, pp. 209-216.

9 Haile, W., "Validation of a Simple Formula for Force Limits in Vibration Testing", *Journal of the Institute of Environmental Sciences and Technology*, Vol. 41, No. 4, August 1998, pp. 24-29.

10 Salter, J. P., "Taming the General-Purpose Vibration Test", *Shock and Vibration Bulletin*, U.S. Naval Research Laboratory, Washington, D. C., No. 33, Pt. 3, March 1964, pp. 211-217.

11 Perl E., Do T., Peterson A, and Welch J., "Environmental Testing for Launch and Space Vehicles", *Crosslink* [online], Vol. 6, No. 3, Fall 2005, http://www.aero.org/publications/crosslink/fall2005/02.html [retrieved 10 April 2007].

12 McConnell, K. G., *Vibration Testing Theory and Practice*, John Wiley & Sons, Inc., New York, 1995, pp. 50, 301, 540, 575.

13 Witte, A. F., and Rodeman, R., "Dual Specification In Random Vibration Testing, An Application Of Mechanical Impedance", *Shock and Vibration Bulletin*, U.S. Naval Research Laboratory, Washington, D. C., No. 41, Pt. 44, 1970, pp. 109-118.

14 Hunter, N.F. and J. V. Otts, "The Measurement Of Mechanical Impedance And Its Use In Vibration Testing", *Shock and Vibration Bulletin*, U.S. Naval Research Laboratory, Washington, D. C., No. 42, Pt. 1, 1972, pp. 79-88.

15 Scharton T. D., "In-Flight Measurements of Dynamic Force and Comparison with Methods used to Derive Force Limits for Ground Vibration Tests", *Proceedings of the European Conference on Spacecraft Structures, Material and Mechanical Testing*, ESA SP-428, Paris, February 1999, pp. 583-588.

16 Scharton, T. D., "Force Limits Measured on a Space Shuttle Flight", *Journal of the Institute of Environmental Sciences and Technology*, Vol. 45, No. 1, January 2002, pp. 144-148.

17 Worth D. B., Kaufmand D. S., "Validation of Force-Limited Vibration Testing", *Journal of the Institute of Environmental Sciences and Technology*, Vol. 41, No. 3, 1998, pp. 17-23.

18 Rice, C. E., and Buehrle, R. D., "Validation of Force Limited Vibration Testing at NASA Langley Research Center", NASA TM-2003-212404, May 2003.

19 Ritzmann, S., and Jahn, H., "Comparison of Dynamic Loads to Space Instruments, Depending on the Stage of Development", *Proceeding of the 22nd Aerospace Testing Seminar*, The Aerospace Corporation, El Segundo, March 2005, pp. 1-69 to 1-75.

20 Marchand, P., O'Grady, M., and Singhal, R., "Relating the Value of C^2 of the Semi-Empirical Method of Force Limited Vibration to a 2-DOF System", *Proceeding of the 22nd Aerospace Testing Seminar*, The Aerospace Corporation, El Segundo, March 2005, pp. 6-79 to 6-90.

21 Thomson, William T., *Theory of Vibration with Applications*, 3rd Edition, Prentice Hall, Englewood Cliffs, 1988, pp.54, 72, 75, 126-127, 177, 381.

22 "MATLAB Function Reference", Version 7, The MathWorks Inc., June 2004.

23 Crandall, S. H., and W. D. Mark, "Random Vibration in Mechanical Systems", New York, Academic Press, 1973, pp. 96-97.

24 Scharton, T. D., "Vibration-Test Force Limits Derived from Frequency-Shift Method", *Journal of Spacecraft and Rockets*, Vol. 32, No. 2, 1995, pp. 312-316.

25 Scharton, T. D., and Chang, K. Y., "Force Limited Vibration Testing", Notes from the Force Limited Vibration Seminar presented at the 22nd Aerospace Testing Seminar, The Aerospace Corporation, El Segundo, March 22-24, 2005, p. 40.

26 Steinberg, D. S., *Vibration Analysis for Electronic Equipment*, 3rd Edition, John Wiley & Sons Inc., New York, 2000, pp. 155, 368.

27 Sedaghati, R., Soucy, Y., Etienne N., "Efficient Estimation of Effective Mass for Complex Structures under Base Excitation", *Canadian Aeronautic and Space Journal*, Vol. 49, No. 3, September 2003, pp. 135-143.

28 "COSMOS/Works User's Guide", Version 2006, Structural Research & Analysis Corporation, 2006.

29 "Load Analyses of Spacecrafts and Payloads", NASA-STD-5002, June 21, 1996.

30 Tustin, W., and Mercado, R., *Random Vibration in Perspective*, Tustin Institute of Technology, Santa Barbara, 1984, p.126.

31 Hogg, R. V., and Tanis, E. A., *Probability and Statistical Inference* 3rd edition, Macmillan Publishing Company, New York, 1983, pp. 182, 302, 362, 613.

32 Wirsching, P. H., Paez, T. L., and Ortiz, K., *Random Vibrations Theory and Practice*, Dover Publications, Inc., Mineola, 1995, pp. 60-63.

33 "Material Properties of Sorbothane", *Sorbothane Incorporated website*, http://www.sorbothane.com/PDF/sor_matprop.pdf, [retrieved April 16, 2007].

34 Ewins, D. J., *Modal Testing: Theory and Practice*, John Wiley & Sons Inc., New York, 1984, p. 109.

35 Juvinall, R. C., and Marshek, K. M., *Fundamentals of Machine Component Design*, 2nd Edition, John Wiley & Sons Inc., New York, 1991, pp. 362, 370-375.

36 Oberg, Erik, et al., *Machinery's Handbook*, 24th Edition, Industrial Press Inc., New York, 1992, pp. 1530.

37 "Kistler Models 9251A, 9252A, 9250A4, 9251A4 3-Component Force Sensor", Kistler Instrument Corporation [online], http://www.intertechnology.com/Kistler/Force_Model_9251A_9252A_9250A4_9251A4.htm [retrieved April 10 2007].

38 Feynman, R. P., Leighton R. B., and Sands, M., *The Feynman Lectures on Physics*, Volume I, Addison-Wesley Publishing Company, Reading, 1963, pp. 23-1 to 23-5.

39 Rao, S. S., *Mechanical Vibrations*, 3rd Edition, Addison-Wesley Publishing Company, New York, 1995, p. 226.

40 Popov, E. P., "Engineering Mechanics of Solids", Prentice Hall, Englewood Cliffs, New Jersey, 1990, p. 75, A-2.

APPENDIX A: EXAMPLE OF VIBRATION ABSORBER EFFECT AND FORCE-LIMITED VIBRATION TESTING

Vibration Absorber Effect

The vibration absorber effect is what causes the main resonant frequency encountered during testing to be a frequency of minimal response during flight. The vibration absorber effect arises because of the differences in boundary conditions between the test configuration and the flight configuration. The flight configuration provides a base with finite mechanical impedance while the shaker provides a base with near infinite mechanical impedance.

Vibration Absorber Effect Example

In order to better understand the vibration absorber effect and the force limited method applied to random vibration testing, consider the following simplified arbitrary numerical example.

A 20 kg telescope with an un-coupled natural frequency of 140 Hz and a Q of 50 is mounted on a 50 kg spacecraft with an un-coupled natural frequency of 80 Hz and a Q of 20. The launch vehicle's engines produce a flat spectral acceleration of 0.1 g^2/Hz between 20 and 2000 Hz at the interface to the spacecraft giving an overall acceleration input of 14.07 g RMS.

During testing, the telescope can be represented dynamically as shown in figure A.1, where the position of the mass represents the center-of-mass of the telescope.

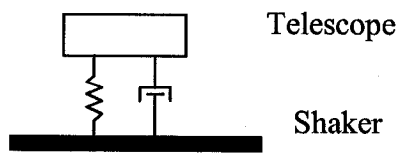

Figure A.1: 1-DOF Dynamics during Test

However, during flight, a more representative dynamic model would include the spacecraft as shown in figure A.2, where again the positions of the masses represent the center-of-mass of the objects.

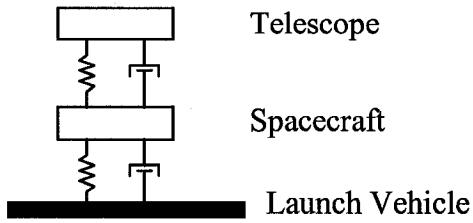

Figure A.2: 2-DOF Dynamics During Flight

Since the telescope is mounted on the spacecraft, it is the acceleration of the spacecraft that is of interest in developing a test spectrum for the telescope. To this end, the acceleration response of the spacecraft and a typical enveloping spectrum are shown in figure A.3. For clarity, in figure A.3, only the frequencies between 20 and 1000 Hz are shown. In aerospace, the slopes of an acceleration spectral density (ASD) are described in decibels (dB) per octave (oct). The slopes of the test spectrum, set to ±6 dB/oct, are representative of the type of slopes encountered in test specifications.

Consider the response of the two degrees-of-freedom system shown in A.2. The given coupled system has two natural frequencies: one at 65 Hz and one at 172 Hz, as shown in figure A.3.

Notice in figure A.3 the pronounced valley occurring at the natural frequency of the telescope at 140 Hz when the telescope is mounted on the shaker. This is the result of the vibration absorber effect. The depth of the valley depends on the mass ratio of the telescope to the spacecraft, the ratio of the un-damped natural frequencies, and the amount of damping present. Thus, the amount of over-testing is a function of these parameters.

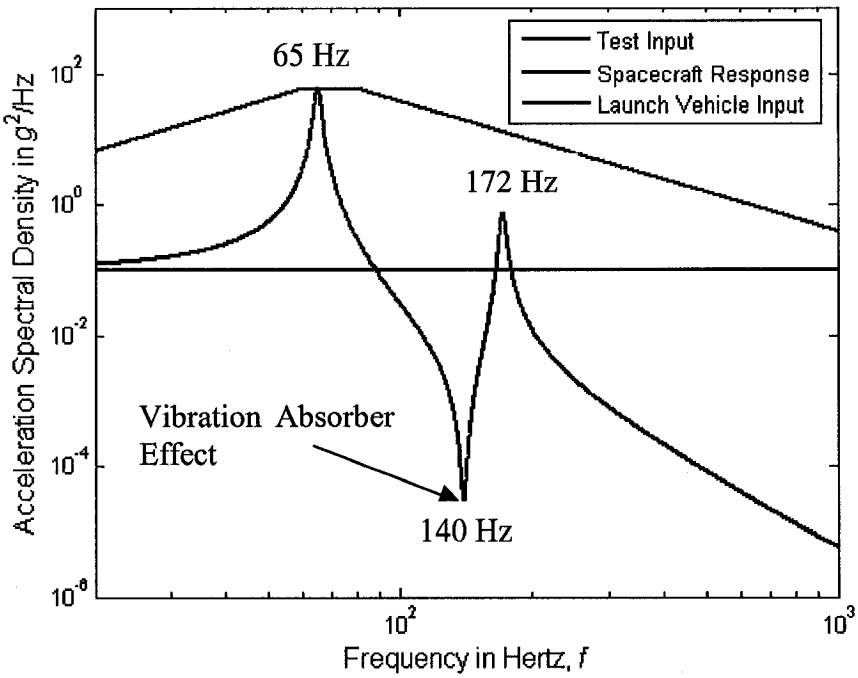

Figure A.3: Test Specification Derivation Based on 2-DOF System

A comparison of the telescope's acceleration response when mounted on the spacecraft and when mounted on the shaker and vibrated with the simplified test spectrum is shown in figure A.4. The figure shows severe over-estimating of the random environment near the natural frequency of the telescope at 140 Hz. For this example, the flight acceleration spectral density response of the telescope at 140 Hz is only 2.7 E-5 g^2/Hz while during testing it is 7600 g^2/Hz!

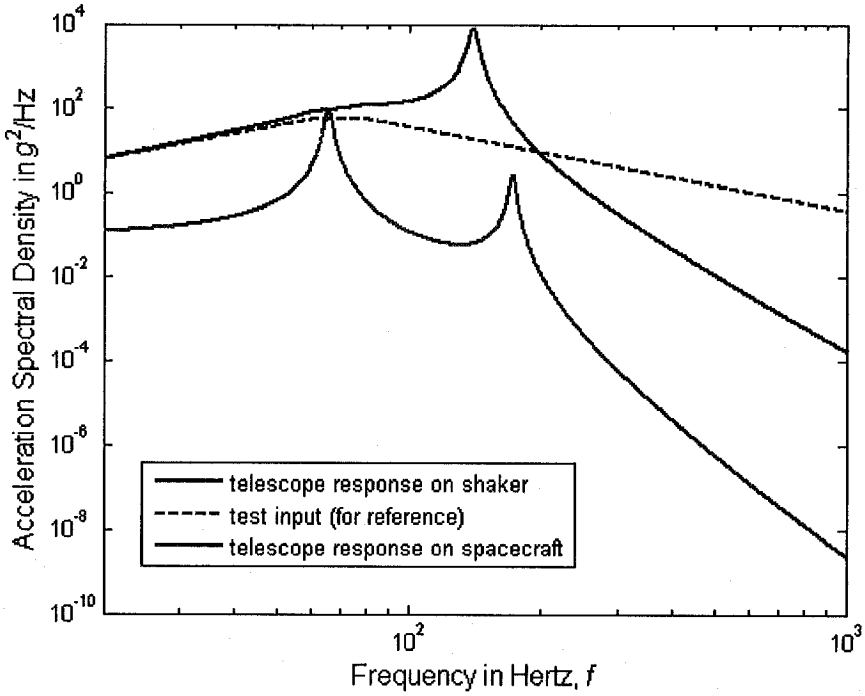

Figure A.4: Telescope Spectral Response Comparison

The final value of interest is 3 times the RMS values of the acceleration, since these will give the peak response for practical purposes. For comparisons, the peak response values are shown in table A.1. The table clearly shows that the derived test spectrum will over-test the telescope by a factor of 15.

Table A.1: Peak Response Comparison without Notching

Flight Configuration	**Peak Response (= 3 x *g* RMS)**
Launch Vehicle Input (for reference)	42 *g*
Spacecraft Peak Response (for reference)	46 *g*
Telescope Peak Response	59 *g*
Test Configuration	
Shaker Input (for reference)	246 *g*
Telescope Peak Response	889 *g*
Over-test	889 *g* / 59 *g* = 15

Force Limited-Vibration Testing Example

Continuing with the previously given example of the telescope on the spacecraft, the idea of force limited testing will be applied to the derived test input to show the benefits of the force-limited vibration testing method.

To perform a force-limited vibration test, the maximum allowable interface force based on the in-flight configuration must be determined. The in-flight force spectral density function, along with its maximum value, is shown in figure A.5. In the given example, the maximum spectral value occurs at 3.12 E6 N^2/Hz. In addition, figure A.5 shows the force spectral density function encountered during testing using the un-notched test input.

Notice that the maximum force spectral density in the flight configuration occurs at 65 Hz while the maximum force spectral density during testing occurs at 140 Hz.

The force limiting method involves placing force sensors between the test article and the shaker during testing. The same input acceleration spectral density is utilized as before but now the input acceleration spectral density is automatically notched such that the maximum force at the interface never exceeds the predetermined value of 3.12 E6 N^2/Hz.

By implementing force limiting notching, the input acceleration spectrum is automatically modified as shown in figure A.6.

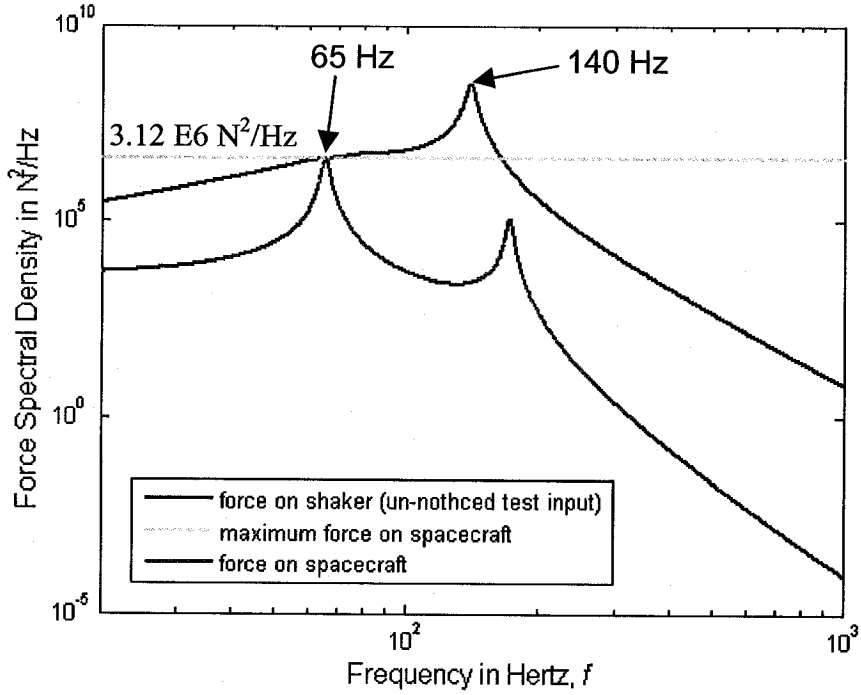

Figure A.5: Telescope to Spacecraft Interface Force Spectral Density

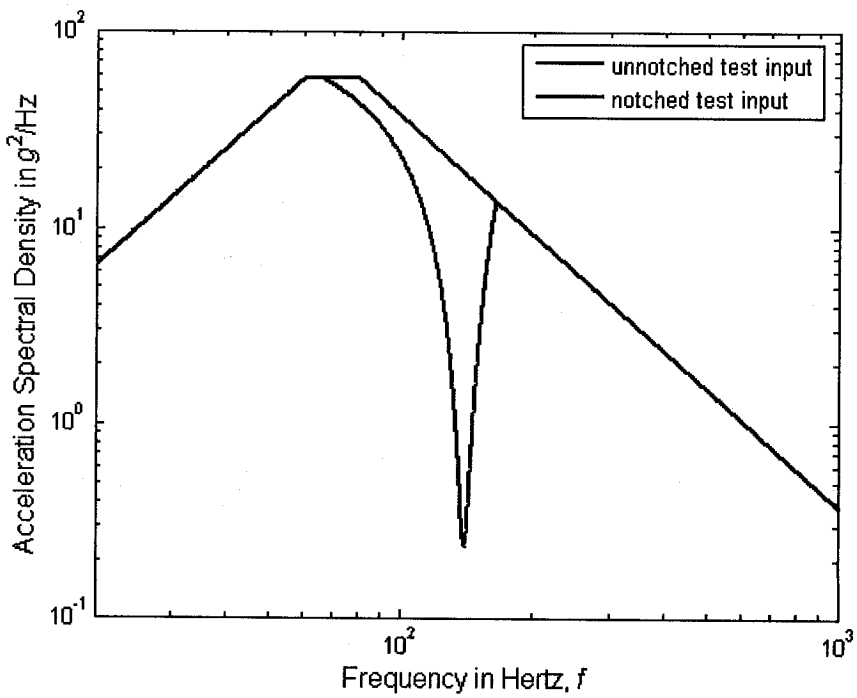

Figure A.6: Test Input Spectrum Before and After Notching

The acceleration spectral density responses of the telescope during testing using the un-notched and the notched test input, along with the actual response of the telescope when on the spacecraft, are compared in figure A.7. The figure shows how force limited-vibration testing has significantly reduced the over-testing occurring near the 140 Hz natural frequency of the telescope by two orders of magnitude for the response acceleration spectral density.

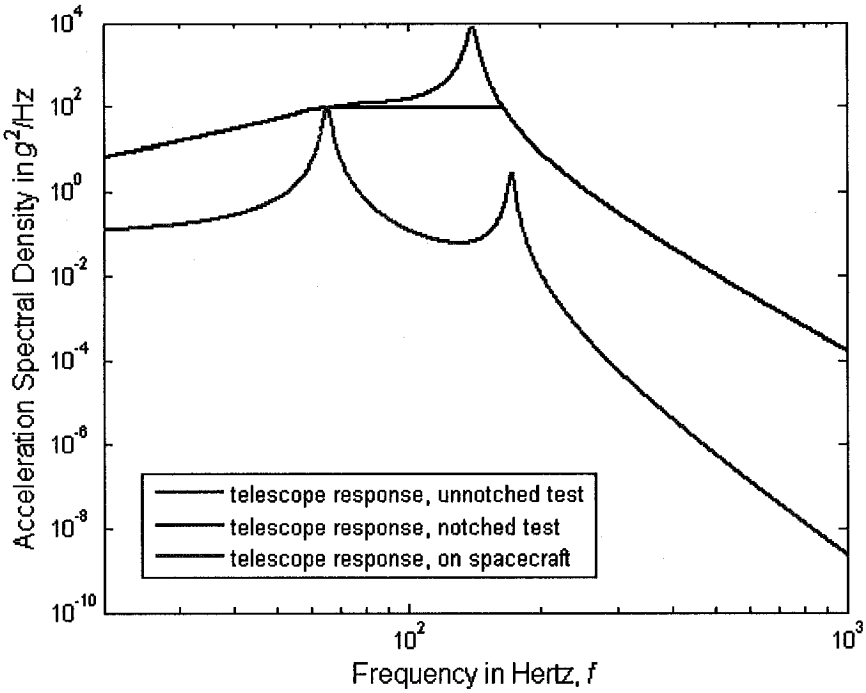

Figure A.7: Telescope Spectral Response Comparison with Notching

The new peak responses can now be computed and compared to the previous peak responses of table A.1. The results are shown in table A.2.

Table A.2: Peak Response Comparison after Notching

Test Configuration	Un-notched Peak Response (= 3 x *g* RMS)	Notched Peak Response (= 3 x *g* RMS)
Shaker Input (for reference)	246 *g*	219 *g*
Telescope Peak Response During Flight (for reference)	59 *g*	59 *g*
Telescope Peak Response During Test	889 *g*	337 *g*
Telescope over-test factor	889 *g* / 59 *g* = 15	337 *g* / 59 *g* = 5.7

The results of figure A.7 and table A.2 show that the force limited-vibration testing produced a significant reduction in the over-testing. The reduction in over-testing was performed while maintaining conservatism in that the telescope's response acceleration spectral density during testing is always greater than the telescope's actual response during flight as shown in figure A.7.

APPENDIX B: RESPONSE OF A BASE EXCITED 2-DOF SYSTEM WITH VISCOUS DAMPING

Consider the base-excited 2-DOF system with viscous damping shown in figure B.1.

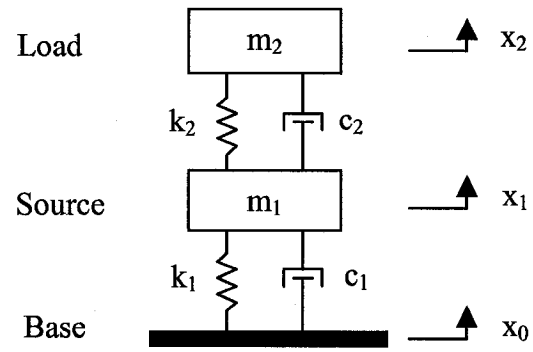

Figure B.1: Base-Excited 2-DOF System with Viscous Damping

In figure B.1, the variables represent the following.

x_0	Base position
x_1	Center-of-mass of source position
m_1	Source mass
k_1	Source spring constant
c_1	Source viscous damping constant
x_2	Center-of-mass of load position
m_2	Load mass
k_2	Load spring constant
c_2	Load viscous damping constant

The base motion is given as a harmonic acceleration as follows

$$\ddot{x}_0 = A_0 \cos(\omega t) \tag{B.1}$$

where

ω	Motion angular frequency
A_0	Zero-to-peak acceleration
t	Time

Defining the following values

Un-damped Fixed-Base Natural frequency of the source

$$\omega_1 \equiv \sqrt{\frac{k_1}{m_1}} \tag{B.2}$$

Un-damped Fixed-Base Natural frequency of the load

$$\omega_2 \equiv \sqrt{\frac{k_2}{m_2}} \tag{B.3}$$

Load-to-source mass Ratio

$$\mu \equiv \frac{m_2}{m_1} \tag{B.4}$$

Load-to-Source un-damped fixed-base natural frequency ratio

$$F \equiv \frac{\omega_2}{\omega_1} \tag{B.5}$$

Critical damping ratio of the source

$$\zeta_1 \equiv \frac{c_1}{2 \cdot m_1 \cdot \omega_1} \tag{B.6}$$

Critical damping ratio of the load

$$\zeta_2 \equiv \frac{c_2}{2 \cdot m_2 \cdot \omega_2} \tag{B.7}$$

For a viscously damped system, the Q of the source is [21]

$$Q_1 = \frac{1}{2\zeta_1} \tag{B.8}$$

Similarly, the Q of the load is

$$Q_2 = \frac{1}{2\zeta_2} \tag{B.9}$$

Base motion frequency to un-damped fixed-base load natural frequency ratio

$$R \equiv \frac{\omega}{\omega_2} \tag{B.10}$$

The free body diagrams for the load and the source are shown in figures B.2 and B.3 respectively. Each dot above a variable indicates a derivative with respect to time.

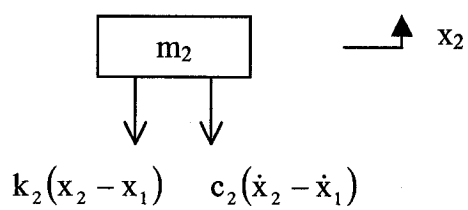

Figure B.2: Load Free Body Diagram (Viscous Damping)

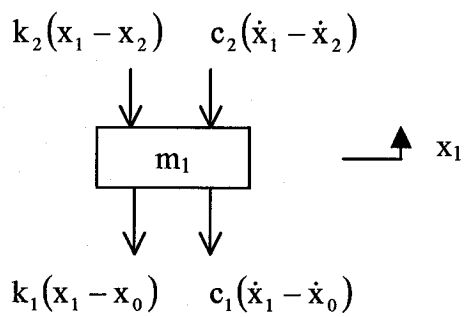

Figure B.3: Source Free Body Diagram (Viscous Damping)

Newton's law can be used to find the equations of motion. Applying Newton's second law to the source gives the following equation of motion.

$$-c_1(\dot{x}_1-\dot{x}_0)-c_2(\dot{x}_1-\dot{x}_2)-k_1(x_1-x_0)-k_2(x_1-x_2)=m_1\ddot{x}_1 \qquad \text{(B.11)}$$

Similarly, applying Newton's second law to the load gives a second equation of motion.

$$-c_2(\dot{x}_2-\dot{x}_1)-k_2(x_2-x_1)=m_2\ddot{x}_2 \qquad \text{(B.12)}$$

Although equations B.11 and B.12 are the correct equations of motion, they are not in a form that is convenient for analysis. As such, the following transformations are applied.

Re-write equation B.11 as

$$m_1\ddot{x}_1+c_1(\dot{x}_1-\dot{x}_0)+c_2(\dot{x}_1-\dot{x}_2)+k_1(x_1-x_0)+k_2(x_1-x_2)=0 \qquad \text{(B.13)}$$

and equation B.12 as

$$m_2\ddot{x}_2+c_2(\dot{x}_2-\dot{x}_1)+k_2(x_2-x_1)=0 \qquad \text{(B.14)}$$

Dividing equation B.13 by m_1 and equation B.14 by m_2 results in equations B.15 and B.16 respectively.

$$\ddot{x}_1+\frac{c_1}{m_1}(\dot{x}_1-\dot{x}_0)+\frac{c_2}{m_1}(\dot{x}_1-\dot{x}_2)+\frac{k_1}{m_1}(x_1-x_0)+\frac{k_2}{m_1}(x_1-x_2)=0 \qquad \text{(B.15)}$$

and

$$\ddot{x}_2+\frac{c_2}{m_2}(\dot{x}_2-\dot{x}_1)+\frac{k_2}{m_2}(x_2-x_1)=0 \qquad \text{(B.16)}$$

Collecting like terms and re-arranging equations B.15 and B.16 gives equations B.17 and B.18 respectively.

$$\ddot{x}_1+\left(\frac{c_1}{m_1}+\frac{c_2}{m_1}\right)\dot{x}_1-\left(\frac{c_2}{m_1}\right)\dot{x}_2+\left(\frac{k_1}{m_1}+\frac{k_2}{m_1}\right)x_1-\left(\frac{k_2}{m_1}\right)x_2=\left(\frac{c_1}{m_1}\right)\dot{x}_0+\left(\frac{k_1}{m_1}\right)x_0 \qquad \text{(B.17)}$$

$$\ddot{x}_2 + \left(\frac{c_2}{m_2}\right)\dot{x}_2 + \left(\frac{k_2}{m_2}\right)x_2 = \left(\frac{c_2}{m_2}\right)\dot{x}_1 + \left(\frac{k_2}{m_2}\right)x_1 \qquad \text{(B.18)}$$

The above equations are the equations of motion of the 2-DOF system. Using the previously defined ratios, equations B.17 and B.18 can be expressed as

$$\ddot{x}_1 + \left(\frac{\omega_1}{Q_1} + \frac{\mu\omega_2}{Q_2}\right)\dot{x}_1 + \left(\omega_1^2 + \mu\omega_2^2\right)x_1 - \frac{\mu\omega_2}{Q_2}\dot{x}_2 - \mu\omega_2^2 x_2 = \frac{\omega_1}{Q_1}\dot{x}_0 + \omega_1^2 x_0 \qquad \text{(B.19)}$$

$$\ddot{x}_2 + \frac{\omega_2}{Q_2}\dot{x}_2 + \omega_2^2 x_2 = \frac{\omega_2}{Q_2}\dot{x}_1 + \omega_2^2 x_1 \qquad \text{(B.20)}$$

The motion of the source x_1 and the load x_2 are assumed to be harmonic. For convenience, the complex notation describing the harmonic motion will be utilized [38]. Although the actual motion is real, not complex, the complex notation is a trick used to simplify the mathematics. The trick works because the equations of motion B.19 and B.20 are linear. The actual motion will be the real part of the final answer for the motion of the load and the source.

The motion of the base was given by equation B.1. Using complex notation, B.1 can be written as

$$\ddot{x}_0 = \mathrm{Re}\left[A_0 e^{i\omega}\right] \qquad \text{(B.21)}$$

For convenience, the descriptor Re[ ], indicating that only the real part of the value must be considered, will be dropped from the notation.

Setting the integration constants to zero, the first and second anti-derivatives of B.21 are

$$\dot{x}_0 = -\frac{A_0}{\omega} i e^{i\omega t} \qquad \text{(B.22)}$$

$$x_0 = -\frac{A_0}{\omega^2} e^{i\omega t} \qquad \text{(B.23)}$$

Similarly, the source and the load acceleration responses are assumed to be harmonic. Their motion can also be described using the complex notation as by the real part of the complex quantities

$$\ddot{x}_1 = A_1 e^{i\omega t} \tag{B.24}$$

$$\ddot{x}_2 = A_2 e^{i\omega t} \tag{B.25}$$

In the two above equations, A_1 and A_2 represent the zero-to-peak acceleration of the harmonic motion and are in general complex quantities. The assumed solution will be the correct solution if the constants A_1 and A_2 are chosen such that both equations of motion B.19 and B.20 are satisfied. Replacing the assumed solution into the equations of motion described by equations B.19 and B.20 and dividing by $e^{i\omega t}$ gives

$$A_1 - \left(\frac{\omega_1}{Q_1} + \frac{\mu\omega_2}{Q_2}\right)\frac{A_1}{\omega} i - \left(\omega_1^2 + \mu\omega_2^2\right)\frac{A_1}{\omega^2} + \frac{\mu\omega_2}{Q_2}\frac{A_2}{\omega} i + \mu\omega_2^2 \frac{A_2}{\omega^2} = -\frac{\omega_1}{Q_1}\frac{A_0}{\omega} i - \omega_1^2 \frac{A_0}{\omega^2} \tag{B.26}$$

$$A_2 - \frac{\omega_2}{Q_2}\frac{A_2}{\omega} i + \omega_2^2 \frac{A_2}{\omega^2} = -\frac{\omega_2}{Q_2}\frac{A_1}{\omega} i - \omega_2^2 \frac{A_1}{\omega^2} \tag{B.27}$$

Multiplying equations B.26 and B.27 by $-\omega^2$ and collecting common terms

$$\left[\omega_1^2 + \mu\omega_2^2 - \omega^2 + i\cdot\left(\frac{\omega_1}{Q_1} + \frac{\mu\omega_2}{Q_2}\right)\omega\right]A_1 - \left[\mu\omega_2^2 + i\cdot\left(\frac{\mu\omega_2}{Q_2}\right)\omega\right]A_2 = \left[\omega_1^2 + i\cdot\left(\frac{\omega_1}{Q_1}\right)\omega\right]A_0 \tag{B.28}$$

$$\left[\omega_2^2 - \omega^2 + i\cdot\left(\frac{\omega_2}{Q_2}\right)\omega\right]A_2 = \left[\omega_2^2 + i\cdot\left(\frac{\omega_2}{Q_2}\right)\omega\right]A_1 \tag{B.29}$$

Dividing the above two equations by ω_2^2 and simplifying them using the previously defined ratios of equations B.2 to B.10, equations B.28 and B.29 can be written as

$$\left[\frac{1}{F^2}+\mu-R^2+i\cdot\left(\frac{1}{FQ_1}+\frac{\mu}{Q_2}\right)R\right]A_1-\left[\mu+i\cdot\left(\frac{\mu R}{Q_2}\right)\right]A_2=\left[\frac{1}{F^2}+i\cdot\left(\frac{R}{FQ_1}\right)\right]A_0 \tag{B.30}$$

$$\left[1-R^2+i\cdot\left(\frac{R}{Q_2}\right)\right]A_2=\left[1+i\cdot\left(\frac{R}{Q_2}\right)\right]A_1 \tag{B.31}$$

Equations B.30 and B.31 can be simplified by defining the following complex quantities.

$$C_1=\left[\frac{1}{F^2}+\mu-R^2+i\cdot\left(\frac{R}{FQ_1}+\frac{\mu R}{Q_2}\right)\right] \tag{B.32}$$

$$C_2=\left[\mu+i\cdot\left(\frac{\mu R}{Q_2}\right)\right] \tag{B.33}$$

$$C_3=\left[\frac{1}{F^2}+i\cdot\left(\frac{R}{FQ_1}\right)\right] \tag{B.34}$$

$$C_4=\left[1-R^2+i\cdot\left(\frac{R}{Q_2}\right)\right] \tag{B.35}$$

$$C_5=\left[1+i\cdot\left(\frac{R}{Q_2}\right)\right] \tag{B.36}$$

Resulting in the following two simple equations

$$C_1A_1-C_2A_2=C_3A_0 \tag{B.37}$$

$$C_4A_2=C_5A_1 \tag{B.38}$$

Solving equations B.37 and B.38 simultaneously for A_1 and A_2

$$A_1=C_4\left[\frac{C_3}{C_1C_4-C_2C_5}\right]A_0 \tag{B.39}$$

$$A_2=C_5\left[\frac{C_3}{C_1C_4-C_2C_5}\right]A_0 \tag{B.40}$$

The complex acceleration frequency response function of the source to the base is

$$H_{10} = \frac{A_1}{A_0} \tag{B.41}$$

The complex acceleration frequency response function of the load to the base is

$$H_{20} = \frac{A_2}{A_0} \tag{B.42}$$

Note that from equations B.39 and B.40, the frequency response function H_{10} and H_{20} are

$$H_{10} = \left[\frac{C_3 C_4}{C_1 C_4 - C_2 C_5}\right] \tag{B.43}$$

$$H_2 = \left[\frac{C_3 C_5}{C_1 C_4 - C_2 C_5}\right] \tag{B.44}$$

In general, the results of equations B.39 and B.40 are complex numbers. As previously described, he motion of the source and the load can be described by the real part of

$$\ddot{x}_1 = A_1 e^{i\omega t} \tag{B.24}$$

$$\ddot{x}_2 = A_2 e^{i\omega t} \tag{B.25}$$

Where A_1 and A_2 are the complex number defined by B.39 and B.40. These complex numbers can be expressed as

$$\ddot{x}_1 = |A_1| e^{i\varphi_1} e^{i\omega t} \tag{B.41}$$

$$\ddot{x}_2 = |A_2| e^{i\varphi_2} e^{i\omega t} \tag{B.42}$$

Where φ_1 and φ_2 are the arguments of the complex numbers A_1 and A_2. Equations B.41 and B.42 can be simplified as

$$\ddot{x}_1 = |A_1| e^{i(\omega t + \varphi_1)} \tag{B.43}$$

$$\ddot{x}_2 = |A_2| e^{i(\omega t + \varphi_2)} \tag{B.44}$$

The real part of which is

$$\ddot{x}_1 = |A_1| \cos(\omega t + \varphi_1) \tag{B.45}$$

$$\ddot{x}_2 = |A_2| \cos(\omega t + \varphi_2) \tag{B.46}$$

APPENDIX C: UN-DAMPED NATURAL FREQUENCIES OF THE BASE EXCITED 2-DOF SYSTEM

Equations B.43 and B.44 are useful equations for determining the un-damped natural frequencies of the system. Without damping, the values of H_{10} and H_{20} are undetermined when the frequency of the motion of the base corresponds to the natural frequency of the coupled system. By examining equations B.43 and B.44, one can see that both equations become undetermined when the denominator is equal to zero. Therefore, the equation defining the un-damped natural frequencies is

$$C_1 C_4 - C_2 C_5 = 0 \tag{C.1}$$

Without damping, the value of the imaginary portion of the complex quantities defined by equations B.32 to B.36 will be zero, resulting in the following simplification.

$$C_1 = \frac{1}{F^2} + \mu - R^2 \qquad \text{No Damping} \tag{C.2}$$

$$C_2 = \mu \qquad \text{No Damping} \tag{C.3}$$

$$C_3 = \frac{1}{F^2} \qquad \text{No Damping} \tag{C.4}$$

$$C_4 = 1 - R^2 \qquad \text{No Damping} \tag{C.5}$$

$$C_5 = 1 \qquad \text{No Damping} \tag{C.6}$$

Inserting the above equations into equation C.1 gives the following simple equation for determining the un-damped natural frequencies.

$$\left(\frac{1}{F^2} + \mu - R^2\right)\left(1 - R^2\right) - \mu = 0 \tag{C.7}$$

Defining

$$\Omega \equiv R^2 \tag{C.8}$$

And multiplying C.7 by the constant F^2 allows one to convert equation C.7 into the following standard quadratic form.

$$F^2\Omega^2 - \left[1 + F^2(1+\mu)\right]\Omega + 1 = 0 \tag{C.9}$$

Solving for the two solutions of Ω gives

$$\Omega_{11} = \frac{1 + F^2(1+\mu) - \sqrt{\left[1 + F^2(1+\mu)\right]^2 - 4F^2}}{2F^2} \tag{C.10}$$

$$\Omega_{22} = \frac{1 + F^2(1+\mu) + \sqrt{\left[1 + F^2(1+\mu)\right]^2 - 4F^2}}{2F^2} \tag{C.11}$$

Where the double subscript has been used to emphasize that the natural frequency is for the coupled system.

In terms of the forcing frequency ratio R, which is the ratio of forcing frequency to the un-damped fixed based natural frequency of the load, the un-damped natural frequencies of the 2-DOF system can be expressed as

$$R_{11}^2 = \frac{1 + F^2(1+\mu) - \sqrt{\left[1 + F^2(1+\mu)\right]^2 - 4F^2}}{2F^2} \tag{C.12}$$

$$R_{22}^2 = \frac{1 + F^2(1+\mu) + \sqrt{\left[1 + F^2(1+\mu)\right]^2 - 4F^2}}{2F^2} \tag{C.13}$$

or in general as

$$R_{ff}^2 = \frac{1 + F^2(1+\mu) \mp \sqrt{\left[1 + F^2(1+\mu)\right]^2 - 4F^2}}{2F^2} \tag{C.14}$$

APPENDIX D: MATLAB ROUTINES FOR 2-DOF INVESTIGATION

Program 1

```
%%%%%%%%%%%%%%%%%%%%%%%%%%%%%%%%%%%%%%%%%%%%%%%%%%%%%%%%%%%%%%%%%%%%%%%%
%   This program calculates the value of C^2 for
%   variable values of the frequency ratio F
%   for a 2-DOF system with viscous damping
%%%%%%%%%%%%%%%%%%%%%%%%%%%%%%%%%%%%%%%%%%%%%%%%%%%%%%%%%%%%%%%%%%%%%%%%

clear   %clears all variables
close   %closes all figures

%INPUT
Q1=10                                       %Define Q of the source
Q2=20                                       %Define Q of the load
u=[0.00001 0.0001 0.001 0.01 0.1 1 10]; %Define mass ratios to analyze

for j=1:length(u)
    F=0.001:0.001:2.5;          %Define frequency ratios to analyze
    for k=1:length(F)

        %Natural Frequencies
        R_1(k)=sqrt((1+F(k)^2*(1+u(j))-sqrt((1+F(k)^2*(1+u(j)))^2 ...
            -4*F(k)^2))/(2*F(k)^2));
        R_2(k)=sqrt((1+F(k)^2*(1+u(j))+sqrt((1+F(k)^2*(1+u(j)))^2 ...
            -4*F(k)^2))/(2*F(k)^2));

        %First mode calculations
        R=R_1(k);
        C1=1/F(k)^2+u(j)-R^2+i*(R/(F(k)*Q1)+u(j)*R/Q2);
        C2=u(j)+i*(u(j)*R/Q2);
        C3=1/F(k)^2+i*(R/(F(k)*Q1));
        C4=1-R^2+i*(R/Q2);
        C5=1+i*(R/Q2);
        H10_1=abs(C3*C4/(C1*C4-C2*C5));
        H20_1=abs(C3*C5/(C1*C4-C2*C5));

        %Second mode calculations
        R=R_2(k);
        C1=1/F(k)^2+u(j)-R^2+i*(R/(F(k)*Q1)+u(j)*R/Q2);
        C2=u(j)+i*(u(j)*R/Q2);
        C3=1/F(k)^2+i*(R/(F(k)*Q1));
        C4=1-R^2+i*(R/Q2);
        C5=1+i*(R/Q2);
        H10_2=abs(C3*C4/(C1*C4-C2*C5));
        H20_2=abs(C3*C5/(C1*C4-C2*C5));

        %C^2 calculations
        H10_max(k)=max(max(H10_1),max(H10_2));
        H20_max(k)=max(max(H20_1),max(H20_2));
        C_squared(k)=(H20_max(k)/H10_max(k))^2;
    end

    %Plot Results with different coloured lines
```

```
    if j==1
        semilogy(F,C_squared,'r', 'linewidth', 2)
        hold on     %futures curves will be added to the initial plot
    end

    if j==2
        semilogy(F,C_squared,'m', 'linewidth', 2)
    end

    if j==3
        semilogy(F,C_squared,'g', 'linewidth', 2)
    end

    if j==4
        semilogy(F,C_squared,'b', 'linewidth', 2)
     end

    if j==5
        semilogy(F,C_squared,'color',([1 0.8 0.1]), 'linewidth', 2)
    end

    if j==6
        semilogy(F,C_squared,'color',[.25 0.8 0.8], 'linewidth', 2)
    end

    if j==7
        semilogy(F,C_squared,'k', 'linewidth', 2)
    end
end

%Plot Labels
grid on
xlabel('Frequency Ratio, F','FontSize',12)
ylabel('C^2','FontSize',12)
legend('{\mu}=0.00001','{\mu}=0.0001','{\mu}=0.001','{\mu}=0.01', ...
    '{\mu}=0.1','{\mu}=1','{\mu}=10');


%%%%%%%%%%%%%%%%%%%%%%%%%%%%%%%%%%%%%%%%%%%%%%%%%%%%%%%%%%%%%%%%%%%%%%%
```

Program 2

```
%%%%%%%%%%%%%%%%%%%%%%%%%%%%%%%%%%%%%%%%%%%%%%%%%%%%%%%%%%%%%%%%%%%%%%%
%   This program calculates the value of C^2 for
%   variable values of the mass ratio u
%   for a 2-DOF system with viscous damping
%%%%%%%%%%%%%%%%%%%%%%%%%%%%%%%%%%%%%%%%%%%%%%%%%%%%%%%%%%%%%%%%%%%%%%%

clear   %clears all variables
close   %closes all figures

%INPUT
Q1=10                               %Define Q of the source
Q2=20                               %Define Q of the load
F=[0.5 0.75 0.9 1 1.1 1.5 2];       %Define frequency ratios to analyze

for j=1:length(F)
    u=logspace(-5,1,1000);          %Define mass ratios to analyze
    for k=1:length(u)

        %Natural Frequencies
        R_1(k)=sqrt((1+F(j)^2*(1+u(k))-sqrt((1+F(j)^2*(1+u(k)))^2 ...
            -4*F(j)^2))/(2*F(j)^2));
        R_2(k)=sqrt((1+F(j)^2*(1+u(k))+sqrt((1+F(j)^2*(1+u(k)))^2 ...
            -4*F(j)^2))/(2*F(j)^2));

        %First mode calculations
        R=R_1(k);
        C1=1/F(j)^2+u(k)-R^2+i*(R/(F(j)*Q1)+u(k)*R/Q2);
        C2=u(k)+i*(u(k)*R/Q2);
        C3=1/F(j)^2+i*(R/(F(j)*Q1));
        C4=1-R^2+i*(R/Q2);
        C5=1+i*(R/Q2);
        H10_1=abs(C3*C4/(C1*C4-C2*C5));
        H20_1=abs(C3*C5/(C1*C4-C2*C5));

        %Second mode calculations
        R=R_2(k);
        C1=1/F(j)^2+u(k)-R^2+i*(R/(F(j)*Q1)+u(k)*R/Q2);
        C2=u(k)+i*(u(k)*R/Q2);
        C3=1/F(j)^2+i*(R/(F(j)*Q1));
        C4=1-R^2+i*(R/Q2);
        C5=1+i*(R/Q2);
        H10_2=abs(C3*C4/(C1*C4-C2*C5));
        H20_2=abs(C3*C5/(C1*C4-C2*C5));

        %C^2 calculations
        H10_max(k)=max(max(H10_1),max(H10_2));
        H20_max(k)=max(max(H20_1),max(H20_2));
        C_squared(k)=(H20_max(k)/H10_max(k))^2;
    end

    %Plot Results with different coloured lines
    if j==1
        loglog(u,C_squared,'r', 'linewidth', 2)
        hold on     %future curves will be added to the initial plot
```

```
    end

    if j==2
        loglog(u,C_squared,'m', 'linewidth', 2)
    end

    if j==3
        loglog(u,C_squared,'g', 'linewidth', 2)
    end

    if j==4
        loglog(u,C_squared,'b', 'linewidth', 2)
     end

    if j==5
        loglog(u,C_squared,'color',([1 0.8 0.1]), 'linewidth', 2)
    end

    if j==6
        loglog(u,C_squared,'color',[.25 0.8 0.8], 'linewidth', 2)
    end

    if j==7
        loglog(u,C_squared,'k', 'linewidth', 2)
    end
end

%Plot Labels
grid on
xlabel('Mass Ratio, \mu','FontSize',12)
ylabel('C^2','FontSize',12)
legend('F=0.5','F=0.75','F=0.9','F=1','F=1.1','F=1.5','F=2');

%%%%%%%%%%%%%%%%%%%%%%%%%%%%%%%%%%%%%%%%%%%%%%%%%%%%%%%%%%%%%%%%%%%%%%%%%%%
```

Program 3

```
%%%%%%%%%%%%%%%%%%%%%%%%%%%%%%%%%%%%%%%%%%%%%%%%%%%%%%%%%%%%%%%%%%%%%%%
%   This program calculates the value of C^2 for
%   variable values of the frequency ratio F
%   for a 2-DOF system with structural damping
%%%%%%%%%%%%%%%%%%%%%%%%%%%%%%%%%%%%%%%%%%%%%%%%%%%%%%%%%%%%%%%%%%%%%%%

clear   %clears all variables
close   %closes all figures

%INPUT
Q1=10                                       %Define Q of the source
Q2=100                                      %Define Q of the load
u=[0.00001 0.0001 0.001 0.01 0.1 1 10]; %Define mass ratios to analyze

for j=1:length(u)
    F=0.001:0.001:2.5;              %Define frequency ratios to analyze
    for k=1:length(F)

        %Natural Frequencies
        R_1(k)=sqrt((1+F(k)^2*(1+u(j))-sqrt((1+F(k)^2*(1+u(j)))^2 ...
            -4*F(k)^2))/(2*F(k)^2));
        R_2(k)=sqrt((1+F(k)^2*(1+u(j))+sqrt((1+F(k)^2*(1+u(j)))^2 ...
            -4*F(k)^2))/(2*F(k)^2));

        %First mode calculations
        R=R_1(k);
        C6=1/F(k)^2+u(j)-R^2+i*(1/(F(k)^2*Q1)+u(j)/Q2);
        C7=u(j)+i*(u(j)/Q2);
        C8=1/F(k)^2+i*(1/(F(k)^2*Q1));
        C9=1-R^2+i*(1/Q2);
        C10=1+i*(1/Q2);
        H10_1=abs(C8*C9/(C6*C9-C7*C10));
        H20_1=abs(C8*C10/(C6*C9-C7*C10));

        %Second mode calculations
        R=R_2(k);
        C6=1/F(k)^2+u(j)-R^2+i*(1/(F(k)^2*Q1)+u(j)/Q2);
        C7=u(j)+i*(u(j)/Q2);
        C8=1/F(k)^2+i*(1/(F(k)^2*Q1));
        C9=1-R^2+i*(1/Q2);
        C10=1+i*(1/Q2);
        H10_2=abs(C8*C9/(C6*C9-C7*C10));
        H20_2=abs(C8*C10/(C6*C9-C7*C10));

        %C^2 calculation
        H10_max(k)=max(max(H10_1),max(H10_2));
        H20_max(k)=max(max(H20_1),max(H20_2));
        C_squared(k)=(H20_max(k)/H10_max(k))^2;
    end

    %Plot Results with different coloured lines
    if j==1
        semilogy(F,C_squared,'r', 'linewidth', 2)
        hold on     %future curves will be added to the initial plot
```

```
    end

    if j==2
        semilogy(F,C_squared,'m', 'linewidth', 2)
    end

    if j==3
        semilogy(F,C_squared,'g', 'linewidth', 2)
    end

    if j==4
        semilogy(F,C_squared,'b', 'linewidth', 2)
     end

    if j==5
        semilogy(F,C_squared,'color',([1 0.8 0.1]), 'linewidth', 2)
    end

    if j==6
        semilogy(F,C_squared,'color',[.25 0.8 0.8], 'linewidth', 2)
    end

    if j==7
        semilogy(F,C_squared,'k', 'linewidth', 2)
    end
end

%Plot Labels
grid on
xlabel('Frequency Ratio, F','FontSize',12)
ylabel('C^2','FontSize',12)
legend('{\mu}=0.00001','{\mu}=0.0001','{\mu}=0.001','{\mu}=0.01', ...
    '{\mu}=0.1','{\mu}=1','{\mu}=10');

%%%%%%%%%%%%%%%%%%%%%%%%%%%%%%%%%%%%%%%%%%%%%%%%%%%%%%%%%%%%%%%%%%%%%%%%
```

Program 4

```
%%%%%%%%%%%%%%%%%%%%%%%%%%%%%%%%%%%%%%%%%%%%%%%%%%%%%%%%%%%%%%%%%%%%%%%
%   This program calculates whether a given set of
%   system parameters will lead to the maximum
%   frequency responses H10 and H20 to occur at
%   the first natural frequency of the
%   coupled 2-DOF system with viscous damping
%%%%%%%%%%%%%%%%%%%%%%%%%%%%%%%%%%%%%%%%%%%%%%%%%%%%%%%%%%%%%%%%%%%%%%%

clear   %clears all variables
close   %closes all figures

%INPUT
F=0.01:0.001:2.5;                   %Define frequency ratios to analyze
u=0.001:0.001:0.5;                  %Define mass ratios to analyze
Q1=10                               %Define Q of the source
Q2=100                              %Define Q of the load

%CALCULATIONS

for j=1:length(u)
    for k=1:length(F)

    %Natural Frequencies
    R_1=sqrt((1+F(k)^2*(1+u(j))...
        -sqrt((1+F(k)^2*(1+u(j)))^2-4*F(k)^2))/(2*F(k)^2));
    R_2=sqrt((1+F(k)^2*(1+u(j))...
        +sqrt((1+F(k)^2*(1+u(j)))^2-4*F(k)^2))/(2*F(k)^2));

    %First mode calculations
    R=R_1;
    C1=1/F(k)^2+u(j)-R^2+i*(R/(F(k)*Q1)+u(j)*R/Q2);
    C2=u(j)+i*(u(j)*R/Q2);
    C3=1/F(k)^2+i*(R/(F(k)*Q1));
    C4=1-R^2+i*(R/Q2);
    C5=1+i*(R/Q2);
    H10_1=abs(C3*C4/(C1*C4-C2*C5));
    H20_1=abs(C3*C5/(C1*C4-C2*C5));

    %Second mode calculations
    R=R_2;
    C1=1/F(k)^2+u(j)-R^2+i*(R/(F(k)*Q1)+u(j)*R/Q2);
    C2=u(j)+i*(u(j)*R/Q2);
    C3=1/F(k)^2+i*(R/(F(k)*Q1));
    C4=1-R^2+i*(R/Q2);
    C5=1+i*(R/Q2);
    H10_2=abs(C3*C4/(C1*C4-C2*C5));
    H20_2=abs(C3*C5/(C1*C4-C2*C5));

    %Ratio calculation
    ratio_H10=H10_1/H10_2;
    ratio_H20=H20_1/H20_2;

    if ratio_H10>=1 & ratio_H20>=1
        region(j,k)=0;
```

```
    else
        region(j,k)=1;
    end
    end
end

contourf(F,u,region)
hidden on
view([0 0 1])
xlabel('Frequency Ratio, F','FontSize',16)
ylabel('Mass Ratio, \mu','FontSize',16)

%%%%%%%%%%%%%%%%%%%%%%%%%%%%%%%%%%%%%%%%%%%%%%%%%%%%%%%%%%%%%%%%%%%%%%%%%%%%
```

Program 5

```
%%%%%%%%%%%%%%%%%%%%%%%%%%%%%%%%%%%%%%%%%%%%%%%%%%%%%%%%%%%%%%%%%%%%%%%
%   This program calculates the differences
%   in the value of C^2 between
%   a 2-DOF system with viscous damping and
%   a 2-DOF system with structural damping
%%%%%%%%%%%%%%%%%%%%%%%%%%%%%%%%%%%%%%%%%%%%%%%%%%%%%%%%%%%%%%%%%%%%%%%

clear   %clears all variables
close   %closes all figures

%INPUT
Q1=10                                       %Define Q of the source
Q2=100                                      %Define Q of the load
u=[0.00001 0.0001 0.001 0.01 0.1 1 10]; %Define mass ratios to analyze

for j=1:length(u)
    F=0.001:0.001:2.5;                      %Define frequency ratios to
analyze
    for k=1:length(F)

        %Natural Frequencies
        R_1(k)=sqrt((1+F(k)^2*(1+u(j))-sqrt((1+F(k)^2*(1+u(j)))^2 ...
            -4*F(k)^2))/(2*F(k)^2));
        R_2(k)=sqrt((1+F(k)^2*(1+u(j))+sqrt((1+F(k)^2*(1+u(j)))^2 ...
            -4*F(k)^2))/(2*F(k)^2));

        %First mode calculations
        R=R_1(k);
        C1=1/F(k)^2+u(j)-R^2+i*(R/(F(k)*Q1)+u(j)*R/Q2);
        C2=u(j)+i*(u(j)*R/Q2);
        C3=1/F(k)^2+i*(R/(F(k)*Q1));
        C4=1-R^2+i*(R/Q2);
        C5=1+i*(R/Q2);
        H10_1_viscous=abs(C3*C4/(C1*C4-C2*C5));
        H20_1_viscous=abs(C3*C5/(C1*C4-C2*C5));
        C6=1/F(k)^2+u(j)-R^2+i*(1/(F(k)^2*Q1)+u(j)/Q2);
        C7=u(j)+i*(u(j)/Q2);
        C8=1/F(k)^2+i*(1/(F(k)^2*Q1));
        C9=1-R^2+i*(1/Q2);
        C10=1+i*(1/Q2);
        H10_1_structural=abs(C8*C9/(C6*C9-C7*C10));
        H20_1_structural=abs(C8*C10/(C6*C9-C7*C10));

        %Second mode calculations
        R=R_2(k);
        C1=1/F(k)^2+u(j)-R^2+i*(R/(F(k)*Q1)+u(j)*R/Q2);
        C2=u(j)+i*(u(j)*R/Q2);
        C3=1/F(k)^2+i*(R/(F(k)*Q1));
        C4=1-R^2+i*(R/Q2);
        C5=1+i*(R/Q2);
        H10_2_viscous=abs(C3*C4/(C1*C4-C2*C5));
        H20_2_viscous=abs(C3*C5/(C1*C4-C2*C5));
        C6=1/F(k)^2+u(j)-R^2+i*(1/(F(k)^2*Q1)+u(j)/Q2);
        C7=u(j)+i*(u(j)/Q2);
```

```
        C8=1/F(k)^2+i*(1/(F(k)^2*Q1));
        C9=1-R^2+i*(1/Q2);
        C10=1+i*(1/Q2);
        H10_2_structural=abs(C8*C9/(C6*C9-C7*C10));
        H20_2_structural=abs(C8*C10/(C6*C9-C7*C10));

       %C^2 difference calculation
        H10_max_viscous(k)=max(max(H10_1_viscous),max(H10_2_viscous));
        H20_max_viscous(k)=max(max(H20_1_viscous),max(H20_2_viscous));
        C_squared_viscous(k)=(H20_max_viscous(k)/H10_max_viscous(k))^2;

        H10_max_structural(k)=...
            max(max(H10_1_structural),max(H10_2_structural));
        H20_max_structural(k)...
            =max(max(H20_1_structural),max(H20_2_structural));
        C_squared_structural(k)=...
            (H20_max_structural(k)/H10_max_structural(k))^2;

        C_squared_difference(k)=...
            C_squared_viscous(k)-C_squared_structural(k);
    end

    %Plot Results with different coloured lines
    if j==1
     plot(F,C_squared_difference,'r', 'linewidth', 2)
     hold on     %future curves will be added to the initial plot
    end

    if j==2
     plot(F,C_squared_difference,'m', 'linewidth', 2)
    end

    if j==3
     plot(F,C_squared_difference,'g', 'linewidth', 2)
    end

    if j==4
     plot(F,C_squared_difference,'b', 'linewidth', 2)
     end

    if j==5
     plot(F,C_squared_difference,'color',([1 0.8 0.1]), 'linewidth', 2)
    end

    if j==6
     plot(F,C_squared_difference,'color',[.25 0.8 0.8], 'linewidth', 2)
    end

    if j==7
     plot(F,C_squared_difference,'k', 'linewidth', 2)
    end
end

%Plot Labels
grid on
xlabel('Frequency Ratio, F','FontSize',12)
ylabel('\itC\rm^2 Difference (Viscous - Structural)','FontSize',12)
```

```
legend('{\mu}=0.00001','{\mu}=0.0001','{\mu}=0.001','{\mu}=0.01', ...
    '{\mu}=0.1','{\mu}=1','{\mu}=10');

%%%%%%%%%%%%%%%%%%%%%%%%%%%%%%%%%%%%%%%%%%%%%%%%%%%%%%%%%%%%%%%%%%%%%%%%%%%%%%%
```

Program 6

```
%%%%%%%%%%%%%%%%%%%%%%%%%%%%%%%%%%%%%%%%%%%%%%%%%%%%%%%%%%%%%%%%%%%%%%%
%   This program calculates the apparent mass function
%   of two different systems with the same total mass
%%%%%%%%%%%%%%%%%%%%%%%%%%%%%%%%%%%%%%%%%%%%%%%%%%%%%%%%%%%%%%%%%%%%%%%

clear   %clears all variables
close   %closes all figures


%INPUT

M=2.16;             %Total mass of object in kg

%D matrix values from finite element analysis results
%D matrix contains the following information
%First column = mode ID
%Second column = natural frequency in Hz
%Third column = effective mass in kg
%Fourth column = Q

D_simply_supported=...
   [1   241.81  1.4203296   20;...
    2   605.14  7.45718E-12 20;...
    3   605.16  1.39892E-12 20;...
    4   966.52  1.24621E-08 20;...
    5   1210.8  0.289656    20;...
    6   1210.9  0.02553336  20;...
    7   1570.5  2.48357E-10 20;...
    8   1570.7  1.29155E-10 20;...
    9   2057.6  1.4558E-08  20;...
    10  2057.7  5.66266E-09 20;...
    11  2172.2  0.017273304 20;...
    12  2416.1  1.08927E-09 20;...
    13  2416.2  2.72678E-11 20;...
    14  3015    3.41064E-08 20;...
    15  3015.7  3.28147E-08 20;...
    16  3143.9  0.09640512  20;...
    17  3144    0.01719576  20;...
    18  3501.4  3.07627E-10 20;...
    19  3501.5  4.36968E-09 20;...
    20  3855.6  1.84959E-07 20;...
    21  4098.5  0.00811188  20;...
    22  4098.7  0.004292784 20;...
    23  4468.1  1.41124E-09 20;...
    24  4468.2  1.38849E-12 20;...
    25  4824.4  3.34217E-10 20;...
    26  4824.8  1.18586E-11 20;...
    27  4934.8  2.63434E-08 20;...
    28  4936.6  1.85203E-10 20;...
    29  5419.5  4.18219E-08 20;...
    30  5420    1.64192E-09 20;...
    31  6012.1  0.00281124  20;...
    32  6027.9  0.02783592  20;...
    33  6028.8  0.02955528  20;...
```

```
    34  6253.4  4.52174E-09 20;...
    35  6254.4  1.43266E-09 20;...
    36  6383.4  6.1411E-09  20;...
    37  6383.8  2.56824E-09 20;...
    38  6976.2  0.006133536 20;...
    39  6977.3  0.000192825 20;...
    40  7324.3  4.67532E-08 20;...
    41  7328.7  4.35823E-09 20;...
    42  7807.3  3.71412E-09 20;...
    43  7808.5  9.43358E-13 20;...
    44  7821    2.04412E-10 20;...
    45  7822.6  9.28066E-12 20;...
    46  8175.5  5.70629E-10 20;...
    47  8176.4  1.1872E-10  20;...
    48  8636.4  9.08928E-07 20;...
    49  8766.7  4.9613E-07  20;...
    50  8767.5  5.78383E-08 20];

D_simply_supported_four_point_fixed=...
    [1  684.86  0.7307496   20;...
    2   1170.8  8.42962E-07 20;...
    3   1171    1.13195E-06 20;...
    4   1289    5.87909E-08 20;...
    5   1794.5  0.5690952   20;...
    6   2146.9  4.59994E-06 20;...
    7   2147.4  2.85422E-07 20;...
    8   2547    4.91681E-06 20;...
    9   2554.8  1.30773E-05 20;...
    10  2555.9  4.8397E-05  20;...
    11  2577.8  0.000127544 20;...
    12  2581.6  6.75994E-06 20;...
    13  2635.2  0.511272    20;...
    14  3087.5  3.36096E-07 20;...
    15  3088.7  3.09571E-06 20;...
    16  3175.2  7.47619E-09 20;...
    17  3643.7  0.01264248  20;...
    18  3861.2  2.11576E-06 20;...
    19  3969.8  2.01468E-07 20;...
    20  3971    3.37284E-07 20;...
    21  4203.4  5.78578E-11 20;...
    22  4829.5  3.30242E-09 20;...
    23  4949.3  0.0373464   20;...
    24  4976.7  2.63002E-06 20;...
    25  4977.5  1.62328E-05 20;...
    26  4983.7  6.59275E-05 20;...
    27  4991    3.90463E-08 20;...
    28  5929.3  5.05354E-08 20;...
    29  5932.3  5.98579E-06 20;...
    30  6101.7  6.46164E-06 20;...
    31  6111.2  0.02976912  20;...
    32  6325.6  8.47022E-06 20;...
    33  6329    4.53946E-08 20;...
    34  6633.8  0.000199554 20;...
    35  7004.4  2.21335E-11 20;...
    36  7041.8  6.00286E-10 20;...
    37  7043.6  6.26681E-08 20;...
    38  7080.9  3.16073E-07 20;...
```

```
    39  7825    1.06898E-06 20;...
    40  7828.1  1.44297E-07 20;...
    41  7945.3  0.000695326 20;...
    42  7948.6  1.20617E-06 20;...
    43  7949.4  0.004152384 20;...
    44  8388.6  2.78489E-08 20;...
    45  8394.8  1.32084E-10 20;...
    46  8538.8  1.08091E-07 20;...
    47  8551.6  6.85843E-08 20;...
    48  8885.3  3.49315E-09 20;...
    49  8885.4  4.78591E-10 20;...
    50  9005.7  2.39544E-10 20];

%Frequencies to output apparent mass
f_min=10;                   %minimum frequency of interest, in Hz
f_max=10000;                %maximum frequency of interest, in Hz
f_step_size=1;              %resolution in Hz

%CALCULATIONS FOR SIMPLY SUPPORTED PLATE
fn=D_simply_supported(:,2);     %extract natural frequencies
m_eff=D_simply_supported(:,3);  %extract effective masses
Q=D_simply_supported(:,4);      %extract Q
M_res=M-sum(m_eff);             %calculates residual mass

i=sqrt(-1);     %defines i as the imaginary number sqrt(-1)
f=f_min:f_step_size:f_max;
for j=1:length(f)
    for k=1:length(fn)
        H_1DOF_H(j,k)=(1+i*(f(j)/fn(k))/Q(k))/(1-(f(j)/fn(k))^2+...
            i*(f(j)/fn(k))/Q(k));
        M_app_k_H(j,k)=m_eff(k)*H_1DOF_H(j,k);
    end
end
M_app_simply_supported=M_res+abs(sum(M_app_k_H')'); %apparent mass
M_app_N_simply_supported=M_app_simply_supported/M;
                                            %normalized apparent mass

%CALCULATIONS FOR SIMPLY SUPPORTED PLATE WITH FOUR INTERIOR POINTS
FIXED
fn=D_simply_supported_four_point_fixed(:,2);
      %extract natural frequencies
m_eff=D_simply_supported_four_point_fixed(:,3);
      %extract effective masses
Q=D_simply_supported_four_point_fixed(:,4);   %extract Q
M_res=M-sum(m_eff);                           %calculates residual mass

i=sqrt(-1);     %defines i as the imaginary number sqrt(-1)
f=f_min:f_step_size:f_max;
for j=1:length(f)
    for k=1:length(fn)
        H_1DOF_H(j,k)=(1+i*(f(j)/fn(k))/Q(k))/(1-(f(j)/fn(k))^2+...
            i*(f(j)/fn(k))/Q(k));
        M_app_k_H(j,k)=m_eff(k)*H_1DOF_H(j,k);
    end
end
M_app_simply_supported_four_point_fixed=M_res+abs(sum(M_app_k_H')');
      %apparent mass
```

```
M_app_N_simply_supported_four_point_fixed=...
    M_app_simply_supported_four_point_fixed/M;
      %normalized apparent mass

%Plots results of source acceleration and force response
figure(1)
loglog(f,M_app_N_simply_supported,'k','linewidth',2)
title('Simply Supported','fontsize',16)
xlabel('Frequency in Hz, \itf','fontsize',14)
ylabel('Normalized Apparent Mass, M_ \it_{app}\rm /M_0','fontsize',14)
ylim([0.1 100])
grid

figure(2)
loglog(f,M_app_N_simply_supported_four_point_fixed,'k','linewidth',2)
title('Simply Supported and Four Interior Points Fixed','fontsize',16)
xlabel('Frequency in Hz, \itf','fontsize',14)
ylabel('Normalized Apparent Mass, M_ \it_{app}\rm /M_0','fontsize',14)

ylim([0.1 100])
grid

%%%%%%%%%%%%%%%%%%%%%%%%%%%%%%%%%%%%%%%%%%%%%%%%%%%%%%%%%%%%%%%%%%%%%%%%%%%%%%%
```

Program 7

```
%%%%%%%%%%%%%%%%%%%%%%%%%%%%%%%%%%%%%%%%%%%%%%%%%%%%%%%%%%%%%%%%%%%%%%%
%This program calculates the interface acceleration
%and the value of C^2 for a 4-DOF system and compares
%the results to the apparent mass method
%%%%%%%%%%%%%%%%%%%%%%%%%%%%%%%%%%%%%%%%%%%%%%%%%%%%%%%%%%%%%%%%%%%%%%%

clear   %clears all variables
close   %closes all figures

%INPUT
%System Parameters
m1=150;      %kg
m2=50;       %kg
m3=10;       %kg
m4=2;        %kg

k1=1E7;      %N/m
k2=1E7;      %N/m
k3=4.2E6;    %N/m
k4=1E6;      %N/m

c1=4000;     %N*s/m
c2=50;       %N*s/m
c3=20;       %N*s/m
c4=10;       %N*s/m

%Base excitation
Saa_base=0.001     %g^2/Hz
f_min=10;          %Hz
f_max=1000;        %Hz
f_step=0.1;        %Hz

%%%%%%%%%%%%%%%%%%%%%%%%%%%%%%%%%%%%%%%%%%%%%%%%%%%%%%%%%%%%%%%%%%%%%%%


%%%%%%%%%%%%%%%%%%%%%%%%%%%%%%%%%%%%%%%%%%%%%%%%%%%%%%%%%%%%%%%%%%%%%%%
%Calculations
%%%%%%%%%%%%%%%%%%%%%%%%%%%%%%%%%%%%%%%%%%%%%%%%%%%%%%%%%%%%%%%%%%%%%%%
%Define useful quantities
m_source=m1+m2;    %total mass of source
m_load=m3+m4;      %total mass of load
i=sqrt(-1);              %define i to be the square root of -1
f=f_min:f_step:f_max;    %frequency point definition

%%%%%%%%%%%%%%%%%%%%%%%%%%%%%%%%%%%%%%%%%%%%%%%%%%%%%%%%%%%%%%%%%%%%%%%


%%%%%%%%%%%%%%%%%%%%%%%%%%%%%%%%%%%%%%%%%%%%%%%%%%%%%%%%%%%%%%%%%%%%%%%
%Calculations for source with free interface: 2-DOF
%%%%%%%%%%%%%%%%%%%%%%%%%%%%%%%%%%%%%%%%%%%%%%%%%%%%%%%%%%%%%%%%%%%%%%%
%Matrix definition
M_source=[m1 0 ;0 m2];
C_source=[c1+c2 -c2;-c2 c2];
K_source=[k1+k2 -k2;-k2 k2];
```

```
%Source Natural Frequencies
[phi_source,lambda_source]=eig(K_source,M_source);
fn_source=sqrt(lambda_source)/(2*pi);
fn1_source=fn_source(1,1)
fn2_source=fn_source(2,2)

%Source Responses
for j=1:length(f)
    w(j)=f(j)*2*pi;                    %angular frequency vector
    F_source=[i*w(j)*c1+k1 0]';        %Force matrix definition
    H_source=(K_source-w(j)^2*M_source+i*w(j)*C_source)\F_source;
            %Solve for responses (same as inv(A)*B but is much faster)
    H1_source(j)=H_source(1);    %FRF acceleration response of mass m1
    H2_source(j)=H_source(2);    %FRF acceleration response of mass m2
    Saa_m2_source(j)=abs(H2_source(j))^2*Saa_base; %ASD of m2 in g^2/Hz
end

%Find test ASD based on enveloping process
Saa_test=max(Saa_m2_source)          %in g^2/Hz

%%%%%%%%%%%%%%%%%%%%%%%%%%%%%%%%%%%%%%%%%%%%%%%%%%%%

%%%%%%%%%%%%%%%%%%%%%%%%%%%%%%%%%%%%%%%%%%%%%%%%%%%%
%Calculations for load in test configuration: 2-DOF
%%%%%%%%%%%%%%%%%%%%%%%%%%%%%%%%%%%%%%%%%%%%%%%%%%%%
M_load=[m3 0 ;0 m4];
C_load=[c3+c4 -c4;-c4 c4];
K_load=[k3+k4 -k4;-k4 k4];

%Load Natural Frequencies
[phi_load,lambda_load]=eig(K_load,M_load);
fn_load=sqrt(lambda_load)/(2*pi);
fn1_load=fn_load(1,1)
fn2_load=fn_load(2,2)

%Load Responses
for j=1:length(f)
    w(j)=f(j)*2*pi;              %angular frequency vector
    F_load=[i*w(j)*c3+k3 0]'; %Force matrix definition
    H_load=(K_load-w(j)^2*M_load+i*w(j)*C_load)\F_load;
            %Solve for responses (same as inv(A)*B but is much faster)
    H3_load(j)=H_load(1);        %FRF acceleration response of mass m3
    H4_load(j)=H_load(2);        %FRF acceleration response of mass m4
    Sff_load(j)=abs(m3*H3_load(j)+m4*H4_load(j))^2*Saa_test*9.81^2;
                                 %FSD force at base in N^2/Hz
    Mapp_load(j)=sqrt(Sff_load(j)/(Saa_test*9.81^2));
                                 %apparent mass of load at base in kg
end

%Calculate Load Normalized Apparent Mass
Mapp_load_N=Mapp_load/m_load; %normalize the apparent mass of the load

%%%%%%%%%%%%%%%%%%%%%%%%%%%%%%%%%%%%%%%%%%%%%%%%%%%%


%%%%%%%%%%%%%%%%%%%%%%%%%%%%%%%%%%%%%%%%%%%%%%%%%%%%
```

```
Calculation for Coupled System in Flight Configuration: 4-DOF
%%%%%%%%%%%%%%%%%%%%%%%%%%%%%%%%%%%%%%%%%%%%%%%%%%%%
M=[m1 0 0 0;0 m2 0 0;0 0 m3 0;0 0 0 m4];
C=[c1+c2 -c2 0 0;-c2 c2+c3 -c3 0;0 -c3 c3+c4 -c4;0 0 -c4 c4];
K=[k1+k2 -k2 0 0;-k2 k2+k3 -k3 0;0 -k3 k3+k4 -k4;0 0 -k4 k4];

%Flight System Natural Frequencies
[V,lambda]=eig(K,M);
fn_4DOF=sqrt(lambda)/(2*pi);
fn1_4DOF=fn_4DOF(1,1)
fn2_4DOF=fn_4DOF(2,2)
fn3_4DOF=fn_4DOF(3,3)
fn4_4DOF=fn_4DOF(4,4)

%Flight System Responses
for j=1:length(f)
    w(j)=f(j)*2*pi;            %angular frequency vector
    F=[i*w(j)*c1+k1 0 0 0]';   %Force matrix definition
    H=(K-w(j)^2*M+i*w(j)*C)\F;
            %Solve for responses (same as inv(A)*B but is much faster)
    H1(j)=H(1);                %FRF acceleration response of mass 1
    H2(j)=H(2);                %FRF acceleration response of mass 2
    H3(j)=H(3);                %FRF acceleration response of mass 3
    H4(j)=H(4);                %FRF acceleration response of mass 4
    Saa_m2_flight(j)=abs(H2(j))^2*Saa_base;   %ASD of m2 in g^2/Hz
    Sff_interface_flight(j)=abs(m3*H3(j)+m4*H4(j))^2*Saa_base*9.81^2;
                               %FSD in N^2/Hz at interface
    Mapp_load_flight(j)=...
      sqrt(Sff_interface_flight(j)/(Saa_m2_flight(j)*9.81^2));
                               %apparent mass of load in kg at interface
end

%Calculate Normalized Apparent Mass of the Load
Mapp_load_flight_N=Mapp_load_flight/m_load;

%Find test ASD based on enveloping process
Saa_test=max(Saa_m2_flight)    %in g^2/Hz

%Find the frequency corresponding to the largest force
f_max=f(find(Sff_interface_flight==max(Sff_interface_flight)))
                               %frequency in Hz
f_max_index=find(Sff_interface_flight==max(Sff_interface_flight));
                               %corresponding frequency index for f_max

%%%%%%%%%%%%%%%%%%%%%%%%%%%%%%%%%%%%%%%%%%%%%%%%%%%%


% C^2 Calculations
% Actual value of C^2 based on 4-DOF system
C_squared_actual=...
      max(Sff_interface_flight)/(m_load^2*max(Saa_m2_flight)*9.81^2)

%Predicted value of C^2 based on apparent mass
C_squared_mapp_predicted_max=(Mapp_load_flight_N(f_max_index))^2
            %assumes maximum force occurs at same frequency as maximum
            %acceleration
C_squared_mapp_predicted=...
```

```
      C_squared_mapp_predicted_max...
      *(Saa_m2_flight(f_max_index)/max(Saa_m2_flight))

%%%%%%%%%%%%%%%%%%%%%%%%%%%%%%%%%%%%%%%%%%%%%%%%%%%%


%%%%%%%%%%%%%%%%%%%%%%%%%%%%%%%%%%%%%%%%%%%%%%%%%%%%
%Figures
%%%%%%%%%%%%%%%%%%%%%%%%%%%%%%%%%%%%%%%%%%%%%%%%%%%%
figure(1)
loglog(f,Sff_interface_flight,'k','linewidth',2)
title('Flight Force Spectral Density vs. Frequency','FontSize',12)
xlabel('Frequency in Hertz, \itf','FontSize',12)
ylabel('Force Spectral Density in N^2/Hz,
      \itS_{ff\rm\_flight}','FontSize',12)
grid on

figure(2)
loglog(f,Saa_m2_flight,'k','linewidth',2)
title('Flight Acceleration Spectral Density for m_2 vs.
      Frequency','FontSize',12)
xlabel('Frequency in Hertz, \itf','FontSize',12)
ylabel('Acceleration Spectral Density in \it g\rm^2/Hz,
      \itS_{aa\rm\_flight}','FontSize',12)
grid on

figure(3)
loglog(f,Saa_m2_source,'k','linewidth',2)
title('Free Acceleration Spectral Density for m_2 vs.
      Frequency','FontSize',12)
xlabel('Frequency in Hertz, \itf','FontSize',12)
ylabel('Acceleration Spectral Density in \it g\rm^2/Hz,
      \itS_{aa\rm\_free}','FontSize',12)
grid on

figure(4)
loglog(f,Mapp_load_N,'k','linewidth',2)
title('Normalized Apparent Mass vs. Frequency','FontSize',12)
xlabel('Frequency in Hertz, \itf','FontSize',12)
ylabel('Normalized Apparent Mass (dimensionless),
      M_{\itapp}','FontSize',12)
grid on


%%%%%%%%%%%%%%%%%%%%%%%%%%%%%%%%%%%%%%%%%%%%%%%%%%%%%%%%%%%%%%%%%%%%%%%%%%%%%%%%
```

APPENDIX E: RESPONSE OF A BASE EXCITED 2-DOF SYSTEM WITH STRUCTURAL DAMPING

Consider the base-excited 2-DOF system with structural damping shown in figure E.1.

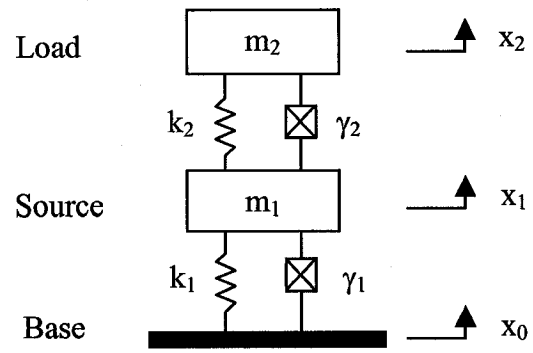

Figure E.1: Base-Excited 2-DOF System with Structural Damping

In figure E.1, the variables represent the following.

x_0	Base position
x_1	Center-of-mass of source position
m_1	Source mass
k_1	Source spring constant
γ_1	Source structural damping constant
x_2	Center-of-mass of load position
m_2	Load mass
k_2	Load spring constant
γ_2	Load structural damping constant

The un-damped fixed-base natural frequencies of the source and the load are defined as:

Un-damped fixed-base natural frequency of the source

$$\omega_1 \equiv \sqrt{\frac{k_1}{m_1}} \tag{E.1}$$

Un-damped fixed-base natural frequency of the load

$$\omega_2 \equiv \sqrt{\frac{k_2}{m_2}} \tag{E.2}$$

The base is assumed to describe harmonic acceleration as follows

$$x_0 = A_0 \cos(\omega t) \tag{E.3}$$

where

ω	Motion angular frequency
A_0	Zero-to-peak acceleration
t	Time

The following ratios are defined.

Mass ratio

$$\mu \equiv \frac{m_2}{m_1} \tag{E.4}$$

Load-to-source un-damped fixed-base frequency ratio

$$F \equiv \frac{\omega_2}{\omega_1} \tag{E.5}$$

For structural damping, the Q of the source is [21]

$$Q_1 = \frac{1}{\gamma_1} \tag{E.6}$$

Similarly, the Q of the load is

$$Q_2 = \frac{1}{\gamma_2} \tag{E.7}$$

Base motion frequency to load un-damped fixed-base natural frequency ratio

$$R \equiv \frac{\omega}{\omega_2} \tag{E.8}$$

The definition of the Q, shown in equations E.6 and E.7, are based on a system with structural damping exhibiting harmonic motion dissipating the same amount of energy per cycle as a system with viscous damping [21].

Because the system is assumed to exhibit harmonic motion, the spring stiffness and the structural damping can be expressed as a complex stiffness as follows [21]

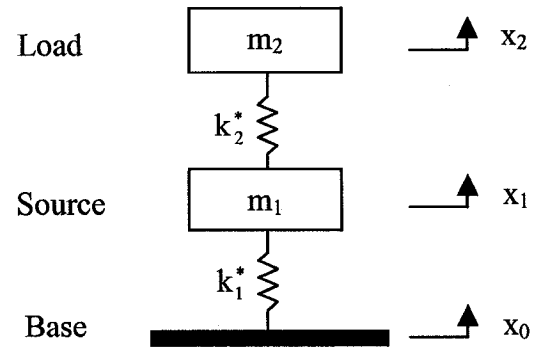

Figure E.2: Base-Excited 2-DOF System with Complex Stiffness

Where the values k_1^* and k_2^* are the complex stiffness of the system. These values are defined as follows.

$$k_1^* \equiv k_1(1 + i \cdot \gamma_1) \tag{E.9}$$

$$k_2^* \equiv k_2(1 + i \cdot \gamma_2) \tag{E.10}$$

One way to derive the equations of motion is to apply Newton's second law on the free body diagrams of the load and the source. The free body diagrams for the load and the source are shown in figures E.2 and E.3 respectively.

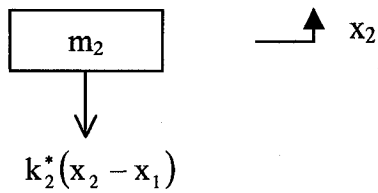

Figure E.3: Load Free Body Diagram (Complex Stiffness)

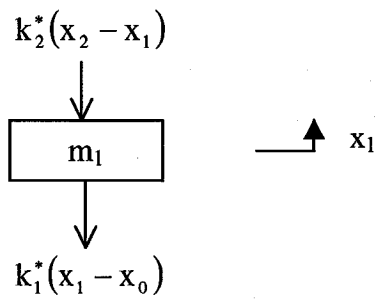

Figure E.4: Source Free Body Diagram (Complex Stiffness)

Applying Newton's second law to the source gives the following equation of motion.

$$-k_1(1+i\cdot\gamma_1)(x_1-x_0)-k_2(1+i\cdot\gamma_2)(x_1-x_2)=m_1\ddot{x}_1 \qquad \text{(E.11)}$$

Similarly, applying Newton's second law to the load gives a second equation of motion.

$$-k_2(1+i\cdot\gamma_2)(x_2-x_1)=m_2\ddot{x}_2 \qquad \text{(E.12)}$$

Re-writing equation E.11 as

$$m_1\ddot{x}_1+k_1(1+i\cdot\gamma_1)(x_1-x_0)+k_2(1+i\cdot\gamma_2)(x_1-x_2)=0 \qquad \text{(E.13)}$$

and equation E.12 as

$$m_2\ddot{x}_2+k_2(1+i\cdot\gamma_2)(x_2-x_1)=0 \qquad \text{(E.14)}$$

Dividing equation E.13 by m_1 and equation E.14 by m_2

$$\ddot{x}_1 + \frac{k_1}{m_1}(1 + i \cdot \gamma_1)(x_1 - x_0) + \frac{k_2}{m_1}(1 + i \cdot \gamma_2)(x_1 - x_2) = 0 \tag{E.15}$$

$$\ddot{x}_2 + \frac{k_2}{m_2}(1 + i \cdot \gamma_2)(x_2 - x_1) = 0 \tag{E.16}$$

Collecting like terms and re-arranging equations E.15 and E.16

$$\ddot{x}_1 + \left[\frac{k_1}{m_1} + \frac{k_2}{m_1} + i \cdot \left(\frac{k_1}{m_1}\gamma_1 + \frac{k_2}{m_1}\gamma_2\right)\right]x_1 - \left[\frac{k_2}{m_1} + i \cdot \left(\frac{k_2}{m_1}\gamma_2\right)\right]x_2 = \left[\frac{k_1}{m_1} + i \cdot \left(\frac{k_1}{m_1}\gamma_1\right)\right]x_0 \tag{E.17}$$

$$\ddot{x}_2 + \left[\frac{k_2}{m_2} + i \cdot \left(\frac{k_2}{m_2}\gamma_2\right)\right]x_2 = \left[\frac{k_2}{m_2} + i \cdot \left(\frac{k_2}{m_2}\gamma_2\right)\right]x_1 \tag{E.18}$$

Simplifying using the previously defined ratios

$$\ddot{x}_1 + \left(\omega_1^2 + \mu\omega_2^2 + i \cdot \left(\frac{\omega_1^2}{Q_1} + \frac{\mu\omega_2^2}{Q_2}\right)\right)x_1 - \left(\mu\omega_2^2 + i \cdot \frac{\mu\omega_2^2}{Q_2}\right)x_2 = \left(\omega_1^2 + i \cdot \frac{\omega_1^2}{Q_1}\right)x_0 \tag{E.19}$$

$$\ddot{x}_2 + \left(\omega_2^2 + i \cdot \frac{\omega_2^2}{Q_2}\right)x_2 = \left(\omega_2^2 + i \cdot \frac{\omega_2^2}{Q_2}\right)x_1 \tag{E.20}$$

With the above equations of motion, the resulting motion of the source and the load to a given harmonic acceleration motion of the base can be determined.

For convenience, the complex notation describing the harmonic motion will be utilized [38]. In this notation, the actual motion is replaced by a complex number whose real part represents the actual motion. Thus, the actual motion of the source and the load will be the real part of the resulting complex number.

Using the complex notation, equation E.3 describing the acceleration motion of the base can be expressed as follows.

$$\ddot{x}_0 = A_0 e^{i\omega} \tag{E.21}$$

Setting the integration constants to zero, the first and second anti-derivatives of E.21 are

$$\dot{x}_0 = -\frac{A_0}{\omega} i e^{i\omega t} \tag{E.22}$$

$$x_0 = -\frac{A_0}{\omega^2} e^{i\omega t} \tag{E.23}$$

Since the source and the load are also assumed to exhibit harmonic motion, their motion can be described by the real part of the complex number shown below.

$$\ddot{x}_1 = A_1 e^{i\omega t} \tag{E.24}$$

$$\ddot{x}_2 = A_2 e^{i\omega t} \tag{E.25}$$

In the above equations, A_1 and A_2 represent the zero-to-peak acceleration of the harmonic motion and are in general complex quantities. The assumed solution will be correct if A_1 and A_2 are chosen such that the equations of motion are both satisfied. Replacing the assumed solution into the equations of motion described by equations E.19 and E.20 then dividing by $e^{i\omega t}$, multiplying by ω^2, and collecting common terms gives

$$\left[\omega_1^2 + \mu\omega_2^2 - \omega^2 + i\cdot\left(\frac{\omega_1^2}{Q_1} + \frac{\mu\omega_2^2}{Q_2}\right)\right]A_1 - \left[\mu\omega_2^2 + i\cdot\frac{\mu\omega_2^2}{Q_2}\right]A_2 = \left[\omega_1^2 + i\cdot\frac{\omega_1^2}{Q_1}\right]A_0 \tag{E.26}$$

$$\left[\omega_2^2 - \omega^2 + i\cdot\frac{\omega_2^2}{Q_2}\right]A_2 = \left[\omega_2^2 + i\cdot\frac{\omega_2^2}{Q_2}\right]A_1 \tag{E.27}$$

Dividing the two above equations by ω_2^2 and simplifying using the previously defined ratios.

$$\left[\frac{1}{F^2} + \mu - R^2 + i\cdot\left(\frac{1}{F^2 Q_1} + \frac{\mu}{Q_2}\right)\right]A_1 - \left[\mu + i\cdot\left(\frac{\mu}{Q_2}\right)\right]A_2 = \left[\frac{1}{F^2} + i\cdot\left(\frac{1}{F^2 Q_1}\right)\right]A_0 \tag{E.28}$$

$$\left[1-R^2+i\cdot\left(\frac{1}{Q_2}\right)\right]A_2=\left[1+i\cdot\left(\frac{1}{Q_2}\right)\right]A_1 \tag{E.29}$$

Equations E.28 and E.29 can be simplified by defining the following complex quantities.

$$C_6=\left[\frac{1}{F^2}+\mu-R^2+i\cdot\left(\frac{1}{F^2Q_1}+\frac{\mu}{Q_2}\right)\right] \tag{E.30}$$

$$C_7=\left[\mu+i\cdot\left(\frac{\mu}{Q_2}\right)\right] \tag{E.31}$$

$$C_8=\left[\frac{1}{F^2}+i\cdot\left(\frac{1}{F^2Q_1}\right)\right] \tag{E.32}$$

$$C_9=\left[1-R^2+i\cdot\left(\frac{1}{Q_2}\right)\right] \tag{E.33}$$

$$C_{10}=\left[1+i\cdot\left(\frac{1}{Q_2}\right)\right] \tag{E.34}$$

Resulting in the following two simple equations

$$C_6A_1-C_7A_2=C_8A_0 \tag{E.35}$$

$$C_9A_2=C_{10}A_1 \tag{E.36}$$

Solving equations E.35 and E.36 simultaneously for A_1 and A_2

$$A_1=C_9\left[\frac{C_8}{C_6C_9-C_7C_{10}}\right]A_0 \tag{E.37}$$

$$A_2=C_{10}\left[\frac{C_8}{C_6C_9-C_7C_{10}}\right]A_0 \tag{E.38}$$

In general, the results of equations E.37 and E.38 are complex numbers. As previously described, the motion of the source and the load can be described by the real part of

$$\ddot{x}_1 = A_1 e^{i\omega t} \tag{E.24}$$

$$\ddot{x}_2 = A_2 e^{i\omega t} \tag{E.25}$$

Where A_1 and A_2 are the complex numbers defined by E.37 and E.38. These complex numbers can be expressed as

$$\ddot{x}_1 = |A_1| e^{i\varphi_1} e^{i\omega t} \tag{E.39}$$

$$\ddot{x}_2 = |A_2| e^{i\varphi_2} e^{i\omega t} \tag{E.40}$$

Where φ_1 and φ_2 are the arguments of the complex numbers A_1 and A_2.

Equations E.39 and E.40 can be simplified as

$$\ddot{x}_1 = |A_1| e^{i(\omega t+\varphi_1)} \tag{E.41}$$

$$\ddot{x}_2 = |A_2| e^{i(\omega t+\varphi_2)} \tag{E.42}$$

The real part of which is

$$\ddot{x}_1 = |A_1| \cos(\omega t + \varphi_1) \tag{E.43}$$

$$\ddot{x}_2 = |A_2| \cos(\omega t + \varphi_2) \tag{E.44}$$

Where φ_1 and φ_2 are the arguments of the complex numbers A_1 and A_2.

The complex acceleration frequency response function of the source to the base is

$$H_{10} = \frac{A_1}{A_0} \tag{E.45}$$

The complex acceleration frequency response function of the load to the base is

$$H_{20} = \frac{A_2}{A_0} \tag{E.46}$$

Combining equations E.37 and E.38 with E.45 and E.46,

$$|H_{10}| = \left| \frac{C_8 C_9}{C_6 C_9 - C_7 C_{10}} \right| \tag{E.47}$$

$$|H_{20}| = \left| \frac{C_8 C_{10}}{C_6 C_9 - C_7 C_{10}} \right| \tag{E.48}$$

APPENDIX F: VALUE OF R^2 FOR MAXIMUM C^2

Consider the following equation

$$C^2 \approx \frac{1}{\left(1-R_{ff}^2\right)^2} \tag{F.1}$$

The above equation is valid for very lightly damped systems where the maximum acceleration of the source and the load both occur at the same natural frequency identified as R_{ff}.

The value of R_{ff} is the ratio of the one of the natural frequencies of the coupled system to the natural frequency of the uncoupled load. This ratio has been previously determined in appendix B as

$$R_{ff}^2 = \frac{1+F^2(1+\mu) \mp \sqrt{\left[1+F^2(1+\mu)\right]^2 - 4F^2}}{2F^2} \tag{F.2}$$

By inspection of F.1, the value of C^2 will approach infinity as the ratio R_{ff}^2 approaches unity.

Thus, of interest is the condition where

$$\frac{1+F^2(1+\mu) \mp \sqrt{\left[1+F^2(1+\mu)\right]^2 - 4F^2}}{2F^2} \rightarrow 1 \tag{F.3}$$

Re-written as

$$\mp \sqrt{\left[1+F^2(1+\mu)\right]^2 - 4F^2} \rightarrow 2F^2 - \left[1+F^2(1+\mu)\right] \tag{F.4}$$

Squaring both sides

$$\left[1+F^2(1+\mu)\right]^2 - 4F^2 \rightarrow 4F^4 - 4F^2\left(1+F^2(1+\mu)\right) + \left[1+F^2(1+\mu)\right]^2 \tag{F.5}$$

Simplifying and re-arranging terms

$$F^4\mu \to 0 \tag{F.6}$$

For any given non-zero value of F, the equation can be simplified as

$$\mu \to 0 \tag{F.7}$$

Thus, for any given non-zero value of F, the value of R_{ff}^2 will be closest to unity when the mass ratio tends towards zero provided that the maximum acceleration of the source and the load both occur at the same natural frequency.

Therefore, the value of R_{ff}^2 that will give the largest value of C^2 for any given F provided that the acceleration of the source and the load occur at the same frequency will be determined by

$$R_{ff,\mu\to 0}^2 = \lim_{\mu \to 0} \frac{1+F^2(1+\mu) \mp \sqrt{\left[1+F^2(1+\mu)\right]^2 - 4F^2}}{2F^2} \tag{F.8}$$

which gives

$$R_{ff,\mu\to 0}^2 = \frac{1+F^2 \mp \sqrt{\left[1+F^2\right]^2 - 4F^2}}{2F^2} \tag{F.9}$$

The factor under the square root can be factorized as either

$$\left(1+F^2\right)^2 - 4F^2 = \left(1-F^2\right)^2 \tag{F.10}$$

or

$$\left(1+F^2\right)^2 - 4F^2 = \left(F^2-1\right)^2 \tag{F.11}$$

Assuming that the maximum acceleration of the source and the load both occur at R_{11}, using either factorization leads to the following results

$$R_{11,\mu\to 0}^2 = 1 \qquad \text{if } F \le 1 \tag{F.12}$$

$$R_{11,\mu\to 0}^2 = \frac{1}{F^2} \qquad \text{if } F \ge 1 \tag{F.13}$$

Combining equations F.13 with F.1 gives

$$C^2 \approx \frac{1}{\left(1-\frac{1}{F^2}\right)^2} \qquad \text{maximum responses at } R_{11} \qquad \text{(F.18)}$$

APPENDIX G: FORCE TRANSMISSIBILITY FOR BASE EXCITED 1-DOF SYSTEM WITH STRUCTURAL DAMPING

Consider the force excited fixed-base 1-DOF system with structural damping shown in figure G.1.

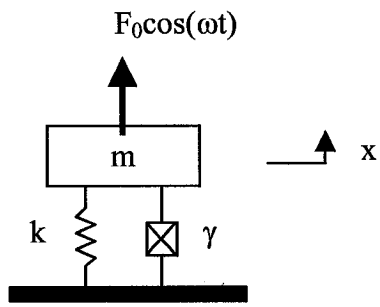

Figure G.1: Fixed-Base 1-DOF System with Structural Damping

Using complex notation, the equation of motion for this system can be expressed as [39]

$$m\ddot{x} + k(1 + i\gamma)x = F_0 e^{i\omega t} \tag{G.1}$$

Defining the un-damped natural frequency as

$$\omega_n \equiv \sqrt{\frac{k}{m}} \tag{G.2}$$

And assuming that the solution can be expressed as

$$x = Xe^{i\omega t} \tag{G.3}$$

Equation G.1 can be re-written as

$$\left[1 - \left(\frac{\omega}{\omega_n}\right)^2 + i\gamma\right] X = \frac{F_0}{\omega_n^2 m} \tag{G.4}$$

Solving for X

$$X = \frac{\frac{F_0}{\omega_n^2 m}}{1 - \left(\frac{\omega}{\omega_n}\right)^2 + i\gamma} \tag{G.5}$$

Equation G.5 shows the displacement response to the force. From equation G.3,

$$\ddot{x} = -\omega^2 X e^{i\omega t} \tag{G.6}$$

According to Newton's law, the forcing load F_0 must be equal to the vector sum of the transmitted force F_{trans} plus the acceleration of the mass. This can be expressed in complex notation as

$$\overline{F}_0 = \overline{F}_{trans} + m\ddot{x} \tag{G.7}$$

Where

$$\overline{F}_0 = F_0 e^{i\omega t} \tag{G.8}$$

and

$$\overline{F}_{trans} = F_{trans} e^{i\omega t} \tag{G.9}$$

Since by definition the force transmissibility is the ratio $\frac{\overline{F}_{trans}}{\overline{F}_0}$, equation G.7 can be re-written as

$$\frac{F_{trans}}{F_0} = 1 - \frac{m\ddot{x}}{\overline{F}_0} \tag{G.10}$$

Combining equations G.10, G.6, and G.5, then dividing by $e^{i\omega t}$ gives

$$\frac{F_{trans}}{F_0} = 1 + \frac{\frac{\omega^2}{\omega_n^2}}{1 - \left(\frac{\omega}{\omega_n}\right)^2 + i\gamma} \tag{G.5}$$

Which can equivalently be written as

$$\frac{F_{trans}}{F_0} = \frac{1 + i\gamma}{1 - \left(\frac{\omega}{\omega_n}\right)^2 + i\gamma} \tag{G.6}$$

The Q factor for structural damping is [21]

$$Q = \frac{1}{\gamma} \tag{G.7}$$

Therefore, the force transmissibility for structural damping is

$$\frac{F_{trans}}{F_0} = \frac{1 + \frac{i}{Q}}{1 - \left(\frac{\omega}{\omega_n}\right)^2 + \frac{i}{Q}} \tag{G.8}$$

Converting the frequencies from radians per second to Hertz and using H to describe the force transmissibility frequency response function, the transmissibility can be expressed as

$$H = \frac{1 + \frac{i}{Q}}{1 - \left(\frac{f}{f_n}\right)^2 + \frac{i}{Q}} \tag{G.9}$$

APPENDIX H: APPARENT MASS METHOD EXAMPLE EQUATIONS

Consider the following base excited viscously damped 4-DOF system as shown in figure H.1.

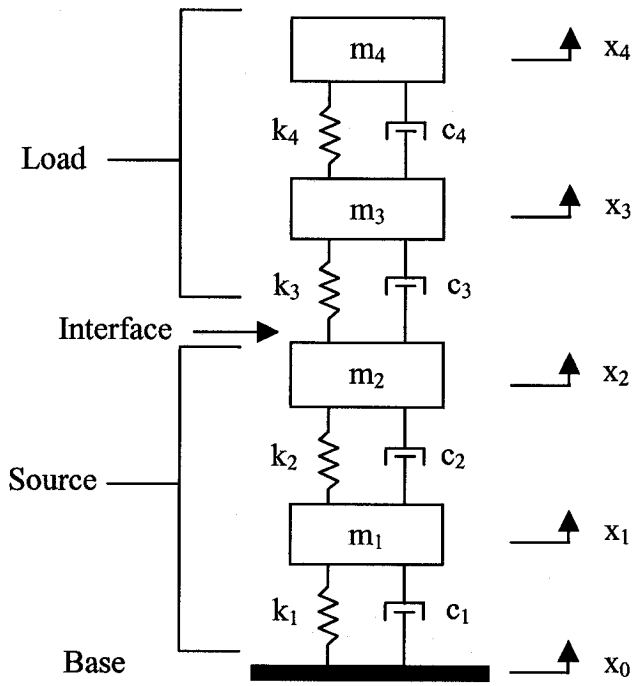

Figure H.1: 4-DOF System

The force balance on any given mass j can be expressed described as shown in figure H.2.

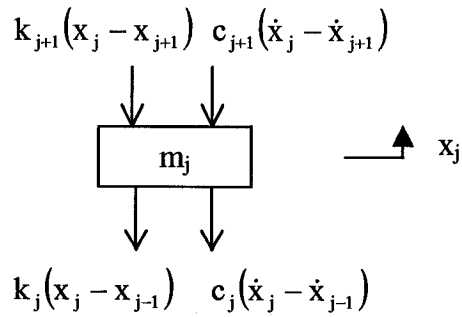

Figure H.2: General Force Balance on Mass j

Applying Newton's second law at each mass gives the following four equations of motion.

$$-c_1(\dot{x}_1-\dot{x}_0)-c_2(\dot{x}_1-\dot{x}_2)-k_1(x_1-x_0)-k_2(x_1-x_2)=m_1\ddot{x}_1 \tag{H.1}$$

$$-c_2(\dot{x}_2-\dot{x}_1)-c_3(\dot{x}_2-\dot{x}_3)-k_2(x_2-x_1)-k_3(x_2-x_3)=m_2\ddot{x}_2 \tag{H.2}$$

$$-c_3(\dot{x}_3-\dot{x}_2)-c_4(\dot{x}_3-\dot{x}_4)-k_3(x_3-x_2)-k_4(x_3-x_4)=m_3\ddot{x}_3 \tag{H.3}$$

$$-c_4(\dot{x}_4-\dot{x}_3)-k_4(x_4-x_3)=m_4\ddot{x}_4 \tag{H.4}$$

Re-arranged as

$$m_1\ddot{x}_1+(c_1+c_2)\dot{x}_1+(k_1+k_2)x_1-c_2\dot{x}_2-k_2x_2=c_1\dot{x}_0+k_1x_0 \tag{H.5}$$

$$-c_2\dot{x}_1-k_2x_1+m_2\ddot{x}_2+(c_2+c_3)\dot{x}_2+(k_2+k_3)x_2-c_3\dot{x}_3-k_3x_3=0 \tag{H.6}$$

$$-c_3\dot{x}_2-k_3x_2+m_3\ddot{x}_3+(c_3+c_4)\dot{x}_3+(k_3+k_4)x_3-c_4\dot{x}_4-k_4x_4=0 \tag{H.7}$$

$$-c_4\dot{x}_3-k_4x_3+m_4\ddot{x}_4+c_4\dot{x}_4+k_4x_4=0 \tag{H.8}$$

The above four equations can be written in the matrix form

$$[M]\{\ddot{X}\}+[C]\{\dot{X}\}+[K]\{X\}=\{C_f\}\dot{x}_0+\{K_f\}x_0 \tag{H.9}$$

where

$$[M]=\begin{bmatrix} m_1 & 0 & 0 & 0 \\ 0 & m_2 & 0 & 0 \\ 0 & 0 & m_3 & 0 \\ 0 & 0 & 0 & m_4 \end{bmatrix} \tag{H.10}$$

$$[C]=\begin{bmatrix} c_1+c_2 & -c_2 & 0 & 0 \\ -c_2 & c_2+c_3 & -c_3 & 0 \\ 0 & -c_3 & c_3+c_4 & -c_4 \\ 0 & 0 & -c_4 & c_4 \end{bmatrix} \tag{H.11}$$

$$[K]=\begin{bmatrix} k_1+k_2 & -k_2 & 0 & 0 \\ -k_2 & k_2+k_3 & -k_3 & 0 \\ 0 & -k_3 & k_3+k_4 & -k_4 \\ 0 & 0 & -k_4 & k_4 \end{bmatrix} \tag{H.12}$$

$$\{C_f\}=\begin{Bmatrix} c_1 \\ 0 \\ 0 \\ 0 \end{Bmatrix} \tag{H.13}$$

$$\{K_f\}=\begin{Bmatrix} k_1 \\ 0 \\ 0 \\ 0 \end{Bmatrix} \tag{H.14}$$

Assuming that the solution to the individual displacements can be expressed as

$$x_j = \mathrm{Re}\left[X_j e^{i\omega t}\right] \tag{H.15}$$

Equation H.9 can be written as

$$\left([K]-\omega^2[M]+i\omega[C]\right)\{X\}=\{F\}x_0 \tag{H.16}$$

Where

$$\{F\}=\begin{Bmatrix} i\omega c_1+k_1 \\ 0 \\ 0 \\ 0 \end{Bmatrix} \tag{H.17}$$

The un-damped natural frequencies are the eigenvalues of the problem

$$([K]-\omega^2[M])\{X\}=0 \tag{H.18}$$

Let the H be a column vector whose elements are defined as the ratio

$$H_j=\frac{x_j}{x_0} \tag{H.19}$$

Then equation H.16 can be written as

$$([K]-\omega^2[M]+i\omega[C])\{H\}=\{F\} \tag{H.20}$$

where by equation H.15, $\{H\}$ simplifies to

$$\{H\}=\begin{Bmatrix} X_1/X_0 \\ X_2/X_0 \\ X_3/X_0 \\ X_4/X_0 \end{Bmatrix} \tag{H.21}$$

Solving for H given ω

$$\{H\}=([K]-\omega^2[M]+i\omega[C])^{-1}\{F\} \tag{H.22}$$

The algorithm for finding the frequency response function H involves choosing a frequency then evaluating the quantities in equation H.22. Then the process is repeated as many times as required to get any desired frequency response function resolution and bandwidth.

The above algorithm can also be used to solve for the 2-DOF systems shown in figure H.3.

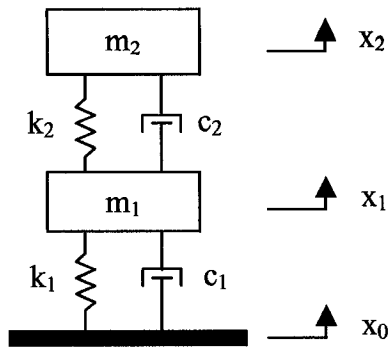

Figure H.3: 2-DOF Systems for Source and Load

However, in the case of the source, the matrices are

$$[M]_{source} = \begin{bmatrix} m_1 & 0 \\ 0 & m_2 \end{bmatrix} \tag{H.23}$$

$$[C]_{source} = \begin{bmatrix} c_1 + c_2 & -c_2 \\ -c_2 & c_2 \end{bmatrix} \tag{H.24}$$

$$[K]_{source} = \begin{bmatrix} k_1 + k_2 & -k_2 \\ -k_2 & k_2 \end{bmatrix} \tag{H.25}$$

$$\{F\}_{source} = \begin{bmatrix} i\omega c_1 + k_1 \\ 0 \end{bmatrix} \tag{H.26}$$

And in the case of the load, the matrices are

$$[M]_{load} = \begin{bmatrix} m_3 & 0 \\ 0 & m_4 \end{bmatrix} \tag{H.27}$$

$$[C]_{load} = \begin{bmatrix} c_3 + c_4 & -c_4 \\ -c_4 & c_4 \end{bmatrix} \tag{H.28}$$

$$[K]_{load} = \begin{bmatrix} k_3 + k_4 & -k_4 \\ -k_4 & k_4 \end{bmatrix} \tag{H.29}$$

$$\{F\}_{load} = \begin{bmatrix} i\omega c_3 + k_3 \\ 0 \end{bmatrix} \tag{H.30}$$

To calculate the values of the acceleration spectral density, the following relationship was utilized.

$$S_{aa\_output} = |H|^2 S_{aa\_input} \tag{H.31}$$

Where H is the frequency response function between the input and the output. Similarly,

$$S_{ff} = |M_{app}|^2 S_{aa\_input} \tag{H.32}$$

Where M_{app} is the apparent mass calculated as

$$M_{app} = \sum_{j=1}^{N} m_j H_j \tag{H.33}$$

Where N represents the number of discrete masses on one side of the interface of interest and H is a complex number representing the frequency response function of acceleration of mass j to the base input acceleration.

The above equations and algorithm was programmed into the MATLAB language. The resulting script file is shown in program 7 of appendix C.

APPENDIX I: BOLT SCALING FACTOR CALCULATIONS

The scaling factor is calculated as

$$\alpha = \frac{k_{bolt} + k_{clamped}}{k_{clamped}} \tag{I.1}$$

The stiffness of a structural member can be established using the relation [40]

$$k = \frac{AE}{L} \tag{I.2}$$

Where A is the compressed area, E is the modulus of elasticity of the material, and the L is the length of the compressed area.

Now consider the problem of determining the scaling factor for the geometry shown in figure I.1.

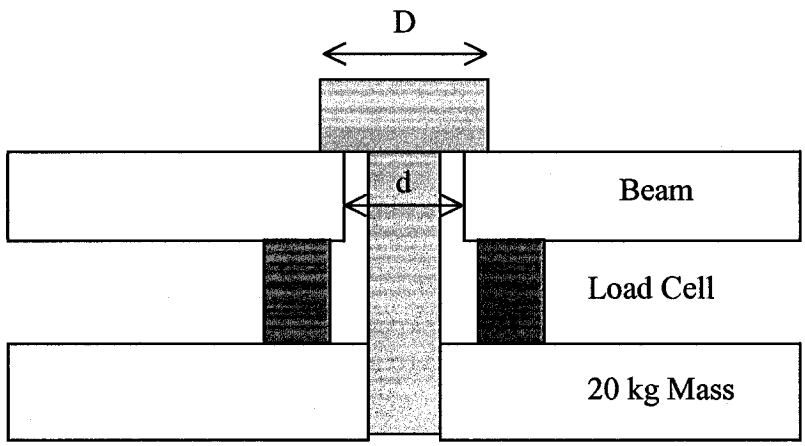

Figure I.1: Joint Geometry

The compressed area of the load can be estimated by assuming that the compressed volume makes a 30° cone as shown in figure I.2 [35].

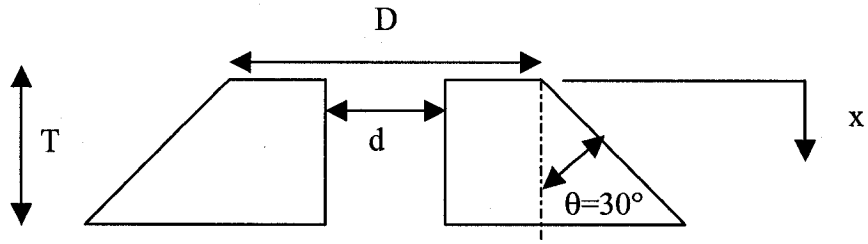

Figure I.2: Compressed Volume

Now consider the compliance of an infinitesimally thin horizontal slice of the above geometry. The differential compliance dC can be expressed as

$$dC = \frac{dx}{A_x E} \tag{I.3}$$

Where A_x can be expressed in terms of the cone angle θ and the position x as

$$A_x = \frac{\pi}{4}\left[(D + 2x\tan\theta)^2 - d^2\right] \tag{I.4}$$

Using calculus, the total compliance of the volume can be calculated as

$$C = \int_0^T \frac{dx}{\frac{\pi}{4}\left[(D + 2x\tan\theta)^2 - d^2\right]E} \tag{I.5}$$

Solving the above integral gives

$$C = \frac{\ln\left[\frac{(2T\tan\theta + D - d)(D + d)}{(2T\tan\theta + D + d)(D - d)}\right]}{\pi E d \tan\theta} \tag{I.6}$$

The stiffness is the inverse of the compliance, thus

$$k = \frac{\pi E d \tan\theta}{\ln\left[\frac{(2T\tan\theta + D - d)(D + d)}{(2T\tan\theta + D + d)(D - d)}\right]} \tag{I.7}$$

The thickness T is 0.200 inches for the experimental setup with the 2 kg mass and 0.350 inches for the setup with the 10 kg mass. Both setups have a value of D = 0.375 inches and d = 0.226 inches. The modulus of elasticity of steel is taken as 29E6 psi [40]. Using a compression angle of 30°, the stiffness of the beam as calculated by equation I.7 is

k_{beam} = 1.95 E7 lb/in for the setup with the 2 kg load mass

k_{beam} = 1.49 E7 E6 lb/in for the setup with the 10 kg load mass

The stiffness of the force sensor is given by the manufacture and is

k_{sensor} = 14.7 E6 lb/in

Since the beam and the sensor are in series, the value of the clamped stiffness is

$$k_{clamped} = \frac{1}{\frac{1}{k_{beam}} + \frac{1}{k_{sensor}}} \tag{I.8}$$

Giving

$k_{clamped}$ = 8.37 E6 lb/in for the setup with the 2 kg load mass

$k_{clamped}$ = 7.40 E6 lb/in for the setup with the 10 kg load mass

The bolt is a steel ¼-20 socket head cap screw. The tensile area of the bolt is given as 0.0318 in^2 [36]. The modulus of elasticity of steel is taken as 29E6 psi [40]. The effective length of the bolt is taken as

$$L_{bolt} = L_{beam} + L_{sensor} \tag{I.9}$$

This gives

k_{bolt} = 1.55 E6 lb/in for the setup with the 2 kg load mass

k_{bolt} = 1.24 E6 lb/in for the setup with the 10 kg load mass

Thus the scaling factor can be calculated with equation I.1. They are

$\alpha = 1.19$ for the setup with the 2 kg load mass

$\alpha = 1.17$ for the setup with the 10 kg load mass

Since these values are approximate, both are considered to have a scaling factor of about 1.2.

APPENDIX J: TYPICAL VIBRATION DATA PLOTS

CSA/DFL Vibration Laboratory

Project : flvt_m
Test : 20F_Sine
Run : 1 RUN_1

Date : 19-01-06
Time : 12: 33: 20
Mode : Sine Vibration Control

Sweeprate : 2.000 Oct/min
Sweep mode : LOG
Start frequency : 10
Sweeps done : 1
Frequency resolution : 1 Hz

Maximum value : 6.49 g

Trace identification : MSX

fixed

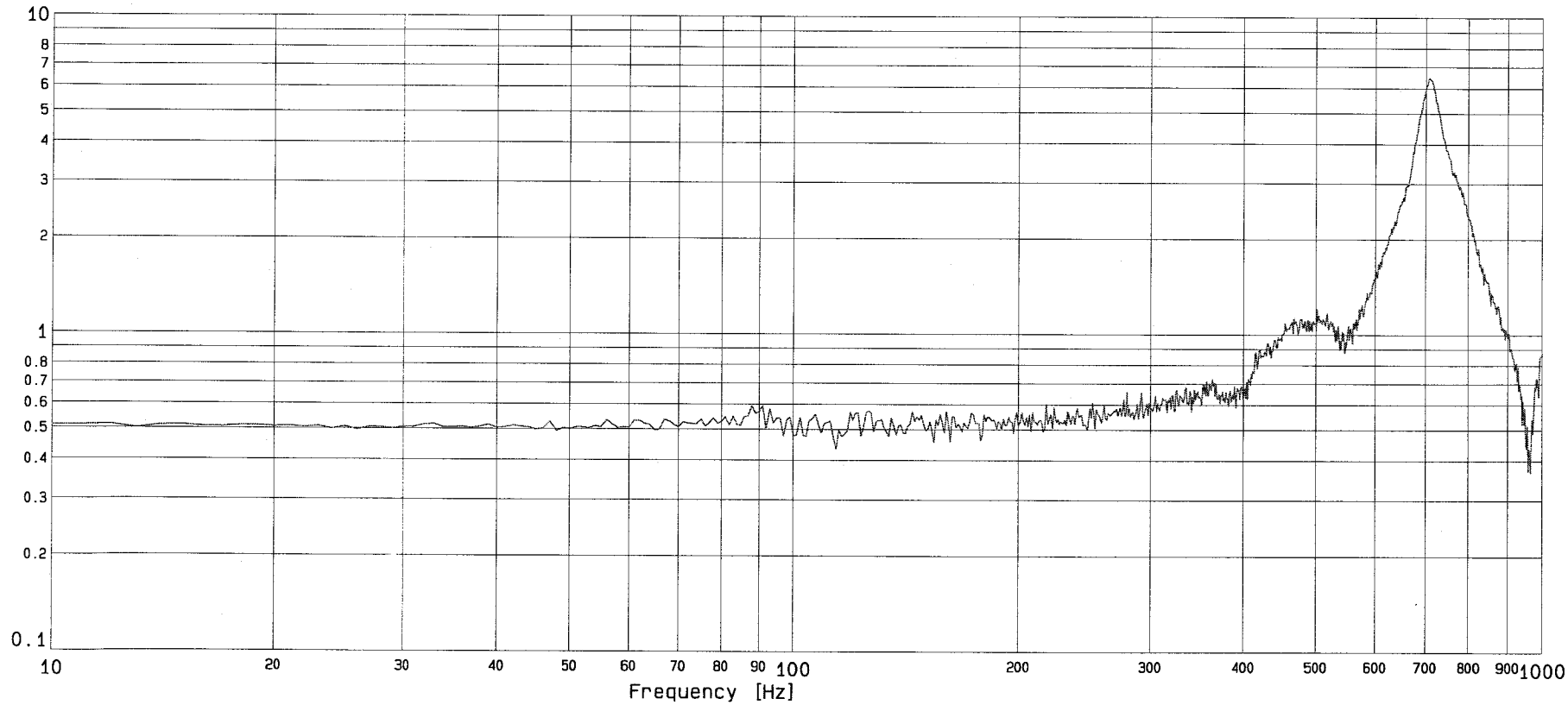

J-2

CSA/DFL Vibration Laboratory

Project : flvt_m
Test : 20F_Rand2007042
Run : 1 20F_rand20070420

Date : 20-04-07
Time : 14: 32: 27
Mode : Random Vibration Control

Test level : 0.00 dB
Elapsed time : 00: 02: 30.0
Degrees of freedom : 150
Control strategy : Average
Frequency resolution : 2 Hz

PSD Level (RMS) : 10.06 g
Number of averages : 215

Trace identification : MSX

fixed

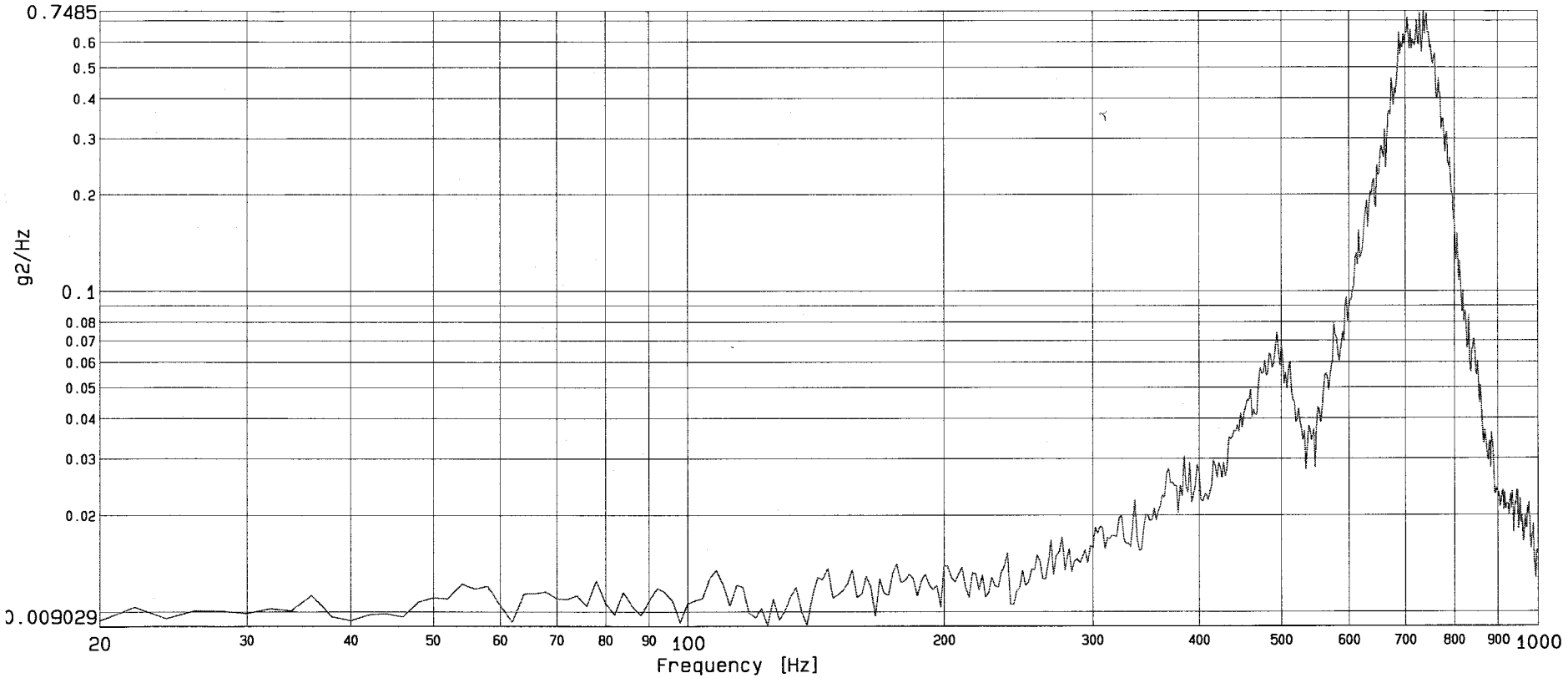

4-3

CSA/DFL Vibration Laboratory

Project : flvt_m
Test : 20U_Sine
Run : 2 RUN_2

Date : 19-01-06
Time : 09:29:49
Mode : Sine Vibration Control

Sweeprate : 2.000 Oct/min
Sweep mode : LOG
Start frequency : 10
Sweeps done : 1
Frequency resolution : 1 Hz

Maximum value : 21.00 g

Trace identification : ——— MSX

fixed

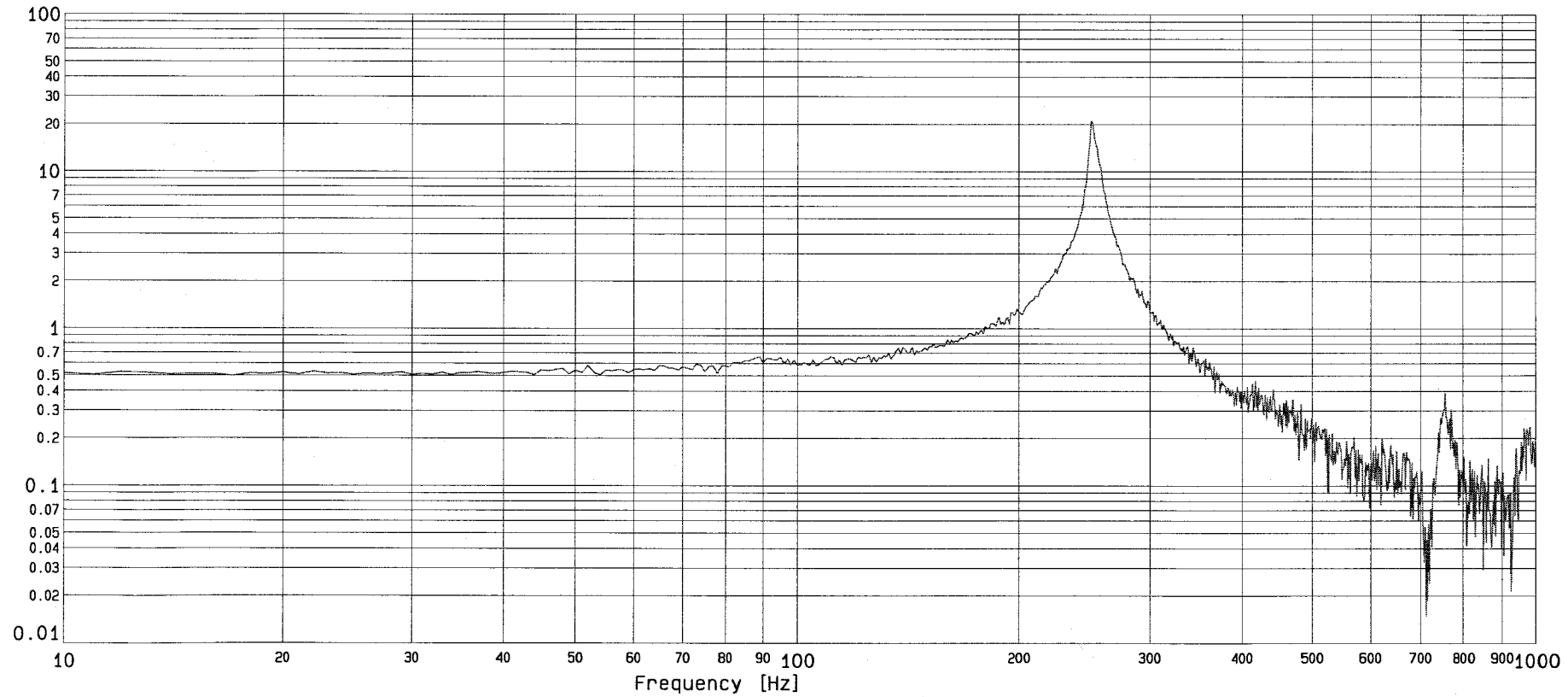

5-4

CSA/DFL Vibration Laboratory

Project	: flvt_m	Date	: 20-04-07
Test	: 20U_Rand20070420	Time	: 10: 42: 50
Run	: 1 20U_Rand20070420	Mode	: Random Vibration Control

Test level	: 0.00 dB	PSD Level (RMS)	: 18.13 g	Trace identification :	MSX
Elapsed time	: 00: 02: 30.0	Number of averages	: 215		
Degrees of freedom	: 150				
Control strategy	: Average				
Frequency resolution	: 2 Hz		fixed		

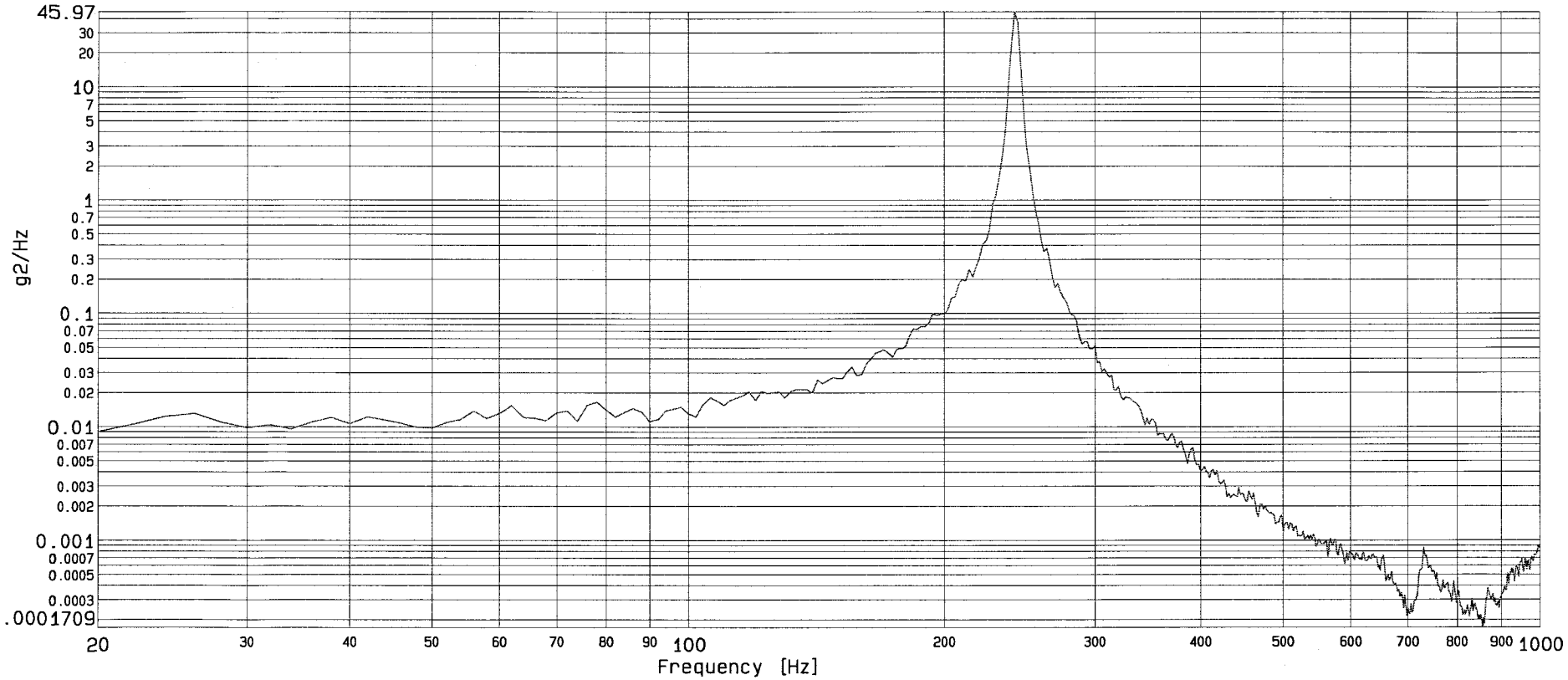

5-5

CSA/DFL Vibration Laboratory

Project : flvt_m
Test : 20D_Sine
Run : 8 RUN_8

Date : 19-01-06
Time : 13: 42: 05
Mode : Sine Vibration Control

Sweeprate : 2.000 Oct/min
Sweep mode : LOG
Start frequency : 10
Sweeps done : 1
Frequency resolution : 1 Hz

Maximum value : 8.54 g

Trace identification : MSX

fixed

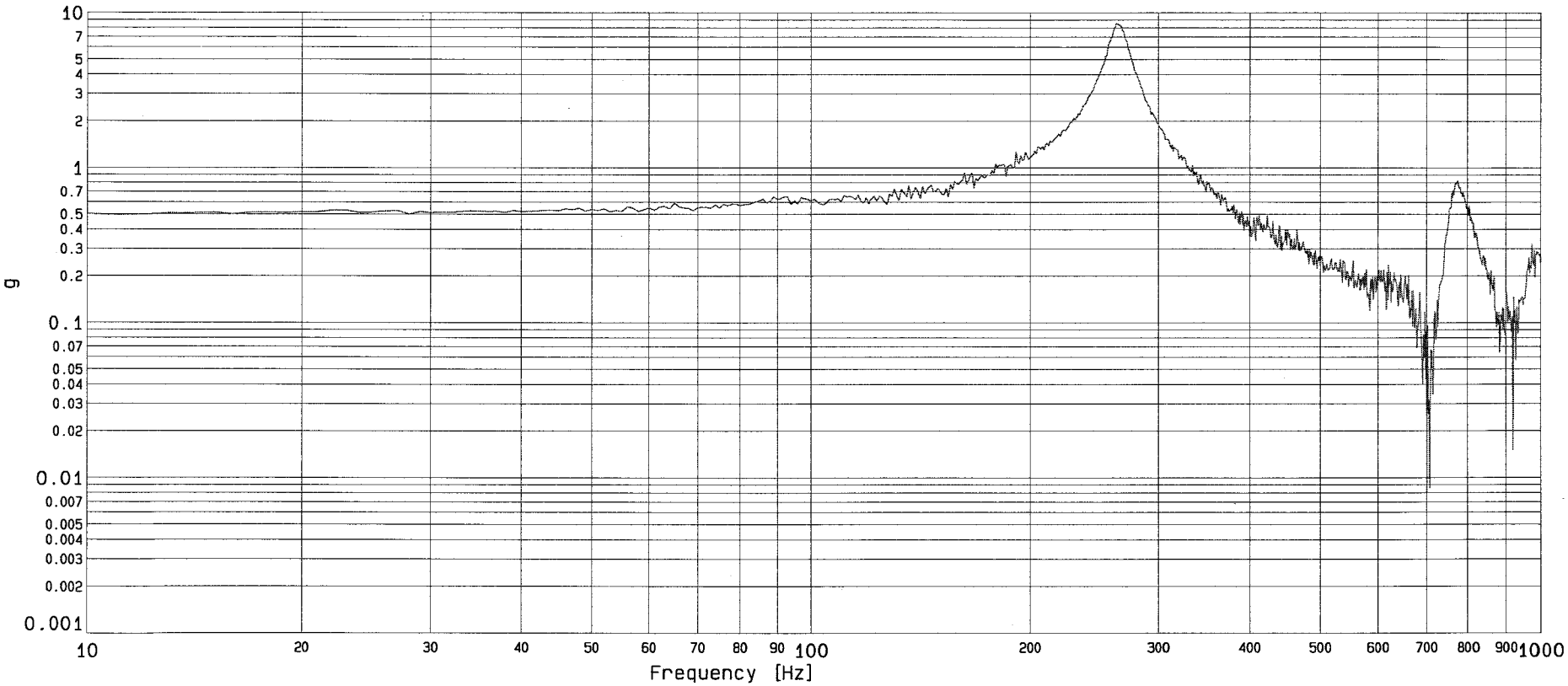

CSA/DFL Vibration Laboratory

Project : flvt_m
Test : 20D_Rand20070420
Run : 1 20D_Rand20070420

Date : 20-04-07
Time : 10:55:03
Mode : Random Vibration Control

Test level	: 0.00 dB	PSD Level (RMS)	: 9.15	g	Trace identification : MSX
Elapsed time	: 00:02:30.0	Number of averages	: 107		
Degrees of freedom	: 150				
Control strategy	: Average				
Frequency resolution	: 1 Hz		fixed		

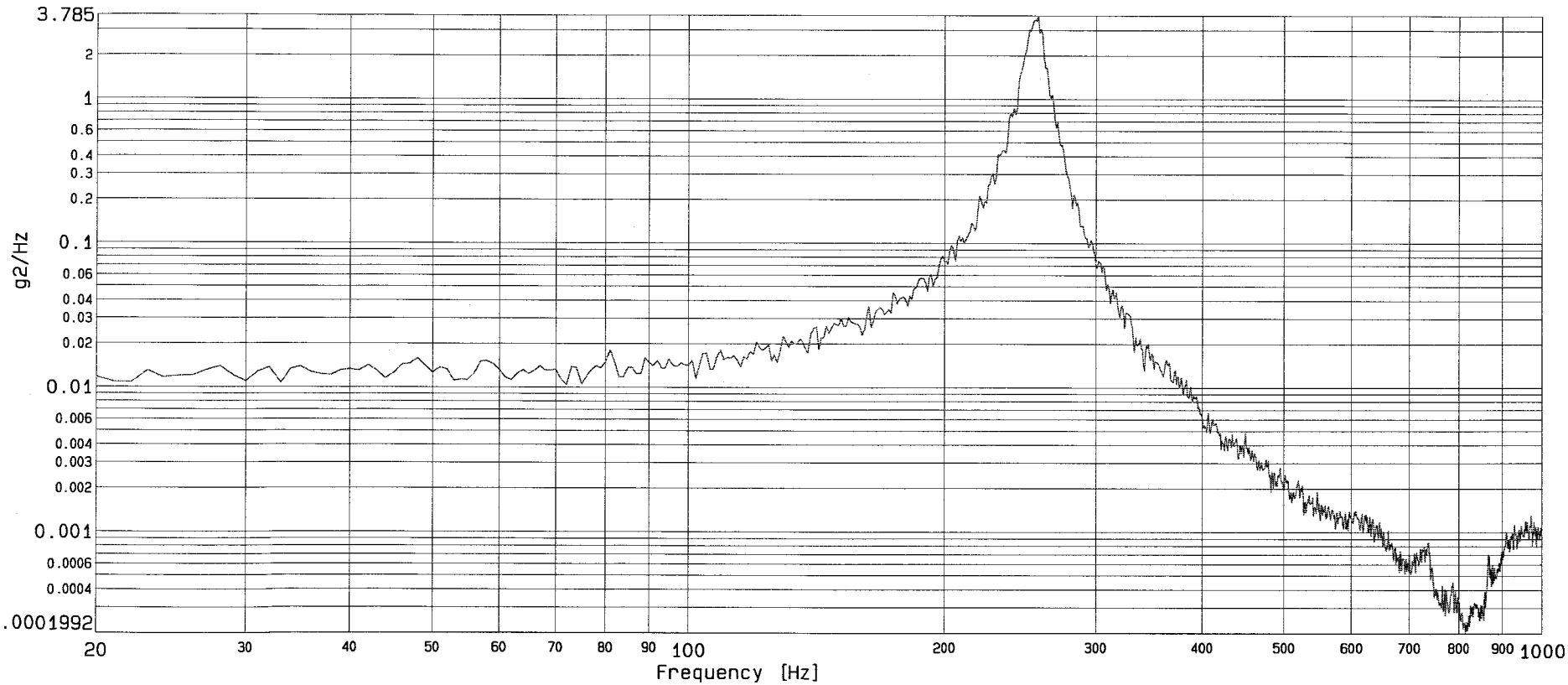

CSA/DFL Vibration Laboratory

Project : flvt_m
Test : 20F2_4_Sine
Run : 1 RUN_1

Date : 09-02-06
Time : 11:02:18
Mode : Sine Vibration Control

Sweeprate : 2.000 Oct/min
Sweep mode : LOG
Start frequency : 20
Sweeps done : 1
Frequency resolution : 1 Hz

Maximum value : 67.53 g

Trace identification : ML1X

fixed

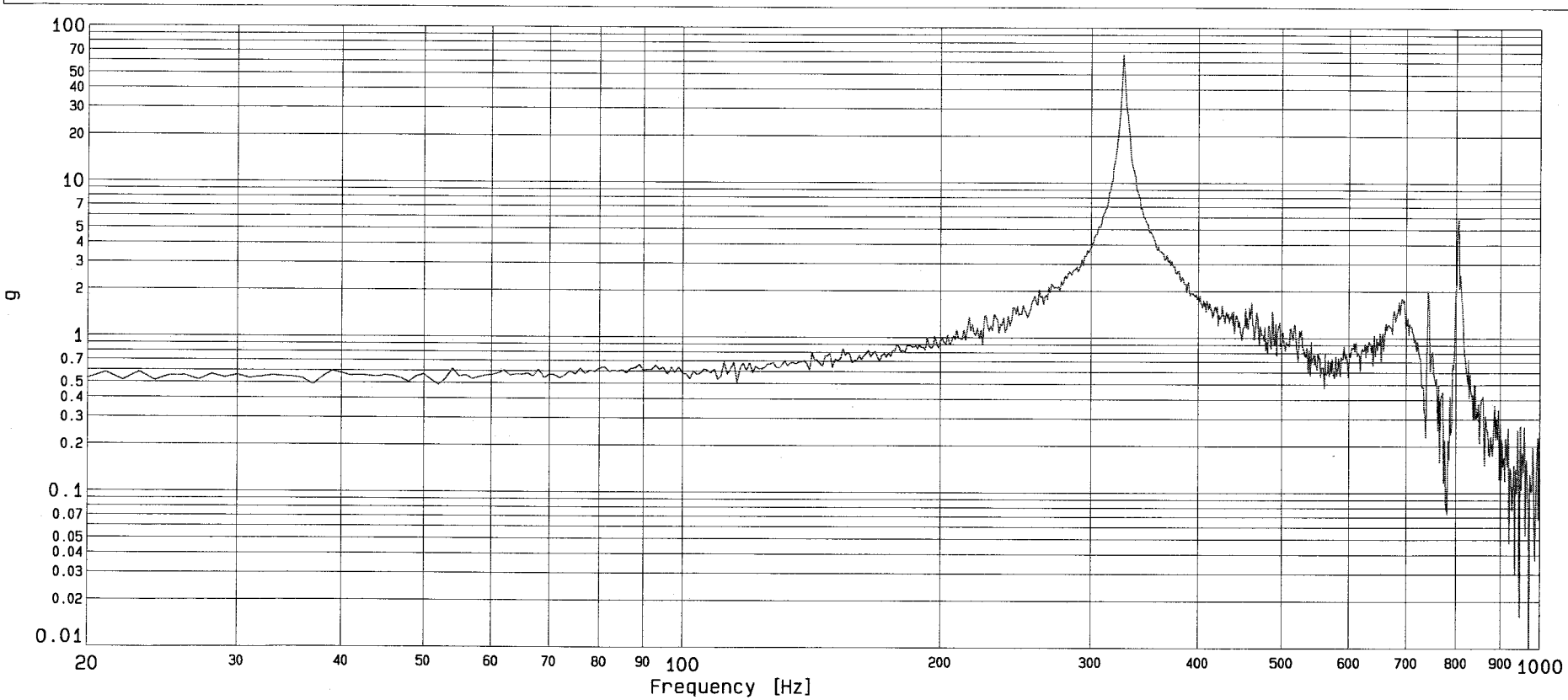

8-5

DFL SQF Vibration

Project : flvt_m
Test : 20F2_4_Rand3_Dec
Run : 1 RUN_12X_Dec_2006

Date : 05-12-06
Time : 11:41:58
Mode : Random Vibration Control

Test level : 0.00 dB
Elapsed time : 00:02:56.1
Degrees of freedom : 150
Control strategy : Average
Frequency resolution : 0.25Hz

Reference identification : C1X
Number of averages : 26

Trace identification : ML1X

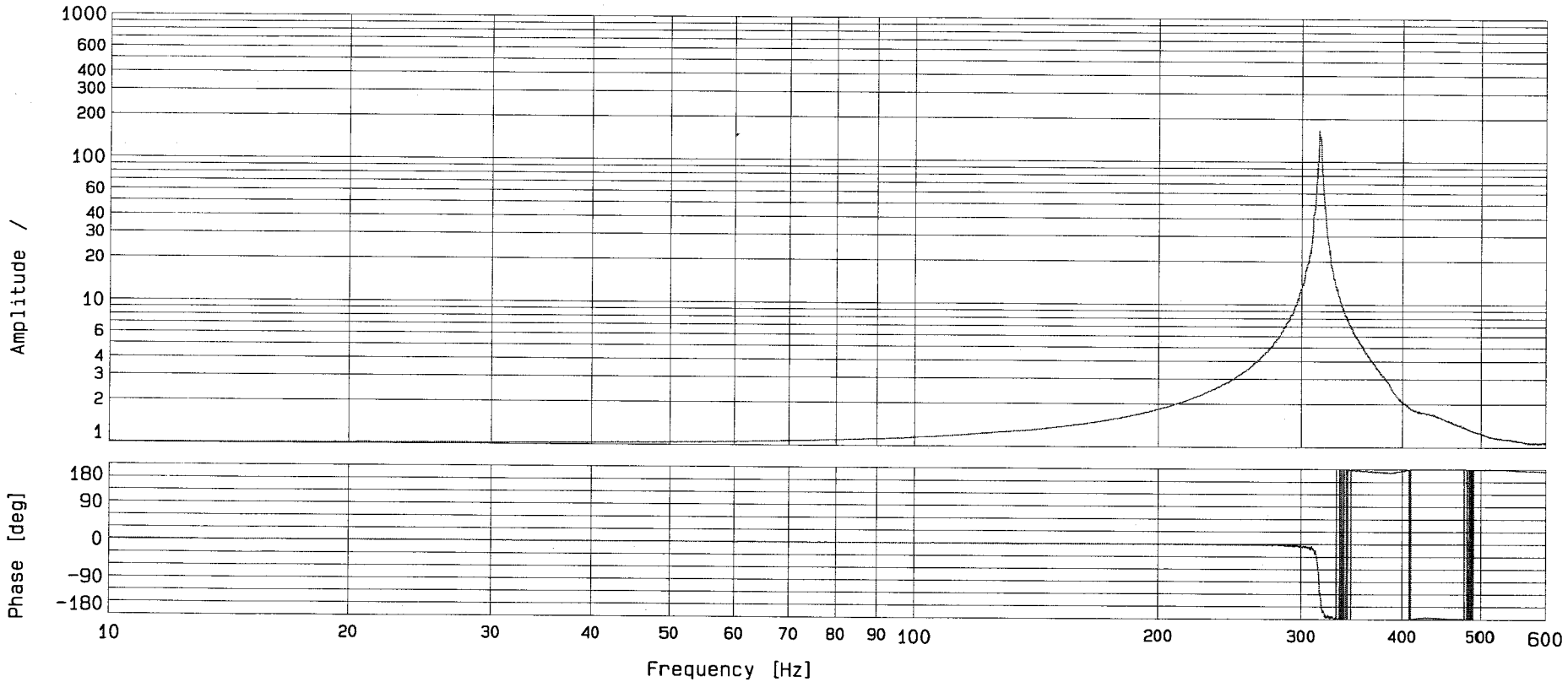

CSA/DFL Vibration Laboratory

Project : flvt_m	Date : 23-01-06
Test : 20D2_4_Random	Time : 09:02:58
Run : 1 RUN_1	Mode : Random Vibration Control

Test level	: 0.00 dB	PSD Level (RMS)	: 25.51 g	Trace identification :	MSX
Elapsed time	: 00:02:30.0	Number of averages	: 107		
Degrees of freedom	: 150				
Control strategy	: Average				
Frequency resolution	: 1 Hz		fixed		

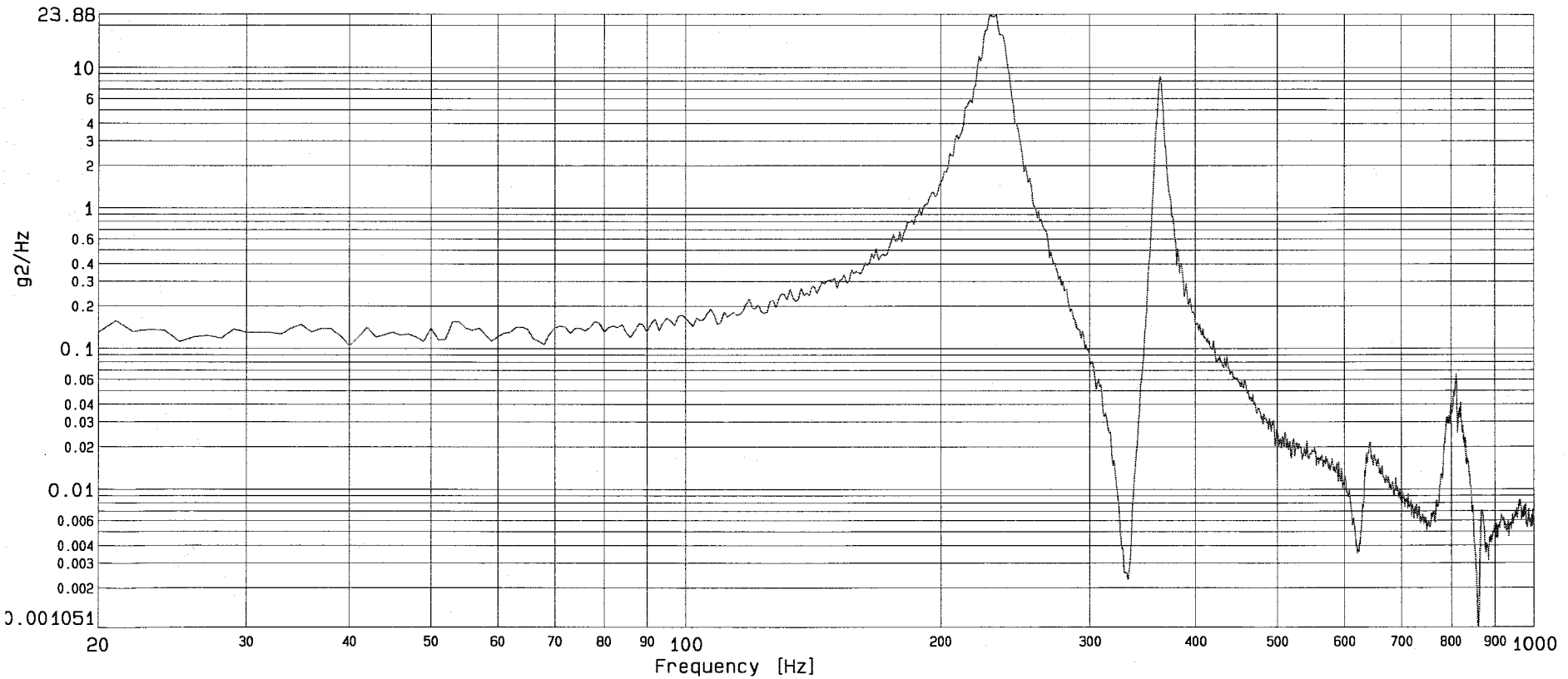

J-10

CSA/DFL Vibration Laboratory

Project : flvt_m
Test : 20D2_4_Random
Run : 1 RUN_1

Date : 23-01-06
Time : 09:02:58
Mode : Random Vibration Control

Test level	: 0.00 dB	PSD Level (RMS)	: 68.82	g	Trace identification : ML1X
Elapsed time	: 00:02:30.0	Number of averages	: 107		
Degrees of freedom	: 150				
Control strategy	: Average				
Frequency resolution	: 1 Hz		fixed		

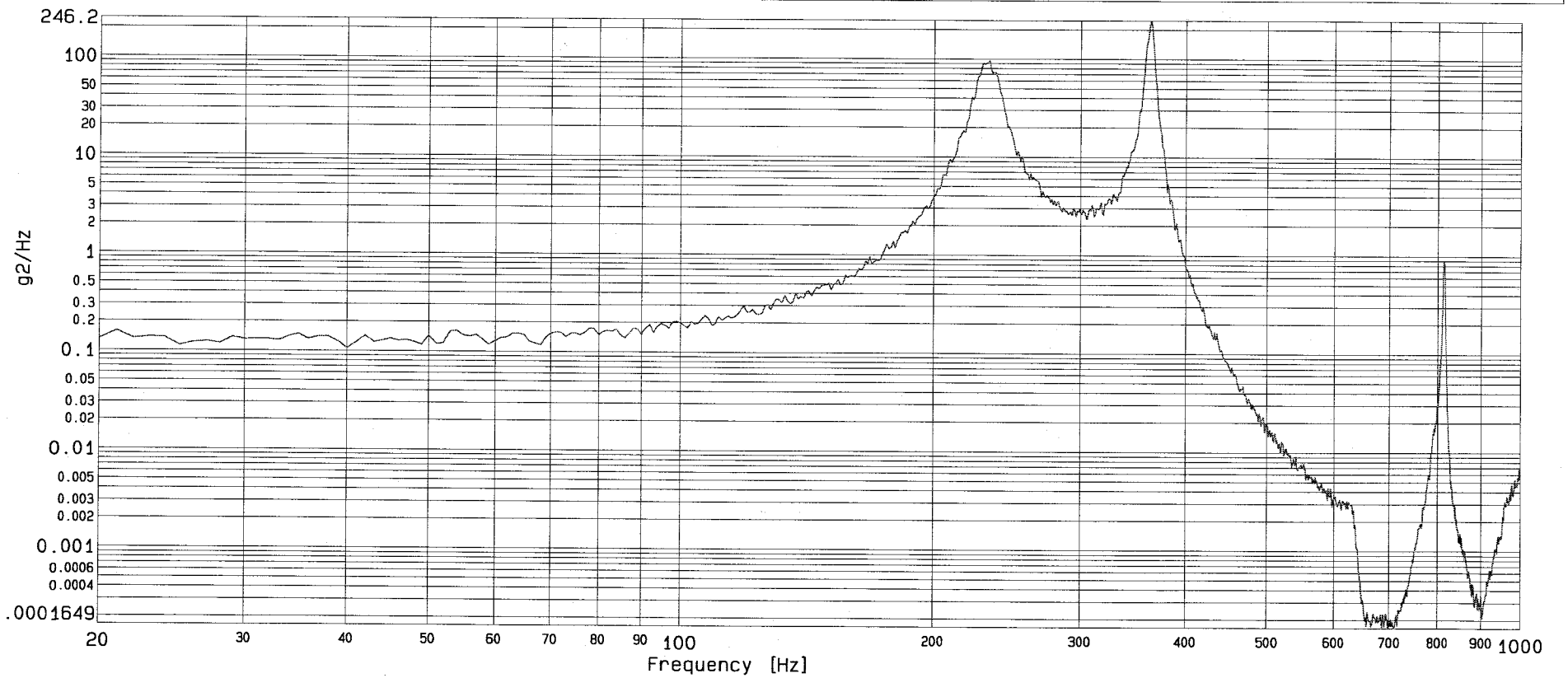

CSA/DFL Vibration Laboratory

Project : flvt_m
Test : 20D2_4_Random
Run : 1 RUN_1

Date : 23-01-06
Time : 09: 02: 58
Mode : Random Vibration Control

Test level	: 0.00 dB	PSD Level (RMS)	: 130.35	lbf	Trace identification : Loadcell1
Elapsed time	: 00: 02: 30.0	Number of averages	: 107		
Degrees of freedom	: 150				
Control strategy	: Average				
Frequency resolution	: 1 Hz		fixed		

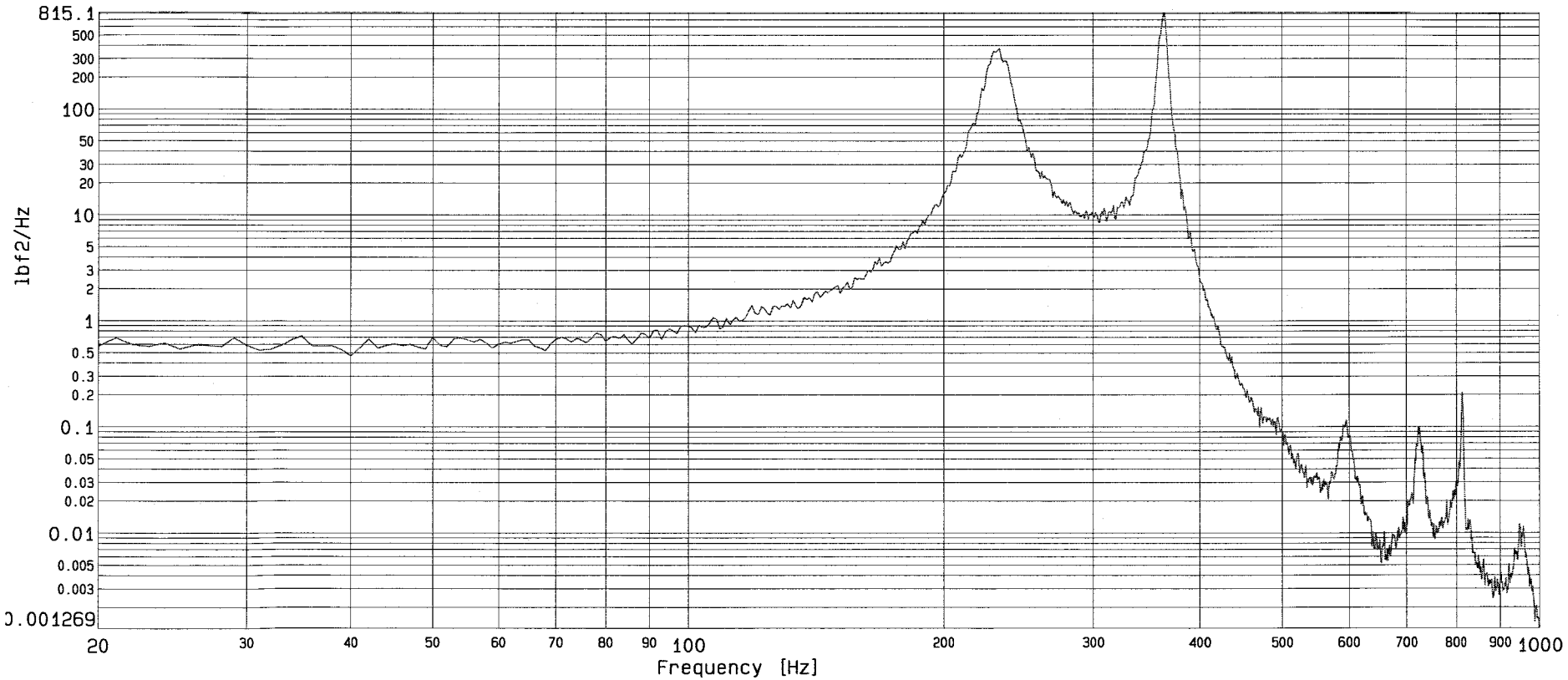

J-12

CSA/DFL Vibration Laboratory

Project : flvt_m
Test : 20D2_4_Random
Run : 1 RUN_1

Date : 23-01-06
Time : 09: 02: 58
Mode : Random Vibration Control

Test level	: 0.00 dB	PSD Level (RMS)	: 137.64	lbf	Trace identification : ——— Loadcell2
Elapsed time	: 00: 02: 30.0	Number of averages	: 107		
Degrees of freedom	: 150				
Control strategy	: Average				
Frequency resolution	: 1 Hz		fixed		

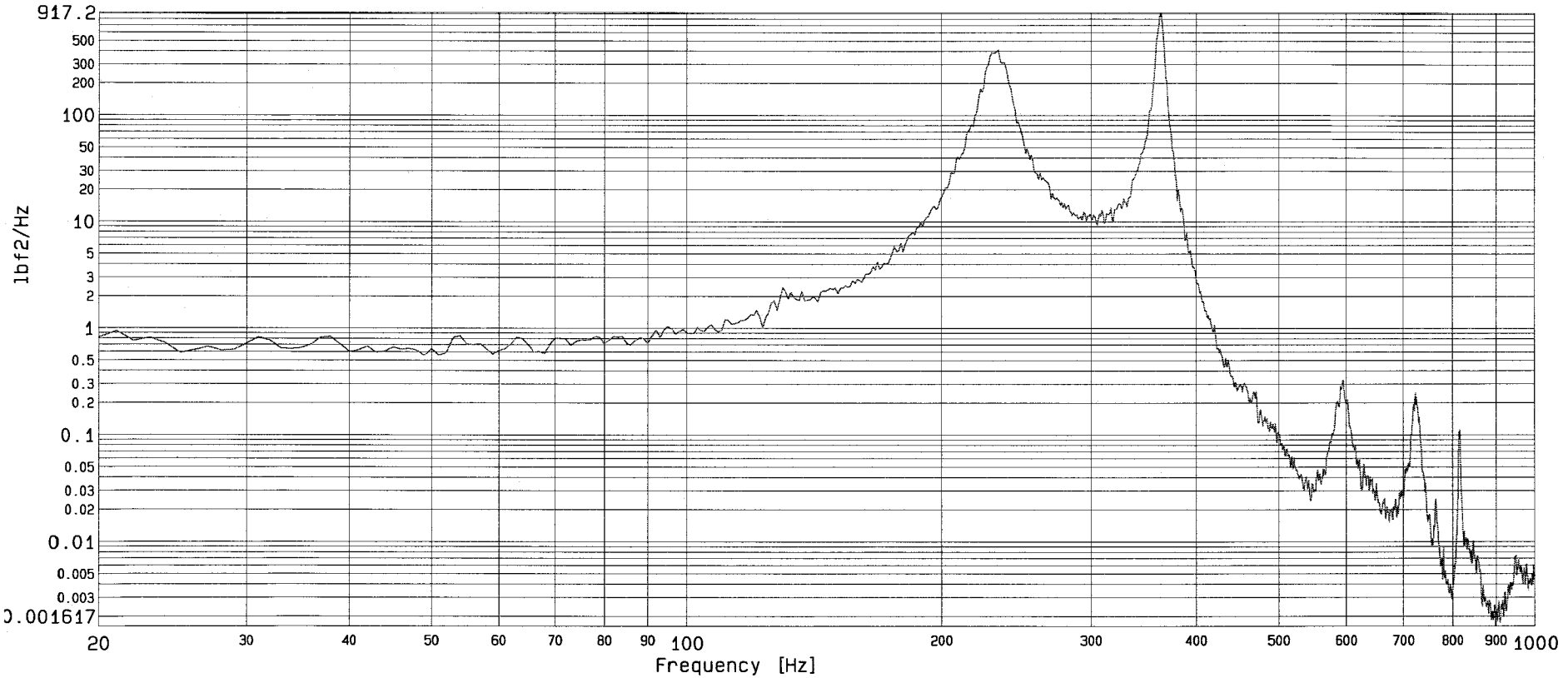

APPENDIX K: C^2 CALCULATIONS EXAMPLES

Example #1

The experimental value, $C^2_{experimental}$, for the coupled 20D2_1 configuration is found using equation 4.30, repeated below.

$$C^2_{experimental} = \left[\frac{\left[S_{ff\_interface}\right]_{max}}{M^2_{load} \cdot \left[S_{aa\_source}\right]_{max}} \right]_{coupled\_system} \tag{4.30}$$

Figure K.1 shows that the value of $[S_{ff\_interface}]_{max}$ is 14 048 lb^2/Hz occurring at 120 Hz. Similarly, figure K.2 shows that the value of $[S_{aa\_source}]_{max}$ is 37.3 g^2/Hz. The value of S_{aa_source} evaluated at 120 Hz, the frequency where the maximum force occurs, is identified as 0.841 g^2/Hz.

Since the actual mass of the load is 2.080 kg or 4.586 lb/g, the value $C^2_{experimental}$ for the 20D2_1 configuration is

$$C^2_{experimental\_20D2\_1} = \frac{14\,048\ lb^2/Hz}{\left(4.586\ lb/g\right)^2 \cdot 37.3\ g^2/Hz} = 17.91$$

In addition, figure K.2 shows that the ratio given by equation 4.31 is

$$\left[\frac{S_{aa\_source}\left(f_{max\_force}\right)}{S_{aa\_source}\left(f_{max\_acc}\right)} \right]_{coupled\_system} \tag{4.31}$$

$$\left[\frac{S_{aa\_source}(120\ Hz)}{S_{aa\_source}(260\ Hz)} \right]_{20D2\_1} = \frac{0.841\ g^2/Hz}{37.3\ g^2/Hz} = 0.02255$$

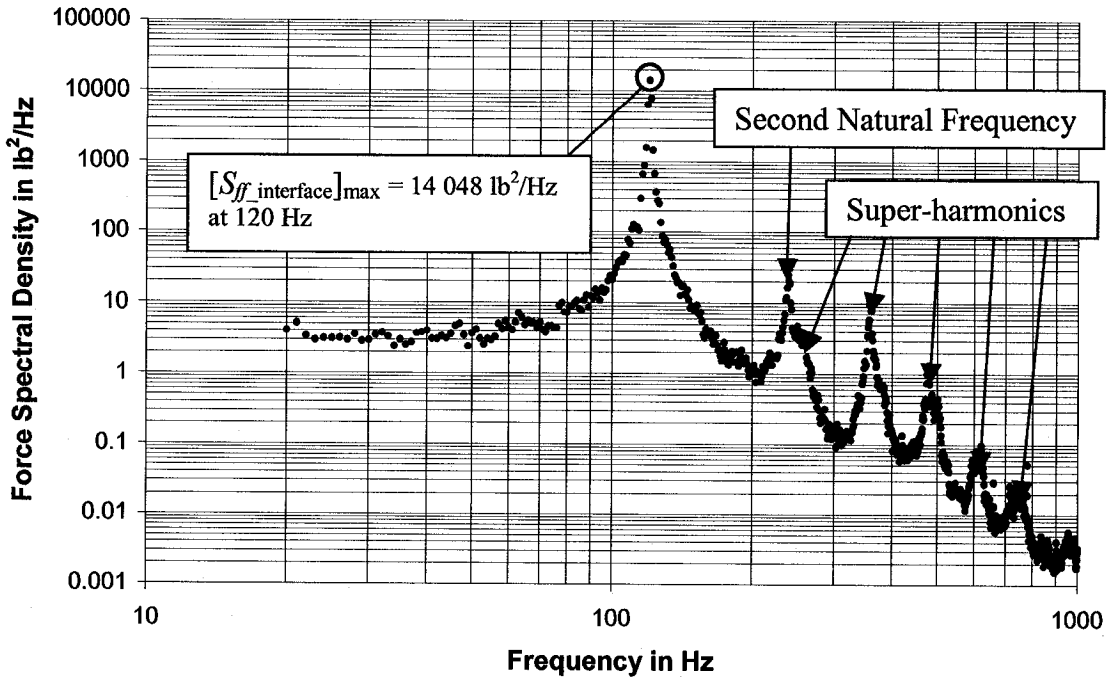

Figure K.1: Summed and Corrected Interface Force Spectral Density Data for Test Configuration 20D2_1

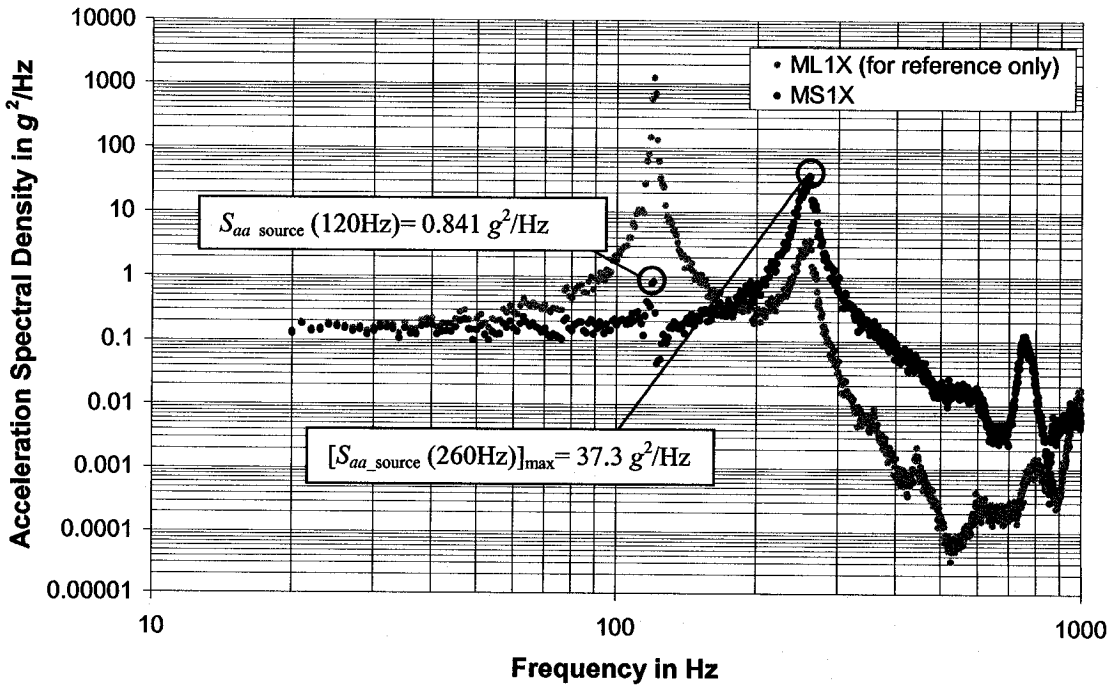

Figure K.2: Acceleration Data for Test Configuration 20D2_1

The value of $C^2_{predicted}$ using the apparent mass method described by equation 4.32 is

$$C^2_{predicted} = \left[\frac{\left|M_{app}\left(f_{max\_force\ (coupled\_system)}\right)\right|}{M_{load}}\right]^2_{uncoupled\_load} \cdot \left[\frac{S_{aa\_source}\left(f_{max\_force}\right)}{S_{aa\_source}\left(f_{max\_acc}\right)}\right]_{coupled\_system} \quad (4.32)$$

From figure K.3, the normalized apparent mass of the load evaluated at f_{max_force} = 120 Hz is 12.92. Thus the predicted value of C^2 is

$$C^2_{predicted\_20D2\_1} = 12.92^2 \cdot 0.02255 = 3.76$$

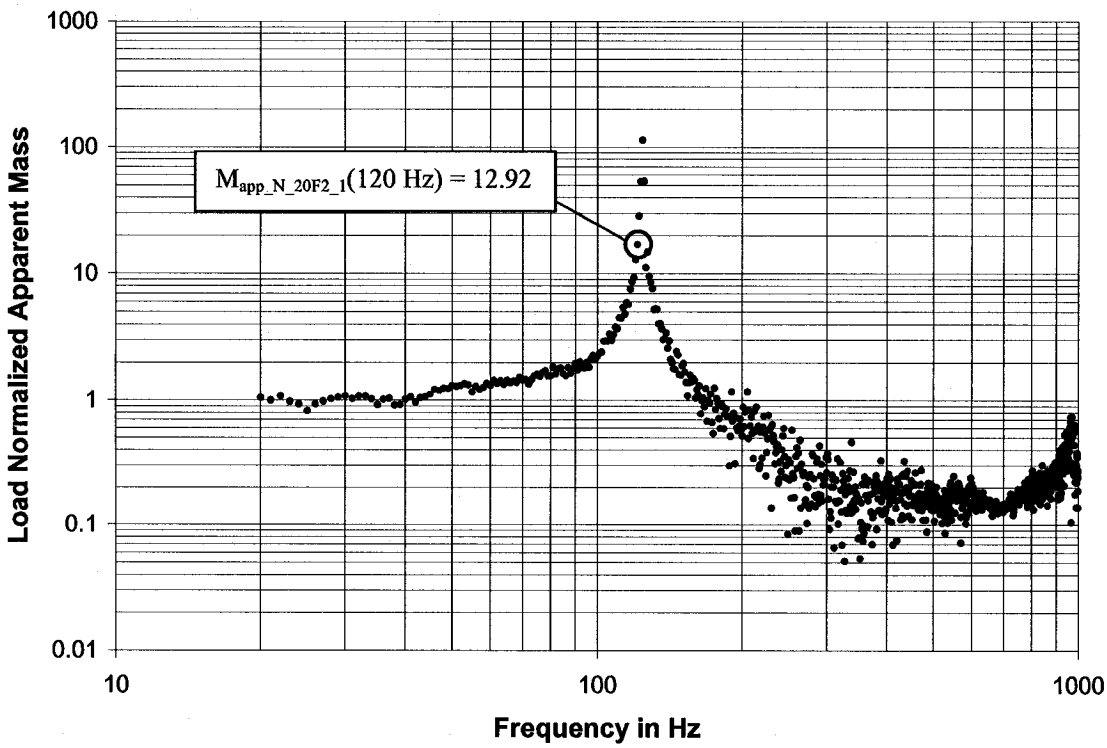

Figure K.3: Load Normalized Apparent Mass for 20F2_1

Example #2

The experimental value, $C^2_{experimental}$, for the coupled system 20U10_3 configuration is found using equation 4.30, repeated below.

$$C^2_{experimental} = \left[\frac{\left[S_{ff\_interface}\right]_{max}}{M^2_{load} \cdot \left[S_{aa\_source}\right]_{max}} \right]_{coupled\_system} \tag{4.30}$$

Figure K.4 shows that the value of $[S_{ff\_interface}]_{max}$ is 35 008 lb^2/Hz occurring at 179 Hz. Similarly, figure K.5 shows that the value of $[S_{aa\_source}]_{max}$ is 22.4 g^2/Hz. The value of S_{aa_source} evaluated at 179 Hz, the frequency where the maximum force occurs, is identified as also 22.4 g^2/Hz because the maximum force and the maximum acceleration occur at the same frequency.

Since the actual mass of the load is 9.224 kg or 20.335 lb/g, the value $C^2_{experimental}$ for the 20U10_3 configuration is

$$C^2_{experimental\_20U10\_3} = \frac{35\,008\ lb^2/Hz}{\left(20.335\ lb/g\right)^2 \cdot 22.4\ g^2/Hz} = 3.78$$

In addition, figure K.5 shows that the ratio given by equation 4.31 is

$$\left[\frac{S_{aa\_source}\left(f_{max\_force}\right)}{S_{aa\_source}\left(f_{max\_acc}\right)} \right]_{coupled\_system} \tag{4.31}$$

$$\left[\frac{S_{aa\_source}(179\ Hz)}{S_{aa\_source}(179\ Hz)} \right]_{20U10\_3} = \frac{22.4\ g^2/Hz}{22.4\ g^2/Hz} = 1$$

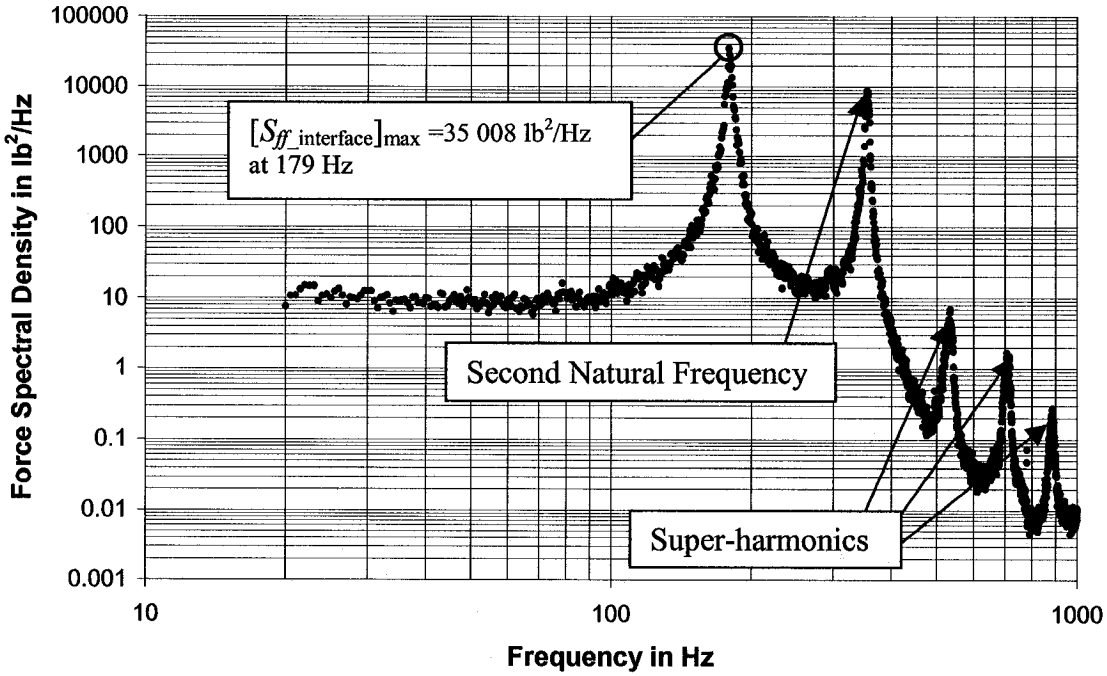

Figure K.4: Summed and Corrected Interface Force Spectral Density Data for Test Configuration 20U10_3

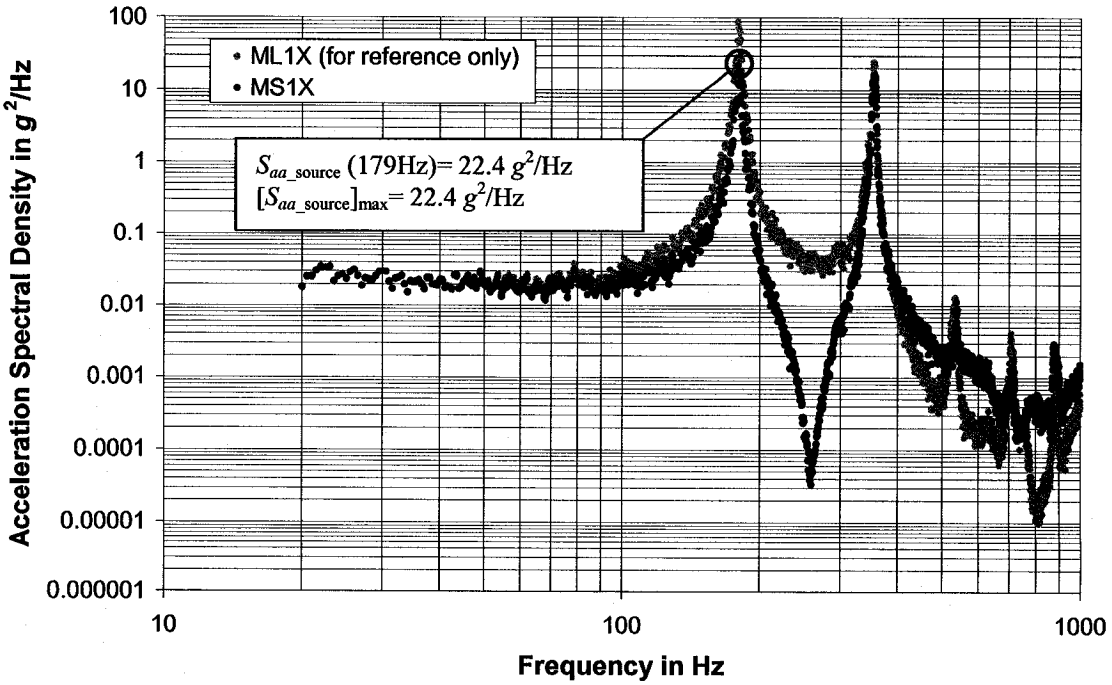

Figure K.5: Acceleration Data for Test Configuration 20U10_3

The value of $C^2_{predicted}$ using the apparent mass method described by equation 4.32 is

$$C^2_{predicted} = \left[\frac{\left|M_{app}\left(f_{max\_force\ (coupled\_system)}\right)\right|}{M_{load}}\right]^2_{uncoupled\_load} \cdot \left[\frac{S_{aa\_source}\left(f_{max\_force}\right)}{S_{aa\_source}\left(f_{max\_acc}\right)}\right]_{coupled\_system} \quad (4.32)$$

From figure K.6, the normalized apparent mass of the load evaluated at f_{max_force} = 179 Hz is 1.995. Thus the predicted value of C^2 is

$$C^2_{predicted\_20U10\_3} = 1.995^2 \cdot 1 = 3.98$$

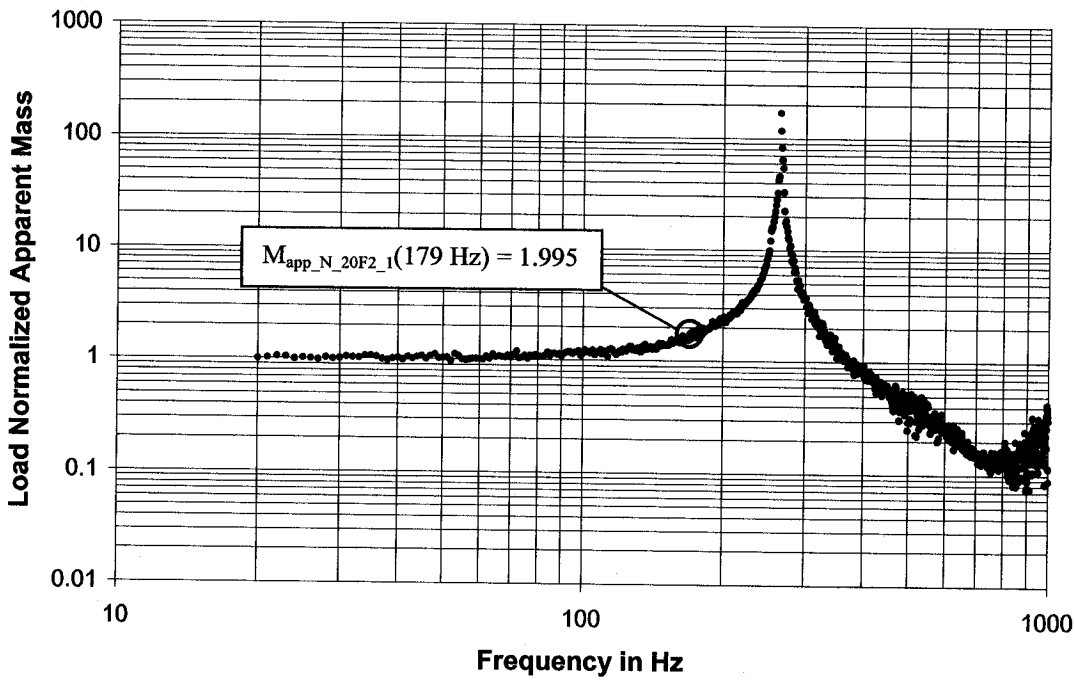

Figure K.6: Load Normalized Apparent Mass for 20F10_3